

Studies on Efficiency Considerations in Conventional and Schottky Barrier Solar Cells

A Thesis

Submitted in partial fulfillment of the
requirements of the degree of

DOCTOR OF PHILOSOPHY

by

NARENDRA KUMAR SWAMI



PHYSICS GROUP

**BIRLA INSTITUTE OF TECHNOLOGY AND SCIENCE
PILANI (RAJASTHAN) INDIA**

OCTOBER, 1979

BIRLA INSTITUTE OF TECHNOLOGY AND SCIENCE

PILANI (RAJASTHAN)

C E R T I F I C A T E

This is to certify that the thesis entitled
"STUDIES ON EFFICIENCY CONSIDERATIONS IN CONVENTIONAL
AND SCHOTTKY BARRIER SOLAR CELLS" and submitted by
Mr. Narendra Kumar Swami, ID NO. 74S65001 for award
of Ph.D. degree of the Institute, embodies original work
done by him under my supervision.

H. M. Ghule

(H. M. Ghule)
Assistant Professor of Physics
Physics Group.

Date: 13.11.79

ACKNOWLEDGEMENTS

It gives me great pleasure to place on record my deep sense of gratitude towards Dr. H.M. Ghule, Asst. Prof. of Physics, B.I.T.S., Pilani (Raj.), who suggested the problem and guided and encourage^d me during the entire course of this work.

I owe my sincere and heartfelt thanks to Dr. S.K. Sharma and Dr. B.R. Marathe for their keen interest and all possible help during the course of this work.

My special thanks are due to Dr.S.C.Jain, Dr.(Mrs.) S.Srivastava, Sri S.C.Bawa, Dr.A.K. Jain, Dr. Chandra Shekhar and Sri K.C. Gupta for their valuable help.

I wish to express my heartfelt thanks to Dr.S.C. Sharma, Dr. G.P.Srivastava, Dr. Ved Prakash, Dr. N.K.Joshi, Dr. M.C. Gupta, Dr. D.C.Tewari, Dr. V.S. Kulhar, Dr. S.K.Jain, Dr. S.Kumar, Dr.(Mrs.) A. Gupta, Dr. P.R.Marwadi, Dr.A.P.Sathe, Dr. Subhash C. Sharma, Sri Raviprakash Saxena, Sri K.S.Yadav, Sri G.S.Tyagi, Sri M.D. Arora, Sri M.K. Madan, Miss Amita Agrawal, Sri S.K. Sharma, Dr. Room Singh, Sri Rakesh Kapila, Sri Lalit Jain and all other friends who made my stay in Pilani a lively and memorable experience in various fields of life.


My thanks are due to Sri Banwari Lal, Sri S.L. Sharma, Sri Ashok Tewathia and Sri B.P. Singh for helping during my

computational work. I also thank Shri S.K. Sinha for efficient typing of the manuscript and Sri K.N. Sharma and Sri B.D. Sukhaja for the drawing work.

I wish to express my deep sense of gratitude towards my parents for their stoic forbearance and continued encouragement.

I lovingly thank my younger sisters, Savita, Savitri and Manju whose affection has been a constant source of inspiration.

In the end I express my grateful thanks to the Director, B.I.T.S., Pilani, Dr. V.K. Tewary, Dean Research and Consultancy Division, Chief I.F.C. and Sri T.N.R.K. Kurup, Group Leader of Physics for providing necessary facilities during the course of this work. The author is also thankful to the University Grants Commission for financial assistance.


13-11-79.
(N. K. SWAMI)

C O N T E N T S

<u>Chapter</u>		<u>Page .</u>
I	Introduction.	1
II	Series resistance of p-n junction solar cells.	45
III	Effect of temperature and concentrated sunlight.	83
IV	Schottky barrier solar cells.	113
V	Electron transmission and donor density effect in schottky barrier solar cells.	141
VI	Effect of hole transmission in schottky barrier solar cells.	167
	Summary.	185
	Appendix-2.1.	188
	List of publications.	191

CHAPTER-I.

INTRODUCTION

1.1	Photovoltaic effect and solar cell	2
1.2	p-n junction solar cells	5
1.3	Efficiency and limiting efficiency of a solar cell.	19
1.4	Other solar cell devices	35
1.5	Aims of the present work in connection with p-n junction solar cells.	38

CHAPTER-I.

INTRODUCTION

1.1 PHOTOVOLTAIC EFFECT AND SOLAR CELL:

Photovoltaic effect⁽¹⁻⁶⁾ constitutes a class of phenomena in which generation of an electromotive force takes place as a result of the absorption of light across a portion of the material absorbing this light. In order for the photovoltaic effect to exist in the system, the generated electrons and holes must be separated by an internal field created by some inhomogeneity in the system. This inhomogeneity can be due to a metal-semiconductor contact⁽⁴⁾ or a junction between two regions of the same semiconductor having different types of conductivities such as a p-n junction⁽⁵⁻⁶⁾. This effect is most pronounced in those semiconductors in which the forbidden energy gap lies between 1.0 and 2.5 eV. An analysis of the effect shows that in the wavelength range 0.40 μm to 2.1 μm , acceptable efficiency for conversion of sunlight into electricity can occur only in such materials. Such a device, which converts incident solar radiation into electricity, is known as a solar cell. This effect has been known for many years, but it has been only in the last 25 years that serious consideration has been given for affecting considerable improvement in the performance of solar cells as well as to a clearer understanding of its

operation (7-31). A high efficiency silicon solar cell was first demonstrated in 1954 by the Bell Telephone Laboratories. It was then clear that direct conversion of solar radiation by means of a solar cell into electricity would some day prove^{to} be a useful source of power. The successful flight of Vanguard I and the numerous space probes that have followed, have confirmed this speculation (32-35). Now a days the use of solar cell has become much more important for terrestrial uses (36-39) on account of fast depleting conventional energy sources. The major advantages of employing solar cells for power generation are:

- (i) highest overall conversion efficiency of solar radiation to electricity as compared to other devices such as thermoelectric solar energy converters;
- (ii) unlimited life;
- (iii) ease of fabrication and
- (iv) high power output/weight ratio.

At the same time there are some disadvantages also.

These are :

- (i) high cost to develop a solar cell;
- (ii) the need of storage devices in most of the applications;

- (iii) degradation in its performance when it is exposed to a humid atmosphere and
- (iv) radiation damage from high energy particles.

The use of solar cells for direct conversion has been largely confined to space applications. However, the increasing need for alternative energy sources, ecological considerations and fast eroding conventional energy sources have made solar energy and photovoltaic conversion an active area of research. The purpose of this chapter is to provide an understanding of the physics of the photovoltaic effect and its application to the conversion of solar radiation to electrical energy by means of a solar cell. On illuminating a homogeneous piece of semiconductor with light, the light generated electrons and holes, having no preferential direction of motion, diffuse in all directions and there is recombination without development of any photovoltage. The built-in internal electrical field of the p-n junction or metal-semiconductor junction causes the separation of photogenerated carriers of opposite kind and photovoltage appears across the junction. This chapter is confined to the discussion of the p-n junction solar cells only. The case of metal semiconductor system will be taken up in fourth chapter.

1.2 p-n JUNCTION SOLAR CELLS

1.2.1(a) p-n JUNCTION DIODE OPERATION:

As indicated above, in order for the electrons and holes, generated internally by the absorption of light, to contribute to the electrical output from the cell, they must be separated from each other. The p-n junction is most suitable for this purpose. In a p-n junction, the donor impurities on the n side provide mobile electrons. The acceptor impurities on the p side on the other hand can accept electrons from other covalent bonds and provide a mechanism for the movement of vacancies called holes. The electrons on the n side constitute the majority carriers while the holes on the n side are called the minority carriers. The majority and minority carriers on the p side are holes and electrons respectively. During the formation of the p-n junction, the electrons diffuse from n side towards the p side as a result of the concentration gradient, leaving the donors positively charged. Similarly the holes diffuse from p side towards the n side and leave behind negatively charged acceptors. On the p side there is thus an excess of immobile negative ions and on the n side that of the positive ions. An electric field is thus established at the interface of the two portions. The region consisting of immobile charges constitutes the space charge region. The diffusion of electrons and holes

continues till the electric field becomes so strong that the net flow of charge carriers on either side of the p-n junction stops and an equilibrium is set up. An internal electric field is thereby established. Under thermal equilibrium, the net flow of current across the junction is zero.

The setting up of the built-in electric field of the p-n junction can also be explained on the basis of electron energy band diagrams of p and n types of semiconductors as shown in figures 1.1(a) and (b). When the p-n junction is formed, the condition of thermal equilibrium requires levelling of the Fermi levels throughout the system as shown in Figure 1.1(c). This realignment brings about setting up of a built-in potential V_{bi} as shown in figure 1.1(c).

1.2.1(b) DIODE EQUATION:

The internal field in the transition region (space charge region) is directed from the n side to the p side. This means that n side is at a higher potential than the p side. In thermal equilibrium the net flow of carriers of any one type should be zero. From n side only those electrons (majority carriers) whose energy is higher than or equal to the barrier height will cross the barrier by diffusion. These constitute the electron diffusion flux J_{nd} . The thermally generated minority carrier electrons on the p side move "down hill" of

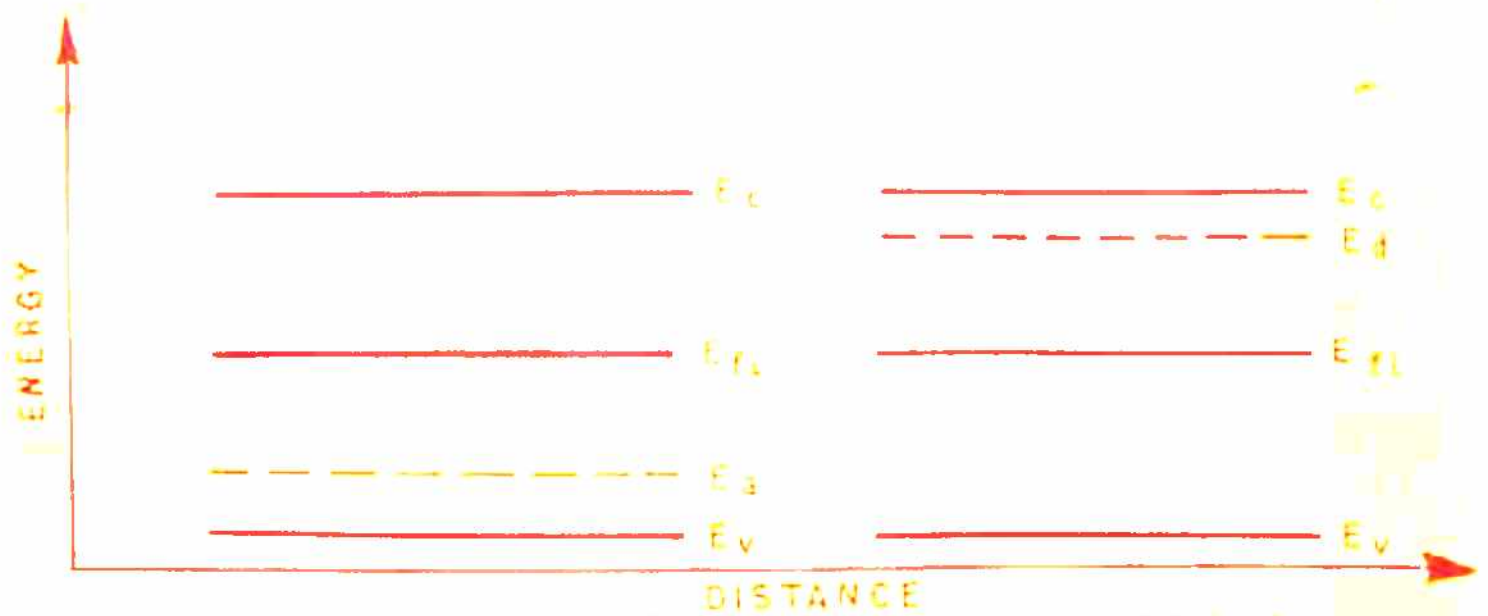


FIG. 1.1 (a)

p TYPE SEMICONDUCTOR

FIG. 1.1 (b)

n TYPE SEMICONDUCTOR

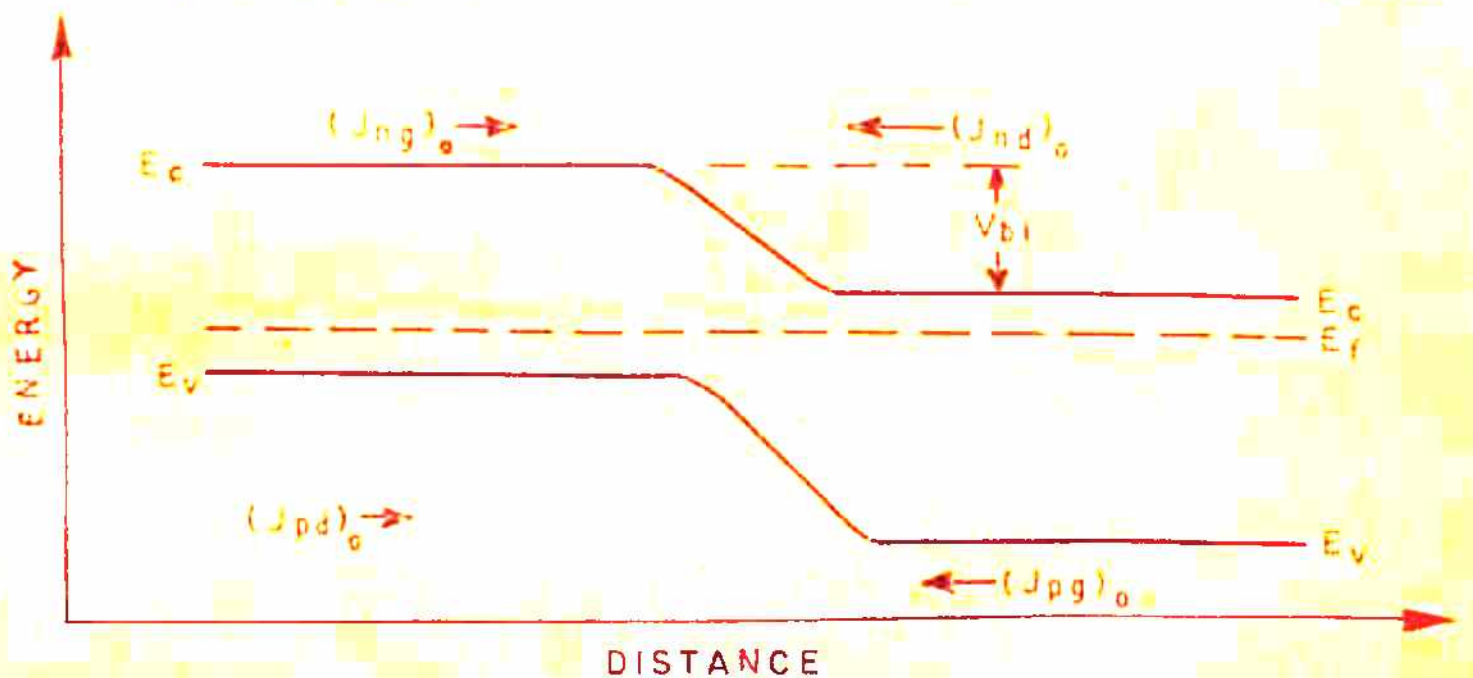


FIG. 1.1 (c) ENERGY BAND DIAGRAM OF A p-n JUNCTION AT THERMAL EQUILIBRIUM.

E_{fp} = FERMI LEVEL ON p SIDE, E_{fn} = FERMI LEVEL ON n SIDE

E_c = CONDUCTION BAND, E_v = VALENCE BAND

E_{fi} = INTRINSIC FERMI LEVEL,

the potential barrier towards the n side. These carriers constitute the generation flux J_{ng} . Similarly holes from p side will diffuse to n side and constitute the diffusion flux J_{pd} and holes from n side constitute the generation flux J_{pg} . In thermal equilibrium

$$(J_{nd})_0 = (J_{ng})_0 \text{ and } (J_{pd})_0 = (J_{pg})_0. \quad (1.1)$$

The basis for the operation of p-n junction diode under reverse and forward bias conditions is as follows: Under reverse bias conditions, the height of the potential barrier at the junction increases by an amount V , where V is the applied voltage. It therefore becomes difficult for majority carriers to surmount the barrier by diffusion, and thus J_{pd} and J_{nd} become small. The generation fluxes $(J_{ng})_0$ and $(J_{pg})_0$, however, depend only upon the temperature and therefore remain unaffected. As the reverse bias V is increased, the current density across the junction approaches a constant small value, called the saturation current density. The physical situation is shown in Figure (1.2a).

When a forward bias voltage V is applied, the barrier height is reduced by an amount V and then it becomes easier for the majority carriers on either side to diffuse over the barrier to the opposite sides. This increases the electron and hole particle fluxes J_{nd} and J_{pd} to $(J_{ng})_0 e^{eV/kT}$ and $(J_{pg})_0 e^{eV/kT}$ respectively.

At the same time the generation of electron and hole fluxes $(J_{ng})_0$ and $(J_{pg})_0$ remains the same. In other words the number of minority carrier electrons on p side (coming from the n side) and the number of minority carrier holes on n side (coming from the p side) increases under forward condition. We say that the junction injects minority carriers into p and n sides respectively. The forward bias condition is illustrated in Figure (1.2b). The particle fluxes for a p-n junction under forward bias are given by

$$J_{pd} = (J_{pg})_0 e^{eV/kT}, \quad J_{nd} = (J_{ng})_0 e^{eV/kT}$$

$$J_p = J_{pd} - (J_{pg})_0 = (J_{pg})_0 (e^{eV/kT} - 1)$$

$$J_n = -J_{nd} + (J_{ng})_0 = -(J_{ng})_0 (e^{eV/kT} - 1)$$

where J_p represents the net hole flux from p to n side and J_n , the net electron flux from n to p side.

The total current I_D is then given by

$$I_D = eA(J_p - J_n) = Ae \left[(J_{pg})_0 + (J_{ng})_0 \right] \left[e^{eV/kT} - 1 \right]$$

$$I_D = I_0 \left[e^{eV/kT} - 1 \right] \quad (1.2)$$

where $I_0 = eA((J_{pg})_0 + (J_{ng})_0)$, e being the electronic charge and A the area of cross section of the junction. Equation 1.2 is the ideal diode equation in which the recombination generation in the depletion region has not been taken into account.

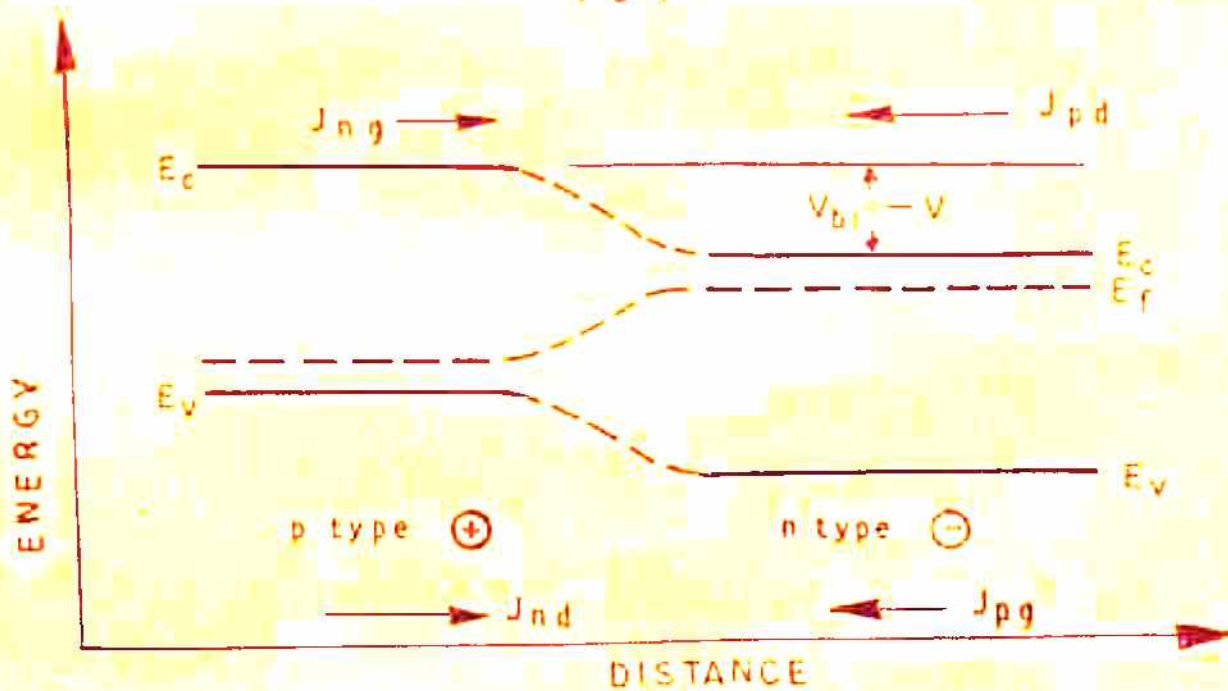
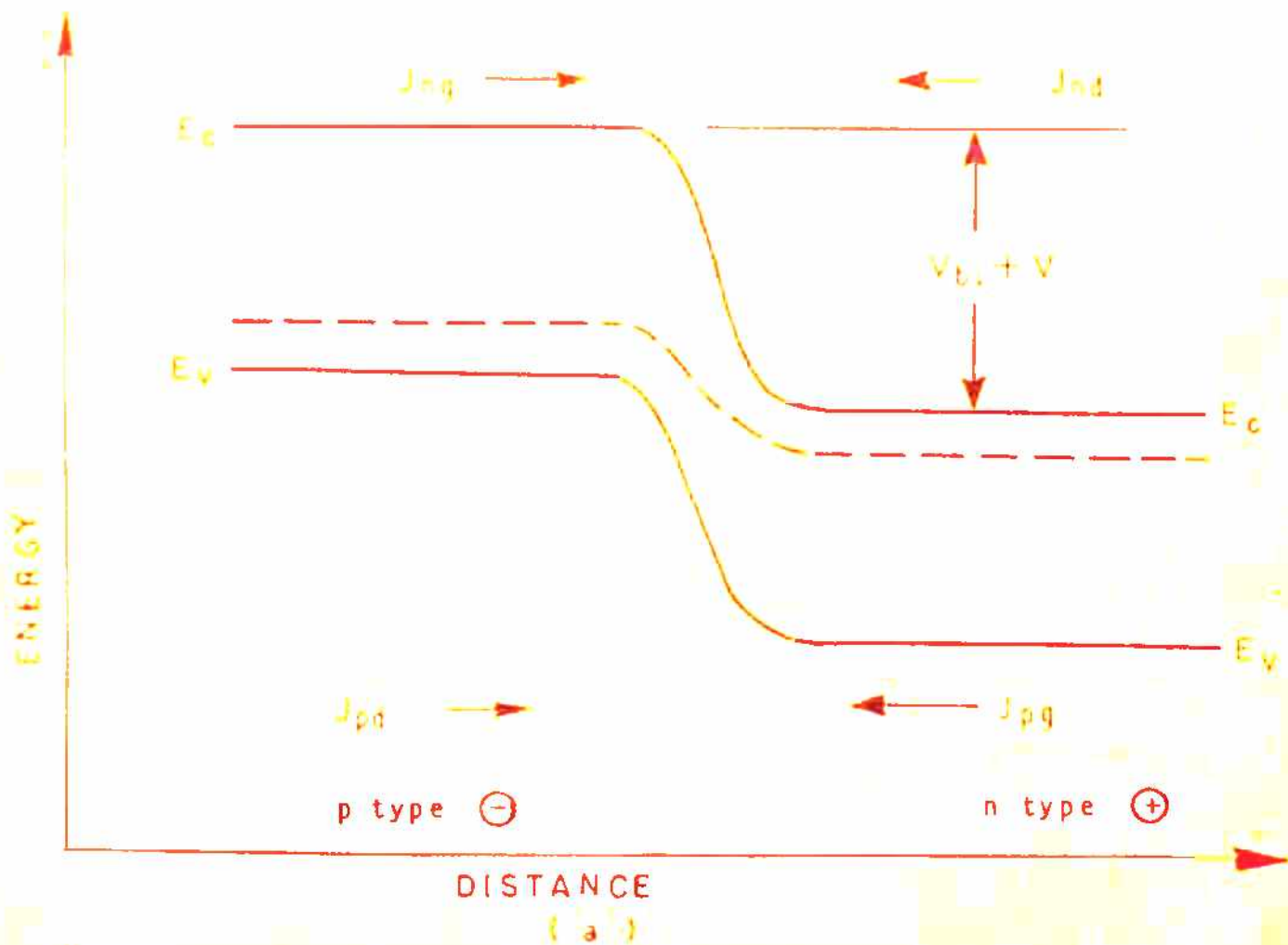


FIG. 1.2 ENERGY BAND DIAGRAM OF A p - n JUNCTION

(a) REVERSE BIAS CONDITION

(b) FORWARD BIAS CONDITION

1.2.1(c) RECOMBINATION GENERATION CURRENT IN SPACE CHARGE REGION:

In addition to the ideal diode current given by equation (1.2), there is a recombination generation current in the device arising from recombination processes occurring in the space charge region. Recombination and generation currents in the space charge region are a consequence of deep levels which serve as recombination centers for electrons and holes. In thermal equilibrium there is a traffic through these centers. Electrons are thermally excited from the valence band into these centers, leaving holes in the valence band and then the electrons can be excited from such a center to the conduction band. The inverse of this process, by which, electrons from conduction band first fall into the recombination centers and then recombine with the holes in the valence band, also occurs. Processes of this type can provide the mechanism for maintaining thermal equilibrium throughout the junction region.

Under forward bias condition, the electrons going from n side to p side and holes from p side to n side through the space charge region recombine there due to the fact that the excess density of carriers in the space charge region causes increased recombination of the carriers in the space charge region as the recombination density increases with carrier

density of each kind. Similarly the electrons going from n side to p side and holes going from p side to n side through the space charge region recombine there due to the fact that the deficit density of carriers in the space charge layer causes decreased recombination of the carriers in the space charge region in the reverse bias condition. At forward bias, the major recombination generation process in the depletion region are the capture processes. On the other hand, under the reverse-bias condition the dominant recombination generation processes in the depletion region are those of emission.

The various steps that occur in the recombination and generation process through intermediate trapping levels are shown in figure 1.3. The arrows in the figure show the transition of the electrons during the particular process. Process(a) is the capture of an electron from the conduction band by the center. Process(b) is the reverse process-the emission of an electron from the center into the conduction band. Process(c) is the capture of a hole from the valence band by a center. This process can also be described as the transition of an electron from the center into the valence band. Finally, process(d) is the emission of a hole from a center into the valence band and this can also be described as the transition of an electron from the valence band to the center, leaving behind a hole in the valence band. The recombination rate of

electrons and holes for a single level trap centres is given by (40)

$$U = \frac{(pn - n_i^2) \sigma_p \cdot \sigma_n V_{th} N_r}{\sigma_n (n + N_c e^{-(E_c - E_t)/kT}) + \sigma_p (p + N_v e^{-(E_t - E_v)/kT})} \quad (1.3)$$

Where $\sigma_{n,p}$ is the cross section for the capture of an electron (hole) by a recombination center located within the band gap at energy E_t , N_r is the density of such centers, N_c is the density of states in the conduction band, N_v is the density of states in the valence band, V_{th} is the thermal velocity, p and n are excess carrier density in n and p regions respectively and n_i is the intrinsic carrier density.

The recombination current is given by

$$I_{rec} = eA \int_{junc} U(x) dx \quad (1.4)$$

For a single level trap centers the recombination generation current in the space charge region can be expressed as (40)

$$I_{rec-gen} = \frac{e n_i W}{(\tau_n \tau_p)^{1/2}} \cdot A \left[e^{eV/2kT} - 1 \right] \quad (1.5)$$

Where A is the area of the device, τ_n and τ_p are the minority carrier life times for electrons and holes respectively and W is the width of the space charge region.

The recombination generation current increases in the forward direction as $\exp (eV/2kT)$ whereas the ideal diffusion (injection) current increases in the forward direction as $\exp (eV/kT)$. In general the actual current can be expressed as

$$I_{\text{Diode}} = I_0 \left[\exp (eV/nkT) - 1 \right] \quad (1.6)$$

Where n is known as the diode quality factor which determines the current voltage characteristics in the diode. In addition to the diffusion current and the recombination generation current in the space charge region, the presence of surface channels in the device leads to leakage current resulting in the values of the diode quality factor n greater than 2⁽⁴¹⁾. The p-n junction diode current-voltage characteristics is shown in Figure (1.4).

1.2.2 p-n JUNCTION AS SOLAR CELL :

The purpose of this article is to give an expression for the current-voltage characteristics of a p-n junction under illumination. We consider the model presented by Cummrow⁽⁶⁾ which is based upon the following assumptions:

1. The thickness of the p-n junction region is small compared to the extent of the p or n regions and the diffusion length of the minority carriers.
2. The electrostatic field is confined to the junction region.

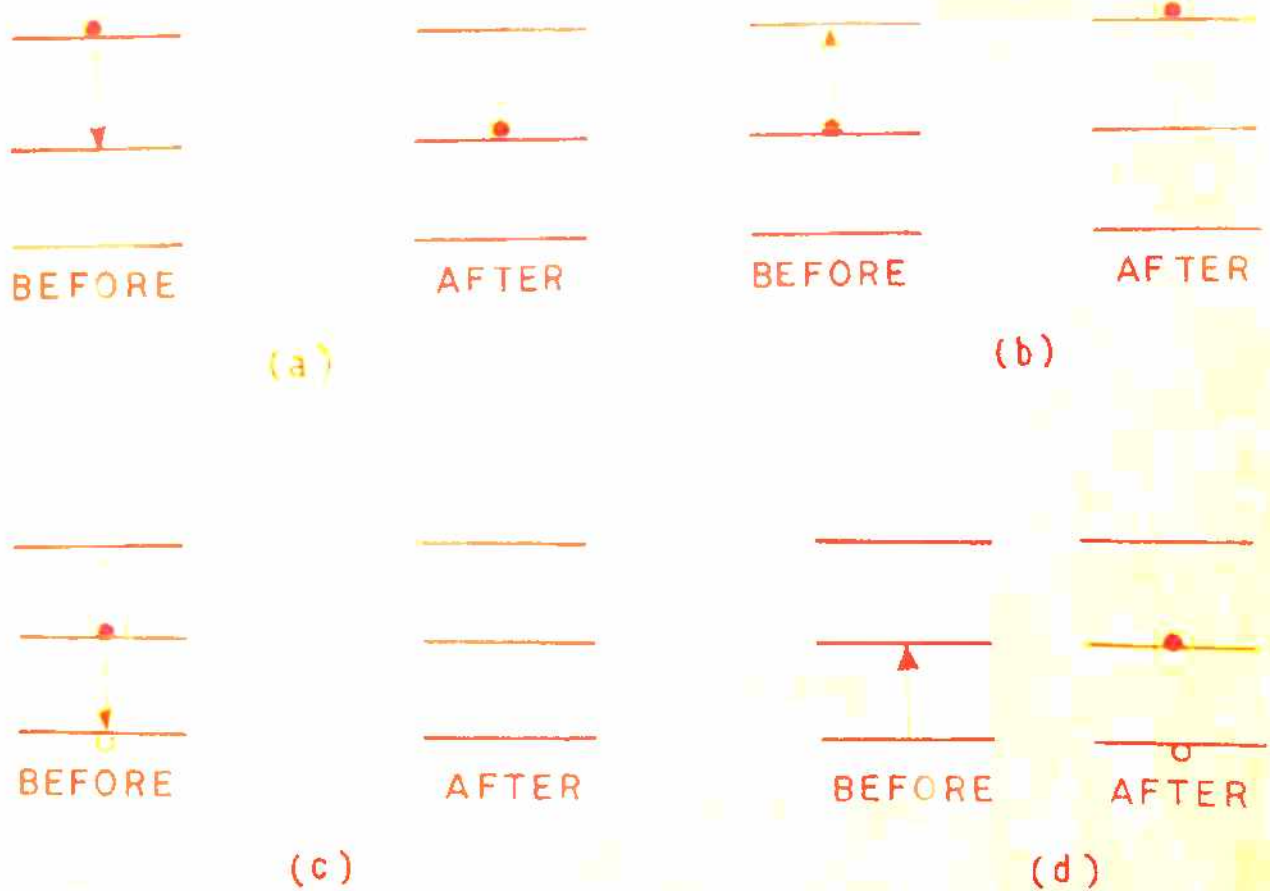


FIG. 1.3 DIAGRAMS SHOWING RECOMBINATION OF CHARGE CARRIERS DUE TO RECOMBINATION CENTERS.
 (a) ELECTRON CAPTURE (b) ELECTRON EMISSION
 (c) HOLE CAPTURE (d) HOLE EMISSION

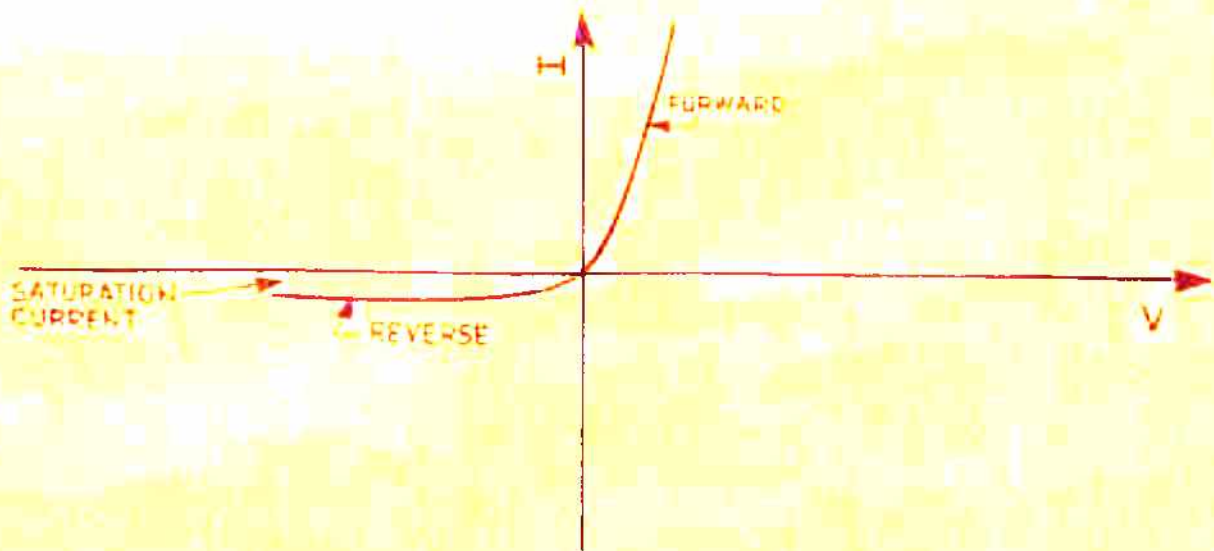


FIG 1.4 CURRENT VOLTAGE CHARACTERISTICS OF A p-n JUNCTION DIODE .

3. The carrier densities are small enough so that Boltzmann statistics can be used.

The junction is represented as a region of width W at $x = 0$ (See Figure 1.5). The carrier concentrations on opposite sides of the junction barrier are related as follows⁽⁴⁰⁾:

$$p_{no} = p_{po} \exp (-eV_{bi}/kT) \quad \text{for } x > 0 \quad (1.7)$$

where p_{no} and p_{po} are the equilibrium hole concentrations in n and p regions respectively, e is the electronic charge and k is the Boltzmann's constant and T is the operating temperature of the cell. On illumination of a solar cell the generation of electron hole pairs takes place and this creates a nonequilibrium situation. The creation of excess carrier concentration due to incident photons and their subsequent separation by the built in electric field results in a net decrease in the charge density in the depletion layer. This in turn lowers the electric field. This is equivalent to a forward bias^[Fig 1.6]. Thus the quasi-equilibrium equations may be written as

$$p_n(0) = p_{po} \exp [-e(V_{bi} - V)/kT] \quad (1.8)$$

where $p_n(0)$ is the value of p_n at $x = \delta_r$ or $x_r = 0$, therefore

$$p_{no}(0) = p_{no} \exp (eV/kT) \quad (1.9)$$

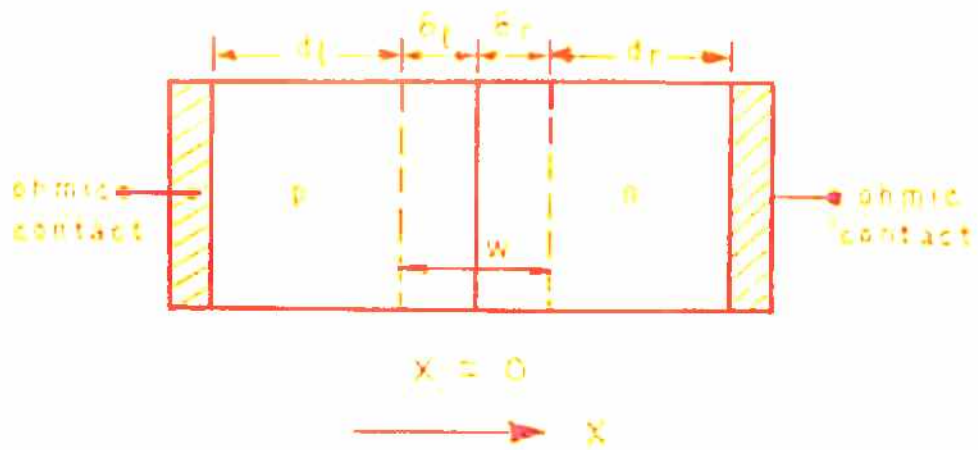


FIG. 1.5 P N JUNCTION AS A REGION OF WIDTH W

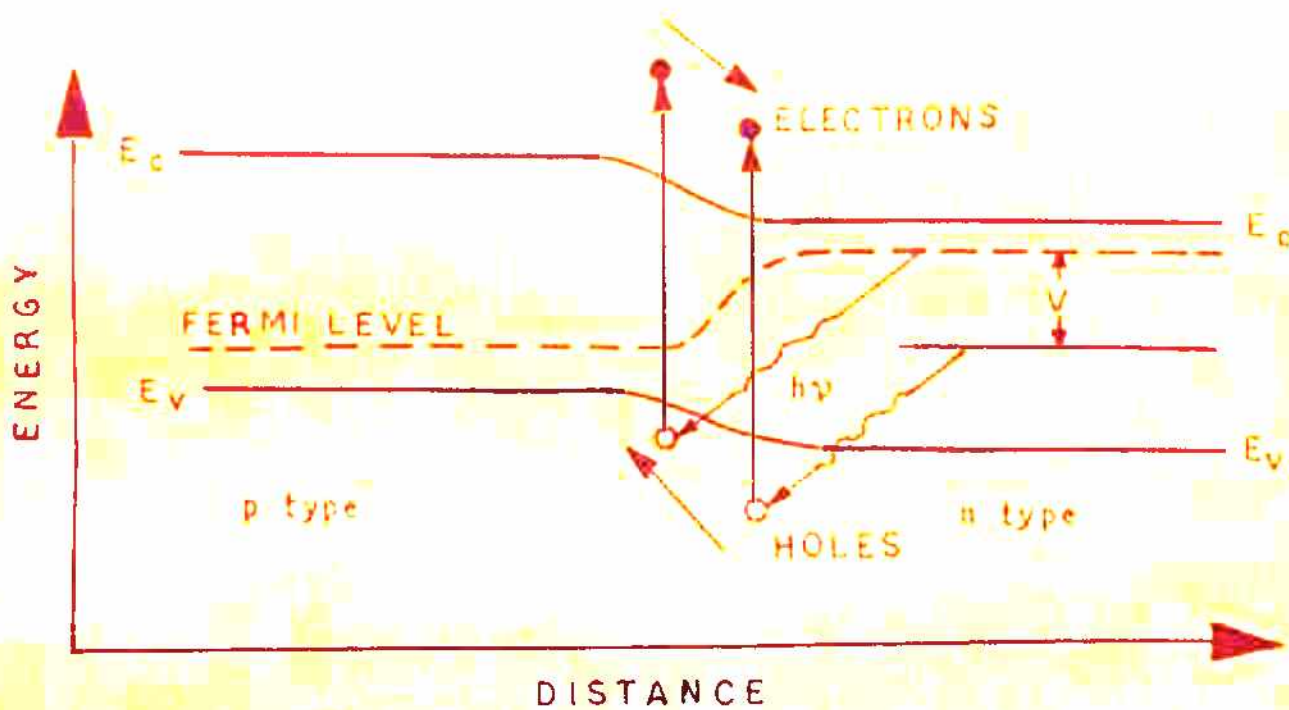


FIG. 1.6 ENERGY BAND DIAGRAM OF A p-n JUNCTION SOLAR CELL UNDER THE ACTION OF LIGHT

and similarly for electrons on p side,

$$n_p(0) = n_{p0} \exp(eV/kT) \text{ at } x = -\delta_e \text{ or } x_e = 0. \quad (1.10)$$

Let \mathcal{G}_p , the rate of thermally generated holes in the n region, be given by $\mathcal{G}_p = p_{no}/\tau_p$. The recombination rate r_p under non equilibrium condition is given by p/τ_p , where τ_p is the hole life time and p is the nonequilibrium hole concentration. On illumination the electron and hole pairs will be generated due to absorption of incident photons with energy greater than or equal to the energy gap of the semiconductor. Let the generation rate of electron hole pairs due to such incident photons be represented by $g(x)$. The net hole generation is then given by

$$\mathcal{G}_p + g(x) - \frac{p}{\tau_p} \quad (1.11)$$

which must equal the net rate at which the holes are leaving the volume under consideration

$$\mathcal{G}_p + g(x) - \frac{p}{\tau_p} = e^{-1} \frac{\partial J_p}{\partial x} \quad (1.12)$$

Where J_p is the diffusion current density* caused by the diffusion of holes and is given by

$$J_p = -e D_p \frac{\partial p}{\partial x} \quad (1.13)$$

* (in article 1.2.1(a) the symbols J_p and J_n have been used for particle fluxes)

where D_p is the diffusion coefficient of holes. Let the electron hole pair generation rate in the junction layer (from $x = -\delta_e$ to $x = +\delta_e$) be uniform and let it be denoted by g_0 . The generation in the n material (to the right of the junction) is

$$g(x_r) = g_0 \exp(-\alpha x_r) \quad (1.14)$$

while the generation rate in the p material (to the left of the junction) is

$$g(x_e) = g_0 \exp(\alpha x_e) \quad (1.15)$$

where $x_e = -(x + \delta_e)$ and is taken positive towards the left. The generation rate on the surface on which the photons are incident is

$$g_s = g_0 \exp(\alpha d_e) \quad (1.16)$$

Combining the equations (1.12) and (1.13) the differential equation for the holes in the n region becomes

$$\frac{d^2 p}{dx^2} - \frac{p}{D_p \tau_p} + \frac{1}{D_p} (g_p + g_0 e^{-\alpha x_r}) \quad (1.17)$$

For a finite p-n junction the solution of the equation (1.17) can be obtained using the following boundary conditions,

$$(i) \quad p = p_{no} \exp(eV/kT) \text{ for } x_r = 0 \quad (1.18a)$$

$$(ii) \quad \partial p / \partial x = 0 \quad \text{for } x_r = d_r \quad (1.18b)$$

The second boundary condition shows that p becomes p_{no} in the neutral region. In the above expressions d_L and d_r represent the width of the regions on the p and n sides respectively. The solution of the differential equation is then given by

$$p = \tau_p \left[\xi_p (e^{eV/kT} - 1) + \frac{g_0}{(a_p^2 - 1)} \right] = \frac{\cosh((d_r - x_r)/L_p)}{\cosh \frac{d_r}{L_p}} \frac{\xi_0 \tau_p}{a_p^2 - 1} + \left[a_p e^{-x_r/L_p} \frac{\sinh x_r/L_p}{\cosh d_r/L_p} + e^{-x_r/L_p} \right] \xi_p \tau_p \quad (1.19)$$

Likewise the flow of electrons in the p side is given by

$$\frac{\partial^2 n}{\partial x^2} - \frac{n}{D_n \tau_n} + \frac{1}{D_n} [g_n + g_0 e^{x_L/L_p}] = 0 \quad (1.20)$$

The solution of this equation (1.20) can also be obtained using the boundary conditions

$$(i) \quad n = n_{po} e^{eV/kT} \quad \text{for } x_L = 0 \quad (1.21a)$$

$$(ii) \quad \frac{\partial n}{\partial x} = 0 \quad \text{for } x_L = d_L \quad (1.21b)$$

This gives

$$n = \tau_n \left[\frac{e^{eV/kT}}{e^{eV/kT} - 1} + \frac{e_0}{a_n^2 - 1} \right] \times \frac{\cosh_n (e_0 - x_e) / L_n}{\cosh (d_e / L_n)}$$

$$= \frac{\tau_n}{(a_n^2 - 1)} \left[\frac{a_n \sinh (x_e / L_n)}{\cosh (d_e / L_n)} e^{x_e / L_n} e^{x_e / L_n} \right] + \epsilon_n \tau_n \quad (1.22)$$

The electron and hole currents are given by

$$I_p(0) = -A e D_p \left. \frac{dp}{dx} \right|_{x=0}$$

$$= A e \epsilon_p L_p (e^{eV/kT} - 1) \tanh \frac{d_p}{L_p} - \frac{A e \epsilon_0 L_p}{(a_p^2 - 1)}$$

$$\left(a_p - a_p e^{-d_p/L_p} \operatorname{sech} \left(\frac{d_p}{L_p} \right) - \tanh \left(\frac{d_p}{L_p} \right) \right)$$

$$I_n(0) = A e D_n \left. \frac{dn}{dx} \right|_{x=0}$$

$$= A e \epsilon_n L_n (e^{eV/kT} - 1) \tanh \left(\frac{d_n}{L_n} \right) - \frac{A e \epsilon_0 L_n}{(a_n^2 - 1)}$$

$$\left(a_n e^{+d_n/L_n} \operatorname{sech} \frac{d_n}{L_n} - a_n - \tanh \frac{d_n}{L_n} \right)$$

Hence, the total current in p-n junction solar cell can be written as

$$I' = I_0 (e^{eV/kT} - 1) - I_{ph} \quad (1.23)$$

where $I_0 = e A [\epsilon_p L_p' + \epsilon_n L_n']$,

$$I_{ph} = e A \epsilon_0 [L_1 + L_2] ,$$

$$L_p' = L_p \tanh \frac{d_r}{L_p} , \quad L_n' = L_n \tanh d_l / L_n ,$$

$$L_1 = \frac{L_p}{a_p^2 - 1} \left[a_p - a_p e^{-d_r/L_\lambda} \operatorname{sech} d_r/L_\lambda - \tanh d_r/L_p \right] ,$$

$$L_2 = \frac{L_n}{(a_n^2 - 1)} \left[a_n e^{d_l/L_\lambda} \operatorname{sech} d_l/L_\lambda - a_n - \tanh d_l/L_n \right] ,$$

$$L_\lambda = 1/\alpha \quad \text{and} \quad a_n = L_n/L_\lambda , \quad a_p = L_p/L_\lambda$$

and α is the absorption coefficient of the semiconductor.

The current voltage characteristics of a solar cell under illumination lies in the fourth quadrant for which the current flowing through the device is $-I'$. The product of current and voltage is negative hence the current flowing through the device is ^apower generating current and ^{is} given by

$$I = I_{ph} - I_0 \left[e^{eV/kT} - 1 \right] , \quad (1.24)$$

where I_{ph} is the photogenerated current and the second term is the diode current, also known as dark current in an ideal p-n junction diode. The current voltage characteristics of a solar cell is shown in Figure 1.7.

The simplest equivalent circuit of a solar cell in the operating mode is shown in figure (1.6). The photogenerated current is represented by a constant current generating source I_{ph} , the dark current of the diode is represented by I_{dark} in opposite direction to the photogenerated current, the shunt resistance is represented by R_{sh} and the series resistance by R_s . The origin and the nature of R_s and R_{sh} will be discussed in the next chapter.

1.3 EFFICIENCY AND LIMITING EFFICIENCY OF A SOLAR CELL :

Before going into the details of the working of a solar cell we introduce and define a number of terms at this stage which will be in common usage throughout hereafter.

1.3.1 (a) ABSORPTION COEFFICIENT:

The ability of a material to absorb light of a given wavelength is measured quantitatively by the absorption coefficient α which is measured in units of reciprocal distance. By definition, the light incident at the surface falls off in intensity by a factor of $1/e$ for each $1/\alpha$ distance in the material. The incident photons, having energy greater than or equal to the energy gap of the semiconductor material, are eligible to create electron hole pairs on absorption. The absorption coefficient rises more steeply with increasing photon

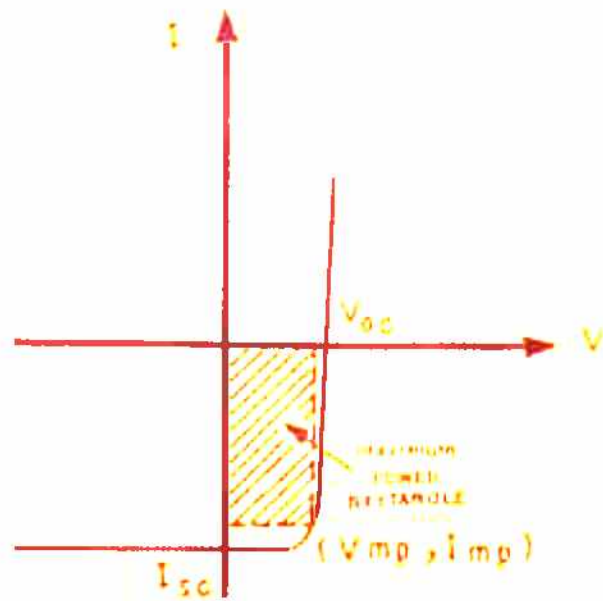


FIG. 1.7 CURRENT-VOLTAGE CHARACTERISTICS OF A SOLAR CELL UNDER ILLUMINATION.

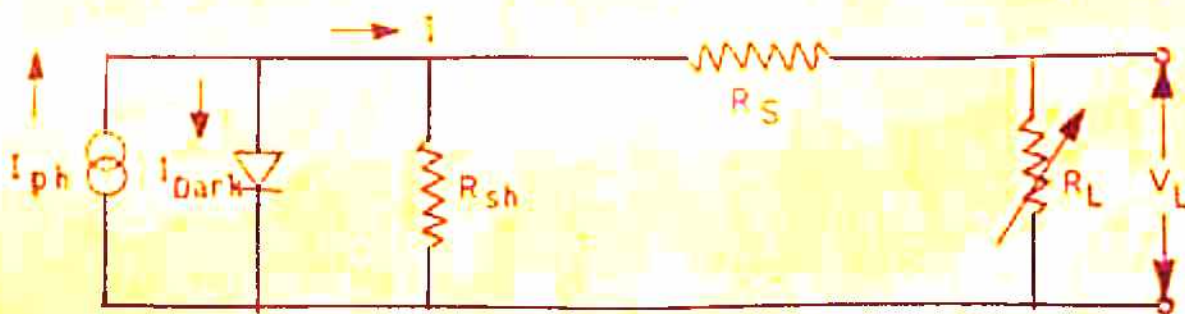


FIG. 1.8 EQUIVALENT CIRCUIT DIAGRAM OF A SOLAR CELL.

energy for direct band gap material than for an indirect gap material, since the later requires an additional scattering event to accompany the photon absorption. The direct and indirect transitions are shown in figure (1.9).

1.3.1(b) SOLAR RADIATION AND PHOTON FLUX :

The spectral distribution of the radiation reaching the earth from the sun depends on various sources of atmospheric absorption namely (a) atmospheric gases (Ozone, nitrogen, oxygen and so on) (b) water vapor and (c) dust. Each of these absorption mechanisms tends to deplete the ultraviolet radiation from the sun in a preferential manner. The effect of these sources of absorption can be described by means of an optical path length m through which the light passes, and by means of the number of centimeters of condensed water droplets w in the atmosphere. The angle which the sun makes with the zenith determines the path length of the light through the atmosphere. The optical path length is defined by the airmass. For outer space it is represented by AM0 (air mass zero) and for terrestrial cases the air mass is represented by AM1, AM2, .. AM _{m} etc. m is a number defined by $m = \frac{1}{\cos \theta}$, where θ is the angle made by the position of the sun from the observer with zenith. This is shown in figure (1.10).

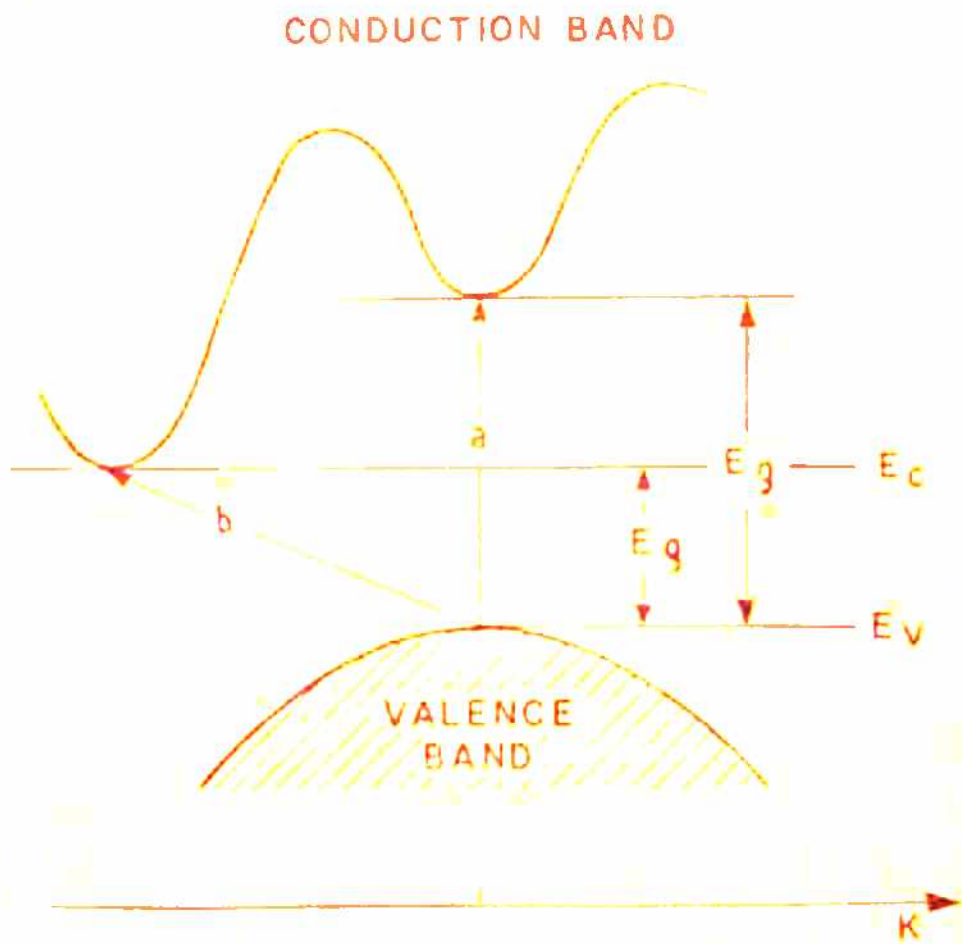


FIG. I.9 OPTICAL TRANSITIONS. (40)
 a - DIRECT TRANSITION
 b - INDIRECT TRANSITION INVOLVING PHONONS.

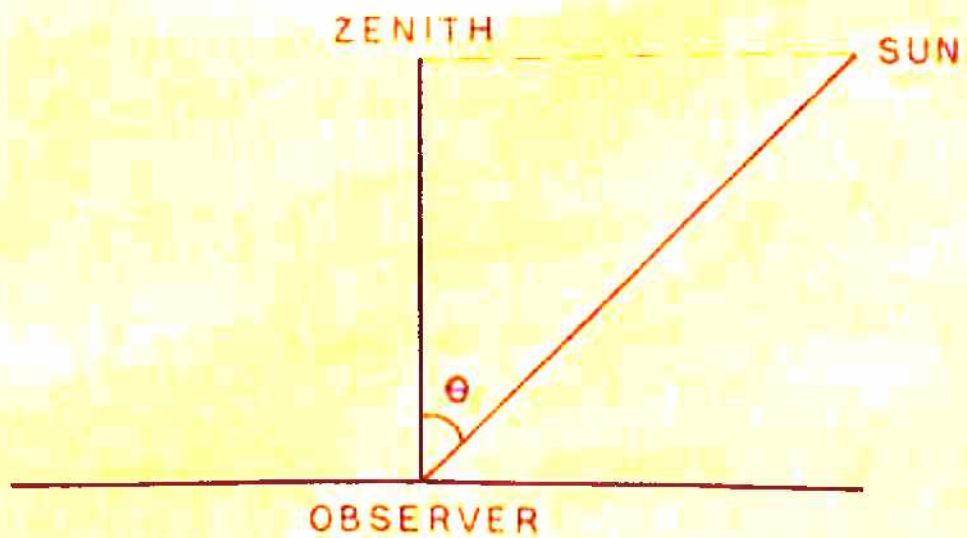


FIG. I.10 AIR MASS = $\frac{1}{\cos \theta}$

In the course of the day θ varies from 90° to a θ_{\min} that occurs at noon. θ_{\min} is also a function of the season of the year between the limits $\theta_{\min} = \text{latitude} \pm 23.5^\circ$. The simplest case is when $\theta_{\min} = 0$ and $m = 1$.

The photon flux is a useful quantity in solar cell calculations. It is defined as the number of photons crossing unit area perpendicular to the light beam per second. If P denotes the intensity of the light in watts per square centimeter, then the number of photons N_{ph} carrying that energy is given by

$$P = N_{ph} \bar{e}$$

where \bar{e} is the average energy of the photons. The parameters of the solar spectrum as a function of absorption conditions are shown in table 1.1⁽¹⁴⁾

1.3.2 EFFICIENCY OF A SOLAR CELL :

The maximum power output of the solar cell is determined from the current voltage characteristics by finding the rectangle with the largest area under the I - V curve in the fourth quadrant. The voltage V_{mp} and the current I_{mp} at the maximum power point give the maximum power $P_{mp} = (I_{mp} V_{mp})$. The ratio of the maximum power output to the product of the open circuit voltage V_{oc}

Parameters of the solar cell as a function of absorption coefficient

m	W	Comments	$P(\text{A/cm}^2)$	$\Delta V(\text{V})$	$\frac{P}{\Delta V}$ (W/cm ²)
0	0	Outside atmosphere	0.135	1.48	0.0915
1	0	Sea level, sun at zenith	0.106	1.32	0.0796
2	0	Sea level, sun at 60° from zenith	0.066	1.33	0.0496
3	0	Sea level, sun at 70.5° from zenith	0.035	1.31	0.0267
1	2	About 50% relative humidity	0.112	1.25	0.0896
3	5	Extreme condition	0.029	1.19	0.0244
1	0	Cloudy dry (7000°K black body)	0.012	1.04	0.0115

and the short circuit current I_{sc} is called the fill factor
 $FF = P_{mp}/(I_{sc} \cdot V_{oc})$. $I_{sc} = I_{ph}$ when $V = 0$ and $V_{oc} = \frac{kT}{e} \ln \frac{I_{ph}}{I_0} + 1$,
 for $I = 0$.

The efficiency is defined as the ratio of the maximum power delivered by the solar cell to the power input.

$$\eta = \frac{P_{mp}}{P_{in}} = FF \cdot \frac{V_{oc} \cdot I_{sc}}{P_{in}} \quad (1.25)$$

V_{oc} represents the maximum voltage that can be obtained from the cell when it is open circuited. Likewise I_{sc} is the maximum attainable current from the cell under short circuit condition.

1.3.3 LIMITATIONS ON PHOTOVOLTAIC ENERGY CONVERTERS :

In this article some of the basic factors are described in brief that prohibit the actual photovoltaic converters from achieving the maximum efficiencies predicted in table 1.2. The major factors are

1. Reflection losses on the surface ,
2. Incomplete absorption ,
3. Utilization of only a part of the photon energy for creation of electron and hole pairs ,

Table-1.2

Performance of solar energy converters

Material	Energy Gap E_g (eV)	Efficiency calculated (%)		Highest measured efficiency η %	Reference
		$m = 0$ $w = 0$	$m = 1$ $w = 2$		
Si	1.12	19.4	20.3	13	18
InP	1.25	21.1	22.1		
Ga As	1.35	21.4	23.7	20	47
Cd Te	1.45	26.0	26.5	7.4	30
CdS	2.20	16.9	-	1.91	51

4. Incomplete collection of electron hole pairs ,
5. voltage factor ,
6. Curve factor related to the operating point at maximum power and
7. Additional degradation of the curve due to internal series resistance .

These factors can be divided into several groups as follows: Factors 1, 2 and 4 can be combined and called the overall collection efficiency. All these factors are related to the absorption characteristics of the material. Factors 1 through 4 determine the short circuit current. The short circuit current I_{sc} is given by⁽¹⁴⁾

$$I_{sc} = \eta_{coll} (1 - r) [1 - \exp(-\alpha l)] e n_{ph} \quad (1.26)$$

Where η_{coll} is the collection efficiency, r is the reflection coefficient, $e^{-\alpha l}$ is the fraction of transmitted intensity at a distance l , l is the thickness of the absorbing material and n_{ph} is the number of photons which are eligible to create electron hole pairs.

Factors 5 and 6 are related to the current voltage characteristics of the device. Factors 1, 4 and 7 are mainly determined by techniques and improvements can be done in these areas. Factors 2, 3, 5 and 6 however, have absolute physical limitations

beyond which improvement is not possible. These factors are discussed here in brief.

REFLECTION LOSSES:

The magnitude of the reflection losses can be estimated from the relation between the index of refraction γ and the reflection coefficient r , namely⁽¹⁴⁾

$$r = \left(\frac{\gamma - 1}{\gamma + 1} \right)^2$$

Reflection losses have been considerably reduced by means of transparent coatings having appropriate thickness and index of refraction. Losses as low as 6% for silicon have been reported in the literature⁽⁴²⁻⁴⁵⁾. Thus reflection can be minimized considerably by the present day available techniques.

INCOMPLETE ABSORPTION:

Figure (1.11) given by P. Moon⁽⁴⁵⁾ shows the energy spectrum of sunlight on a bright clear day on the earth's surface at the sea level and the maximum amount of energy utilized in the generation of electron hole pairs in semiconductors with different band gaps. It is also observed that the amount of solar spectrum utilized increases with decreasing energy gap. It appears from Figure (1.11) that only a part of energy spectrum of the sun can be utilized to generate electron hole pairs.

The problem of incomplete absorption can be minimized by having the materials that have absorption coefficients increasing very rapidly with photon energy. Figure (1.12) shows absorption characteristics of some semiconductors of interest for solar cell use. A rapid rising absorption coefficient, such as that of Ga-As means that a larger fraction of the carriers generated by the absorption of photons will be within a short distance of the surface of incidence. This means that less material will be needed in any solar cell since it will require a thinner film to ensure effective absorption of the incident radiation.

UTILIZATION OF ONLY PART OF THE PHOTON ENERGY FOR CREATION OF ELECTRON AND HOLE PAIRS :

Figure (1.11) shows that a large number of photons that will be absorbed will have more energy than is required to create an electron hole pair. Any photon that has energy greater than or equal to the energy gap ($h\nu \geq E_g$) of the material is eligible to create electron hole pairs. The photons having energy in excess ($h\nu = E_g + \Delta E$) of the energy gap will contribute to the lattice vibrations of the material and will eventually be dissipated as heat. Thus those photons whose energy is less than the energy gap of the material do not contribute at all to electron hole pair generation while those photons whose energy exceeds the energy gap of the material

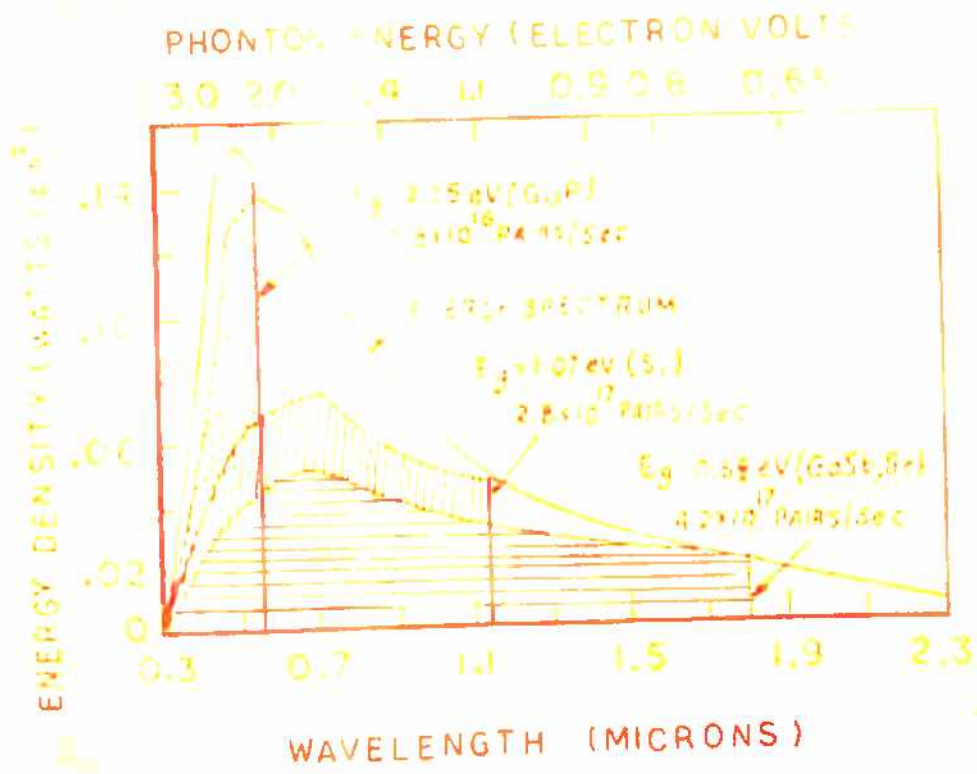


FIG. 1.11 THE ENERGY SPECTRUM OF THE SUN ON A BRIGHT CLEAR DAY AT SEA LEVEL AND THE PARTS OF THIS SPECTRUM UTILIZABLE IN THE GENERATION OF ELECTRON HOLE PAIRS IN SEMICONDUCTORS (46)

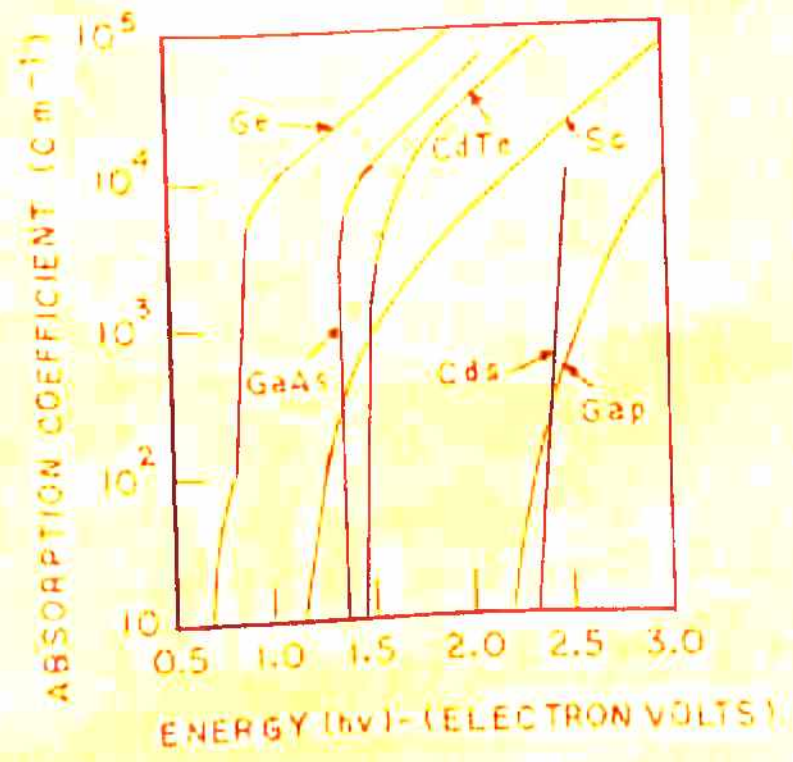


FIG. 1.12 THE OPTICAL ABSORPTION COEFFICIENT AS A FUNCTION OF PHOTON ENERGY (hν) IN ELECTRON VOLTS. (14)

in creating an electron hole pair have their excess energy dissipated as heat. The number of absorbed photons as a function of cut off energy is shown in figure (1.13).

INCOMPLETE COLLECTION OF ELECTRON HOLE PAIRS:

Most of ^{the} electron hole pairs created by photon absorption are not generated within the space charge region of the p-n junction. Therefore, on the average only those electron hole pairs will be collected which are within a diffusion length from the junction. The majority of pairs generated at greater distances from the junction will recombine, causing the collection efficiency to fall below 100 percent. This collection efficiency is defined as the ratio of the electron hole pairs separated by the junction to the total number of electron hole pairs generated and is given by (14)

$$\eta_{\text{coll}} = \frac{I_{\text{sc}}}{(1-r) \cdot (1 - e^{-\alpha l}) e^{n_{\text{ph}}}}$$

The collection efficiency depends upon a number of physical parameters. These are the location where charge carriers are generated, the diffusion length, the minority carrier life time, absorption coefficient and the surface recombination velocity. Improvement in η_{coll} for any given material can be obtained by increasing the minority carrier life time in the p and n material

Collection efficiency as a function of wavelength is shown in figure (1.14) and as a function of surface recombination velocity s , diffusion length L and absorption coefficient α is shown in table 1.3⁽¹⁴⁾.

VOLTAGE FACTOR :

The largest recoverable voltage in a solar cell is the open circuit voltage. The amount of energy utilized in the generation of electron hole pairs is equal to the energy gap of the material. The maximum value that the photovoltage can theoretically have is the built-in potential V_{bi} which is related to the band gap by (40)

$$V_{bi} = \frac{E_g}{e} - (E_c - E_{fp})_p - (E_{fn} - E_v)_n = \frac{kT}{e} \ln \left(\frac{N_A N_D}{n_i^2} \right) \quad (1.27)$$

Where N_D and N_A are the donor and acceptor densities respectively. This shows that the built-in potential is determined by difference in Fermi levels in the p and n type materials on both sides of the junction. The Fermi levels are functions of impurity concentrations and temperature and are normally located within the forbidden gap for nondegenerate semiconductors. The net effect is that the built in potential is less than the energy gap. The maximum open circuit voltage from the solar cell is equal to

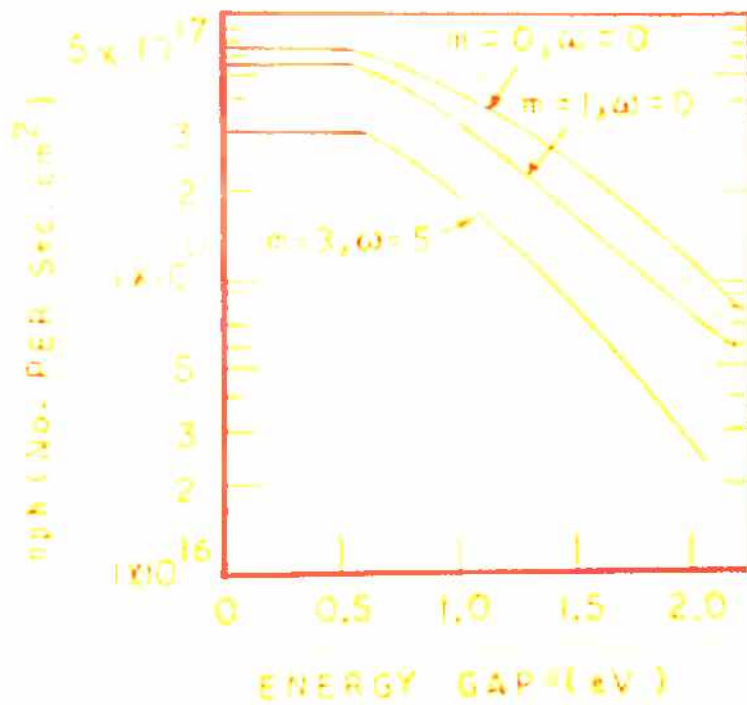


FIG. 1.13 THE TOTAL NUMBER OF ABSORBED PHOTONS AS A FUNCTION OF CUT OFF ENERGY. (14)

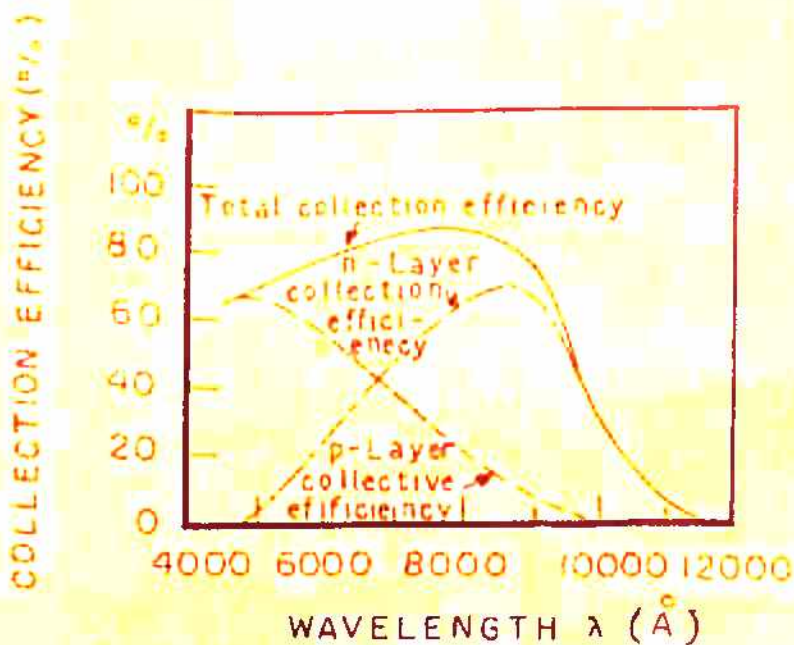


FIG. 1.14 COLLECTION EFFICIENCY V/S WAVELENGTH. COLLECTION EFFICIENCY FROM THE p-LAYER ALONE (DASHED), FROM THE n-LAYER ALONE (DASHED DOTTED) AND FROM THE SUM OF BOTH (SOLID) ARE SHOWN. (19)

TABLE-1.2

The collection efficiency as a function of surface recombination velocity S , diffusion length L , and absorption coefficient α

Surface recombination velocity (cm/sec.)	L (cm)	α (cm ⁻¹)	η_{coll}
0	10 ⁻²	10 ³	0.61
0	10 ⁻³	10 ³	0.47
0	10 ⁻³	10 ⁶	0.65
100	10 ⁻³	10 ³	0.61
∞	10 ⁻²	10 ³	0.25
∞	10 ⁻³	10 ³	0.23
∞	10 ⁻³	10 ⁶	0.001
∞	10 ⁻⁶	10 ³	6x10 ⁻⁵

the built in potential and thus is less than E_g/e . The voltage factor is defined as the ratio of the open circuit voltage V_{oc} and E_g/e where E_g is the energy band gap and is given by

$$V.F = V_{oc}(E_g/e) = \frac{kT}{E_g} \ln \left(\frac{I_{ph}}{I_0} + 1 \right) \quad (1.28)$$

The increase in voltage factor with energy gap is shown in figure (1.15). From the above expression (1.28) it appears that a voltage equal to the built in potential will only be obtained at extremely high injection levels which can never be reached by photon absorption from direct sun.

CURVE OR FILL FACTOR :

The maximum power that can be obtained from a solar cell at that point for which the largest rectangle can be inscribed into the current voltage characteristics is shown in figure (1.7). This point is the maximum power point (V_{mp}, I_{mp}) . The fill factor $(FF = (V_{mp} \cdot I_{mp}) / (V_{oc} \cdot I_{sc}))$ and the voltage factor depends upon the saturation current I_0 and the photo-generated current I_{ph} . The saturation current I_0 depends upon the material properties and operating temperature of the cell. The product of curve and voltage factors is called the characteristic factor. All these factors increase on increasing the band gap of the material and are shown in figure (1.15).

INTERNAL SERIES RESISTANCE LOSSES:

It is found that in actual silicon solar cells a large internal series resistance causes a deviation of the current volt characteristics from its ideal curve (Figure 1.16). This deviation from its ideal curve results in a reduction in the net power output. It is found that if the doped layer of the material on top of the junction was reduced in thickness, the collection efficiency improved because of the large photon absorption. This solution of improving the collection efficiency conflicts with resistance requirements, because as the layer is reduced it increases the resistance due to the doped layer. The ohmic contacts applied to the cell also cause an additional increase to the internal series resistance. Improvements in the techniques of applying contacts have helped in reducing this resistance to negligible values. This problem of internal series resistance will be discussed in detail in the next chapter.

The various energy loss mechanisms in solar cell are shown in table 1.4.

1.3.4 RADIATION EFFECT :

The most important application of solar cell is in satellite and space vehicles. The high energy particles radiation in outer space produces defects in semiconductors which

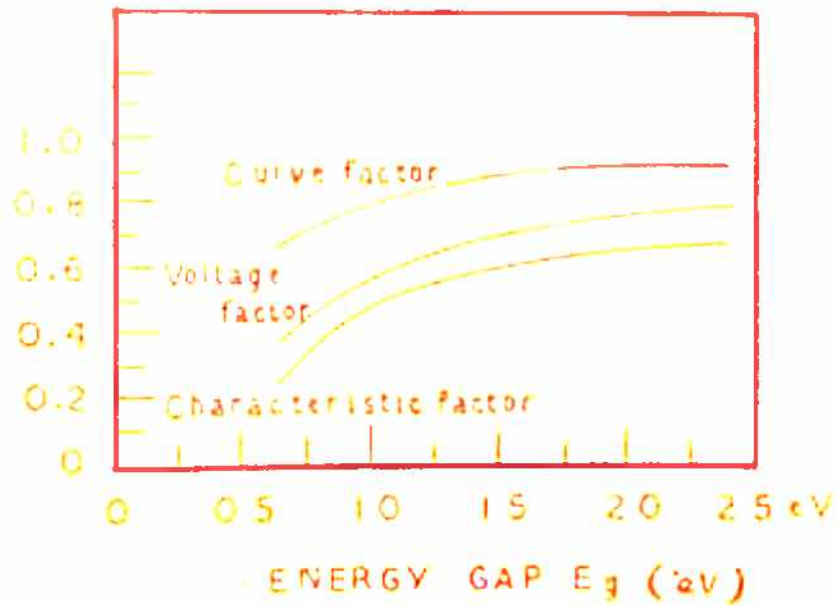


FIG. 1.15 VOLTAGE FACTOR, CURVE FACTOR AND CHARACTERISTICS FACTOR AS A FUNCTION OF ENERGY GAP. (19)

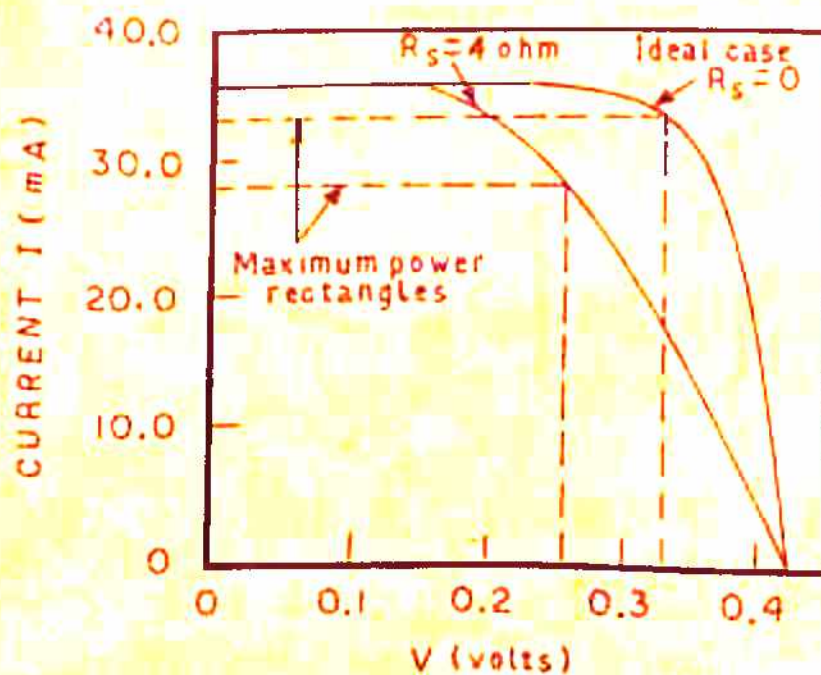


FIG. 1.16 CURRENT VOLTAGE CHARACTERISTICS OF A SOLAR CELL FOR DIFFERENT VALUES OF SERIES RESISTANCE R_s . (47)

The various energy loss mechanism in solar cell.

Region	Mechanism	Form of energy lost
<u>Photon Losses</u>		
Protective or anti reflection layer	Reflection, Absorption	Reflection (at back surface) Heat Generation
Grid	Shading	Reflection (at back surface) Heat Generation
Active layer	a) Reflection at front and back surface b) Absorption at back contact -Non-generative photon losses to free carriers or transitions amongst defect levels c) Incomplete utilization of photon energy - $\Delta E = h\nu - E_g$ is wasted	Heat Generation Heat Generation
<u>Carrier Losses</u>		
Front and rear surfaces	Surface recombination	Heat Generation
Active layer's junction	a) recombination of light generated carriers b) Recombination of forward current carriers	Heat Generation Heat Generation
<u>Power Losses</u>		
Active layer	Resistance ohmic losses	Heat Generation
Contact	Resistive ohmic losses	Heat Generation

causes a reduction in solar cell power output. It is most important to assess the expected useful life of the solar cell power plant. Its life time is the length of the time the power plant is capable of delivering the electrical power necessary for successful operation of the satellite. The life time of the excess minority carriers at any point in the bombardment is given by (1.28)

$$\frac{1}{\tau} = \frac{1}{\tau_0} + k' \phi_{\text{Bomb}} \quad (1.29)$$

Where τ_0 is the initial life time, k' is a constant and ϕ_{Bomb} is the bombardment flux. When these particles impinge on a solar cell, they knock atoms from their normal position in a crystal and a defect is produced. Such imperfections have marked effect on excess minority carrier life time as given above (Equation 1.29) and that minority carrier life time in turn influences almost all the important transport parameters. In the case of silicon, it turns out ^{that} τ_p changes much more slowly with radiation than τ_n . For that reason silicon solar cells are now made with a thin n layer on top of a p layer. Two things can be done to alleviate this situation. One is to cover the solar cell with a glass cover, such that most of the damage occurs in the glass rather than in the cell. The other, more desirable one, is to add an impurity to the base material which has a great mobility, and which will quickly migrate to the defects in the crystal and neutralize the broken bonds.

1.4 OTHER SOLAR CELL DEVICES:

At present most of the solar cells are made with p-n junctions using silicon as the host lattice. There are also several other types of solar cells that could exhibit unique advantages of one kind or other, such as schottky barriers, heterojunctions, vertical multijunctions, grating cells and back surface field solar cells. These solar cells are discussed only in brief in the present article.

1.4.1 SCHOTTKY BARRIER SOLAR CELLS:

A schottky diode solar cell is a metal semiconductor contact. When a metal is brought in contact with a semiconductor, a readjustment of charge takes place and the thermal equilibrium gets established. This results in setting up of a built-in potential. In these cells the light is incident on a very thin optically transparent metal film and transmitted through it to the adjacent semiconductor. This results in the generation of electron hole pairs and gives rise to photogenerated current. These cells are very simple and economical to fabricate. Their main advantage is their response to short wavelength light and high short circuit current can be obtained. The dark currents are higher in schottky barrier solar cells than in p-n junctions and this

leads to lower open circuit voltage. However, the open circuit voltage and conversion efficiency can be improved by introducing a thin interfacial oxide layer between the metal and semiconductor.

1.4.2 HETEROJUNCTION SOLAR CELLS:

Heterojunction solar cells can be obtained by forming the junction with two different semiconductors with unequal band gaps. Heterojunction solar cells have many similarities and a few differences to schottky barriers cells. The most important similarity is that short wavelength photons can be absorbed within or very near the depletion region of the device under most circumstances, leading to good high photon energy response. The most important difference is that the open circuit voltage can be quite high as in a p-n junction, without the need of carefully controlled interfacial layers.

1.4.3 VERTICAL MULTIJUNCTIONS SOLAR CELLS :

The vertical multijunction solar cell is an interesting device concept where light is incident in a direction parallel to the junction rather than perpendicular to it as in a conventional solar cell. This has some important consequences, chief of which is that the spectral response (in

the ideal case) becomes very high at all wavelengths, leading to a high potential efficiency. The surface recombination velocity at the front of the device is more important than in conventional cells, and should be 10^3 cm/sec or less for good photocurrent collection.

1.4.4 GRATING SOLAR CELLS :

If a semiconductor wafer is contacted by schottky barriers, heterojunctions or p-n junctions in the form of strips, the resulting device is known as a grating solar cell. Carriers generated by light at some depth beneath the surface must diffuse both vertically and horizontally to the junction region to be collected. If the spacing between the grids is less than about one minority carrier diffusion length, the carriers will have a high probability of being collected, and in particular, if the surface recombination velocity on the surface of the substrate between the grids is low, the spectral response to short wavelengths will be considerably better than in conventional diffused structures with their short life time, high recombination velocity "dead" regions. In addition, the dark current can be lower in the grating cell than in a conventional cell because of the smaller junction area, so that both the voltage and current

output from the grating cell can theoretically be higher than ^{that} from a conventional cell of the same base doping level, provided the grating cell is properly designed to prevent series resistance problem.

1.4.5 BACK SURFACE FIELD SOLAR CELL:

A significant improvement in the output voltage of silicon solar cell can be obtained with the advent of the back surface field solar cell. In this device, the front (junction) part of the cell is made in the normal way but the back of the cell, instead of containing just a metallic contact to the moderately high resistivity base, has a very heavily doped region adjacent to contact. The response at long wavelengths depends mostly on the base minority carrier life time and diffusion length. If the diffusion length is low, the response can be improved by the presence of an electric field in the base adjacent to the depletion region. A back surface field can improve the response by minimizing the number of photocarriers that would ordinarily recombine at back contact.

1.5 AIM OF THE PRESENT WORK IN CONNECTION WITH p-n JUNCTION SOLAR CELLS:

The present work in connection with p-n junction solar cells consists of three parts, namely (i) the series resis-

tance of the solar cell (ii) the effect of temperature on solar cell parameters and (iii) the effect of concentration of incident solar radiation on the solar cell parameters. In the first part the origin of the internal series resistance is discussed. The internal series resistance of the solar cell affects the I-V characteristics of the solar cell as well as the area of maximum power rectangle. This resistance depends on various factors such as the resistance of the doped layer, resistance of the base region, resistance of the ohmic contacts between metal and substrates and the resistance of the metallic contacts. A lowering of this resistance increases the efficiency of the solar cell. In the present work a simple method to evaluate the resistance of the doped layer for various types of grid structures has been employed and the results obtained are compared with those of Bordina et al⁽⁵²⁾. Total internal series resistance is also calculated taking into account the other remaining factors enumerated before. The internal series resistance is experimentally determined and results obtained are compared with theoretical calculations. These studies form the subject matter of chapter II.

The third chapter describes the second and third part, that is, the effect of temperature and concentrated sunlight on various parameters which determine the fill factor and maximum power point of a solar cell. Since the cost of

silicon solar cells and other semiconducting material is high, and is likely to remain that way, the use of almost any method to get more power output from a given set of solar cells is justified. One technique that has received considerable attention to get more power output from a solar cell is the use of concentrators. The concentrated sunlight also increases the operating temperature of the solar cell. The effect of operating temperature and concentrated sunlight on various parameters has been studied experimentally and results presented in third chapter.

REFERENCES:

1. H.E. Cassel, J. of Chemical Physics, Vol. 9 pp 377 (1941).
2. E. Adler, J. of Chemical Physics Vol. 9 pp 486 (1941).
3. K. Lehovec, Physical Review Vol. 74, pp 463 (1948).
4. S. Benzer, Physical Review Vol. 73, pp. 1256 (1948).
5. H.Y.Fan, Physical Review Vol. 75, pp 1631 (1949).
6. R.L. Cumberow, Physical Review Vol. 95,pp 16 (1954).
7. D.M. Chapin et al, J. Appl. Phys. Vol. 25, pp 676 (1954).
8. G.L. Pearson et al, Bell Laboratories Record Vol. 32, pp 232 (1954).
9. C.S. Fuller, The indicator Vol. 35, pp 54 (1954).
10. R.L. Cumberow, Physical Review Vol. 95, pp 561 (1954).
11. D. Rittener, Physical Review Vol. 96, pp 1708 (1954).
12. M.B. Prince, J.Appl. Phys. Vol. 26, pp 534 (1955).
13. D.M. Chapin et al, Bell Laboratories Record Vol. 33, pp 241 (1955).
14. J.J. Loferski, J. Appl. Phys. Vol. 27, pp 777 (1956).
15. G.L. Pearson, American J. of Physics Vol. 25,pp 591(1957).
16. M.B. Prince and M. Wolf, J. Brit. IRE Vol. 18,pp 583(1958).
17. J. Kalman , Electronics, Vol. 32, pp 59 (1959).
18. P. Rappaport, R.C. Review, Vol. 20, pp 373 ,(1959).
19. M. Wolf, Proc. IRE Vol. 48, pp 1248 (1960).
20. W. Shockley and H.J. Quessier, J. Appl. Phys. Vol. 33, pp 510 (1961).

21. H.J. Quessier, Solid State Electronics Vol. 5, pp 1 (1962)
22. J. Korn Mandel, J. of Electrochemical Society, Vol. 109, pp 313 (1962).
23. J.J. Loferski, Proc. of IEEE Vol. 51, pp 667 (1963).
24. R.B. Gangadhar et al, Indian J. of Pure and Applied Physics Vol. 5, pp 593 (1967).
25. H.J. Hovel, Semiconductors and Semimetals (Solar Cells), Academic Press, New York San Francisco London (1975).
26. A Rohwarf and K.W.Boer, Progress in Solid State Chemistry, Vol. 10, pp 71 (1975).
27. P.T. Landsberg, Solid State Electronics Vol. 18, pp 1043 (1975).
28. E. Charles Buckus, Solar Cells, The Institute of IEEE, Inc. New York (1976).
29. F.A Lindholm and C.T. Sah, IEEE Trans. on Electron Devices Vol. ED-24, pp 299 (1977).
30. J.R. Houser and P.M. Dunbar, IEEE Trans. on Electron Devices Vol. ED-24, pp 305 (1977).
31. G.C. Jain, Silicon Solar Photovoltaic Energy Conversion (A Review), NPL New Delhi, India Jan. (1978).
32. R.P. Housen et al, J. of the British IRE, Vol. 26, pp 519 (1961).
33. N.W. Snyder, IEEE Trans. on Military Electronics Vol. MIL 6, pp 84 (1964).
34. G. Barna and R. Newell, Intersociety Energy Conversion Engineering Conference, Miami FL Aug. (1967).

35. W.G. Cussen, *Electronics and Power* Vol. 18, pp 93(1972).
36. E.L. Ralf, *Solar Energy* Vol. 10, pp 67 (1966).
37. P.A. Bermaⁿ, *Solar Energy* Vol. 11, pp 180 (1967).
38. J.J. Loferski, *Mechanical Engineering* Vol. 95,pp 28(1973).
39. K.W. Boer, *J. of Environmental Science* Vol. 17,pp 8 (1974).
40. S.M. Sze, *Physics of Semiconductor Devices*, John Wiley & Sons, Inc. New York, Chapters 3 & 12 (1969).
41. V.M. Evdokimov, *Applied Solar Energy* Vol. 8,pp 63 (1972).
42. E.L. Ralf and M. Wolf, *IEEE Trans. on Electron Devices* Vol. ED-12, pp 493 (1965).
43. D.L. Reynard and A. Andrew, *Applied Optics*, Vol. 5, pp 23 (1966).
44. E.Y. Wang, 10th IEEE Photovoltaic Specialists Conference, Palo Alto, CA pp 168 (1973).
45. A.G. Revcesz, 10th IEEE Photovoltaic Specialists Conference, Palo Alto, CA pp 180 (1973).
46. P. Moon, *J. Franklin Inst.* Vol. 230, pp 583 (1940).
47. L.V. Azaroff and J.J. Brophy, *Electronic Processes in Materials*, MC Graw-Hill Book Co., Inc. New York,pp 282(1963).
48. S.V. Shiang, B.G. Carbajal and G.W. Wakefield, *Proc. of the International Conference on Photovoltaic Solar Energy*, Luxembourg, pp 27 (1977).
49. J.G.G. Fan, C.O. Bozler and R.L. Chapman, *Appl. Phys. Lett.* Vol. 32, No. 6, pp 390 (1978).

50. G.W. Sutton, Direct Energy Conversion, McGraw-Hill Book Co., Inc., New York pp 33 (1966).
51. Walter E. Devaney et al, IEEE Trans. on Electron Devices Vol. ED-26, pp 268 (1979).
52. N.M. Bordina et al, Radio Engineering and Electronics Physics Vol. 10, pt I pp 617 (1965).

CHAPTER-II

SERIES RESISTANCE OF p-n JUNCTION SOLAR CELLS

2.1	Introduction.	46
2.2	Diffused layer contribution.	50
2.3	Contribution due to other factors.	62
2.4	shunt resistance.	71
2.5	Experimental determination of series resistance.	72
2.6	Fabrication of the solar cells.	77
2.7	Experimental results and discussions.	77

CHAPTER-II

SERIES RESISTANCE OF p-n JUNCTION SOLAR CELLS

2.1 INTRODUCTION:

There are a number of factors which limit the efficiency of the solar cells. Some of these factors, such as incomplete absorption of photons, utilization of only a part of the photon energy for creation of electron-hole pairs, voltage factor and curve factor, are basic limiting factors for a given semiconductor and these have absolute physical limitations beyond which improvement is not possible. There are other factors, such as reflection losses at the surface, incomplete collection of electron hole pairs and additional degradation of the V-I characteristics due to internal series resistance R_s , which are dependent on the technique of fabricating solar cells. The internal series resistance of the solar cell belongs to the second category and its undesirable effects can be minimized using improved fabrication techniques. In the actual p-n junction silicon solar cells, if the internal series resistance is sufficiently high, there is a large deviation from the ideal current voltage characteristics. It was first pointed out by Prince⁽¹⁾ that the fill factor and the efficiency of p-n junction solar cells, are greatly influenced by the internal series resistance of the solar cell. The shunt resistance also affects, although to a lesser extent,

these factors. A larger series resistance and smaller shunt resistance reduce the maximum power rectangle of the current voltage characteristics and lower the fill factor there by reducing the efficiency of the solar cell (Fig. 2.1). The internal series resistance of the solar cell depends on a number of factors which are discussed in the following paragraphs.

In the first chapter it was pointed out that if the thickness of the diffused layer of the material on the top of the junction is reduced, the collection efficiency of the solar cell is improved. In the solar cell quite a large number of electron hole pairs are generated outside the space charge region of the p-n junction. Only those electron hole pairs are collected which lie within a diffusion length from the junction. The electron hole pairs generated at greater distance from the junction will therefore recombine before being separated by the junction thereby causing the collection efficiency to fall below 100%. If the thickness of the diffused layer at the top of the junction is reduced, majority of carriers will be collected by the junction resulting in an improvement in the collection efficiency. This method, however, results in an increase in the resistance of the cell. The light generated carriers, after crossing the junction, flow along the surface towards the conducting grids. For such

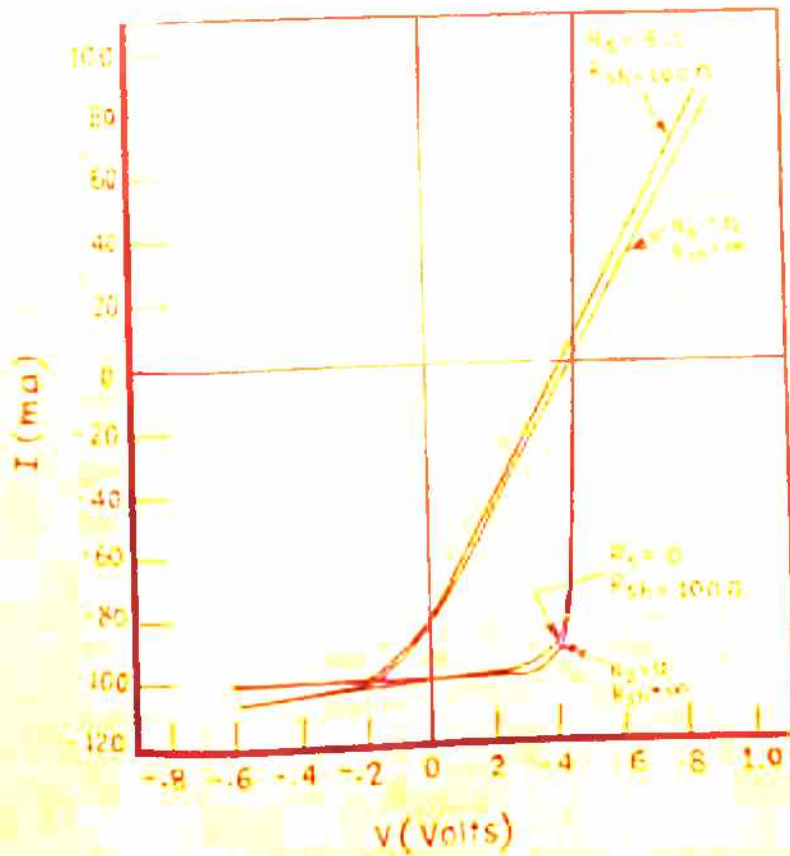


FIG. 2.1 THEORETICAL I-V CHARACTERISTIC OF A SOLAR CELL FOR DIFFERENT VALUES OF SERIES AND SHUNT RESISTANCE. (1)

a flow of the charge carriers along the surface, a smaller thickness of the diffused layer implies a smaller area of cross section. The resistance offered by the diffused region therefore increases as the thickness is reduced, which in turn adversely affects the efficiency. This is in contrast with the improvement in collection efficiency resulting on account of smaller thickness. Therefore in order to achieve the highest possible over all conversion efficiency in a solar cell, a compromise is obtained between the doped layer thickness for achieving good collection efficiency and that for a lower value of the doped layer series resistance.

Techniques allow applications of grids, called fingers to be placed at suitable distances from each other. Wolf⁽²⁾ was the first to calculate the optimum spacing S between the grids and the width T of the grid lines for minimizing the resistance of the doped region. The use of the conducting grids on the active surface of the present day solar cell reduces the average path length of a carrier in the diffused region which greatly minimizes the resistance of the diffused region. The use of many grid lines, however, reduces the optically generated carriers due to decrease in the area exposed to incident light.

The internal series resistance R_s itself is actually made up of several components. The excess carriers in the base

region have to move through the base region and the back electrode before finding themselves in the external circuit. On the way the carriers have to face the resistance due to the semiconductor base R_b , the contact resistance between the base and the back electrode R_{cbe} and the resistance of the back electrode R_{be} . Similarly the excess carriers on the active surface of the p-n junction solar cell will move through the resistance offered by the doped layer R_d , the contact resistance between the doped layer and the front electrode R_{cfe} and the resistance of the grids R_g . The various regions contributing to ^{the} total internal series resistance R_s of a solar cell are shown in Figure 2.2.

The total internal series resistance of the solar cell is given by the sum,

$$R_s = R_b + R_{cbe} + R_{be} + R_{cfe} + R_g + R_d \quad (2.1)$$

of the various components stated above. Whereas the resistance due to the doped region and grids is a distributed element due to each element of the doped region being a current generator, the other remaining components are lumped elements. Thus the series resistance of the solar cell can be modelled by two distinct types of series resistance components, namely a distributed resistance and a lumped resistance.

This chapter deals with the evaluation of the component of the series resistance due to doped layer of the solar

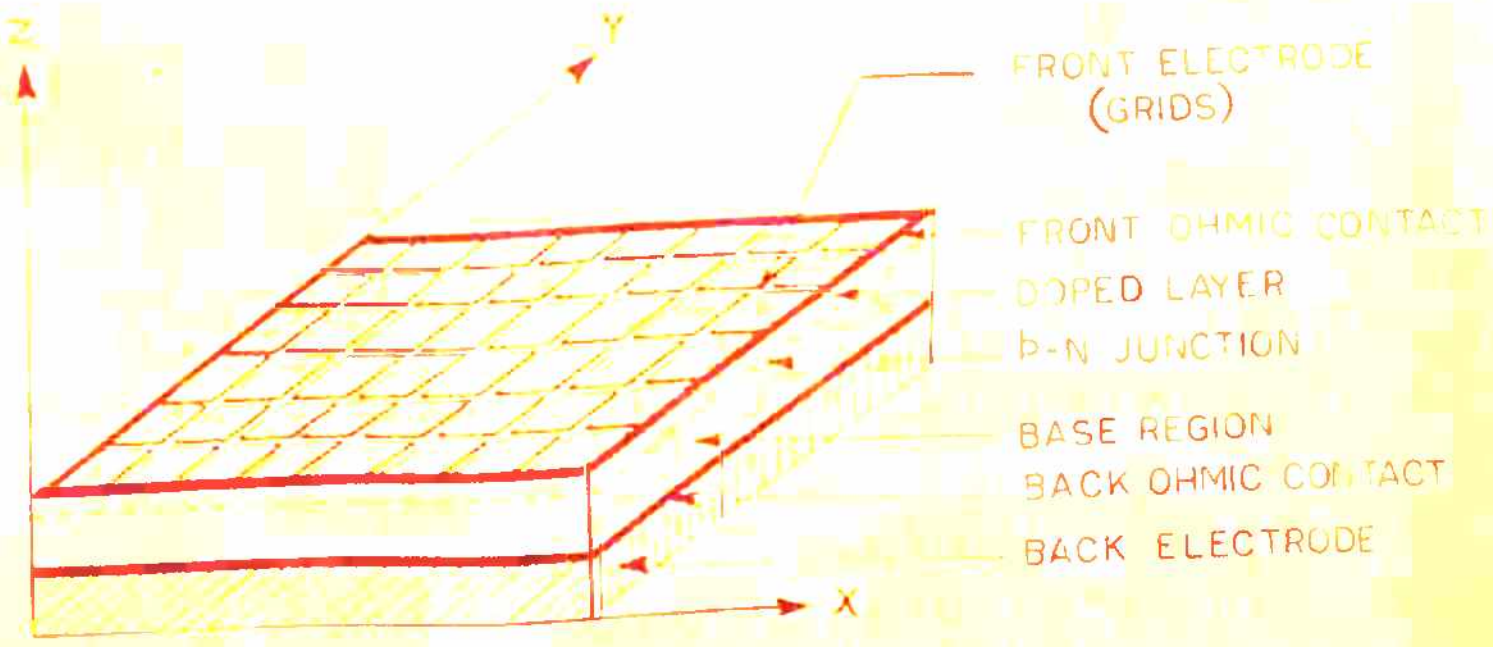
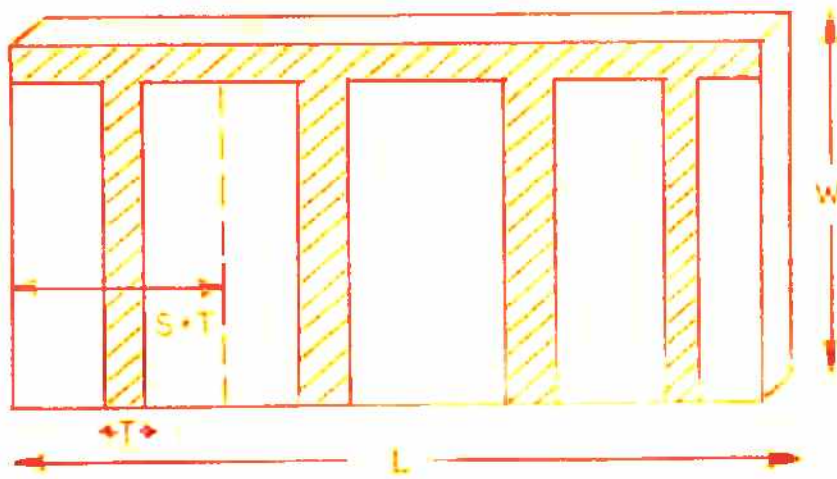


FIG. 2.2 GEOMETRY AND DIFFERENT COMPONENTS OF THE INTERNAL SERIES RESISTANCE OF A P-N JUNCTION SOLAR CELL.

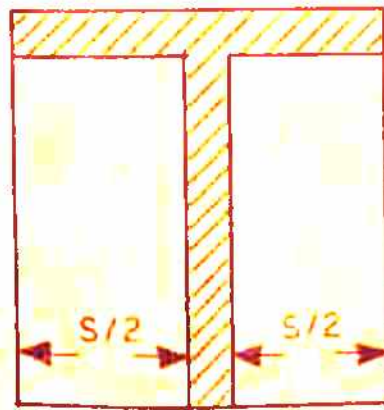
cell for various types of grid structures. The results obtained are compared with the results given by Bordina et al⁽³⁾. The internal series resistance is also calculated taking into account the other remaining factors enumerated before. The total series resistance is experimentally determined and results obtained are compared with the theoretical calculations.

2.2 DIFFUSED LAYER CONTRIBUTION:

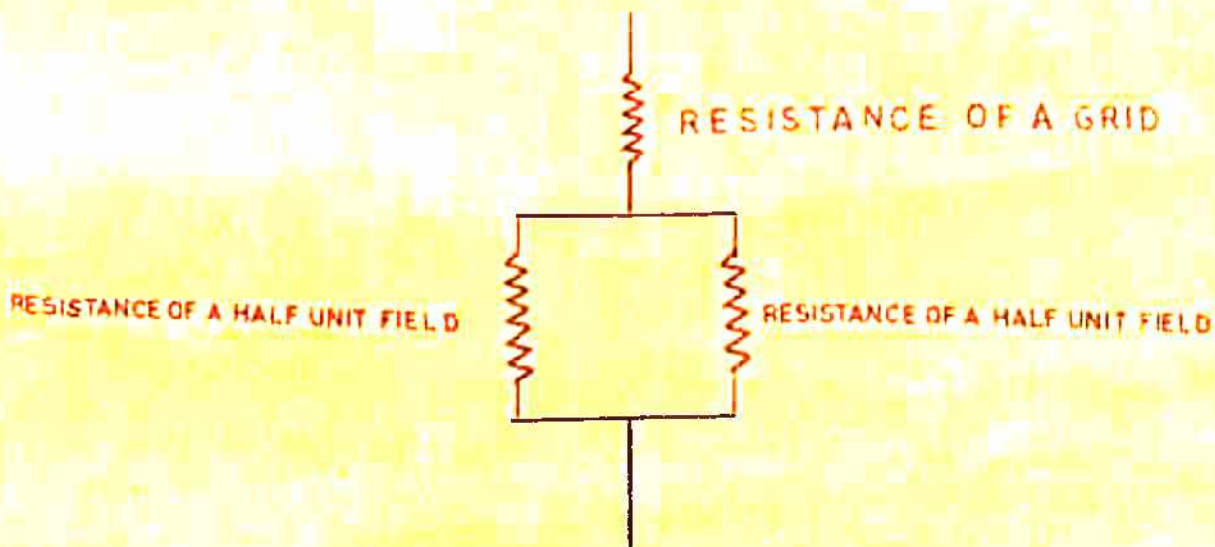
The resistance component due to diffused sheet can be quite high. In many cases it can be the dominant component to the series resistance. Wolf⁽²⁾ suggested the application of conducting grids to minimize the series resistance component due to doped layer. The resistance of the diffused sheet was first calculated by Wolf⁽²⁾ for a simple geometry shown in figure 2.3(a). The distance, which the carriers travel through the diffused sheet to reach the highly conducting grids, is dependent on the location where the carriers enter the diffused region. Therefore the resistance of the diffused sheet depends upon the shape and geometry of the grids. The entire active surface (diffused sheet) can be supposed to be divided into identical units called the unit fields. Figures 2.3(b,c) show the unit field and the equivalent resistance circuit of the unit field as used by Wolf⁽²⁾ for calculating the resistance of the diffused sheet. Wolf⁽²⁾ proceeded under the following assumptions:



(a)



(b)



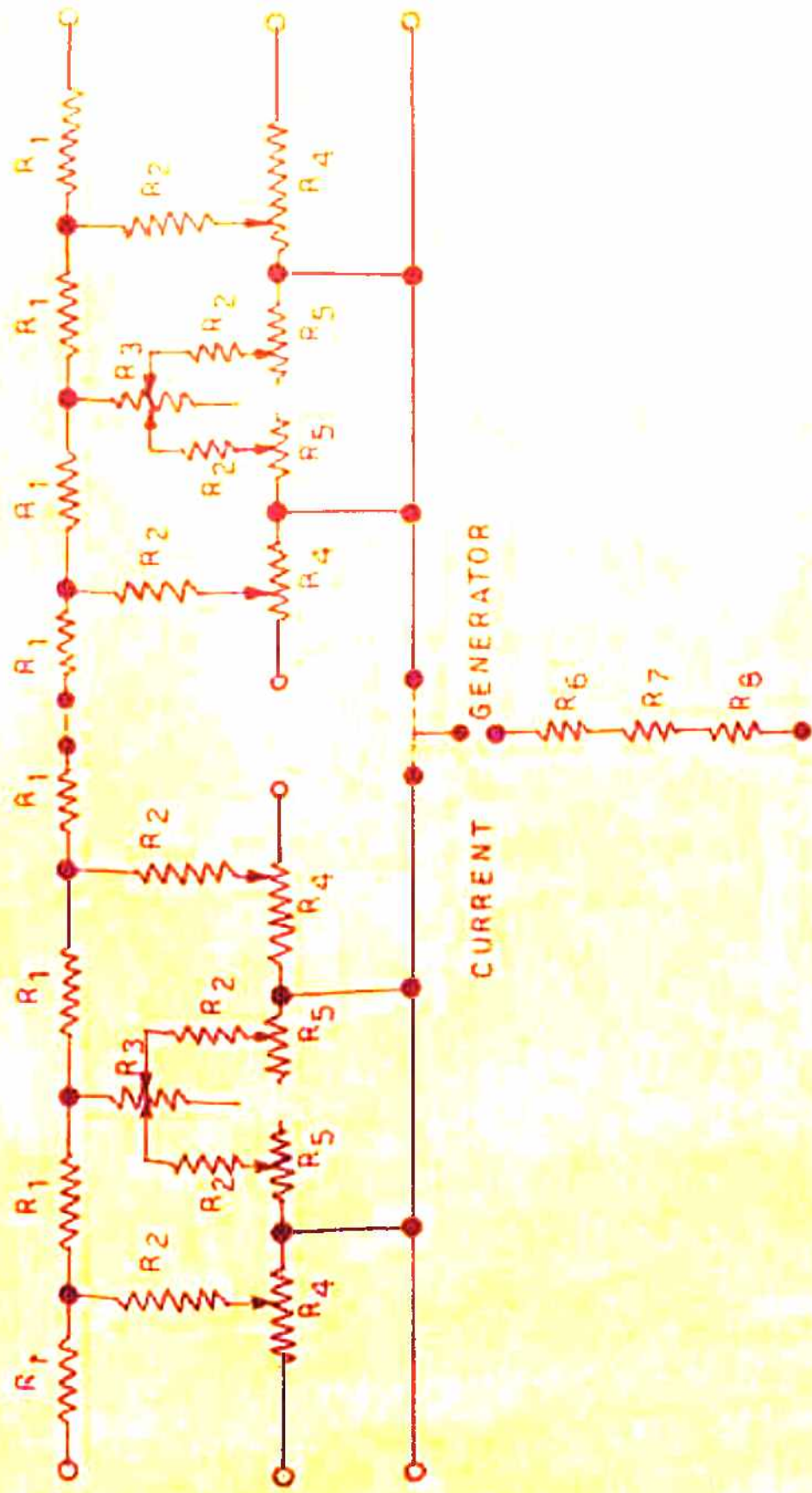
(c)

FIG. 2.3 (a) CONFIGURATION OF A CONTACT GRID STRUCTURE
 (b) CONFIGURATION OF A UNIT FEELD
 (c) EQUIVALENT SERIES RESISTANCE OF A UNIT FIELD

- (i) There is uniform generation of current over the entire active area of the cell.
- (ii) No recombination is taken into account, that is the collection efficiency is assumed to be 100 percent.
- (iii) The metal contact strip at the edge of the cell is assumed to have zero resistance .
- (iv) None of the carriers are collected directly by the contact strip, that is the entire collection is done by fingers.

Under these^e assumptions Wolf⁽²⁾ determined the current flowing through an element of area dA and evaluated the voltage drop $\delta I \cdot dR$ across the element , where δI is the current flowing through the element of resistance dR . Integrating the voltage drop across the elements of a unit field gives V for the field which, when divided by the total current I through the field, gives the resistance of the unit field. The total resistance R_{Ω} of the doped layer is then determined by combining these unit field resistances.

Handy⁽⁴⁾ has presented an equivalent resistance circuit of a solar cell which takes into account all the sources contributing to the internal resistance of a solar cell. The equivalent circuit is shown in Figure (2.4). Handy's calculations are also based on the assumption that carriers are generated uniformly in a plane parallel to the junction plane.



R_1 = RESISTANCE OF THE CONTACT STRIP.

R_2 = CONTACT RESISTANCE BETWEEN DIFFUSED SHEET AND ELECTRODE.

R_3 = RESISTANCE OF GRID STRIP, R_4 = RESISTANCE OF DIFFUSED REGION FOR CARRIERS FLOWING TO CONTACT STRIP.

R_5 = RESISTANCE OF DIFFUSED REGION FOR CARRIER FLOWING TO GRID.

R_6 = RESISTANCE OF BASE REGION. R_7 = RESISTANCE OF THE BACK CONTACT.

R_8 = RESISTANCE OF THE BACK ELECTRODE.

FIG. 2.4 EQUIVALENT RESISTANCE CIRCUIT FOR AN n UNIT FIELD SOLAR CELL (4)

Bordina et al⁽³⁾ analysed the doped layer contribution to the series resistance by solving the associated Poisson's equation. The method, which is mathematically quite rigorous, is based on the series solution for the determination of the general current-voltage characteristics and is as follows: The potential of the doped layer relative to the rear layer satisfies the equation

$$\nabla^2 \phi = \frac{\rho_d}{d_j} j_0 \left[e^{e\phi/nkT} - 1 \right] - \frac{\rho_d}{d_j} j_{ph} \quad (2.2)$$

Where ϕ is the potential of the doped layer relative to the rear contact, ρ_d is the resistivity of the doped layer, d_j is the thickness of the doped layer (junction depth), j_{ph} is the density of the photogenerated current, j_0 is the saturation current density, n is the diode quality factor, k is Boltzmann's constant and T is the operating temperature of the solar cell.

The solution of the above equation is obtained using the following boundary conditions.

- (1) At the edge, where there is no contact, the derivative of the potential with respect to the normal to the photo-element boundary vanishes, since no current exists in this direction:

$$\frac{\partial \phi}{\partial n_s} = 0 \quad (2.3a)$$

- (2) The potential at the contact of the photoelement is constant:

$$\phi(k) = V \quad (2.3b)$$

The constant V is determined by the condition that the total current at the contact be equal to the load current I

$$\oint_k \frac{\partial \phi}{\partial n_s} dl = - \frac{\rho_d}{d_j} I \quad (2.4)$$

Where \oint_k is an integral along the contour of the contact and dl is a length element of the contact.

The solution of the Poisson's equation is obtained in form of a series in the small dimensionless parameter λ_E ,

$$\lambda_E = \alpha_E \frac{\rho_d}{d_j} j_{ph} A / \frac{nkT}{e} \quad (2.5)$$

Where A is the area of the solar cell, α_E is a factor that depends on the geometry of the solar cell and the deposition of the contacts on the surface of the doped layer. The general solution is represented in the form

$$\phi = \phi_0 + \phi_1 + \phi_2 + \dots + \phi_i + \dots \quad (2.6)$$

Where the subscript of ϕ indicates the order of magnitude of the corresponding term with respect to the parameter λ_E . By substituting the values of ϕ in equation (2.2) and comparing the terms of the same order in λ_E , a system of equations is obtained

$$\nabla^2 \phi_0 = 0 \quad (2.7a)$$

$$\nabla^2 \phi_1 = \frac{L_d}{d_j} j_0 (e^{e\phi_0/nkT} - 1) - \frac{L_d}{d_j} j_{ph} \quad (2.7b)$$

$$\nabla^2 \phi_2 = \frac{L_d}{d_j} j_0 e^{e\phi_0/nkT} \frac{e \phi_1}{nkT} \quad (2.7c)$$

$$\nabla^2 \phi_3 = \frac{L_d}{d_j} j_0 e^{e\phi_0/nkT} \frac{e}{nkT} \left(\phi_2 + \frac{e}{nkT} \frac{\phi_1^2}{2} \right) \quad (2.7d)$$

The boundary conditions for the introduced functions ϕ_i are written in a form, analogous to conditions (2.3a & 2.3b):

$$\frac{\partial \phi_i}{\partial n_s} = 0 \quad (\text{at the boundary without a contact})$$

$$\phi_i(k) = V_i \quad (i = 0, 1, 2, \dots), \quad (2.8)$$

where V_i are the terms of the series representing the voltage at the contact:

$$V = V_0 + V_1 + V_2 + V_3 + \dots$$

Thereby condition (2.4) yields

$$\oint_k \frac{\partial \phi_i}{\partial n_s} dl = \begin{cases} 0 & \text{for } i \neq 1 \\ -\frac{L_d}{d_j} I & \text{for } i = 1 \end{cases} \quad (2.9)$$

By integrating the equations of system (2.7) over the area of the solar cell, and taking into consideration that

$$\iint_S \nabla^2 \phi_i \cdot dS = \oint \frac{\partial \phi_i}{\partial n} dl = \oint \frac{\partial \phi_i}{\partial n} dl$$

it is possible to represent the conditions (2.9) in the form

$$I = \iint_S [j_{ph} - j_0 (e^{e\phi_0/nkT} - 1)] dS = A [j_{ph} - j_0 (e^{e\phi_0/nkT} - 1)] \quad (2.10a)$$

$$\iint_S \phi_1 dS = 0 \quad (2.10b)$$

$$\iint_S \left(\phi_2 + \frac{e}{nkT} \frac{\phi_1^2}{2} \right) dS = 0 \quad (2.10c)$$

Where ϕ_0 is assumed to be a constant. In view of

$$\phi_0 = V_0 = V - V_1 - V_2 - V_3 \dots\dots\dots$$

with the help of equation (2.10a), the general expression for the load characteristics of a solar cell has the form

$$V = \frac{nkT}{e} \ln \left[\frac{(j_{ph} A - I)}{j_0 A} + 1 \right] + V_1 + V_2 + V_3 + \dots\dots\dots \quad (2.11)$$

The resistance of the doped layer can be obtained by determining $V_1, V_2, V_3, \dots\dots\dots$ as function of ^{the} power generating current (load current) I .

2.2.1 A SOLAR CELL OF SIMPLEST DESIGN :

For example, to determine the resistance component of the doped layer from the method suggested by Bordina et al (3)

consider a solar cell of simplest design as shown in figure (2.5). Under the assumption of uniform illumination of the solar cell surface and the fulfilment of boundary conditions (2.8),

$$\left. \frac{\partial \phi_i}{\partial y} \right|_{y=0} = \left. \frac{\partial \phi_i}{\partial y} \right|_{y=w} = 0$$

$$\phi_i(k) = V_i \quad (2.12)$$

the problem can be regarded as one dimensional. In this case the equation for V_1 has the form

$$\frac{d^2 \phi_1}{dx^2} = \frac{\rho_d}{d_j} \frac{I}{A} \quad (2.13)$$

The solution for the boundary condition (2.8) and (2.10b) is (3)

$$\phi_1 = - \frac{\rho_d}{d_j} \frac{L}{w} \frac{I}{2} \left[(x/L)^2 - \frac{1}{3} \right] \quad (2.14)$$

hence $V_1 = \phi_1(L) = - \frac{\rho_d}{d_j} \frac{L}{w} \frac{I}{2} \left(1 - \frac{1}{3} \right)$

$$V_1 = - \frac{\rho_d}{d_j} \frac{L}{w} \frac{I}{3} \quad (2.15)$$

Thus the resistance obtained for the simplest case, as shown in Figure (2.5), is given by

$$R_d = \frac{1}{3} \frac{\rho_d}{d_j} \frac{L}{w} \quad (2.16)$$

Where L is the length of the solar cell and w is the width of the cell. These authors obtained V_1, V_2, V_3, \dots as function of power generating current and obtained the resistance of the doped layer for various types of grid structures. The results are presented in table number 2.1.

The method described above as suggested by Bordina et al ⁽³⁾ is quite strenuous to evaluate the resistance of the diffused layer for various types of grid structures. The present work describes a simpler method to evaluate the series resistance component of the diffused layer for various types of grid structures and it is named as power formulation.

2.2.2 POWER FORMULATION *

In this method one evaluates the quantity $(\delta I)^2 dR$ for an element. Integrating this across all the elements of a unit field gives, $P = \int (\delta I)^2 dR$ for the unit field. Dividing this P by the square of the total current flowing through the unit field gives ^{the} resistance R of the unit field. It is found that this simple method for evaluating the doped layer contribution to the series resistance yields values agreeing with those of Bordina et al ⁽³⁾ for most of the cases. The total resistance contributed by the diffused layer is found by

*This method was developed by the group consisting of the supervisor Dr. H.M. Ghule, Km. Abha Ghemawat and the author.

calculating the equivalent resistance due to all the unit fields.

Let us evaluate the resistance of the doped layer for the simplest geometry as shown in Figure (2.5). The resistance of the diffused region depends upon the resistivity of the doped layer ρ_d , junction depth d_j , the grid spacing and the grid geometry. To evaluate the resistance of the diffused region the following assumptions are made:

- (1) Uniform photo-current generation over the entire active area of the solar cell.
- (2) Recombinations are not taken into account.
- (3) The grid geometries are divided in various subunits.
- (4) Current collected by each leg is transferred, equally to both of its ends provided this leg does not lie next to the edge.

To evaluate the series resistance component of diffused layer for simplest geometry, let j be the current density and dx be the width of element of the unit at a distance x , then the total current flowing in the element dx is

$$\delta I = j w x \quad \text{and}$$

$$dR = \frac{\rho_d}{d_j} \frac{dx}{w} \quad (2.17)$$

The power dissipated across the element is δP and δR is given by

$$\delta P = (\delta I)^2 dR = \frac{j^2 w^2 x^2}{w \cdot d_j} dx \quad (2.18)$$

The total power dissipated across the entire diffused sheet is

$$P = \int_0^L \delta P = \frac{1}{3} \frac{\rho_d}{d_j} \frac{L}{w} I^2 \quad (2.19)$$

This gives,

$$R_d = \frac{1}{3} \frac{\rho_d}{d_j} \frac{L}{w} \quad (2.20)$$

The series resistance component of the various type of grid structures (Figure 2.6) can be obtained from the method described above. The resistance of these grid structures can be evaluated by breaking these units into various subunits. The various subunits and their current profiles are shown in figure (2.7). Figure (2.7a) shows the current profile of the simplest unit as shown in figure (2.5). The series resistance component for the grid structure of the type (2.6b) can be obtained dividing this into two subunits of the type (2.7a) of length $L/2$ and width W . These two subunits are in parallel and resistance is given by

$$R_d = \frac{1}{12} \frac{\rho_d}{d_j} \frac{L}{W} \quad (2.21)$$

Similarly the resistance of (2.6b,c,d,e) can also be obtained and are shown in table 2.1. The calculations are presented in Appendix 2.1.

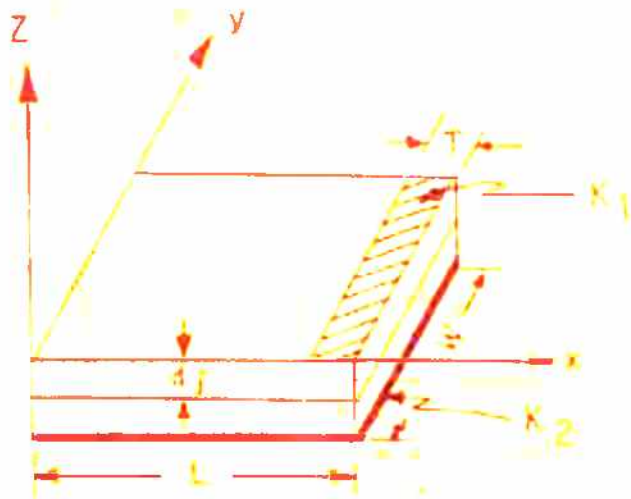


FIG. 2.5 SIMPLE GRID STRUCTURE OF ONE CONTACT

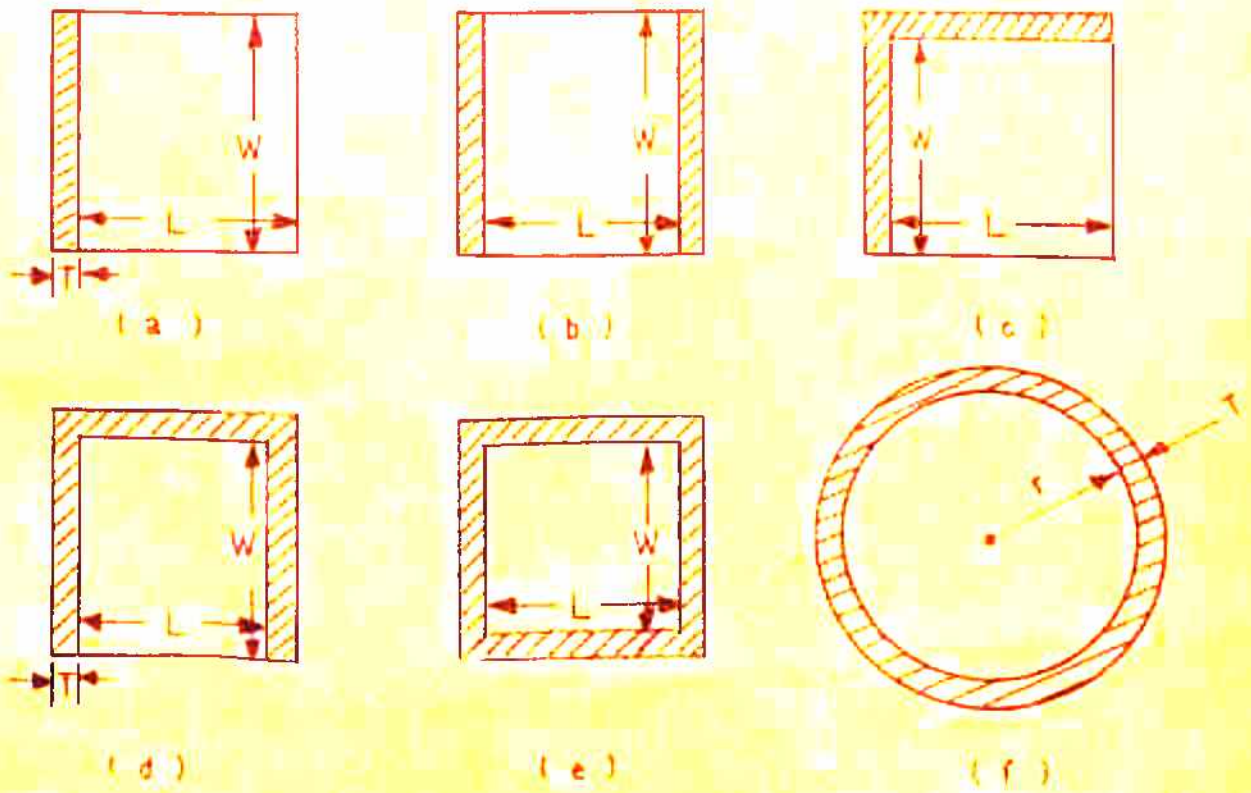
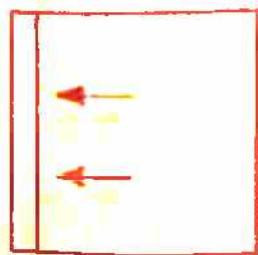
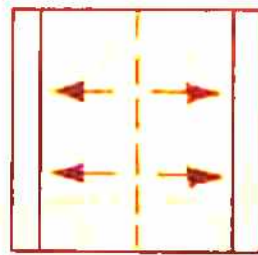


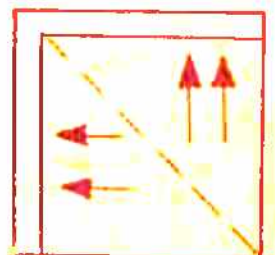
FIG. 2.6 VARIOUS TYPES OF GIRD STRUCTURES



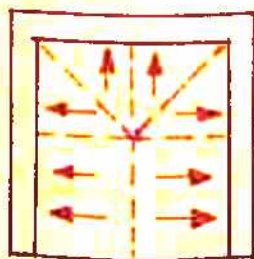
(a)



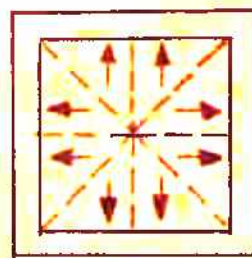
(b)



(c)



(d)



(e)



(f)

FIG. 2.7 VARIOUS TYPES OF SUBUNITS AND THEIR CURRENT PROFILES.

2.2.3 SQUAREMESH GRID STRUCTURE:

As is indicated above, we note that the use of grid structure simply reduces the distance traversed by the carriers before being collected. The same effect can also be obtained by a simple change in geometry. In this article the calculation of the series resistance of the doped layer for the squaremesh grid structure is discussed.

The configuration of the squaremesh grid structure is shown in figure (2.8). To evaluate the resistance of the doped layer with squaremesh grid pattern, divide it in various subunits as described in the previous article. The series resistance component due to doped layer for squaremesh grid pattern can be obtained taking these subunits in parallel. The solar cell with $m \times m$ squaremesh can be modelled by taking

$$(m-1) \times (m-1) \text{ of the type} \quad (2.7e) \quad \dots$$

$$(m-1) \times 4 \text{ of the type} \quad (2.7d) \quad \dots$$

and 1×4 of the type $(2.7c) \quad \dots$

Where all these subunits are in parallel and this gives

$$R_{dsqm} = \frac{\rho_d}{d_j} \frac{1}{32 m^2} \quad (2.22)$$

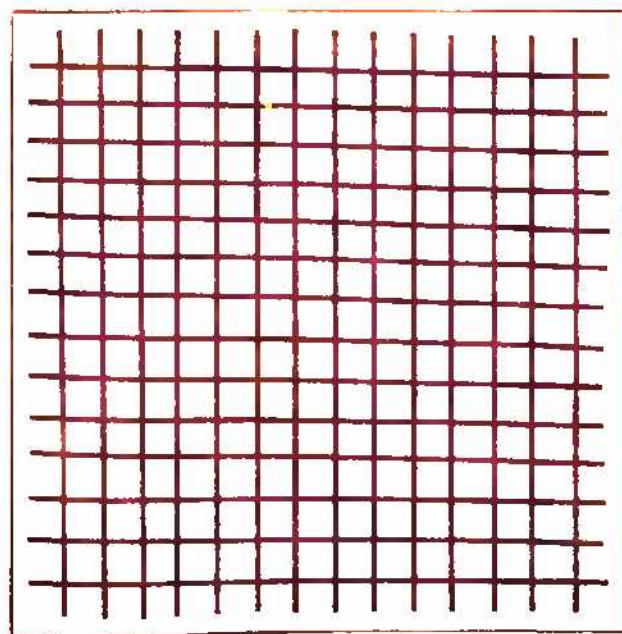


FIG.2.8 SQUARE MESH GRID STRUCTURE.

TABLE-2.1

Comparison of the results obtained, for the resistance components of doped layer, from power formulation with the results that of Bordina et al⁽³⁾

Grid pattern	Results given by Bordina et al ⁽³⁾			Results obtained from power formulation		
2.5	$\frac{1}{3}$	$\frac{\rho_d}{d_j}$	$\frac{L}{W}$	$\frac{1}{3}$	$\frac{\rho_d}{d_j}$	$\frac{L}{W}$
2.6(b)	$\frac{1}{12}$	$\frac{\rho_d}{d_j}$	$\frac{L}{W}$	$\frac{1}{12}$	$\frac{\rho_d}{d_j}$	$\frac{L}{W}$
2.6(c)	$\frac{256}{\pi^6}$	$\frac{\rho_d}{d_j}$	$\frac{WL}{(W^2+L^2)}$	$\frac{\rho_d}{4d_j}$	$\frac{WL}{(W^2+L^2)}$	
2.6(d)	$\frac{256}{\pi^6}$	$\frac{\rho_d}{d_j}$	$\frac{WL}{(4W^2+L^2)}$	$\frac{1}{4}$	$\frac{\rho_d}{d_j}$	$\frac{WL}{(4W^2+L^2)}$
2.6(e)	$\frac{64}{\pi^6}$	$\frac{\rho_d}{d_j}$	$\frac{WL}{(W^2+L^2)}$	$\frac{1}{16}$	$\frac{\rho_d}{d_j}$	$\frac{WL}{(W^2+L^2)}$
2.6(f)	$\frac{1}{8\pi}$	$\frac{\rho_d}{d_j}$		$\frac{1}{8\pi}$	$\frac{\rho_d}{d_j}$	
2.5	$\frac{32}{\pi^6}$	$\frac{1}{m^2}$	$\frac{\rho_d}{d_j}$	$\frac{1}{32}$	$\frac{1}{m^2}$	$\frac{\rho_d}{d_j}$

2.2.4 RESULTS AND DISCUSSION :

The results obtained for various, type of grid structures regarding the series resistance component of the doped layer are presented in table (2.1) and these results are compared with those of Bordina et al.⁽³⁾ The results which are shown in table(2.1) seem to be in good agreement with those of Bordina et al⁽³⁾. Thus the method of calculating the sheet resistance component of series resistance presented here by power formulation simplifies the treatment of the method suggested by Bordina et al⁽³⁾ and allows the prediction of this component for various grid geometries and sheet resistances.

2.3 CONTRIBUTION DUE TO OTHER FACTORS:

The other various components which contribute to the internal series resistance R_s are

- (i) resistance of the contact strips (grids),
- (ii) resistance of the base region,
- (iii) contact resistance between the doped layer and the contact strips and base and the back electrode, and
- (iv) resistance of the back electrode.

The present article deals with the calculations of the resistance of the various other components described above and contributing to ^{the} series resistance R_s .

2.3.1 RESISTANCE OF THE CONTACT STRIPS :

The resistance, contributing to total series resistance R_s of a solar cell due to the metal fingers is also a distributed one and can be evaluated as obtained for the doped layer. The series resistance component of the contact strip with width T_m , thickness t_m of the simplest grid structure described in figure (2.5) is given by

$$R_m = \frac{1}{3} \frac{\rho_m}{t_m} \frac{W}{T_m} \quad (2.23a)$$

Where ρ_m is the resistivity of the metal and W is the width of the solar cell.

The resistance of the metal fingers, as shown in figure (2.6), for other type of grid structures are given below :

$$R_m = \frac{1}{6} \frac{\rho_m}{t_m} \frac{W}{T_m} \quad (2.23b)$$

$$R_m = \frac{8}{15} \frac{\rho_m}{t_m} \frac{WL}{(W+L)T_m} \quad (2.23c)$$

$$R_m = \frac{4}{15} \frac{\rho_m}{t_m} \frac{WL}{T_m(2W+L)} \quad (2.23d)$$

$$R_m = \frac{1}{15} \frac{\rho_m}{t_m} \frac{WL}{T_m(W+L)} \quad (2.23e)$$

and

$$R_m = \frac{2\pi}{3} \frac{\rho_m}{t_m} \frac{a}{T_m} \quad (2.23f)$$

The grid resistance of the square mesh, which is to be evaluated separately from doped layer resistance, is quite complicated as we are left with a $(m+1) \times (m+1)$ interconnected mesh with not all of equal resistance values. For simplicity, all the resistances are taken to be of the same value and this mesh can be broken down into four equivalent $((m+1)/2) \times ((m+1)/2)$ meshes. The assumption of taking all the resistances equal to the resistance of one leg of the subunit is reasonable since all the subunits, except the edge ones, are of the subunit (2.7e) type. It is further assumed that the current, instead of being collected along the entire length of the contact grid, is collected along one leg in each $((m+1)/2) \times ((m+1)/2)$ mesh. This assumption is arbitrary and this assumption allows us to calculate the resistance of a $((m+1) \times ((m+1)/2))$ mesh directly. Under these assumptions Weinberg⁽⁵⁾ gives for a square mesh with equal resistances in each branch,

$$\left(\frac{r_i}{R_{mi}^S} \right)_{av} = \frac{p}{2(p+1)} \quad (2.24)$$

Where $p = (m+1)/2$, R_{mi}^S is the resistance seen by breaking the i -th branch, av denotes the average and r_i is the resistance of the i -th branch and is given by⁽⁶⁾

$$r_i = \frac{1}{6} \frac{\rho_m}{t_m} \frac{s}{T_m}, \quad (2.25)$$

where s is the spacing between two contact strips. From these expressions, the resistance of square mesh grid pattern is

$$R_{sqmg} = \frac{m+3}{12(m+1)} \frac{\rho_m}{t_m} \frac{s}{l_m} \quad (2.26)$$

The total resistance due to metallic fingers and the doped layer is the sum of these two components and is shown in table (2.2). The difference in the resistance expressions for diffused region and metallic fingers as in second and third column of the table (2.2) appear to arise on account of difference in geometry and the change in the direction of current in the metallic fingers.

2.3.2 RESISTANCE OF THE BASE REGION:

The resistance of the base region arises from the substrate resistivity ρ_b , thickness of the substrate t_b and area of the cell A . The resistance of the base is given by

$$R_b = \frac{\rho_b t_b}{A} \quad (2.27)$$

To minimize the bulk resistance, the base region should be relatively thin. However, if the base region is too thin, some of

TABLE-2.2

Series resistance components due to doped layer and metal fingers
for various types of grid structures.

Grid pattern	Doped layer resistance			Grid resistance		
2.5	$\frac{1}{3}$	$\frac{\rho_d}{d_j}$	$\frac{L}{d}$	$\frac{1}{3}$	$\frac{\rho_m}{t_m}$	$\frac{W}{T_m}$
2.6(a)	$\frac{1}{12}$	$\frac{\rho_d}{d_j}$	$\frac{L}{W}$	$\frac{1}{6}$	$\frac{\rho_m}{t_m}$	$\frac{W}{T_m}$
2.6(b)	$\frac{\rho_d}{4d_j}$	$\frac{WL}{(W^2+L^2)}$		$\frac{8}{15}$	$\frac{\rho_m}{t_m}$	$\frac{WL}{T_m(W+L)}$
2.6(d)	$\frac{1}{4}$	$\frac{\rho_d}{d_j}$	$\frac{WL}{(4W^2+L^2)}$	$\frac{4}{15}$	$\frac{\rho_m}{t_m}$	$\frac{WL}{T_m(L+2W)}$
2.6(e)	$\frac{1}{16}$	$\frac{\rho_d}{d_j}$	$\frac{WL}{(W^2+L^2)}$	$\frac{1}{15}$	$\frac{\rho_m}{t_m}$	$\frac{1}{T_m} \frac{WL}{(W+L)}$
2.6(f)	$\frac{1}{3\pi}$	$\frac{\rho_d}{d_j}$		$\frac{2\pi}{3}$	$\frac{\rho_m}{t_m}$	$\frac{a}{t_m}$
2.8	$\frac{1}{32}$	$\frac{1}{m^2}$	$\frac{\rho_d}{d_j}$	$\frac{m+3}{12(m+1)}$	$\frac{\rho_m}{t_m}$	$\frac{S}{T_m}$

the incident photons of long wave wavelength, for whom absorption coefficient α is low will be lost due to transmission and the collection efficiency may be reduced and the dark current increased due to excess recombination at the back surface. Further, handling of such solar cells is likely to be a problem, because if the base region is too thin it will cause the wafer to break. The second method ^{to} minimize the resistance due to base region is by increasing the doping, that is by reducing the resistivity of the base layer. However the minority carrier life time decreases very fast with increased doping⁽⁷⁾. This also results in a low collection efficiency. The optimum resistivity is therefore obtained as a compromise between the life time of the minority carriers and the resistivity of the base layer. Similarly the optimum thickness is a trade off between the transmission of photons and the resistance of the base region. In general 100-300 micron thick cells are used for maximum efficiency. The variation of efficiency with thickness t_b for various values of resistivity ρ_b is shown in figure (2.9). Generally 1-10 ohm cm base material is preferred for cells to be used in space; whereas lower resistivity material upto around 0.01 -0.1 ohm cm is used for terrestrial applications.

2.3.3 RESISTANCE DUE TO FRONT AND BACK CONTACTS:

In the solar cell the front and the back surfaces are covered with highly conductive metallic grids and metals respectively. This gives rise to contact resistance. For better

performance of a solar cell, one of the major requirements of an efficient, reliable contact system is that the metallic electrodes must have low contact resistance to both the n and p regions of the solar cell. The theoretical calculations for contact resistance for various types of contacts are available in the literature (9-11). The contact resistance of the back and front surface depends upon the specific contact resistance r_c and the contact area A_c . The contact resistance is given by (12)

$$R_c = r_c / A_c \quad (2.28)$$

The front surface (active surface) of the solar cell is generally heavily doped and the specific contact resistance for heavily doped layer is very small. The experimentally observed (13) specific contact resistances (resistance in $\Omega \text{ cm}^2$) for various types of contacts for different resistivities to n and p silicon are shown in tables (2.3) and (2.4). Thus to obtain a good low contact resistance to n and p regions of the solar cell, a heavily doped n^+ and p^+ layers should be used. For silicon, electrochemically passivated titanium-silver (by using ρ_d sandwiched between Ti/Ag) layer has been found to be satisfactory.

2.3.4 RESISTANCE OF THE BACK ELECTRODE:

The resistance of the back electrode is very small. It can be determined by the same formula as ^{r_{at}} used for the
 \wedge

TABLE-3.3

The contact resistance in ohm cm² of evaporated metal contacts to p silicon.

Si resistivity (ohm cm) and type	Al	V	Mu	Co	Chromel
.002p	3.7×10^{-5}	5.2×10^{-6}	4.4×10^{-6}	-	2.3×10^{-5}
.005p	5.2×10^{-5}	1.3×10^{-5}	1.4×10^{-5}	7.3×10^{-6}	4.2×10^{-4}
.01p		7.4×10^{-5}	-	2.2×10^{-5}	-
.05p	6.0×10^{-4}	6.4×10^{-2}	1.3×10^{-3}	1.1×10^{-3}	-
.10p	5.4×10^{-4}	$1. \times 10^{-2}$	1.1×10^{-2}	-	-
.25p	1.3×10^{-3}	-	-	-	2.2×10^{-2}
.50p	1.1×10^{-3}	1.40	9.4×10^{-2}	1.3×10^{-2}	-

TABLE-2.4

The contact resistance in ohm cm^2 of evaporated contacts to n silicon

Si resistivity (ohm cm) and type	A1	V	NO	\bar{V}_d	\bar{C}_d	channel
0.005 n	4.1×10^{-3}	7.3×10^{-2}	7.8×10^{-5}	7.0×10^{-4}	1.6×10^{-4}	-
0.010 n	8.3×10^{-3}	2.6×10^{-3}	6.1×10^{-2}	1.5×10^{-3}	4.4×10^{-2}	2.2×10^{-4}
0.05 n	6.4×10^{-2}	2.1×10^{-1}	2.0	7.0×10^{-3}	1.6×10^{-1}	-
0.10 n	1.0×10^{-1}	1.1×10^{-1}	-	-	1.0	-
0.50 n	2.9×10^{-1}	2.9	3.6	-	-	-

calculation of the base resistance, where the symbols refer to the metal. The specific resistivity of the conducting metal is of the order of 10^{-6} ohm cm, the thickness of the back electrode is of the order of 1 micron. For 1 cm^2 solar cell this resistance is less than 10^{-9} ohm.

2.3.5 DISCUSSION:

It is clear from the preceding articles that the contributions to the series resistance by various components can be evaluated. Bordina et al⁽³⁾ did not consider the resistance contribution by metallic fingers, which in the cases studied, is nearly of the same order as that due to the doped layer.⁽⁶⁾ By evaluating these contributions one can find as to which one amongst them is dominant. This can help us devise methods to minimize the resistances due to various components.

2.4 SHUNT RESISTANCE:

The shunt resistance arises because of the fact that there are some ionic charges on or outside the semiconductor surface which induce image charges in the semiconductor thereby causing the formation of the so called surface channels or surface depletion layer regions. Once a channel is formed it modifies the junction depletion region and gives rise to surface leakage current for the minority carriers to flow and this

is represented by the shunt resistance R_{sh} in parallel with the diode. Stürn⁽¹⁴⁾ has pointed out that shunt resistance can also arise from small scratches and imperfections on the device surface which become partially or totally covered by the contact metallurgy during the device fabrication, sintering the contact strips to minimize contact resistance can cause small metal particles to enter the scratches and result in leakage across the p-n junction.

Ideally, the shunt resistance should be as large as possible, but a variety of factors, as discussed above, lead to low values of R_{sh} . The decrease in shunt resistance reduces the fill factor and conversion efficiency of the solar cell. The effect of shunt resistance on current voltage characteristics is shown in figure (2.10).

2.5 EXPERIMENTAL DETERMINATION OF SERIES RESISTANCE:

The series resistance has significant effect on the performance of the solar cell especially at high intensity conditions. A knowledge of the value of the series resistance of the solar cell is necessary particularly to design the solar cell with increased efficiency. Although the effect of series resistance on the performance of the solar cell is well known, but the knowledge of the techniques of experimentally determining the series resistance of the solar cell is also important to analyse the solar cell characteristics. The most commonly

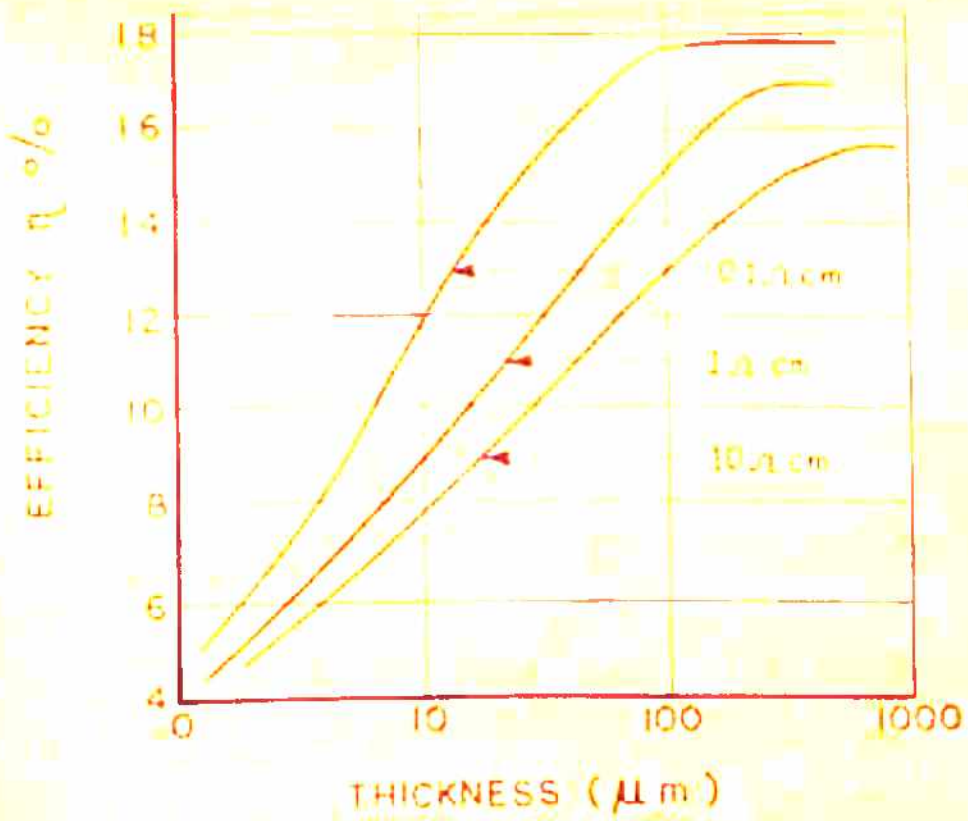


FIG. 2.9 VARIATION OF SOLAR CELL EFFICIENCY WITH THICKNESS FOR VARIOUS BASE RESISTIVITIES. (8)

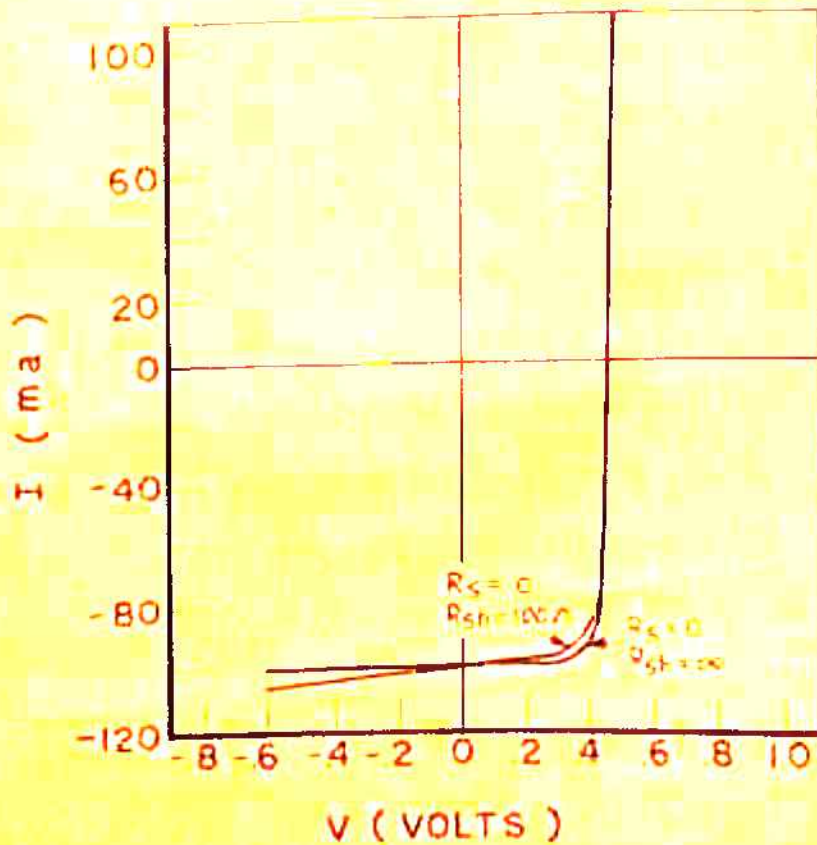


FIG. 2.10 THEORETICAL I - V CHARACTERISTICS OF A SOLAR CELL FOR DIFFERENT VALUES OF SHUNT RESISTANCE (1)

used technique of experimentally determining the series resistance of the solar cell is one described by Wolf and Rauschenback⁽¹⁵⁾ and this is referred^{to} as the illuminated curve technique. Imamura and Portscher⁽¹⁶⁾ have discussed a number of techniques to evaluate the series resistance. The present article discusses in brief the various experimental methods employed for the determination of the series resistance of the solar cell.

2.5.1 ILLUMINATED CURVE TECHNIQUE:

In this method the I-V characteristics of a solar cell under two different light intensities are plotted. A point is marked on each curve at a fixed ΔI from the short-circuit current of that curve, such that the co-ordinates of these points are $P_1(V_1, I_{sc1} - \Delta I)$ and $P_2(V_2, I_{sc2} - \Delta I)$ (Figure 2.11) respectively. The difference ΔI for making^{the} points should be same because it is then possible to connect the marked points of all curves with a straight line. If there were no series resistance present, the line would be parallel to the current axis. If the line is not parallel to the current axis a change in voltage has occurred which is equal to the $(I_{sc1} - I_{sc2})R_s$ drop caused by the series resistance in the cell itself⁽¹⁶⁾. The expression for the series resistance R_s can be obtained by solving the current voltage equations for two different illuminations. The series resistance R_s is given by(16)

$$R_s = \frac{V_1 - V_2}{I_{sc2} - I_{sc1}} \quad (2.29)$$

This expression is obtained under the assumption that $(V_1 - \Delta I_{sc} R_s)$ is very large compared to the magnitude of the thermal voltage nkT/e . This condition can be fulfilled only near the maximum power point of the I-V characteristics. The resistance R_s is also assumed to be independent of light intensity for its evaluation. This method provides the average resistance of the solar cell since the resistance is also dependent on different illumination levels⁽¹⁷⁻¹⁸⁾.

2.5.2 DARK CURVE TECHNIQUE:

In this method the dark I-V characteristics and the I-V characteristics under illumination are plotted as shown in figure 2.12. Two points P_1 and P_2 are selected on the dark and illuminated I-V characteristics, such that their co-ordinates are $(V_1, \Delta I)$ and $(V_2, I_{sc} - \Delta I)$ where I_{sc} is the short circuit current. The series resistance is then given by the relation⁽¹⁶⁾

$$R_s = \frac{(V_1 - V_2)}{I_{sc}} \quad (2.30)$$

In deriving this equation, I_{sc} is assumed to be equal to the photogenerated current I_{ph} which does not hold good if I_0 and R_s are very high since I_{sc} becomes

$$I_{sc} = I_{ph} - I_0 e^{eI_{sc} R_s / nkT} \quad (2.31)$$

Thus this method is not suitable for evaluation of series resistance R_s for the solar cells having high reverse saturation current I_0 and large internal series resistance R_s .

2.5.3 p-n JUNCTION AND DARK FORWARD CHARACTERISTICS TECHNIQUE:

In this technique a dark forward characteristics is plotted along with a p-n junction characteristics for a given solar cell as shown in figure 2.13. The latter characteristics depicts the relationship between open circuit voltage and short circuit current that is, V_{oc} vs I_{sc} . This is obtained by using different intensities of the incident illumination. If V_1 and V_2 are the voltages on the two curves corresponding to the same current I , R_s is given by

$$R_s = \frac{V_1 - V_2}{I} \quad (2.32)$$

This expression can only be obtained under the same assumptions as made for the method described in the previous article (2.5.2). This method too is suitable only for the solar cells with low series resistance, low diode quality factor, low saturation current and high shunt resistance that is for good quality solar cells.

2.5.4 EVDOKIMOV'S SINGLE CURVE TECHNIQUE:

In this method a single experimental current voltage characteristics is used for the evaluation of the series resistance

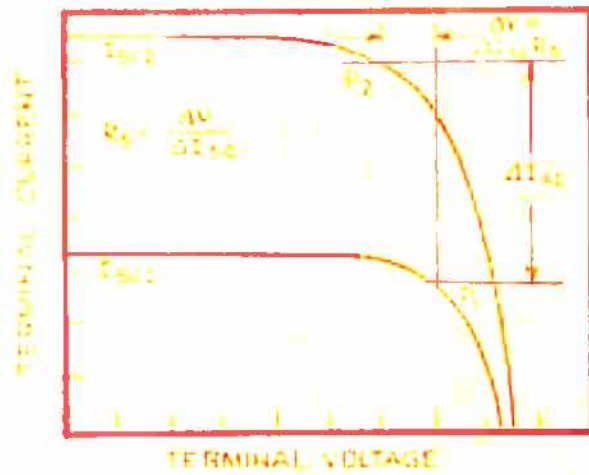


FIG.2.11 ILLUMINATED CURVE METHOD OF DETERMINING R_s .

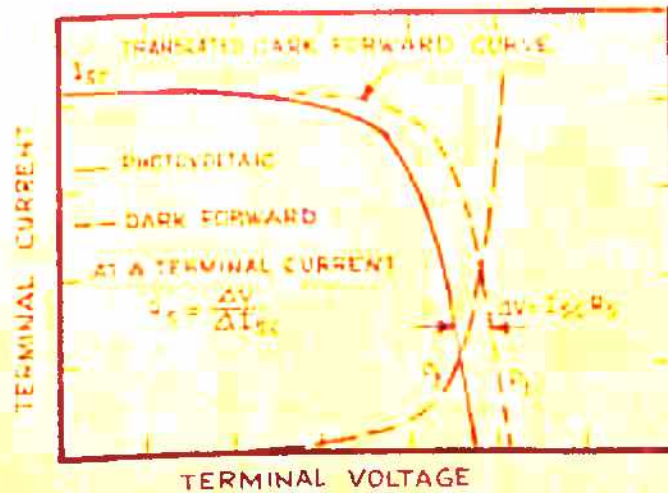


FIG. 2.12 DARK CURVE METHOD OF DETERMINING R_s .

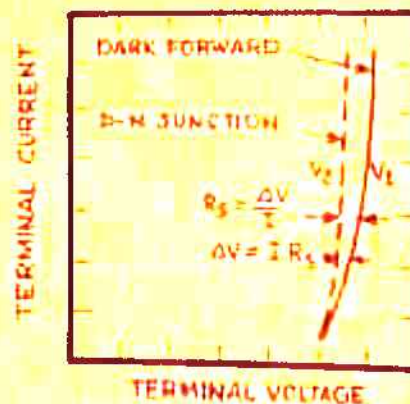


FIG.2.13 DETERMINATION OF R_s USING p-n JUNCTION AND DARK FORWARD CHARACTERISTICS.

and other parameters such as the shunt resistance, diode quality factor n and reverse saturation current I_0 of the solar cell. This method was suggested by Evdokimov⁽¹⁹⁾. In this method the area under the I-V curve (Figure 2.14a) is denoted by P_0 , the cell power VI-I curve is denoted by P_1 (Figure 2.14b) and the value of $\tan \beta$ for I-V curve at $I = 0$ is given by $-\left. \frac{\partial V}{\partial I} \right|_{I=0}$. From these informations the value of the series resistance can be obtained and is given by⁽¹⁹⁾

$$R_s = \frac{12 P_0}{I_{sc}^2} - \frac{12 P_1}{I_{sc}^3} - \frac{6 V_{oc}}{I_{sc}} + 3 \tan \beta \quad (2.33)$$

The importance of this experimental technique lies in the fact that R_s , R_{sh} , I_0 and the diode quality factor n can all be obtained from a single experimental set-up. The shunt resistance R_{sh} , diode quality factor n , and reverse saturation current I_0 can be determined from the following expressions⁽¹⁹⁾

$$\frac{1}{R_{sh}} = \frac{1}{V_{oc}^2} (10 P_0 - \frac{12 P_1}{I_{sc}} + I_{sc}^2 \tan \beta - 4 I_{sc} V_{oc}) \quad (2.34)$$

$$V_T = I_{sc} (\tan \beta - R_s) \quad (2.35)$$

$$n = \frac{e}{kT} I_{sc} (\tan \beta - R_s) \quad (2.36)$$

$$I_0 = I_{sc} e^{-V_{oc}/V_T} \quad (2.37)$$

While employing this method a large number of sets of readings are necessary to determine P_0 , P_1 and $\tan \beta$ with a high degree of accuracy. This enables determination of the series resistance with good precision.

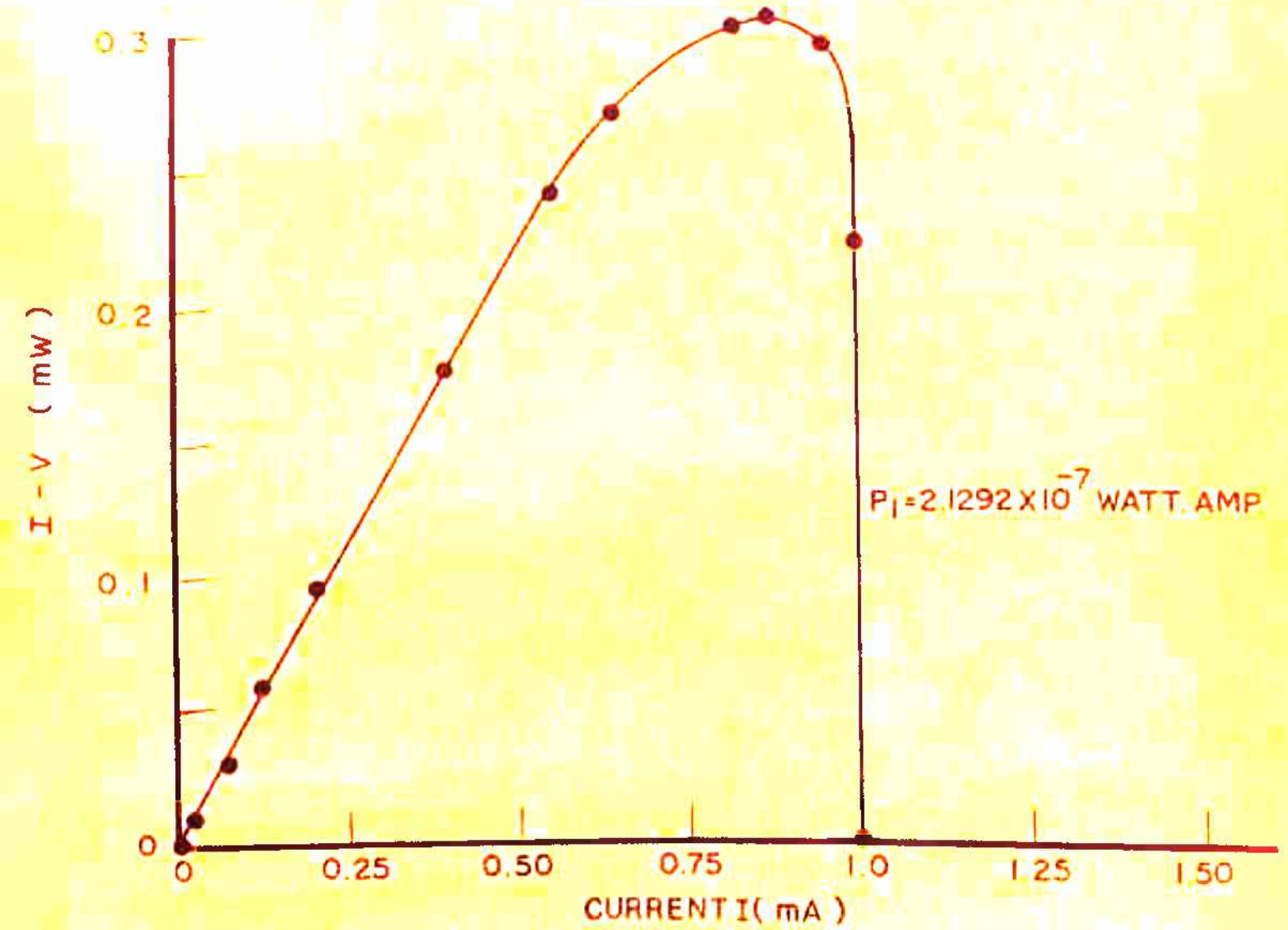
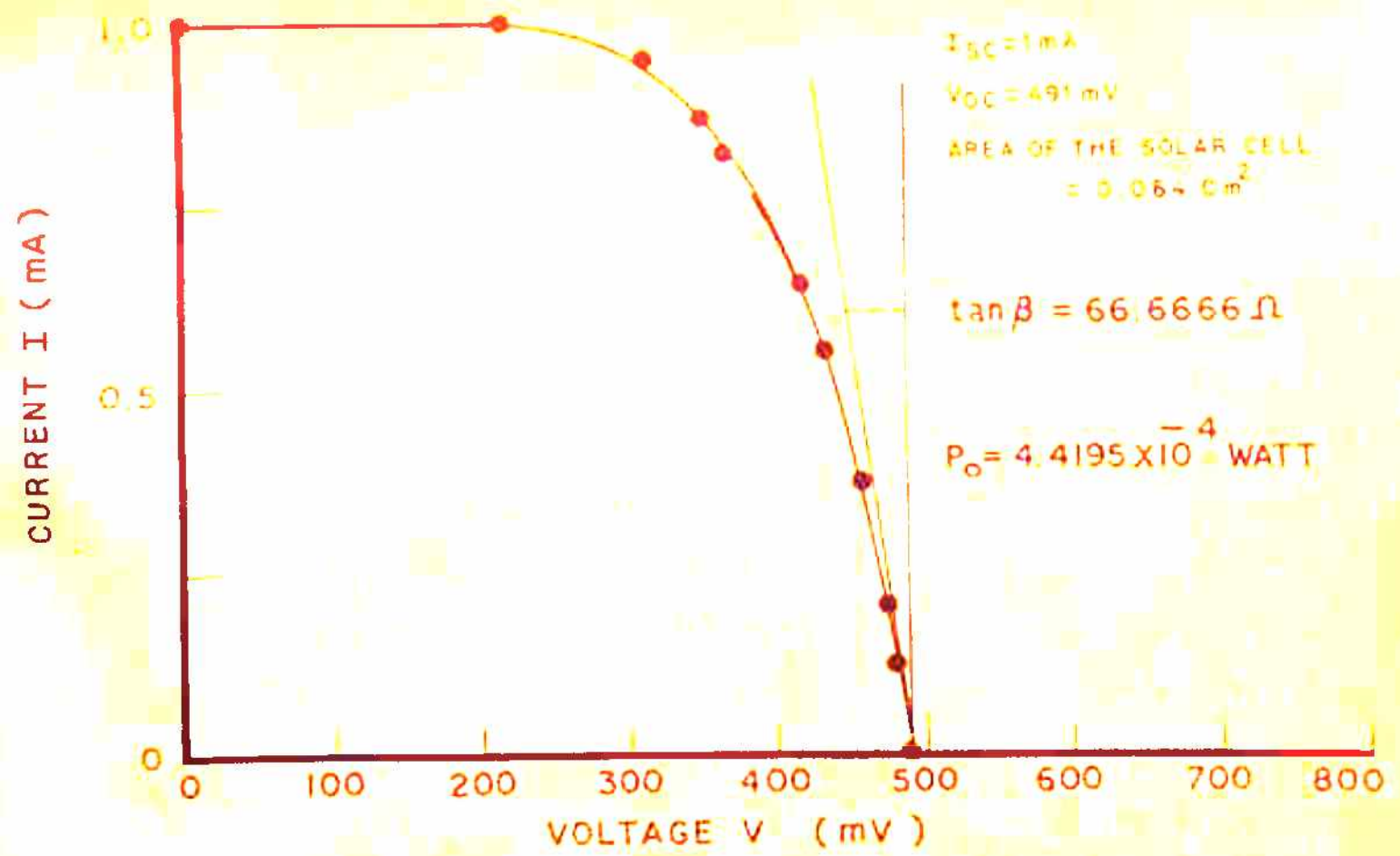


FIG.2.14 EVDOKIMOV'S METHOD OF DETERMINING R_s FOR P-n JUNCTION SOLAR CELL WITH SQUARE MESH GRID STRUCTURE.

(a) I - V CURVE FOR P_0 (b) IV - I CURVE FOR P_1

2.6. FABRICATION OF THE SOLAR CELLS:

p/n single crystal silicon solar cells were used for study. These solar cells were fabricated at CEERI, Pilani and made available for the present investigations. The solar cells were fabricated using conventional silicon integrated circuit fabrication techniques. Emitter was diffused at 900°C using boron dopant. The junction depth was kept in the range of 0.3 to 0.6 micron. Sheet resistance was controlled in the range of $100\ \text{ohm}/\square$ to $200\ \text{ohm}/\square$. Drive in was carried out with wet oxidation. HCl was introduced during oxidation to improve the minority carrier life time. Oxide growth was used in controlled way to use it as an antireflection coatings. Aluminium was evaporated on the back-side of the wafer and sintered in nitrogen ambient at 650°C for 15 minutes. Aluminium square-mesh grid pattern was evaporated on the front side of the wafer. Metal pattern was defined by using photolithography. Sintering was carried out in nitrogen ambient at 500°C for 15 minutes. Top contact was provided by 13×13 squaremesh grid structures. The various parameters of the solar cell used are presented in table 2.5.

2.7 EXPERIMENTAL RESULTS AND DISCUSSIONS :

To evaluate the internal series resistance of solar cell, the measurements were performed on the solar cell of p/n

TABLE-2.5Parameters of the p-n junction solar cell.

Cell area	0.0434 cm^2
Base resistivity	0.1 to 0.5 ohm cm
Base thickness	150-200 μm
Thickness of the back electrode	1 μm
Resistivity of Aluminium	$2.9 \times 10^{-6} \text{ ohm cm}$
Spacing between two legs	6.3 mil
Width of aluminium finger	10 μm .
Junction depth	0.3 - 0.5 μm
Sheet resistance	$200 \Omega/\square$ - $300 \Omega/\square$
Carrier concentration of the doped layer	$10^{19}/\text{cm}^3$ - $5 \times 10^{19}/\text{cm}^3$

type with 4.84 mm^2 size. The current voltage characteristics were obtained under illumination. The experimental set-up is shown in figure (2.15). The voltage was measured on a vernier potentiometer and the current was measured on an electronic multimeter. The internal series resistance was determined using two different experimental techniques, namely the illuminated curve technique for two different light intensities as described in article (2.5.1) and the method suggested by Evdokimov as described in article (2.54) (Figure (2.14a,b)). The purpose of using the later method was to obtain R_s , R_{sh} , n and I_0 from a single I-V plot. The average value of series resistance obtained from the illuminated curve is 2.25Ω and the value of series resistance obtained from the method suggested by Evdokimov is 2.36Ω . The series resistance was obtained within an accuracy of $\pm 12\%$.

It is found that the observed values of series resistance obtained from the two different methods employed are in fairly good agreement. The series resistance obtained from the illuminated curve technique is some what less compared to that obtained from the Evdokimov's method. This difference in the resistance values is likely to be due to the fact that the series resistance is also a function of light intensity and it decreases with increasing intensity.

The value of the series resistance obtained by taking into account contributions by various factors described before.

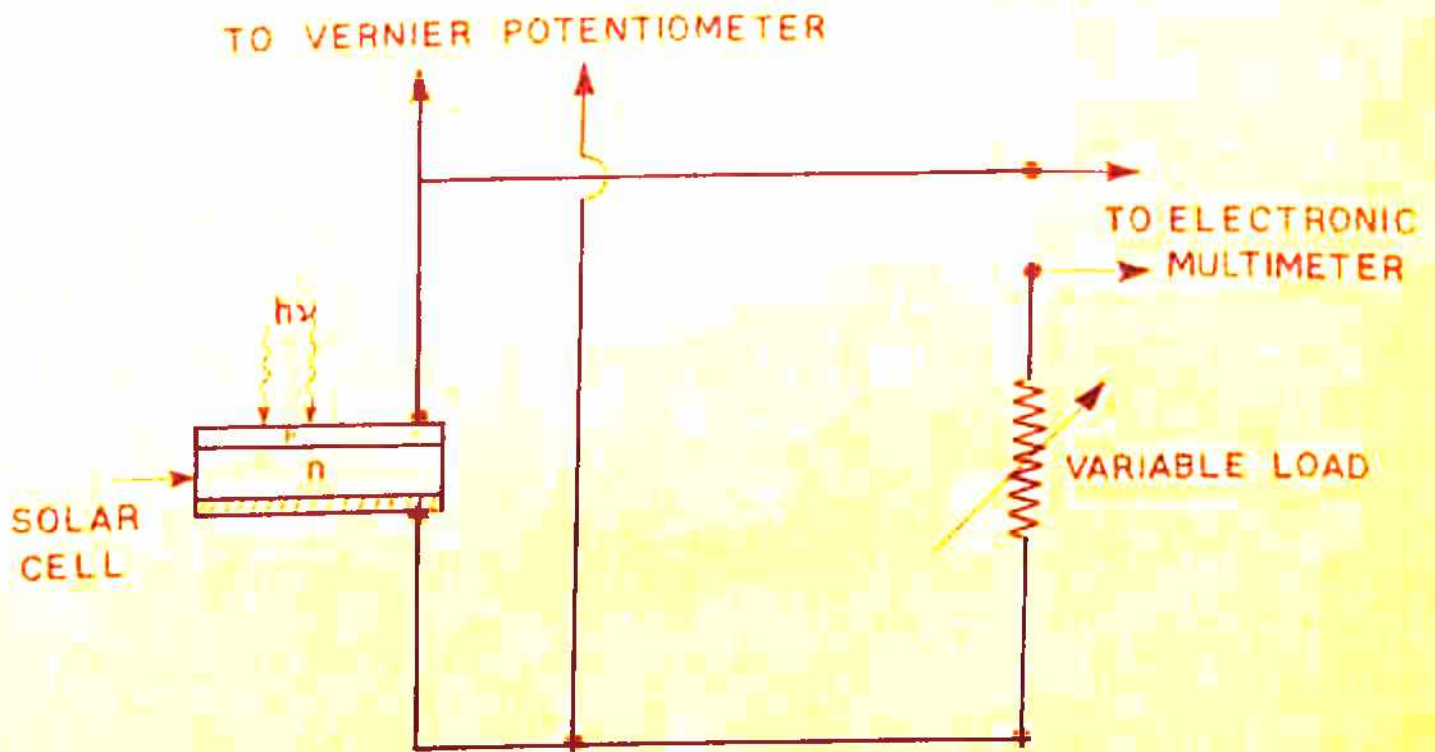


FIG. 2.15 EXPERIMENTAL SET - UP TO DETERMINE CURRENT VOLTAGE CHARACTERISTICS OF A p - n JUNCTION SOLAR CELL .

is 2.34 ohm. This value compares favourably with the experimentally obtained value of 2.36 ohm obtained on using Evdokimov's method. It appears that in the small area solar cell employed, the major contribution is from the contact resistance between the base and the back electrode . This contribution due to contact resistance is going to be small for larger area solar cells.

REFERENCES:

1. M.B. Prince, J. Appl. Phys. Vol. 26, pp 534 (1955).
2. M. Wolf, Proc. IRE, Vol. 48, pp 1246 (1960).
3. N.M. Bordina et al, Radio Engineering and Electronics Physics, Vol. 10, pt I pp. 617 (1965).
4. R.J. Handy, Solid State Electronics Vol. 10, pp 765 (1967).
5. L. Weinber, Network Analysis and Synthesis, McGraw-Hill Book Co., Inc. New York (1962).
6. A Ghemawat, M.Sc. Thesis (1976).
7. J.G. Fossum, Solid State Electronics, Vol.19,pp 269(1977).
8. H.J. Hovel, Semiconductors and Semimetals (Solar Cells) Vol. 11, Academic Press, New York (1975).
9. A.Y.C. Yu, Solid State Electronics, Vol. 13, pp 239 (1970).
10. C.Y. Chang, and Y.K. Fang and S.M. Sze, Solid State Electronics Vol. 14, pp 541 (1971).
11. B. Schwartz, Ohmic Contacts to Semiconductors, Electrochemical Society Inc. New York, U.S.A. pp 31 (1969).
12. R.K. Yasui and L.W. Schmid, 8th IEEE Photovoltaic Specialists Conference, Seattle W.A., Aug. 4-6, pp 110 (1970).
13. R.C. Hooper et al, Solid State Electronics Vol. 8, pp 832 (1965).
14. R.J. Stirn, Conf. Rec. IEEE Phot.Spec. Conf. 9th Silver Spring pp 72 (1972).

15. M. Wolf and H. Rauschenbach, *Advanced Energy Conversion*, Vol. 3, pp 455 (1963).
16. M.S. Imamura and J.I. Porkscheller, *Conference Record of the Eighth IEEE Photovoltaic Specialists Conference*, pp 102 (1970).
17. M.D. Lammert and R.J. Schwartz, *IEEE Trans. on Electron Devices*, Vol. ED-24 pp 237 (1977).
18. N.K. Swami and H.M. Ghule, *Proceedings of National Solar Energy Convention, Bhavnagar* pp 445 (1978).
19. V.M. Evdokimov, *Applied Solar Energy* Vol. 8, pp 63, No. 6 (1972).

CHAPTER-IIIEFFECT OF TEMPERATURE AND CONCENTRATED SUNLIGHT

3.1	Introduction.	84
3.2	Effect of temperature at constant intensity.	86
3.3	Results and discussion.	88
3.4	Effect of concentration of incident solar radiation.	101
3.5	Results and discussion.	104

CHAPTER-III

EFFECT OF TEMPERATURE AND CONCENTRATED SUNLIGHT

3.1 INTRODUCTION:

The concept of generating electricity from sunlight by means of solar cells has become increasingly attractive in a time of uncertain fuel sources, price increases and environmental concerns, for sunlight is a nondepletable resource that can be exploited in space without producing harmful byproducts on earth. There is considerable optimism that the technical hurdles in the way of implementing the use of solar cells for power generation can be surmounted without requiring major scientific breakthroughs. However, the cost of building such a system remains high. Since the cost of silicon solar cells and other semiconducting materials is high and is likely to remain that way, the use of almost any method to obtain power output from a given set of solar cells is justified. One technique that has received considerable attention to get more power output from a solar cell is through the use of concentrator^s.

The use of concentrators results in two main disadvantages. Firstly the increased power generating current I , brought about by higher concentration of incident solar radiation, flowing through the device, causes an additional voltage drop across the cell from the internal series

resistance R_s and as a result the $I^2 R_s$ loss due to the series resistance becomes significant. This in turn affects the maximum power point and degrades the performance of the solar cell. Secondly, the cell operating under concentrated sunlight has a tendency to operate at a temperature higher than the ambient. The increase in temperature increases the dark current which opposes the photogenerated current, which in turn decreases the efficiency of the solar cell. The use of concentrators also necessitates the use of a tracking device which is needed so as to keep the solar cell always in focus. Now a days work is also being done on non-tracking concentrators. The concentration ratio achieved so far has, however, not exceeded 8 to 10 suns. The operating temperature and the concentration of incident solar radiation of the solar cell are important parameters to determine the power output from a given solar cell. In this chapter experimental results giving the temperature and concentration dependence of the various solar cell parameters are presented and physical processes underlying their dependence discussed.

To determine the internal series resistance R_s , the shunt resistance R_{sh} , and the thermal voltage $V_T (= \frac{nkT}{e})$ and the reverse saturation current I_0 as functions of operating temperature and concentration of incident solar radiation, a method suggested by Evdokimov (as described in Chapter II)

was followed. This method yields R_s , R_{sh} , V_T and I_o from a single V-I characteristics. The area under the V-I curve is denoted by P_o , the cell power given by the area under IV-I curve is denoted by P_1 and the value of \tan/β for V-I curve is obtained from the tangent at $I = 0$ and is given by $-\frac{\partial V}{\partial I} \Big|_{I=0}$. P_o , P_1 and \tan/β yields R_s , R_{sh} , V_T and I_o from the following relations (1)

$$R_s = 12P_o/I_{sc}^2 - 12P_1/I_{sc}^3 - 6V_{oc}/I_{sc} + 3 \tan/\beta \quad (3.1)$$

$$1/R_{sh} = \frac{1}{V_{oc}^2} \left[10P_o - \frac{12P_1}{I_{sc}} + I_{sc}^2 \tan/\beta - 4I_{sc}V_{oc} \right] \quad (3.2)$$

$$V_T = I_{sc} (\tan/\beta - R_s) \quad (3.3)$$

and

$$I_o = I_{sc} e^{-V_{oc}/V_T} \quad (3.4)$$

Thus R_s , R_{sh} , V_T and I_o can be determined from the I-V characteristics of the solar cell.

3.2 EFFECT OF TEMPERATURE AT CONSTANT INTENSITY:

The variation of some of the solar cell parameters such as short circuit current I_{sc} , open circuit voltage V_{oc} and the maximum power output P_{mp} from a solar cell at low and high temperatures ranging from -160°C to 150°C has been studied by several authors (2-12). However, a complete study of temperature dependence of solar cell parameters, which determine the

efficiency of solar cell is not available. Wysocki and Rappaport⁽¹³⁾ investigated theoretically the effect of temperature on the open circuit voltage V_{oc} , the dark current voltage characteristics and the conversion efficiency of the solar cell assuming the short circuit current to be insensitive to temperature. It was found experimentally that the short circuit current of the solar cell also depends upon temperature⁽⁵⁾. A quantitative analysis was presented to account for the variation in short circuit current in silicon solar cells with temperature by Alex Shumka⁽¹⁴⁾. However, there are other parameters such as reverse saturation current I_0 , the diode quality factor n , the thermal voltage V_T and the internal series resistance R_s which are also temperature dependent and which play an important role in determining the efficiency, Bawa et al⁽¹⁵⁾ presented experimental results showing the effect of temperature on these parameters. These authors, however, did not give any physical explanation for the temperature dependence of the various parameters studied by them. The present work deals with experimental results concerning temperature effects from 40°C to 110°C on the various parameters of a p-n junction silicon solar cell. The factors which appear to be responsible for the temperature dependence of these parameters have also been analysed. Similar results were presented in the symposium on electron devices held in CEERI Pilani⁽¹⁶⁾.

3.2.1 EXPERIMENTAL SET-UP:

The measurements were performed on p/n type silicon solar cells of 4.84 mm^2 size with 13×13 square mesh grid pattern on the top of the diffused layer and fabricated at CEERI, Pilani. The details of fabrication of the solar cell used for experimental study have been given in Chapter II. The solar cell was kept in a sand bath as shown in Figure (3.1). The cell was illuminated by light from a Tungsten lamp. A slow heating was provided to increase the temperature of the solar cell by adjusting the heater voltage with the help of a variac. The temperature of the solar cell was varied from 40°C to 110°C . The current was measured by an electronic multimeter and the voltage by a vernier potentiometer. The current voltage characteristics of the solar cell was obtained for various temperatures in the range 40°C - 110°C (Figure 3.2). The various parameters were obtained from the expressions (3.1), (3.2), (3.3) and (3.4).

3.3 RESULTS AND DISCUSSION:

3.3.1 EFFECT OF TEMPERATURE ON SHORT CIRCUIT CURRENT:

The variation of short circuit current with temperature is shown in Figure (3.3). The graph shows that the short circuit current increases with increase in temperature. The short circuit current in a solar cell is given by (17)

$$I_{sc} = e g (L_n + L_p) \quad (3.5)$$

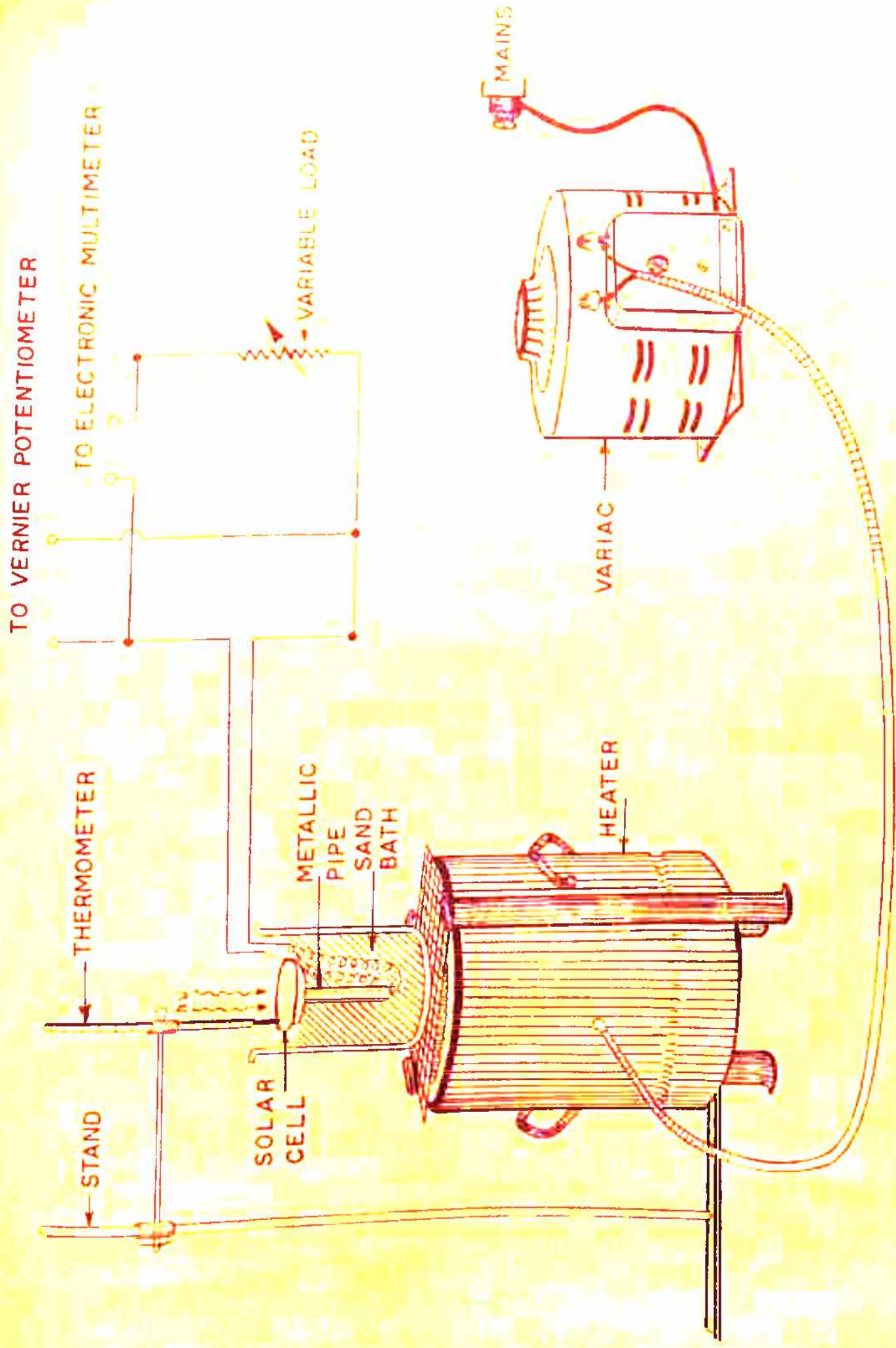


FIG. 3.1 EXPERIMENTAL SET - UP TO STUDY THE EFFECT OF TEMPERATURE ON SOLAR CELL PARAMETERS.

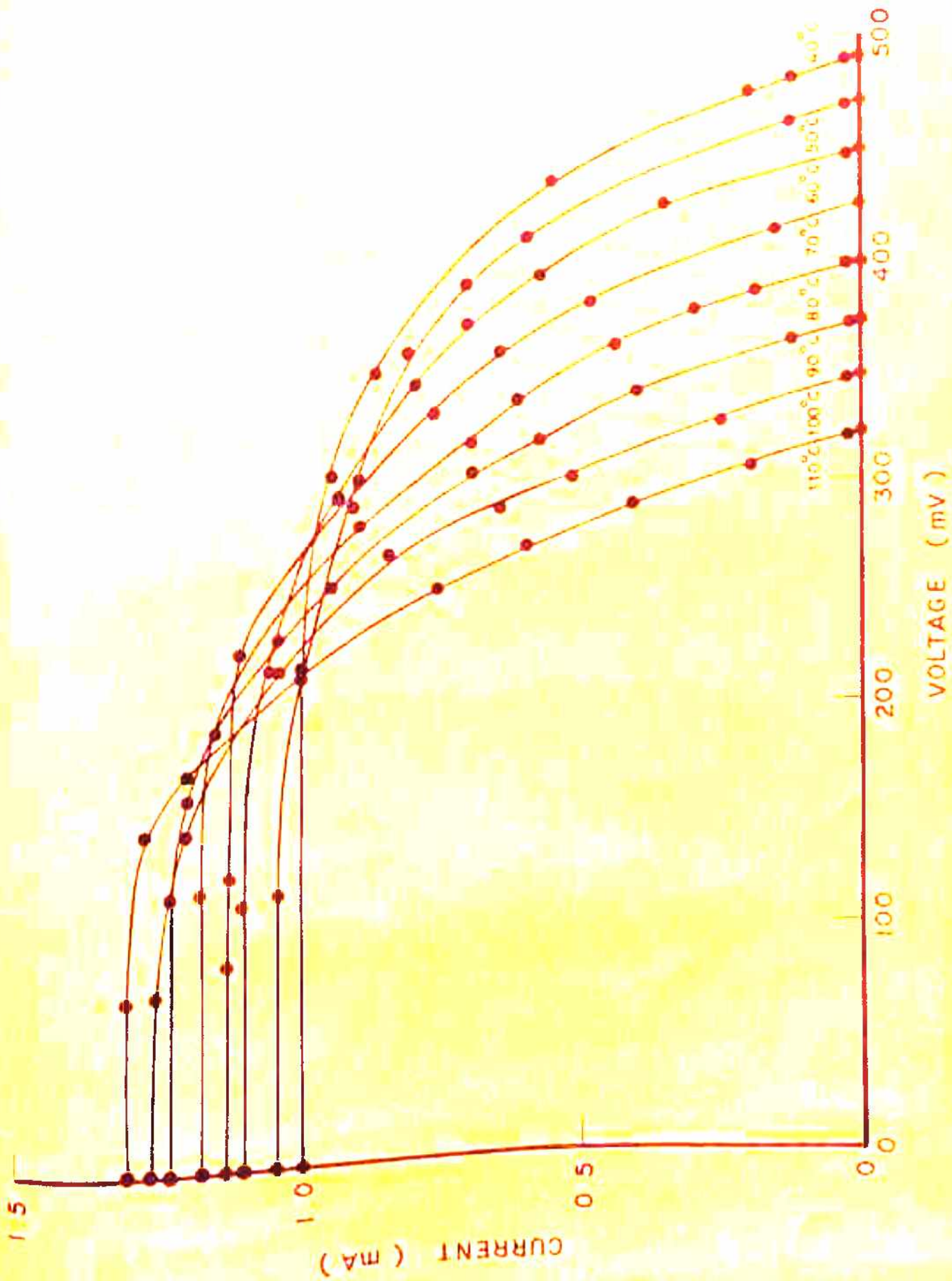


FIG 3.2 CURRENT VOLTAGE CHARACTERISTICS OF A SOLAR CELL FOR VARIOUS VALUES OF TEMPERATURE .

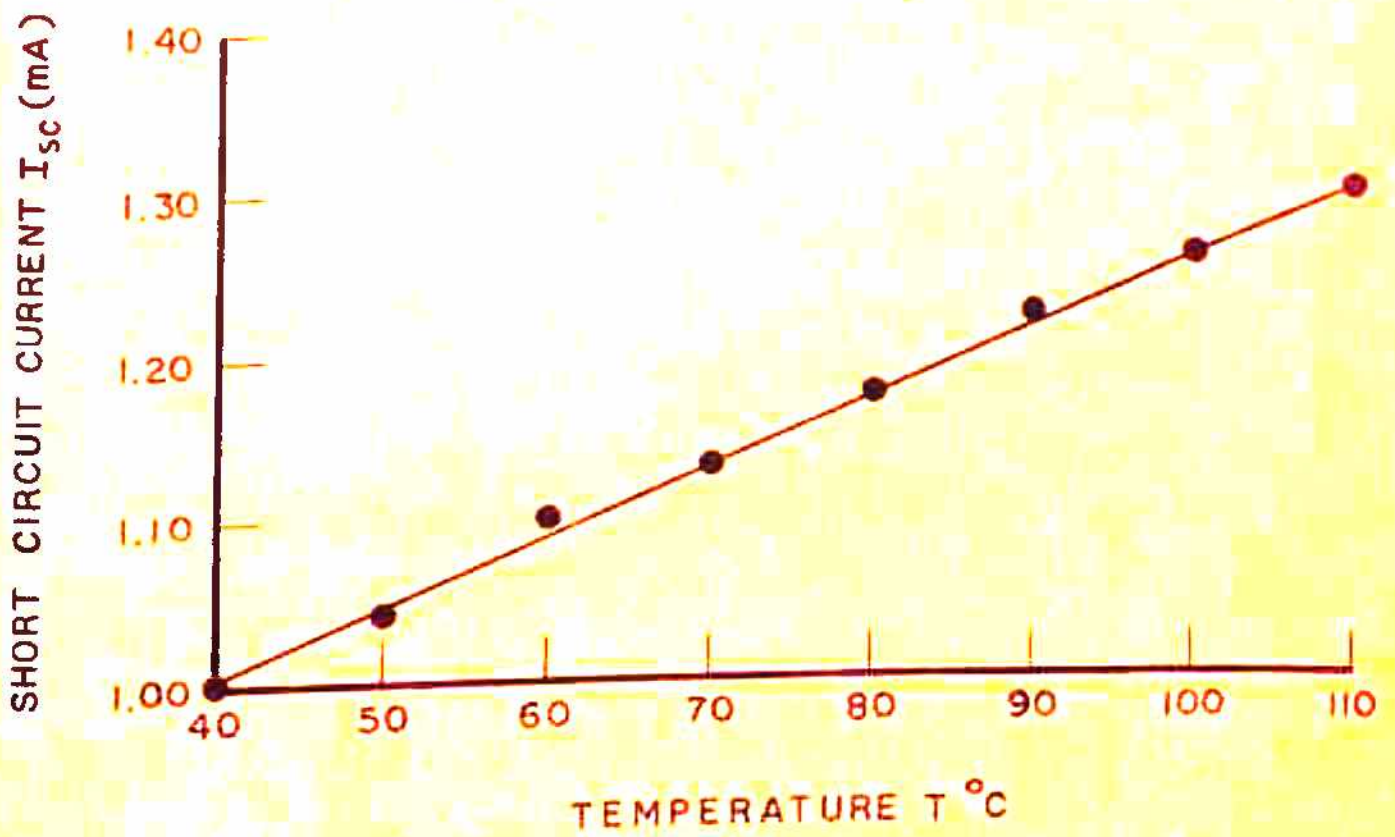


FIG. 3.3 EFFECT OF TEMPERATURE ON SHORT CIRCUIT CURRENT.

where g is the generation rate given by $\propto n_{ph} e^{-\alpha x}$, where n_{ph} is the effective number of photons, x is the distance from the top where the electron-hole pairs are generated, α is the absorption coefficient of the semiconductor and L_n and L_p are the diffusion lengths for minority carrier electrons and holes. The effective number of photons n_{ph} and the absorption coefficient α are determined by the energy gap of the semiconductor while the diffusion lengths of electrons and holes are determined by the mobility, diffusion coefficient and the minority carrier life time. In the case of silicon, the energy gap of the semiconductor decreases with increase in temperature (18). This decrease in energy gap with increase in temperature also affects the absorption coefficient as given by the relation (14)

$$\alpha(\nu, T) = (1.28 \times 10^3 \coth \frac{212}{2T} + 1.13 \coth \frac{670}{2T}) (h\nu - E_g)^2 \quad (3.6),$$

where h is the Planck's constant and ν is the average frequency of the incident radiation. From equation (3.6) it seems that the absorption coefficient α increases with increase in temperature. The variation of α with temperature as given by equation (3.6) is shown in Figure (3.4).

The decrease in energy gap E_g due to increased temperature also increases the effective number of photons as shown

by Wolf⁽¹⁹⁾. The empirical relation to express n_{ph} as a function of energy gap and the total number of photons is given by⁽²⁰⁾

$$n_{ph} = N_{ph} e^{-1.6E_g} \quad (3.7)$$

Where N_{ph} is the total number of photons. It appears from equation (3.7) that the effective number of photons increases with decrease in energy gap. This variation (E_g versus temperature) is also shown in Figure (3.4).

The generation rate in the solar cell is given by

$$g = \alpha n_{ph} e^{-\alpha x} \quad (3.8)$$

In the present case the junction depth is of the order of 1 micron. Most of the electron-hole pairs are generated within a very short distance of the p-n junction due to incident photons. Equation (3.8) shows that the generation rate increases with increase in absorption coefficient α and the effective number of photons n_{ph} . In the present case (p/n junction silicon solar cell), the doping density of the base region is of the order of 10^{17} donors/cm³ and diffused layer is highly doped, having a concentration of 5×10^{19} acceptors/cm³. In the case of silicon the mobility of the minority carrier holes μ_h in the n base region decreases with increase in temperature and the mobility of minority carrier electrons in the doped layer remains

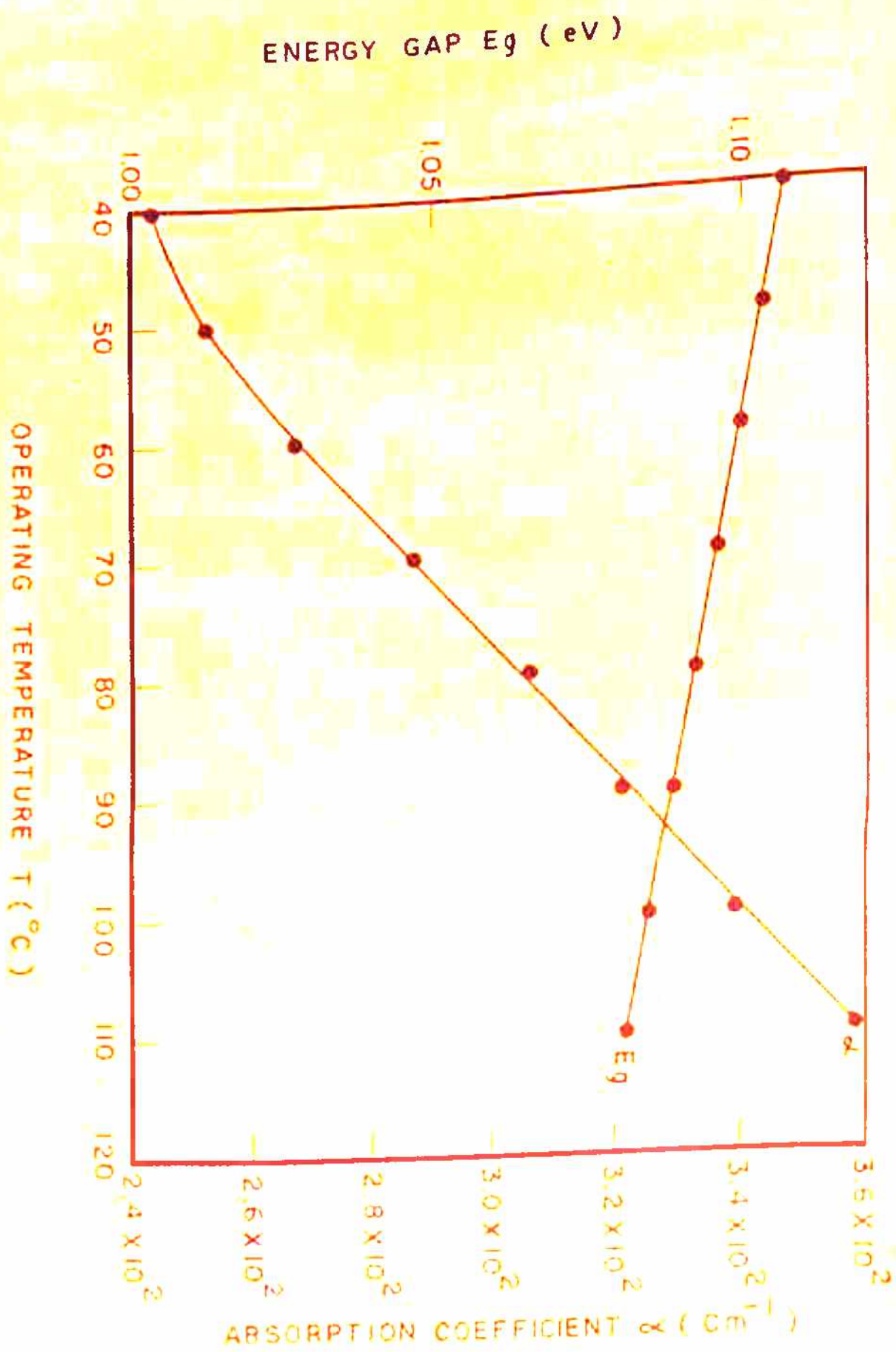


FIG. 3.4 CALCULATED VALUES OF ENERGY GAP E_g AND ABSORPTION COEFFICIENT α FOR VARIOUS VALUES OF TEMPERATURE.

nearly constant over the experimental temperature range $40^{\circ}\text{C} - 110^{\circ}\text{C}$ ⁽²¹⁾. Variations of μ_n and μ_p with temperature are shown in Figure (3.5). The diffusion coefficient is given by the relation $D = \frac{kT}{e} \mu$, where μ is the mobility. The variations of D_n and D_p with temperature are also shown in Figure (3.5). The diffusion length of the minority carriers, given by $(D\tau)^{1/2}$, depends upon their diffusion coefficient D and life time τ . The temperature dependence of the minority carrier life times in p and n regions are given by the following expressions ⁽¹³⁾

$$\tau_n = \tau_{no} + \tau_{po} \exp \left[\frac{E_t - E_f - 2E_i}{kT} \right] \quad (3.9a)$$

and

$$\tau_p = \tau_{po} \left[1 + \exp \left(\frac{E_t - E_f}{kT} \right) \right] \quad (3.9b)$$

where E_f is the Fermi level, E_t is the trap level and E_i is the intrinsic Fermi level. The temperature dependence of the minority carrier lifetime arises from the exponential terms in the equations 3.9a and 3.9b. If the difference between the Fermi level E_f and the trap level E_t is large compared to kT , the exponential terms in equations (3.9a) and (3.9b) are negligible and remain negligible as the temperature is increased until E_f is within a few kT of E_t . The exact position of the trap level not being known, the trap level is assumed to be

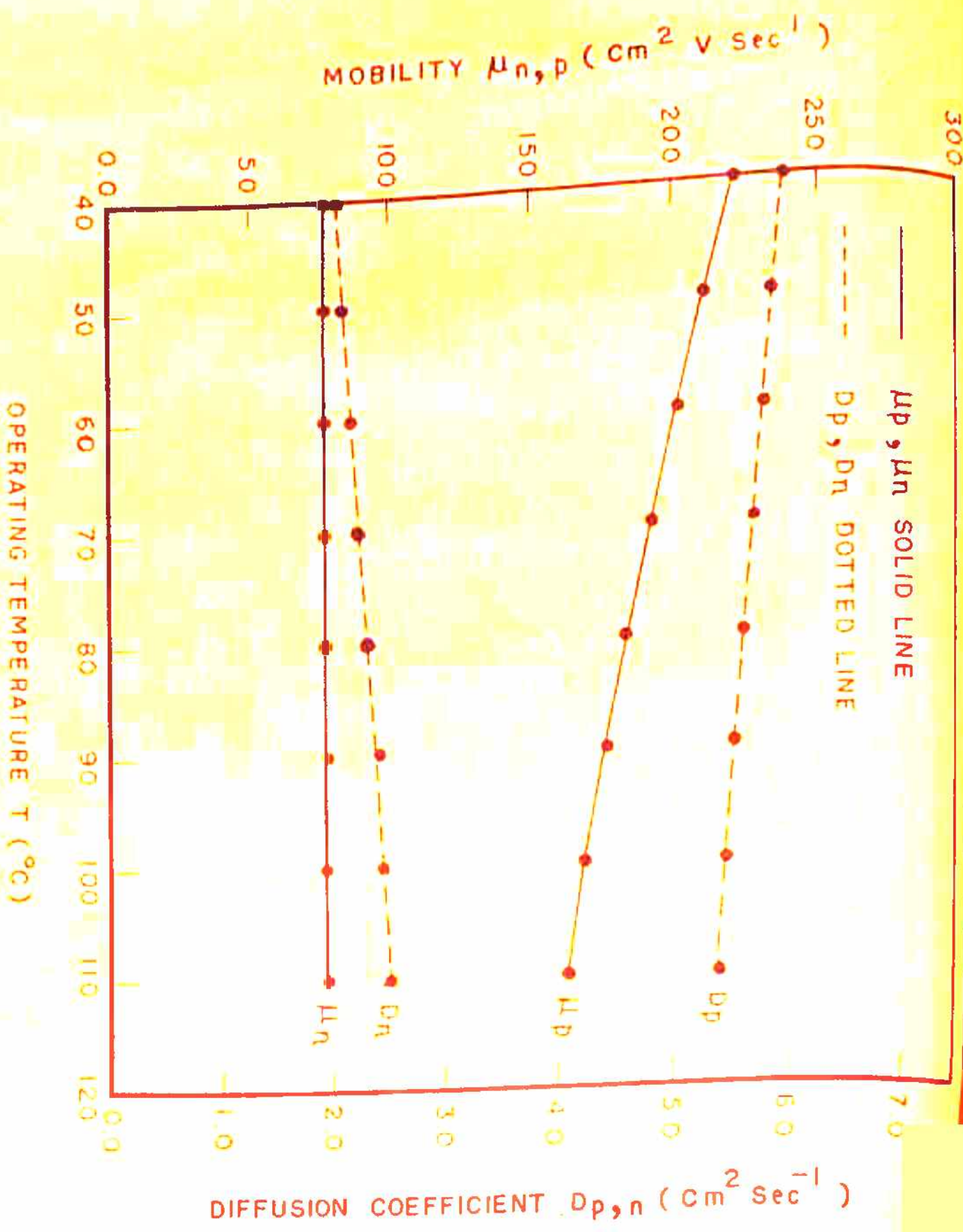


FIG. 3.5 CALCULATED VALUES OF MOBILITY AND DIFFUSION COEFFICIENT $D_{p,n}$ FOR VARIOUS VALUES OF TEMPERATURE

located at the intrinsic Fermi level for convenience in performing calculations. That is, the effect of temperature on minority carrier life times in the temperature range of 40°C - 110°C is regarded as negligible. Thus, an increase in temperature decreases μ_h , which nearly varies at $T^{-2.5}$ in the base region and which in turn causes the diffusion coefficient $D_h (= \frac{kT}{e} \mu_h)$ to decrease. This results in a decreased diffusion length for holes as given by $L_p = (D_p \tau_p)^{1/2}$ for constant value of minority carrier life time τ_p . However, the mobility of electrons in the diffused layer, which is highly doped, is independent of temperature. The diffusion coefficient $D_n = \frac{kT}{e} \mu_n$ increases as appears from the expression for diffusion coefficient. The increase in diffusion coefficient D_n causes an improvement in the diffusion length $L_n = (D_n \tau_n)^{1/2}$ for constant minority carrier life time τ_n with temperature. However, for highly doped p region, the minority carrier life time τ_n and the mobility μ_h are much smaller compared to the minority carrier life time τ_p and mobility μ_n in the base region. Thus, for larger values of minority carrier life time τ_p and mobility μ_h , the diffusion length L_p will also be very much larger than the diffusion length L_n in the highly doped diffused region. Thus, the contribution to the short circuit current I_{sc} is mostly arising from the diffusion length for holes. Thus equation (3.5) can be approximately written as $I_{sc} \approx qg L_p$. However, the short circuit current I_{sc} depends upon the product of the generation rate g

and the diffusion length as given by $I_{sc} = eg (L_n + L_p)$. A much larger increase in generation rate accompanied with a lesser decrease in diffusion length appears to be the reason for the increase in short circuit current with temperature.

The calculated values of various parameters such as diffusion length and generation rate for different temperatures are shown in Figure (3.6-3.7). For the calculation of minority carrier life times τ_p and τ_n which are constants and equal to τ_{p0} and τ_{n0} respectively, the empirical relations⁽²²⁾ given below are used,

$$\tau_{n0,p0} = \frac{3.95 \times 10^{-4}}{1 + N_{A,D}/N_{A0,Do}} \text{ see, where } N_{A0,Do} = 7.1 \times 10^{15} \text{ cm}^{-3}. \quad (3.10)$$

Following expressions⁽²³⁾ are used for determining μ_h and μ_n :

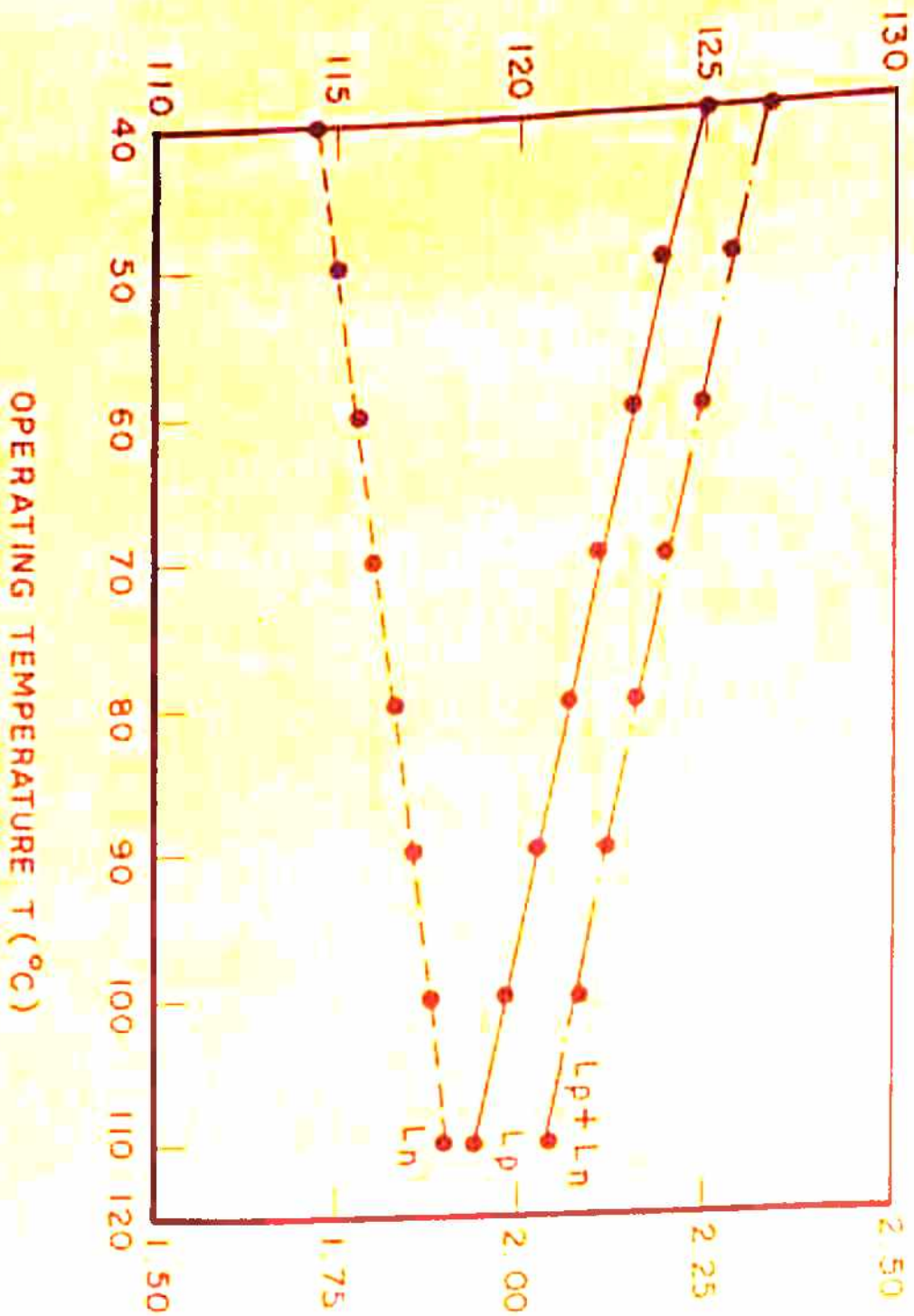
$$\mu_h = 47.7 + 447.3 / [1 + (N_D / 6.3 \times 10^{16})^{0.76}] \text{ cm}^2 \text{V}^{-1} \text{ sec}^{-1} \quad (3.11a)$$

and

$$\mu_n = 65 + 1265 / [1 + (N_A / 8.5 \times 10^{16})^{0.72}] \text{ cm}^2 \text{V}^{-1} \text{ sec}^{-1} \quad (3.11b)$$

The variation of $I_{sc}(T)/I_{sc}(313)$ with temperature for observed and calculated values is shown in Figure (3.8). The calculated and observed $I_{sc}(T)/I_{sc}(313^\circ\text{K})$ values with temperature exhibit a similar trend, namely that of an increase of $I_{sc}(T)/I_{sc}(313^\circ\text{K})$ with temperature.

DIFFUSION LENGTH FOR HOLES L_p (μm) AND $L_n + L_p$ (μm)



DIFFUSION LENGTH FOR MINORITY CARRIER ELECTRONS L_n (μm)

FIG. 3.6 CALCULATED VALUES OF MINORITY CARRIER DIFFUSION LENGTHS FOR VARIOUS VALUES OF TEMPERATURE.

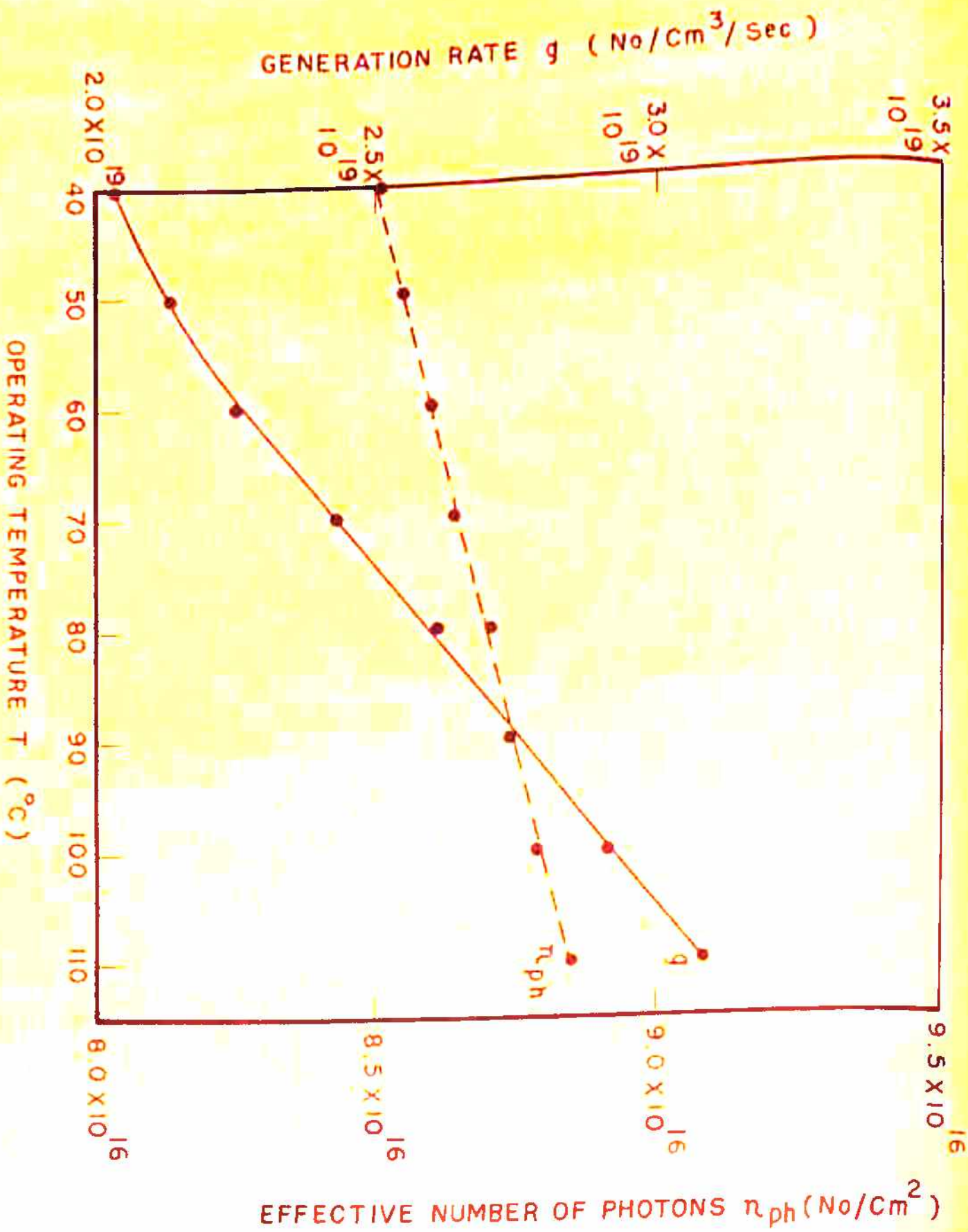


FIG 3.7 CALCULATED VALUES OF GENERATION RATE g AND EFFECTIVE NUMBER OF PHOTONS FOR VARIOUS VALUES OF TEMPERATURE.

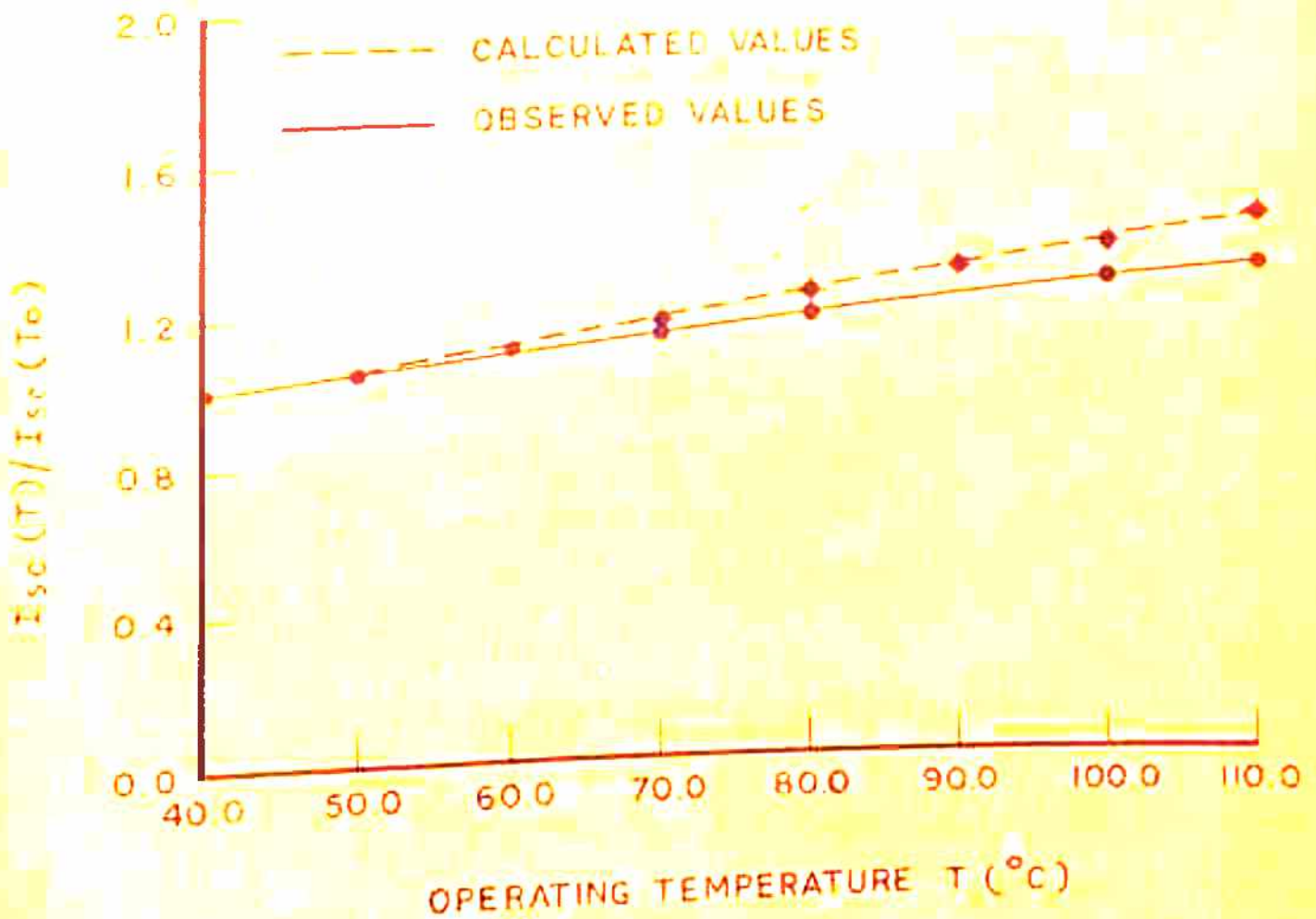


FIG. 3.8 COMPARISON OF CALCULATED AND OBSERVED VARIATION OF $I_{sc}(T)/I_{sc}(T_0)$ FOR VARIOUS VALUES OF TEMPERATURE.

3.3.3 EFFECT OF TEMPERATURE ON REVERSE SATURATION CURRENT I_0 :

The variation of reverse saturation current I_0 is shown in Figure (3.9). The Figure (3.9) shows that the reverse saturation current I_0 increases with temperature. It is seen from the figure (3.9) that the rate of increase in the reverse saturation current I_0 with temperature is small in the initial stages and this rate increases at higher temperatures. In general the dark current I_{Dark} , which opposes the photogenerated current I_{ph} , is given by

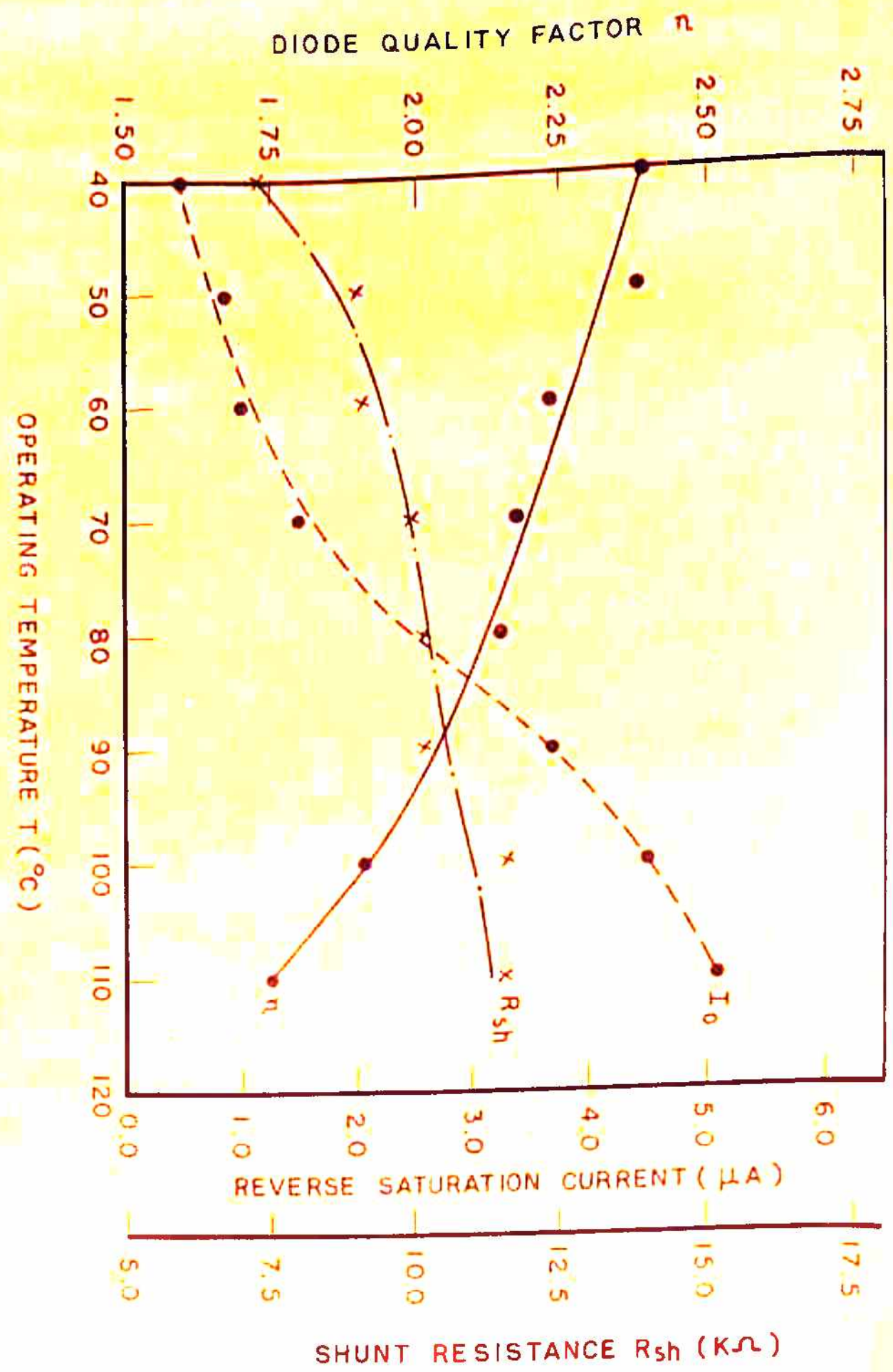
$$I_{\text{Dark}} = \sum_j I_{j0} \left[e^{eV/n_j kT} - 1 \right] \quad (3.12)$$

Where the summation is used to indicate that more than one mechanism may determine the dark current. Each of the components of the dark current is the result of definite processes occurring in the device. In addition to the ideal diffusion current ($n_j = 1$), the most significant contribution is provided by the processes of generation and recombination in the space charge region and also the leakage caused by surface channels. The recombination generation processes in the space charge region yield the value 2 for the diode quality factor n_j . The presence of surface channels leads to the leakage current with values of the diode quality factor n_j (1)

$$2 < n_j < 4$$

These channels play the role of a shunt resistance R_{sh} .

FIG 3.9 EFFECT OF TEMPERATURE ON I_0 , R_{sh} AND η



In the present solar cell, which was under study, the diode quality factor has a value greater than 2. Thus, the surface channel effects on the present p-n junction silicon solar cell appear to be appreciable. At low temperatures the surface channels seem to be quite active and affect the current voltage characteristics of the solar cell. The surface channels in the device are fixed and as the temperature increases, the increase in intrinsic carrier concentration increases the influence of the recombination-generation current in the space charge region and the diffusion current. At higher temperature the recombination-generation current in the space charge region and the diffusion current dominates over the leakage current. Thus the effect of leakage current becomes negligible as temperature increases. This can also be seen from Figure (3.9) showing the variation of diode quality factor n and shunt resistance R_{sh} with temperature. The decrease in diode quality factor n and increase in shunt resistance R_{sh} with temperature is the consequence of decreasing the effect of the leakage current and confirms the inference that at higher temperatures the recombination-generation current in the space charge region and the diffusion current dominate over the leakage current.

Figure (3.9) shows that the rate of increase in the reverse saturation current I_0 with temperature increases at higher temperatures. The reverse saturation current I_0 due to recombination generation current in the space charge region and the diffusion current is given by ⁽¹³⁾

$$I_c = I_{oD} + I_{oR} \quad (3.13)$$

$$\text{where } I_{oD} = en_i^2 \left[\frac{1}{N_A} \left(\frac{D_n}{\tau_n} \right)^{1/2} + \frac{1}{N_D} \left(\frac{D_p}{\tau_p} \right)^{1/2} \right] \text{ and}$$

$$I_{oR} = en_i W / (\tau_p \tau_n)^{1/2}$$

Where n_i is the intrinsic carrier density. N_A and N_D are the acceptor and donor densities respectively and W is the width of the depletion region. The reverse saturation current I_{oD} due to diffusion varies as n_i^2 while that due to recombination generation current in the depletion region I_{oR} varies as n_i , where the intrinsic carrier density n_i varies with temperature according to $T^{3/2} \exp(-E_g/2kT)$.

With further increase in temperature, the number of thermally generated carriers increases and the number of trapping centers which are quite active and available in the depletion region does not change with temperature. Therefore the ratio of the concentration of thermally generated carriers to the trapping centers increases with further rise in temperature. As a result, the relative effectiveness of trapping centers for recombination decreases with rise in temperature. Although, this results in increasing the diffusion current and also generation recombination current but the increase in diffusion current is more as compared to recombination-generation current in the depletion region for higher values of temperature. The

diffusion current which depends on n_i^2 has a temperature dependence $T^3 \exp(-E_g/kT)$ while the current due to recombination generation in the depletion region varying as n_i has a temperature dependence of $T^{3/2} \exp(-E_g/2kT)$. The ratio of these two is given by

$$\frac{I_{oT}}{I_{oD}} \approx \frac{\exp(-E_g/2kT)}{T^{3/2}} \quad (3.14)$$

This shows that at higher values of temperature I_{oD} is the dominant term in I_o . A much larger increase in I_{oD} compared to I_{oT} and an almost near suppression of the leakage current with temperature is responsible for the observed behaviour of I_o versus temperature.

3.3.3 EFFECT OF TEMPERATURE ON OPEN CIRCUIT VOLTAGE V_{oc} , FILL FACTOR FF, AND MAXIMUM POWER P_{mp} :

The variation of open circuit voltage with temperature is shown in Figure (3.10). It shows that the open circuit voltage V_{oc} decreases with increase in temperature. The open circuit voltage of a solar cell is given by

$$V_{oc} = V_T \ln \left(\frac{I_{ph}}{I_o} + 1 \right) \quad (3.15)$$

where $V_T = nkT/e$. The three factors, the thermal voltage V_T , the photogenerated current I_{ph} and the reverse saturation

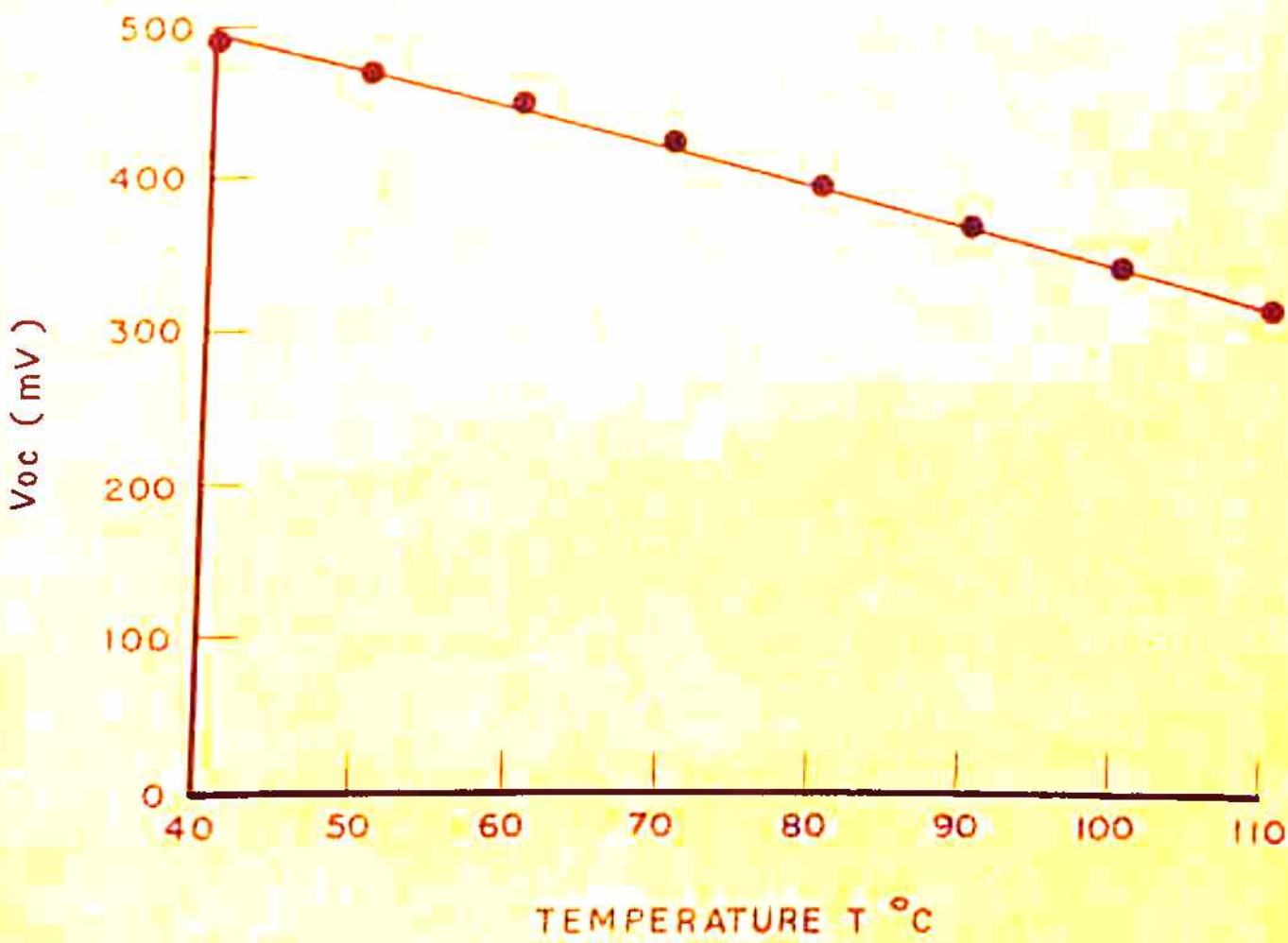


FIG.3.10 EFFECT OF TEMPERATURE T ON OPEN CIRCUIT VOLTAGE Voc.

current I_0 determine the open circuit voltage V_{oc} . The thermally generated intrinsic carriers increase the reverse saturation current I_0 . At the same time the photogenerated current I_{ph} also increases with T . The thermal voltage V_T depends upon n and T and both n and T appear in the numerator in the expression for V_T . Increase in temperature does not affect V_T much. This is because V_T decreases due to decrease of n with T whereas at the same time V_T increases with T as it contains T in the numerator. The increase in I_0 appears to be stronger with T than the increase in the photogenerated current I_{ph} and the net result seems to be a decrease of V_{oc} with temperature (Figure 3.10).

The variations of fill factor FF and the maximum power P_{mp} with temperature T are shown in Figures(3.11,3.12). The Figures(3.11, 3.12) show that the fill factor and the maximum power P_{mp} decrease with increase in temperature. The fill factor of the solar cell is defined as the ratio $V_{mp} \times I_{mp} / (V_{oc} \cdot I_s)$. Where V_{mp} and I_{mp} correspond to the voltage and current at the maximum power point in the current voltage characteristics. The maximum power P_{mp} can be obtained from the area of the maximum power rectangle in the I - V characteristics of the cell. The area of the maximum power rectangle in the I - V characteristics of the cell is determined by the power generating current I flowing through the device and the voltage developed in the solar cell. As the temperature increases, the increase in the reverse saturation

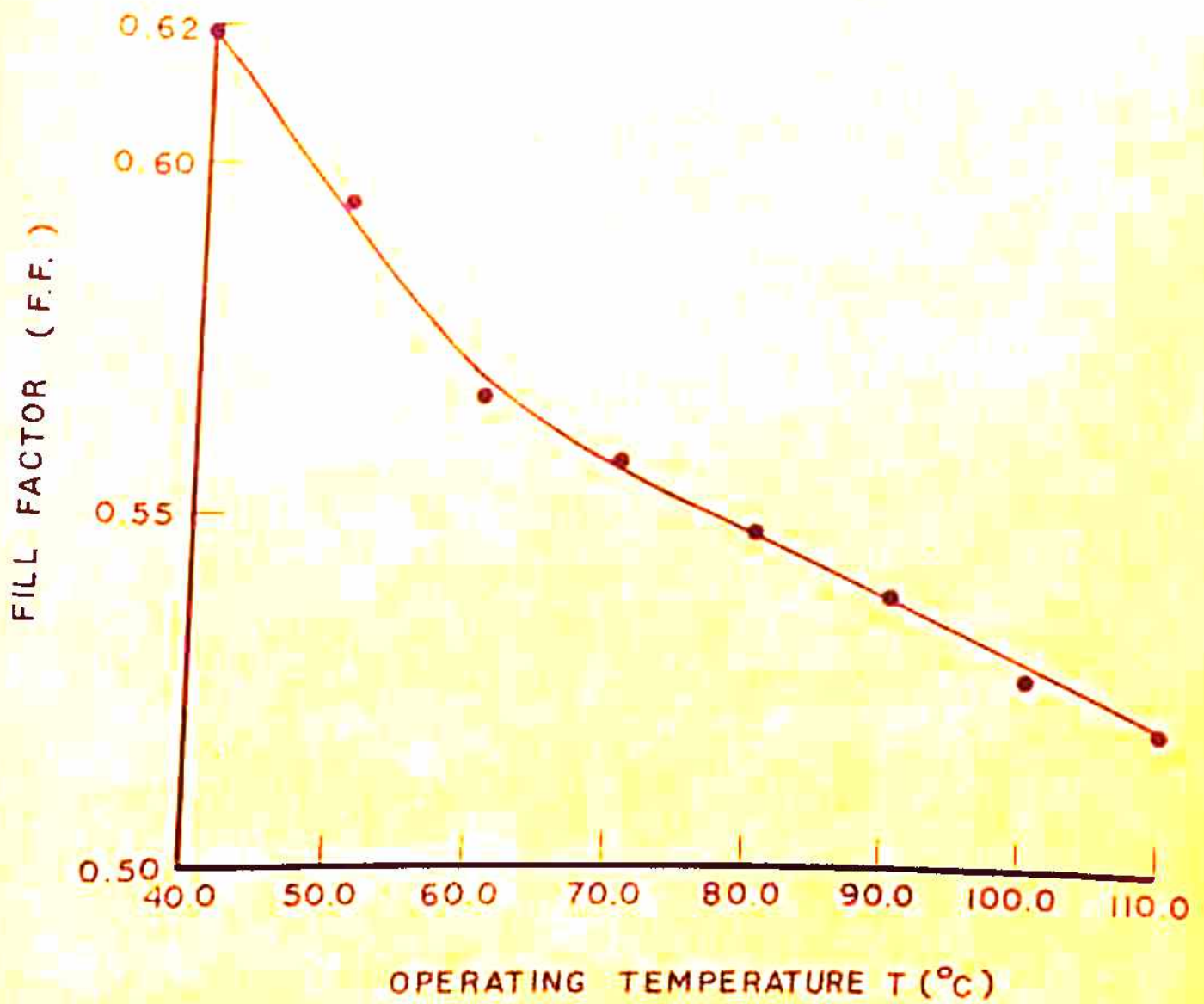


FIG.3.11 EFFECT OF TEMPERATURE ON FILL FACTOR F.F.

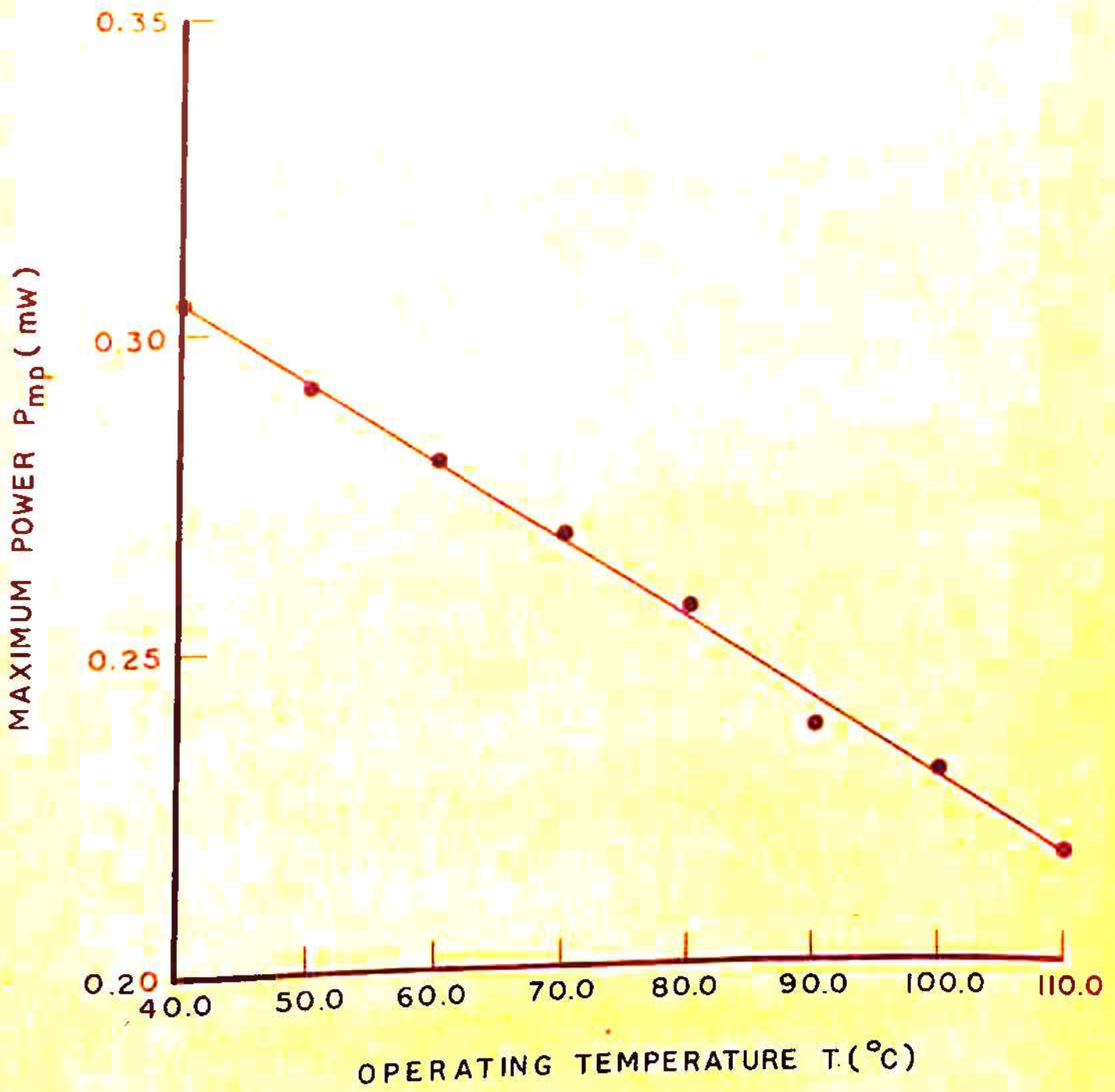


FIG. 3.12 EFFECT OF TEMPERATURE ON MAXIMUM POWER P_{mp} .

current (as shown in Figure (3.9)) results in an increase in the dark current. The increase in dark current results in a decrease in the power generating current I flowing through the device and the decrease in voltage V developed in the cell. Thus the decrease in maximum power P_{mp} and the fill factor are mainly due to increase in the reverse saturation current I_0 , which results in an increase in the dark current and decrease in the area of the maximum power rectangle in the I-V characteristics.

3.3.4 EFFECT OF TEMPERATURE ON INTERNAL SERIES RESISTANCE R_s :

The variation of series resistance R_s with temperature is shown in Figure (3.13). The figure shows that the series resistance decreases with T . Increase of temperature has two effects on the semiconductor. Firstly, in the case of silicon, the bandgap decreases with rise in temperature which results in the generation of more carriers. Secondly, the increase in temperature affects the relaxation time which increases the resistivity of the semiconductor. The mobility μ is generally determined by acoustic phonon scattering and the ionized impurity scattering. The variation of mobility with temperature for silicon shows that at higher temperature (operating temperature in the present case) the mobility is dominated by lattice scattering mechanism. It decreases as temperature increases

as appears from ^{the} equation ⁽²⁴⁾ given below:

$$\mu_L = \frac{(8\pi)^{1/2} e h^4 C_{11}}{3 E_{ds} m^{*5/2} (kT)^{3/2}} \quad (3.16)$$

Where C_{11} is the average longitudinal elastic constant of the semiconductor, E_{ds} the displacement of the edge of the conduction band edge per unit dilation of the lattice and m^* is the conductivity effective mass. The resistivity is given by

$$\rho = \frac{1}{e N_{D,A} \mu_{h,n}} \quad (3.17)$$

Since mobility of the silicon decreases with temperature, the resistivity will increase with temperature as appears from expression (3.17).

The internal series resistance R_s arises on account of a number of factors. These are the resistance due to metallic electrodes and contact between the base and the metal, the resistance of the base layer and the resistance due to doped layer and grids. These various contributions to R_s have been calculated theoretically and presented in Figure (3.13). In the present case the maximum contribution to R_s arises from the contact between the base and the metal. The contact area of the solar cell is very small and it appears that in the small

area solar cell employed, the major contribution is from the contact resistance. This factor decreases with increasing T as shown by the equation⁽²⁵⁾

$$R_{ocbe} = \frac{4 kT/e}{e n_o \bar{v}_n T_{re} A} e^{\phi_o/kT} \quad (3.18)$$

where \bar{v}_n is the average thermal velocity of electrons ($\bar{v}_n = \sqrt{\frac{3kT}{m}}$), n_o the concentration of majority carriers, ϕ_o is the surface barrier, A is the area of the solar cell and T_{re} is the transmission factor of the electrons. The parameters used for the theoretical calculations of the various components contributing to R_s are presented in table 3.1. The decrease in series resistance with increase in temperature, as shown in Figure (3.13), seems to arise from the decrease in the contact resistance contributing to ^{the} total internal series resistance R_s .

The variation of series resistance R_s with temperature agrees with theoretical calculations as far as the trend of decrease with temperature is concerned (Figure 3.13).

3. 4 EFFECT OF CONCENTRATION OF INCIDENT SOLAR RADIATION:

In recent years the theory and fabrication of photovoltaic devices have revealed promising approach to the optimum design and development of solar cells, involving the conversion

TABLE-3.1

The various data used for the calculation of series resistance components

Junction depth	= 0.3 - 0.5 μm
Mass of the electron m	= 9.10×10^{-31} kg.
Boltzmann's constant k	= $1.38 \times 10^{-23} \text{ Joul}^\circ\text{K}^{-1}$
Electronic charge e	= 1.602×10^{-19} Coul.
Surface barrier ϕ_0 (26)	= 0.20 eV
Base resistivity	= 0.10 ohm cm.
Donor density N_D	= $1.0 \times 10^{17} \text{ cm}^{-3}$
Transmission coefficient T_{re}	= 0.01
The cell area	= 0.0434 cm^2
Base thickness	= 150 - 200 μm
Thickness of the back electrode	= 1 μm
Resistivity of Aluminium	= 2.9×10^{-6} ohm cm
Spacing between two legs	= 6.3 mil
Width of aluminium finger	= 10 μm
Sheet resistance	= $200 \Omega/\square$ - 300 Ω/\square
Carrier concentration of the doped layer	= $10^{19} / \text{cm}^3$ - $5 \times 10^{19} / \text{cm}^3$

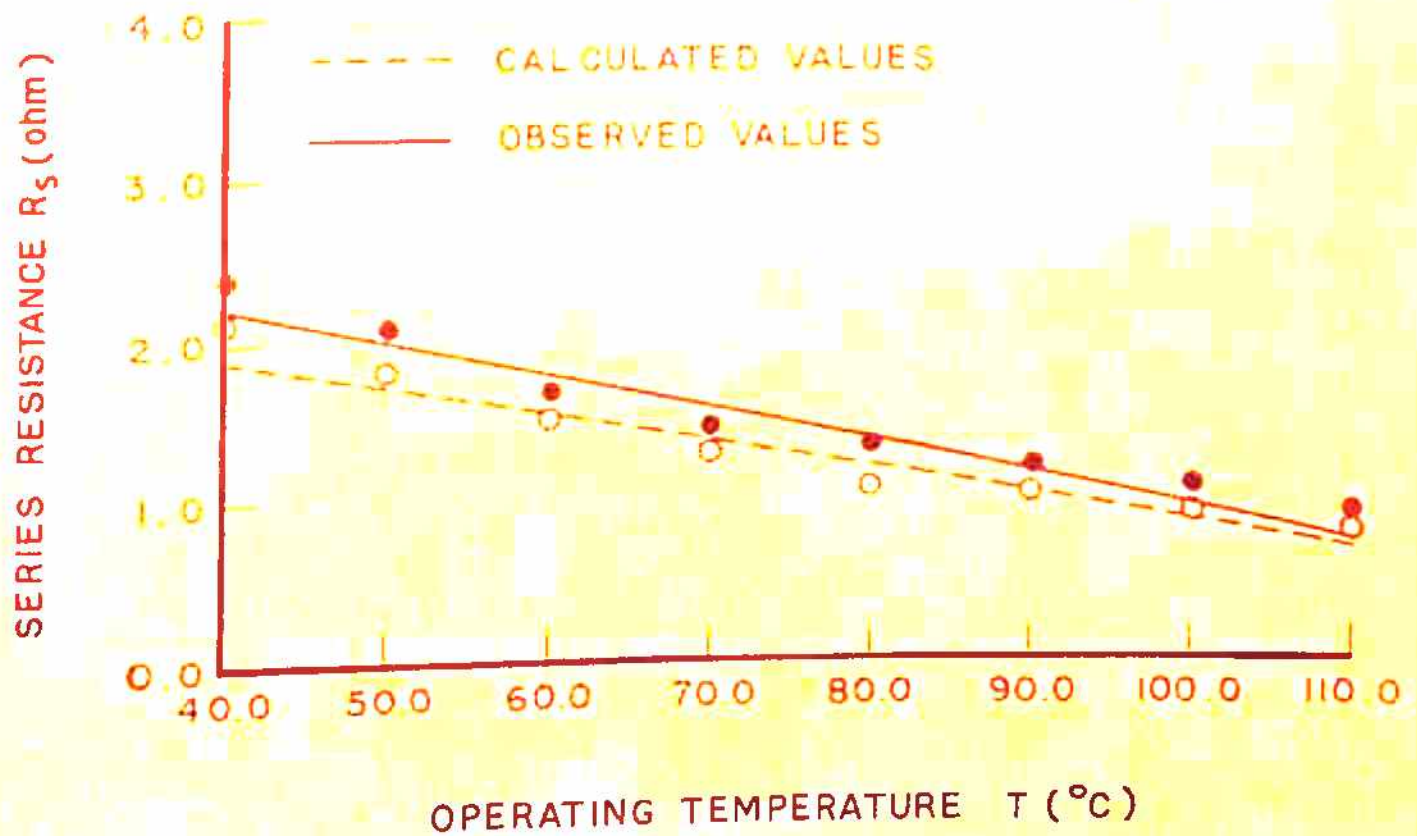


FIG. 3.13 EFFECT OF TEMPERATURE ON SERIES RESISTANCE R_s .

of strongly concentrated solar radiation⁽²⁷⁻⁴¹⁾. When the solar cells are operated under strong illumination, a number of physical phenomena appear that markedly alter the picture of the current carrier diffusion and the photovoltaic effect. Experimental work at high light intensities lagged behind the theoretical work. The earlier high intensity experiments on silicon solar cells were made by Pfeiffer et al⁽⁴²⁾. The measurements were performed for illumination levels upto 17.5 W/cm^2 . Further Sandstrom⁽⁵⁾ studied the effect of intensity varying from 5 mW/cm^2 to 250 mW/cm^2 on n/p silicon solar cells with different values of cell thickness. Hovel⁽¹²⁾ also described the behavior of the solar cell under higher intensity environment and reviewed the work carried out on solar cells under the influence of intense light. However, a detailed analysis and experimental results are not available describing the effect of concentrated sunlight on various parameters which determine the performance of the solar cell. The present work, a part of which was also presented in the National Solar Energy Convention, Bhavnagar, 1978⁽⁴³⁾, deals with the effect of concentrated sunlight on various parameters which influence the performance of a solar cell and a possible explanation is presented accounting for the variation of various parameters of the solar cell as a function of concentration of ^{the} incident solar radiation.

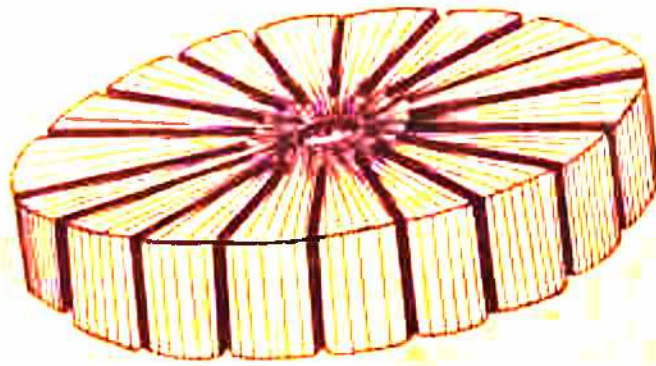
3.4.1 EXPERIMENTAL SET-UP:

The experiments were performed on the same p/n silicon solar cell as the one described earlier, that is, the one used for determination of R_s and for analysing the effect of temperature. To reduce heating of the cell, the cell was surrounded by a heat sink (Figure 3.14). Water circulation was provided to avoid heating of the solar cell. The cell temperature was found to lie in the temperature range of 30.2°C to 32.0°C during the experiment. The incident solar radiation was concentrated using a Fresnel's lens and the current voltage characteristics were obtained for various values of short circuit current varying from 1 mA to 50 mA, I_{sc} being 1 mA at one sun. The various parameters such as internal series resistance R_s , shunt resistance R_{sh} , thermal voltage V_T and the reverse saturation current I_0 were obtained from expressions (3.1), (3.2), (3.3) and (3.4). The current was measured by an electronic multimeter and the voltage was measured by a vernier potentiometer. The experimental set-up is shown in Figure (3.15).

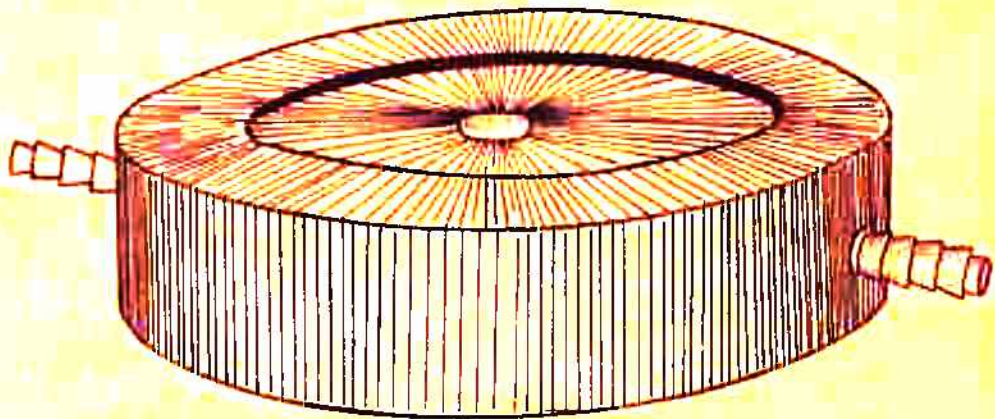
3.5 RESULTS AND DISCUSSION:

3.5.1 EFFECT OF CONCENTRATED SUNLIGHT ON REVERSE SATURATION CURRENT I_0 :

In Figure (3.17) it is shown that initially, the reverse saturation current I_0 does not change with concentration



(a)

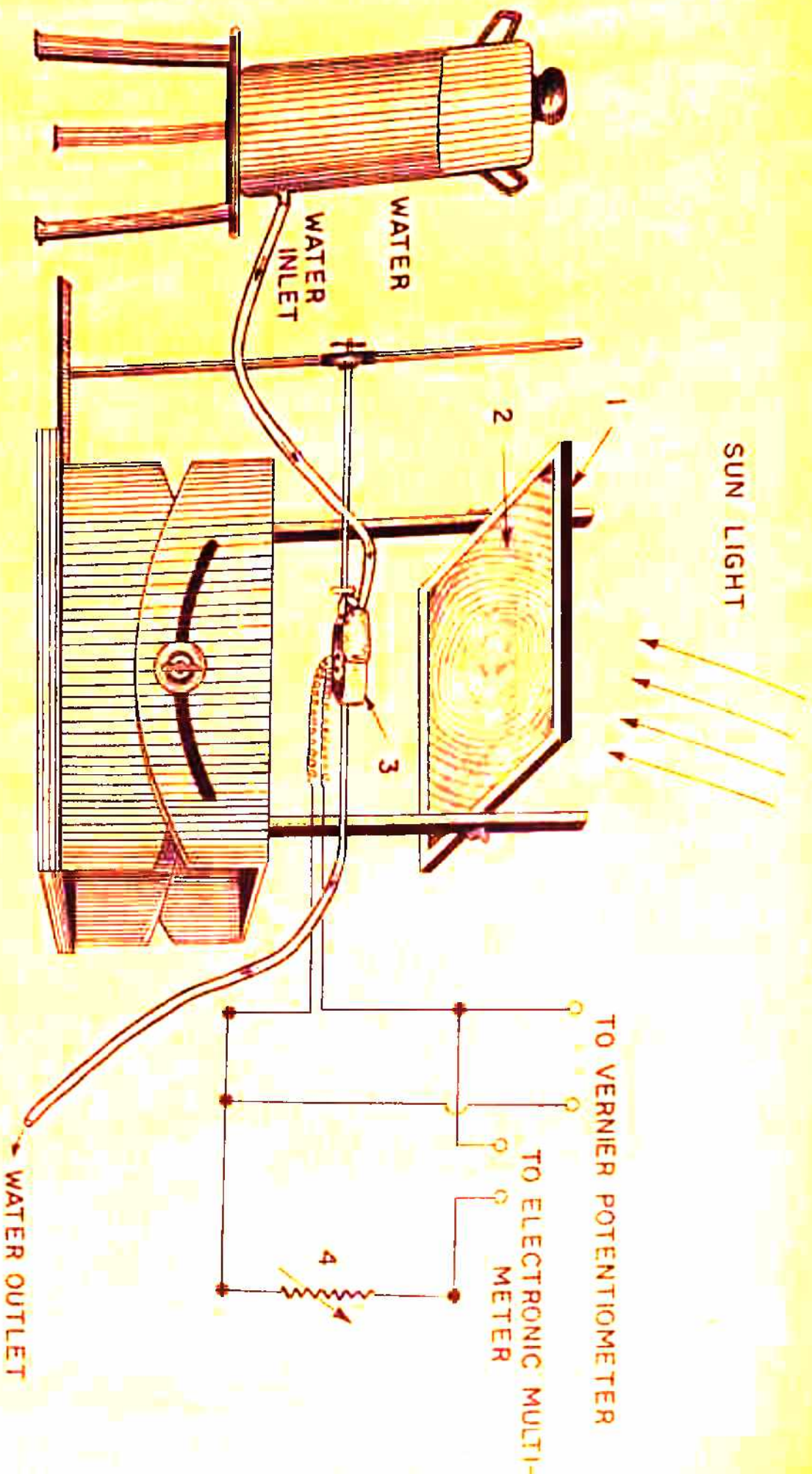


(b)

FIG. 3.14 VARIOUS TYPES OF HEAT SINKS

(a) WITHOUT WATER CIRCULATION

(b) WITH WATER CIRCULATION



(1) STAND (2) FRESNEL'S LENS (3) SOLAR CELL WITH HEAT SINK (4) VARIABLE LOAD

FIG. 3.15 EXPERIMENTAL SET-UP TO STUDY THE EFFECT OF CONCENTRATED SUNLIGHT ON SOLAR CELL PARAMETERS.

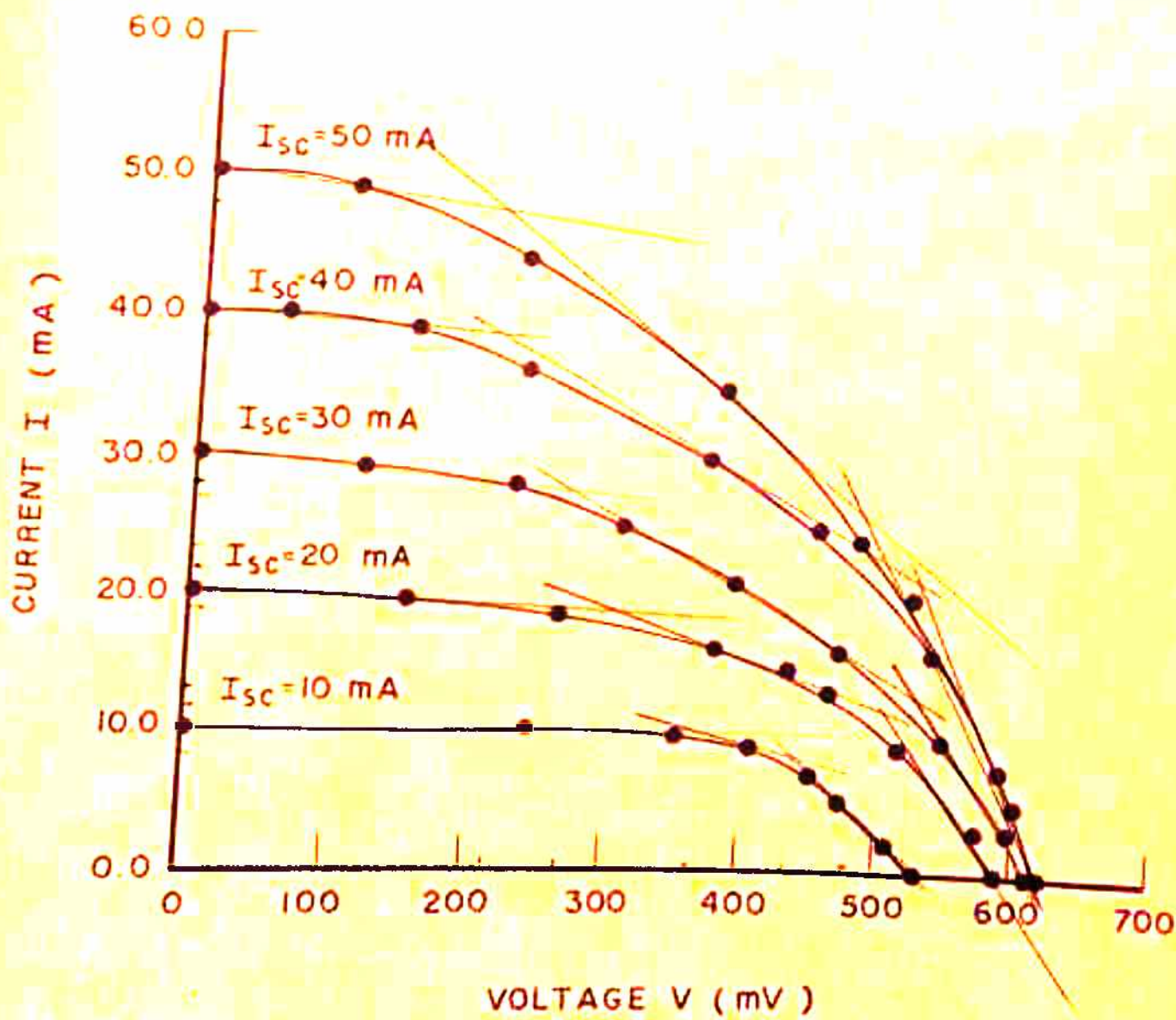


FIG.3.16 CURRENT VOLTAGE CHARACTERISTICS OF p-n JUNCTION SOLAR CELL UNDER CONCENTRATION OF INCIDENT SOLAR RADIATION.

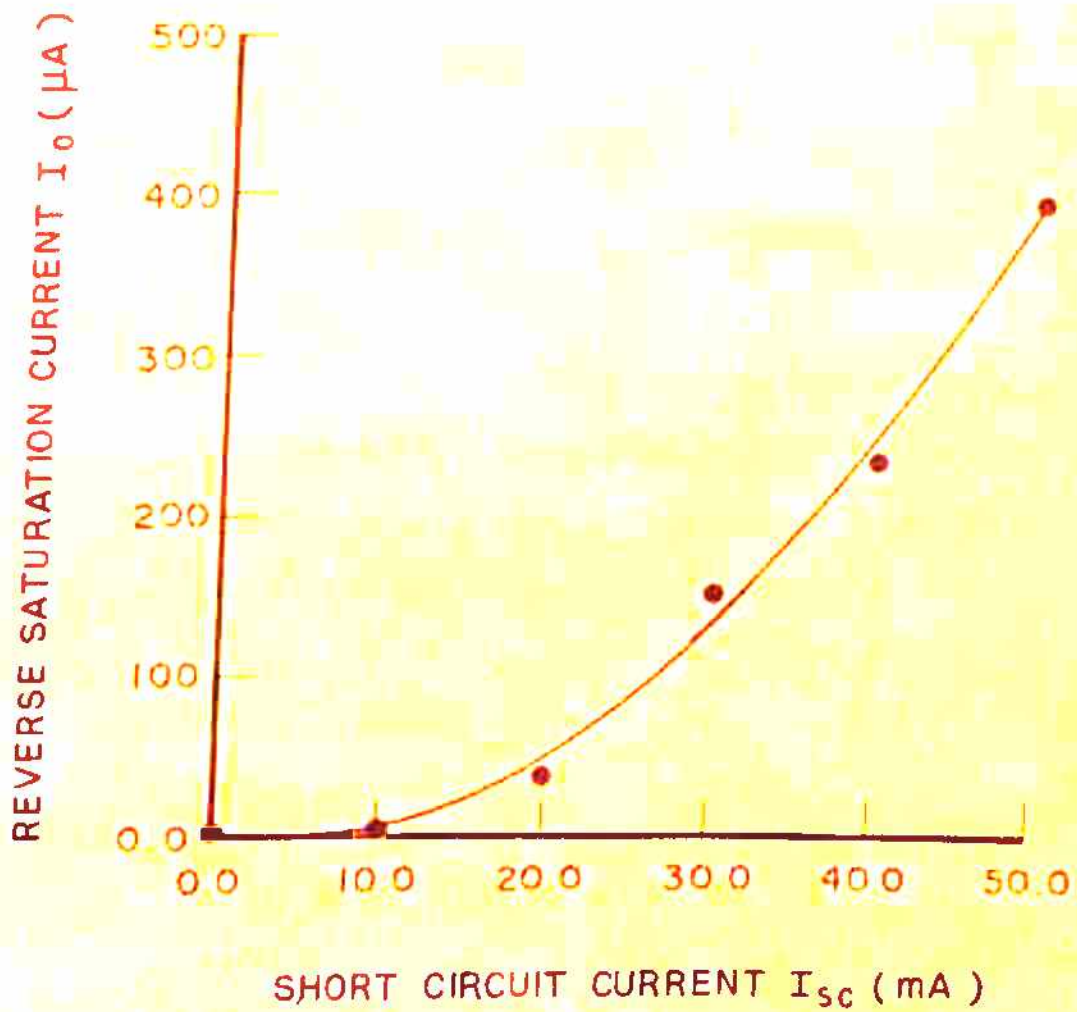


FIG. 3.17 EFFECT OF CONCENTRATION OF INCIDENT SOLAR RADIATION ON REVERSE SATURATION CURRENT I_0 .

the of incident solar radiation upto 10 suns but later on it starts increasing. Howes and Read⁽⁴⁴⁾ have shown that the parameter I_0 is a function of current density. Under concentrated sunlight the simple boundary conditions used in Chapter I for the solution of the continuity equations are no longer valid. This is because of the fact that the concentration of injected minority carriers in the bulk p and n regions near the junction becomes comparable to the equilibrium majority carrier density there. Under such circumstances, the majority carrier distribution, which accompanies the minority carriers to ensure quasi-neutrality, becomes sufficiently dense to seriously perturb the equilibrium value. For such a situation, using exact boundary conditions⁽⁴⁵⁾, the dark current component of the solar cell under concentrated sunlight is given by⁽⁴⁵⁾

$$I_{\text{Dark}} = I'_0 \left[\exp(V/V_T) - 1 \right] \quad (3.19a)$$

where I'_0 is the effective reverse saturation current and is given by

$$I'_0 = \frac{e p_{no} D_p^*}{L_p^*} \left(1 + \frac{n_i^2}{p_{po}^2} e^{eV/kT} \right) + \frac{e n_{po} D_n^*}{L_n^*} \left(1 + \frac{n_i^2}{n_{no}^2} e^{eV/kT} \right) \\ 1 - e^{-2e(V_{bi} - V)/kT} \quad (3.19b)$$

where p_{no} and n_{po} are the respective equilibrium hole and electron

concentrations in n and p regions ; L_p^* and L_n^* are the ambipolar diffusion lengths for minority carrier holes and electrons respectively. D_p^* and D_n^* are the ambipolar diffusion coefficients for holes and electrons respectively and V_{bi} is the built-in potential. It appears from the expression (3.19b) that the reverse saturation current I_0' becomes sensitive to the voltage V developed in the solar cell. It is found from the current voltage characteristics of solar cells (Figures 3.16) under concentrated sunlight that the voltage V appearing in the solar cell increases as the intensity of the incident solar radiation increases. According to the expression (3.19b) an increase in voltage V causes an increase in the reverse current I_0' . Thus the observed increase in I_0' with concentration of incident solar radiation appears to be due to the voltage dependence of I_0' at high concentrations.

3.5.2 EFFECT OF CONCENTRATED SUNLIGHT ON OPEN CIRCUIT VOLTAGE V_{oc} AND FILL FACTOR F.F.:

The variation of the open circuit voltage V_{oc} with concentration of incident solar radiation is shown in Figure (3.18). The graph shows that the open circuit voltage V_{oc} first increases with concentration of incident solar cell and later on it saturates. The increase in open circuit voltage in its initial stages with the concentration of incident solar radiation

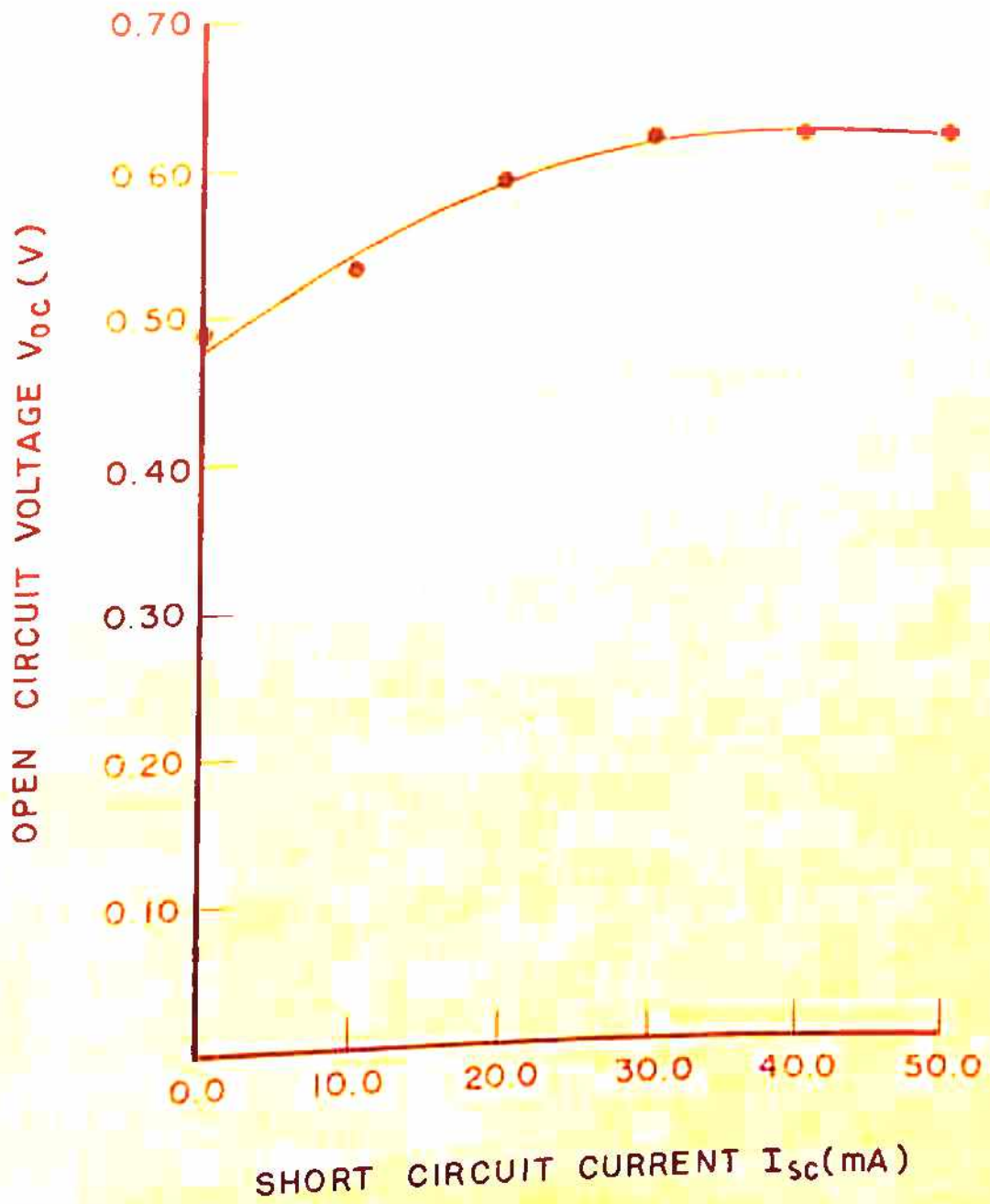


FIG. 3.18 EFFECT OF CONCENTRATED SUNLIGHT ON V_{oc} .

appears because of much larger increase in photogenerated current I_{ph} as compared to changes brought about in I_0 . The saturation of the open circuit voltage V_{oc} for higher concentration of incident solar radiation can be explained by taking into account the changes brought about in the reverse saturation current I_0 at high concentrations. According to equation (3.19b) the reverse saturation current becomes sensitive to the voltage developed by the cell and it increases with increased concentration of incident solar radiation (Figure 3.17). Thus an increase in I_0 at higher concentration causes the open circuit voltage to decrease. Hence, under higher concentration of incident solar radiation the net dependence of concentrations on V_{oc} is to bring about a saturation at high concentrations.

The variation of fill factor with concentration of incident solar radiation is shown in Figure (3.19). The graph shows that the fill factor first increases with concentration of incident solar radiation and after acquiring its maximum it starts decreasing for higher concentrations of incident solar radiation. The fill factor of the solar cell is defined as the ratio of the maximum power point to the product of short circuit current and open circuit voltage, $F.F. = V_{mp} I_{mp} / V_{oc} \cdot I_{sc}$. The increase in fill factor $F.F.$ in its initial stages is mainly due to increase in the open circuit voltage and the photogenerated current I_{ph} which results in a larger area of maximum power rectangle in the current voltage characteristics brought

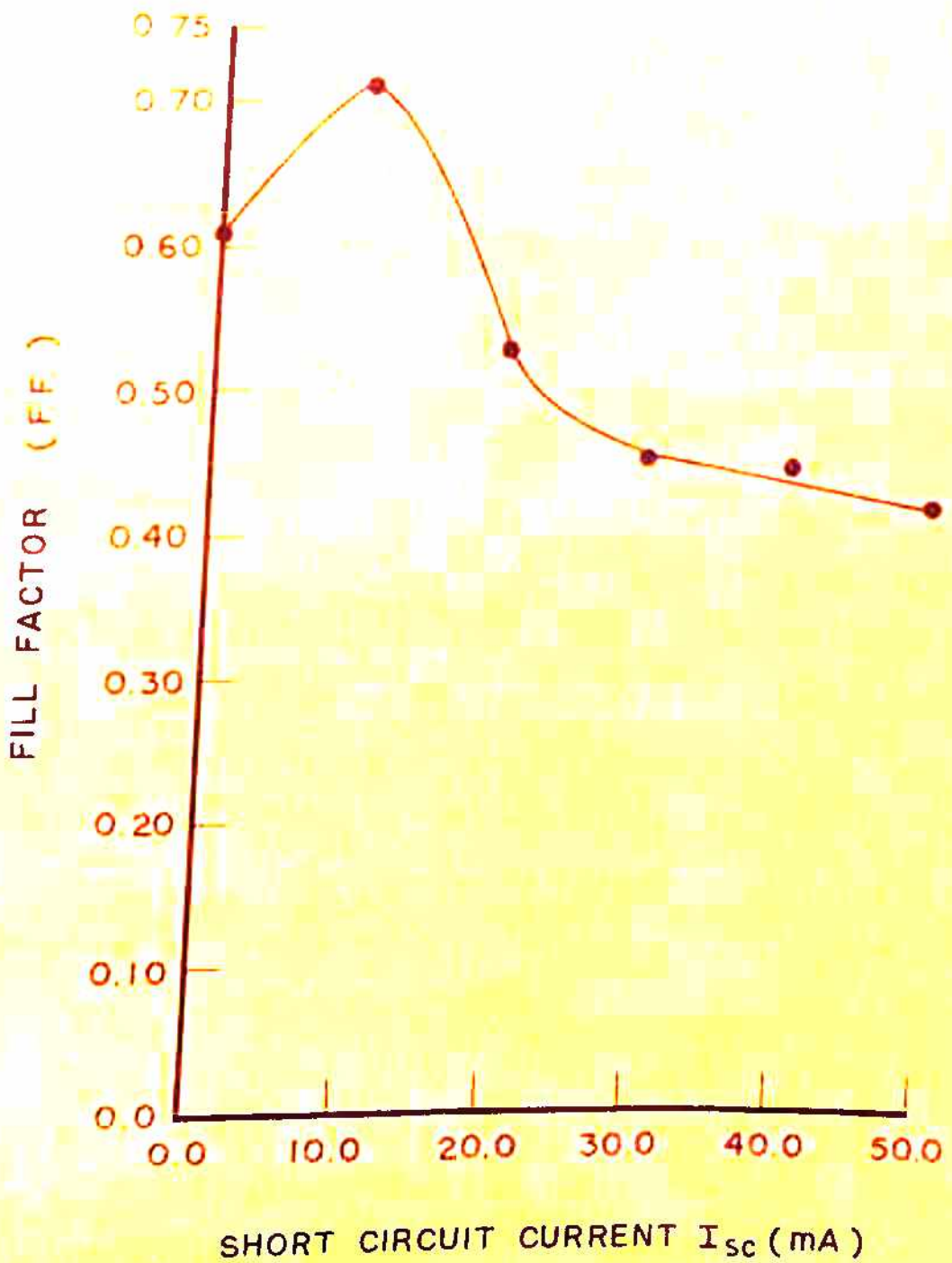


FIG. 3.19 EFFECT OF CONCENTRATED SUNLIGHT ON FILL FACTOR.

about by a decreased internal series resistance R_s values. Later on increase in $I^2 R_s$ loss under higher concentration of incident solar radiation becomes dominant and it seems to cause a reduction of the fill factor.

3.5.3 EFFECT OF CONCENTRATED SUNLIGHT ON INTERNAL SERIES RESISTANCE

R_s :

It is shown in Figure (3.20) that the internal series resistance of the solar cell decreases with concentration of the incident solar radiation. Increased concentration of solar radiation results in larger photogenerated carrier density and lower relaxation time due to collisions. Much larger increase in excess carrier density under concentrated sunlight as compared to decrease in relaxation time results in the decrease of resistivities of the p and n regions. The maximum contribution to the internal series resistance R_s for the solar cell under experimental investigations is mainly due to contact resistance between the base and the back electrode, as discussed in Chapter II. The contact resistance decreases with decrease in resistivities⁽⁴⁶⁾. Thus, the decrease in the resistivity of the base appears to cause a decrease in the contact resistance which in turn decreases the total internal series resistance R_s of the solar cell.

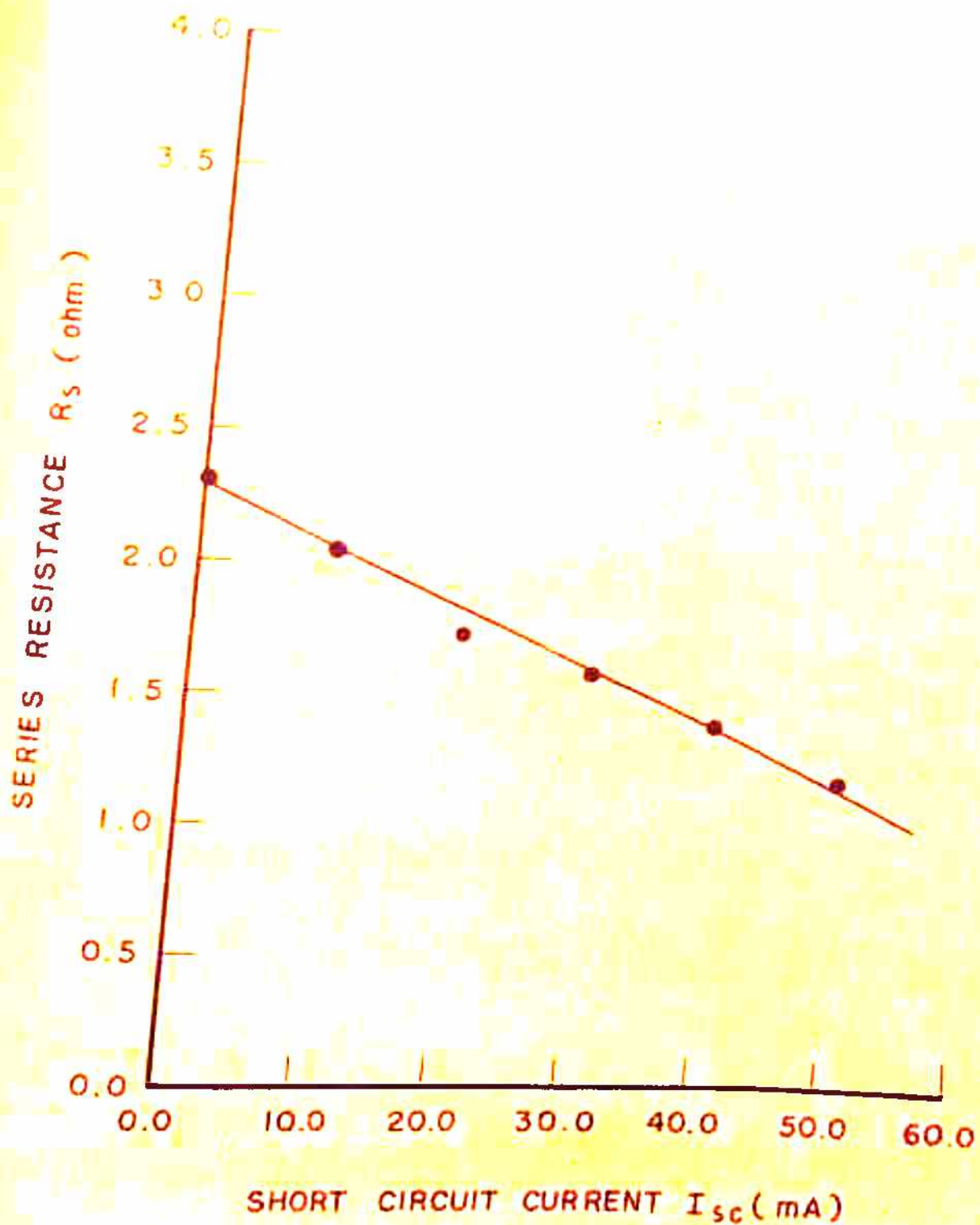


FIG.3.20 EFFECT OF CONCENTRATED SUNLIGHT ON SERIES RESISTANCE .

REFERENCES:

1. V.M. Evdokimov, Applied Solar Energy Vol. 8, No. 6 pp. 63 (1972).
2. K.M. Kennerud, IEEE Trans. On Aerospace and Electronic Systems, Vol. AES 3 pp. 586 (1967).
3. C.H. Liebert, Conference Record of the Seventh photovoltaic specialists conference, IEEE pp 92 (1968).
4. R.J. Lambert, Conference Record of the Seventh photovoltaic specialists conference, IEEE pp 97 (1968).
5. T.D. Sandstrom, Intersociety Energy Conversion Engineering Conference Record, Boulder Colorado pp 138 (1968).
6. C.A. Lewis and J.P. Kirkpatrick, Conference Record of the Eighth IEEE photovoltaic specialists conference pp 123 (1970).
7. Patricia Payne and E.L. Ralph, Conference Record of the Eighth IEEE photovoltaic specialists conference pp 135 (1970).
8. H.W. Brandhorst^S Jr. and R.E. Hurt Jr. Conference Record of the Eighth IEEE photovoltaic specialists conference pp 142 (1970).
9. J.C. Ho, F.T.C. Batels and A.R. Kirkpatrick, Conference Record of the Eighth IEEE photovoltaic specialists conference pp 150 (1970).
10. W. Luft, Conference Record of the Eighth photovoltaic specialists conference pp 161 (1970).
11. W. Luft, IEEE Trans. on Aerospace Electronic System AES-7 pp 332 (1971).

12. H.J. Hovel, Semiconductors and Semimetals (Solar cells) Chapter 8, (1975).
13. J.J. Wysocki and P. Rappaport, J. Appl. Phys. Vol. 31, pp 571 (1960).
14. A Shumka, Conference Record of 8th IEEE photovoltaic specialists conference pp 96 (1970).
15. S.C. Bawa et al. Proc. of the National Solar Energy Convention, Jadavpur (Calcutta) pp 75 (1976).
16. N.K. Swami and H.M. Ghule, Proc. of the Symposium on Electron Devices , CEERI, Pilani pp 114 (1978).
17. A Gremmelmacer, Proc. of IRE Vol. 46 pp 1045 (1958).
18. S.M. Sze, Physics of Semiconductor Devices, A Division of John Wileley and Sons. Chapter 2, (1969).
19. M. Wolf, Proc. IRE Vol. 48, pp 1246 (1960).
20. Manfred Altman, Elements of solid state energy conversion, Van Nostrand Reinhold Company Chapter 4 (1969).
21. Helmut F. Wolf, Silicon Semiconductor Data, Pergamon Press Inc. (1965).
22. J.G. Fossum, Solid State Electronics, Vol. 19, pp 269 (1977).
23. D.M. Caughey and R.E. Thomas, Proc. IEEE Vol. 50, pp 2192 (1967).
24. J. Bardeen and W. Shockley, Phys. Review, Vol. 80, pp. 72 (1950).
25. V.I. Panichevskaya and V.I. Stikhaⁿ, Radio Engng. and Electronics Physics Vol. 20, pp 139 (1975).

26. Dan Dascalu, *Electronic Process in Unipolar Solid State Devices*, Abacus Press Tunbridge Wells, Kent England pp 89 (1977).
27. F. Stezer, *RCA Review* , Vol. 36, pp 316 (1975).
28. R.H. Dean et al, *R.C.A. Review* , Vol. 36 pp 324 (1975).
29. J.G. Fossum and E.L. Burges, *Twelfth Photovoltaic Specialists conference Record* pp 737 (1976).
30. S.R. Dhariwal et al, *IEEE Trans. Electron Devices*, Vol. ED-23 pp 504 (1976).
31. T.T. Tule et al, *Twelfth Photovoltaic Specialists Conference*, pp 744 (1976).
32. J.A. Castle, *Twelfth Photovoltaic Specialists Conference* pp 751 (1976).
33. R.L. Call and W.G. Kerwin, *Twelfth Photovoltaic Specialists Conference* pp 791 (1976).
34. R.G. Ross, *Twelfth Photovoltaic Specialists Conference* pp 801 (1976).
35. R.I. Frank and R. Kalow, *Twelfth IEEE Photovoltaic Specialists Conference* pp 820 (1976).
36. L.S. Napoli et al, *RCA Review*, Vol. 38 pp 76 (1977).
37. L. Dwight Crook and J.R. Yeargan, *IEEE Trans. on Electron Devices* Vol. ED-24 pp 330 (1977).
38. M.D. Lammert and R.J. Schwartz, *IEEE Trans. on Electron Devices*, Vol. ED-24 pp 337 (1977).
39. Chander Goradia and Bernard L. Sater, *IEEE Trans. on Electron Devices*, Vol. ED-24 pp 342 (1977).

40. S.C. Bawa et al, International Solar Energy Congress, New Delhi Abstract No. 28 Vol. 1, pp 426 (1978).
41. Anant G. Sabnis, Solid State Electronics Vol. 21, pp 581 (1978).
42. P. Schoffer and C. Pfeiffer, Trans. of the ASME Vol 85 pp208(1963).
43. N.K. Swami and H.M. Ghule, Proc. of the National Solar Energy Convention, Bhavnagar pp 445 (1978).
44. M.J. Howes and T.G. Read, Proc. IEEE, Vol. 60, pp 329(1972)
45. John P. Mcklvey, Solid State and Semiconductor Physics, Harper and Cow Publishers, Chapter 13 (1966).
46. C. Y. Yang, Y.K. Faug and S.M. Sze, Solid State Electronics Vol. 14, pp 541 (1971).

CHAPTER-IV.

SCHOTTKY BARRIER SOLAR CELLS

4.1	Schottky effect.	115
4.2	Metal-semiconductor contact.	116
4.3	Metal-semiconductor contact rectification.	118
4.4	Expressions for depletion layer width d , built in potential V_{bi} , electric field \mathcal{E} and barrier height ϕ_{Bn}	123
4.5	Charge transport in schottky barriers.	127
4.6	Schottky barrier solar cells.	129
4.7	Aim of the present work in connection with schottky barrier solar cells.	136

CHAPTER-IV.SCHOTTKY BARRIER SOLAR CELLS

The main stress at present in solar energy technology is on the development of cheap and efficient methods for converting incident solar radiation into electrical power. For large scale terrestrial power generation, present technology appears to limit the choice of materials to photovoltaic systems using silicon and cadmium sulphide. This is due to factors such as the availability of appropriate technology and abundance of raw materials. The conventional p-n junction silicon solar cell has had a long history of successful use in many applications, chief among them being the use for space applications. The many well-known advantages of silicon for being used in photovoltaic power systems, include its abundant availability as a raw material, the existence of a well established technology for preparing silicon of desired purity and process of doping and the reliability of the device. The only barrier in the way of current silicon solar cell technology is the cost of these devices. Another device which is drawing the attention of a large number of scientists in recent years is the fabrication of the schottky barrier solar cells⁽¹⁻¹⁵⁾. This is because of the fact that the theoretical limit of the conversion efficiency of these devices can reach that of p-n junction silicon solar cells. Theoretical calculations presented by Mcquat and Pulfrey⁽¹⁶⁾ predicted a maximum efficiency of 25% for schottky barrier solar cells. Schottky barrier solar cells have an additional advantage in terms of cost of production which is quite low compared to the conventional p-n junction silicon solar cells. The present

chapter deals with an introduction to schottky effect, metal-semiconductor contact, the current voltage characteristics of schottky diodes and the theory of schottky barrier solar cells.

4.1 SCHOTTKY EFFECT :

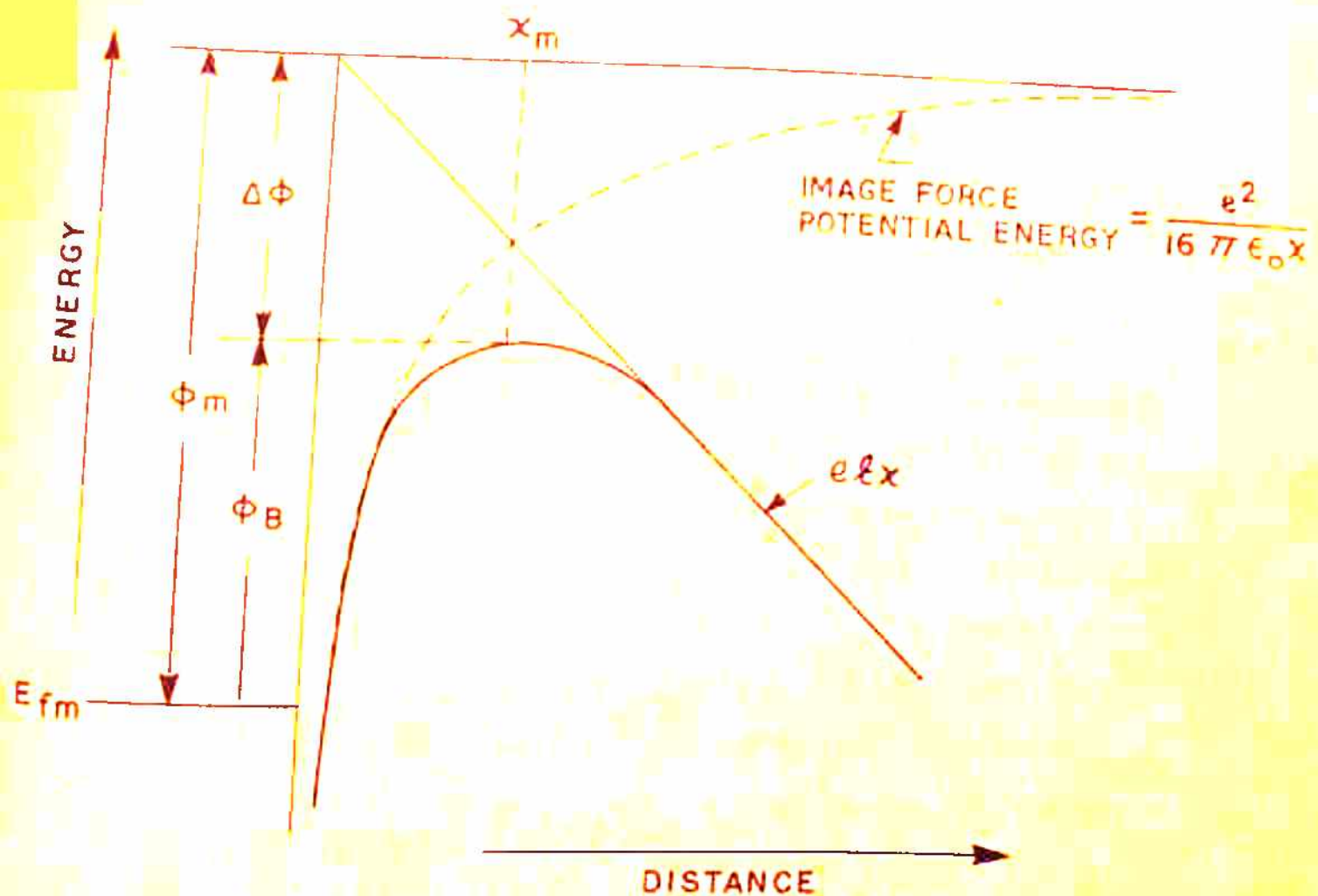
A lowering in the metal work function for a metal vacuum system is brought about by the combined action of the image force and the force due to an applied electric field \mathcal{E} . This lowering is known as the schottky barrier lowering or the image force lowering. The image force is the force between the induced positive charge and the electron. This force can be calculated by assuming that the electron at a distance $+x$ from the metallic surface induces an equal positive charge at a distance $-x$ from the surface. The total potential energy of the electron is given by (17)

$$P.E = \frac{e^2}{16\pi\epsilon_0 x} + e\mathcal{E}x \quad (4.1)$$

The maximum potential energy of the electron for a metal-vacuum system occurs at a distance x_m given by $x_m = (e/16\pi\epsilon_0\mathcal{E})^{1/2}$ and the barrier lowering produced $\Delta\phi$ is given by (17)

$$\Delta\phi = (e\mathcal{E}/4\pi\epsilon_0)^{1/2} \quad (4.2)$$

where ϵ_0 is the permittivity of the free space. This is shown in Figure (4.1). For example if $\mathcal{E} = 10^5$ V/cm, then barrier



E_{fm} = FERMI LEVEL OF METAL

ϕ_m = METAL WORK FUNCTION

ϕ_B = BARRIER HEIGHT OF METAL VACUUM SYSTEM

ℓ = APPLIED ELECTRIC FIELD

$\Delta\phi$ = IMAGE FORCE BARRIER LOWERING

FIG. 4.1 ENERGY BAND DIAGRAM BETWEEN A METAL SURFACE AND VACUUM.

lowering $\Delta\phi$ is 0.12 V and $x_m \approx 60 \text{ \AA}$. If \mathcal{E} be 10^7 V/cm, then $\Delta\phi$ is 1.2 V and $x_m \approx 6 \text{ \AA}$. Thus at higher fields, there is considerable schottky barrier lowering and the effective metal work function is reduced.

If the metal vacuum system is replaced by metal semiconductor system, the schottky barrier lowering and the location of the potential maximum can also be calculated. For a metal semiconductor system, the external applied field in the case of metal vacuum system should be replaced by the maximum field \mathcal{E}_s at the interface and the free space permittivity should be replaced by an appropriate permittivity ϵ_s characterizing the semiconductor medium. $\Delta\phi$ is then given by⁽¹⁷⁾

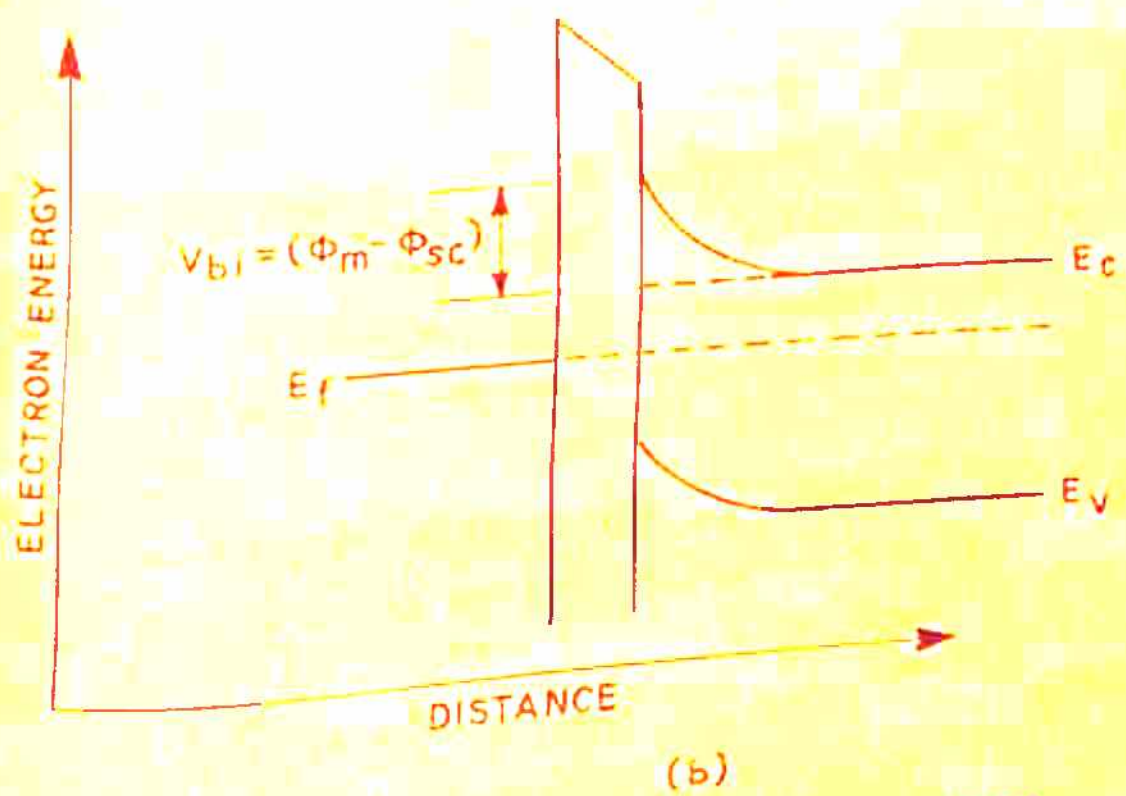
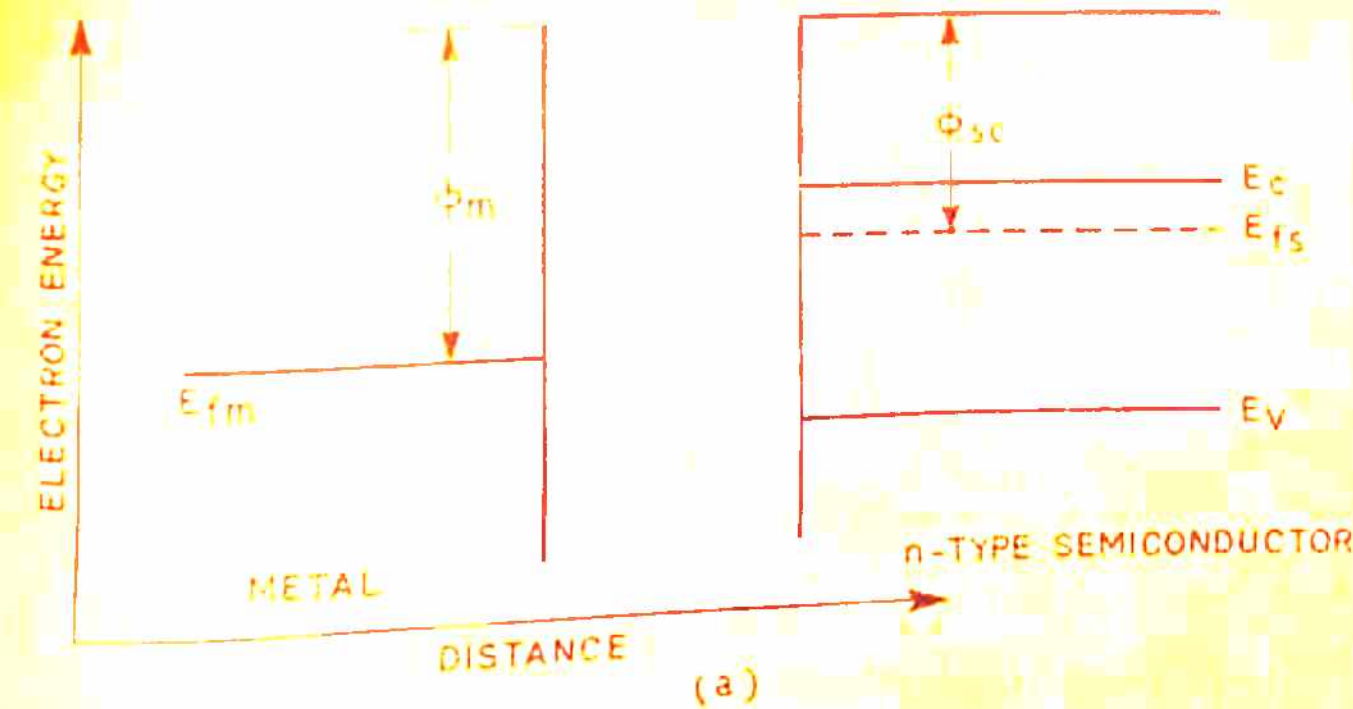
$$\Delta\phi = (e\mathcal{E}_s / 4\pi\epsilon_s)^{1/2} \quad (4.3)$$

Taking $\mathcal{E}_s = 10^5$ V/cm and $\epsilon_s = 16\epsilon_0$ for silicon, $\Delta\phi$ is only 0.03 V as compared to a value of 0.12 V for the metal vacuum system. Thus the barrier lowering is reduced for a metal semiconductor system.

4.2 METAL SEMICONDUCTOR CONTACT :

Consider a contact between a metal and n type semiconductor (Figure 4.2a). Let the metal work function ϕ_m be greater than the semiconductor work function ϕ_{sv} . When the metal and the semiconductor are brought into intimate contact; the electrons flow from semiconductor to metal. This flow of

electrons from semiconductor to metal, leaves ionized donors behind and they provide a positive space charge region. Thermal equilibrium is reached when the Fermi level of the metal E_{fm} and that of the semiconductor E_{fs} coincide. When thermal equilibrium is attained, there is no net flow of charge. In equilibrium the net carrier density near the surface of the semiconductor is reduced from its bulk equilibrium and a contact potential difference is set up at the semiconductor surface. The field arising due to the contact potential difference exists now largely within the semiconductor. The potential energy of an electron at rest at the bottom of the conduction band in the interior of the crystal differs from the potential energy of such an electron at the surface by an amount $(\phi_m - \phi_{sc})$, and as a result the conduction and valence band edges are shifted with respect to the Fermi level as illustrated by Figure (4.2b). The positive space charge density in the surface region, due to the excess concentration of ionized donors over the electron population (in connection with electrons which tunnel through the metal) is just such as to produce a field sufficient to maintain a potential difference $(\phi_m - \phi_{sc})$ between the metal and the semiconductor. The situation within the semiconductor is not essentially different from that which was discussed in connection with the space charge layer of a p-n junction. It is important to note that in the present example a potential barrier V_{bi} of height $(\phi_m - \phi_{sc})$ is formed



Φ_{sc} = WORK FUNCTION OF SEMICONDUCTOR.
 E_c = CONDUCTION BAND.
 E_v = VALENCE BAND.
 E_{fs} = FERMI LEVEL OF SEMICONDUCTOR.
 V_{bi} = BUILT-IN-POTENTIAL.

FIG. 4.2 ESTABLISHMENT OF EQUILIBRIUM BETWEEN AN n-TYPE SEMICONDUCTOR AND A METAL HAVING A GREATER WORK FUNCTION
 (a) BEFORE CONTACT.
 (b) AFTER CONTACT.

at the surface. The formation of this potential barrier and the existence of the depletion region are the basis of the explanation of how a metal-semiconductor contact rectifier operates as is discussed later.

In Figure (4.3) the situation which arises at the contact interface between a metal and an n type semiconductor where ϕ_{sc} is greater than ϕ_m is shown. In this case the electrons flow from metal to semiconductor till the thermal equilibrium is reached. Here the semiconductor must acquire a negative charge, the metal a positive one, and the bands shift downward at the surface. As a result, instead of a potential barrier, an accumulation region in which the electron concentration is greater than the concentration of ionized donor atoms, is formed. The excess electron concentration in the surface accumulation region gives rise to negative space charge necessary to support the contact potential between the two substances.

4.3 METAL SEMICONDUCTOR CONTACT RECTIFICATION :

The metal semiconductor contact, as discussed in article 4.2, behaves as a rectifier in the same manner as a p+n junction. Since the concentration of carriers within the depletion region is much smaller than ^{that} in the other parts of the system, any externally applied voltage will tend to appear primarily across this high resistivity layer. The applied voltage will thus tend

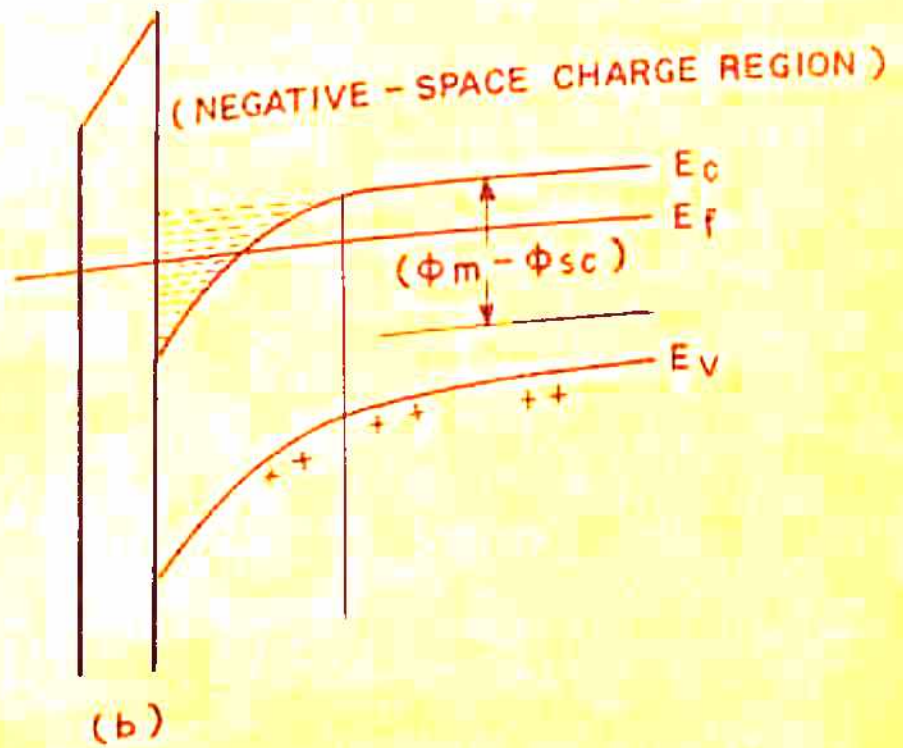
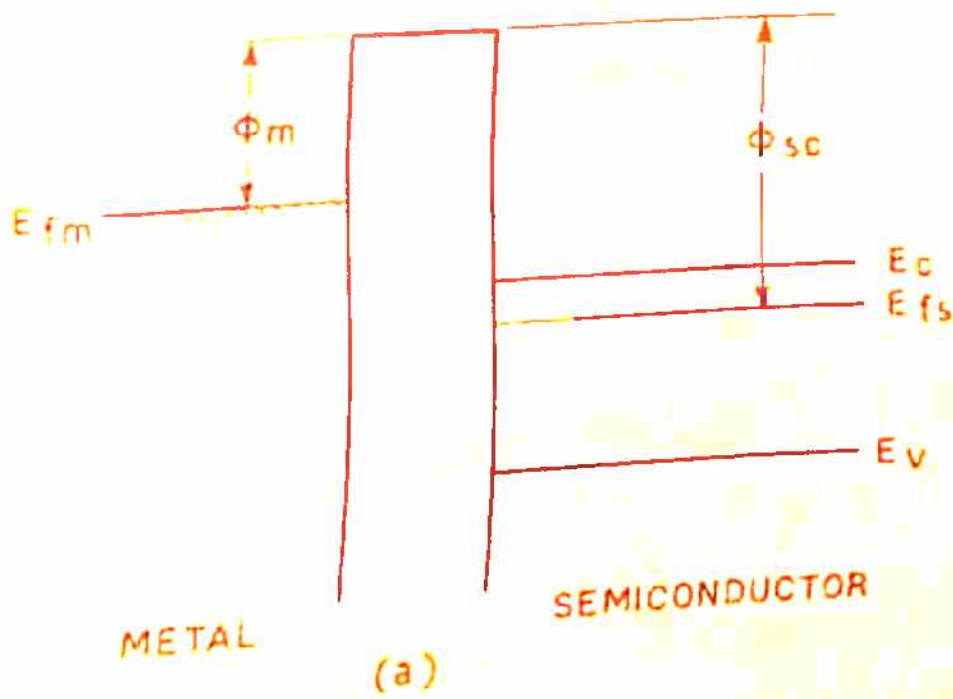


FIG. 4.3 SUCESSIVE STAGES IN THE ESTABLISHMENT OF EQUILIBRIUM BETWEEN AN n-TYPE SEMICONDUCTOR AND A METAL HAVING A SMALLER WORK FUNCTION.

(a) METAL AND SEMICONDUCTOR WITHOUT CONTACT.

(b) FORMATION OF ACCUMULATION REGION AND THERMAL EQUILIBRIUM.

either to increase (reverse bias) or reduce (forward bias) the barrier height, as shown in Figure (4.4) for the case of an n type semiconductor and a metal having a larger work function. In thermal equilibrium, a certain fraction of the electrons in the conduction band of the semiconductor will have sufficient energy to surmount the surface potential barrier and go over to the metal. These electrons will cause a current density J_n^- to flow from metal to the semiconductor. A current density J_n^+ (arising from a small fraction of electrons in the metal which can surmount the barrier and flow to the semiconductor.) will also flow from the semiconductor to metal. These two current densities must be equal in magnitude in equilibrium. Under these circumstances there is no net current due to electrons. In a similar way, there are two current densities J_p^+ and J_p^- due to holes. The former consists of holes which are generated at the semiconductor surface (by electrons from the valence band occupying occasional empty electronic states in the electron distribution of the metal) having sufficient energy to overcome the potential barrier and enter the interior of the semiconductor. Thus J_p^+ is from metal to semiconductor. The other component J_p^- is made up of holes from the interior of the semiconductor which diffuse to the surface and disappear there by extracting an electron from the Fermi distribution of the metal. Thus J_p^- is from semiconductor to metal. Again, at equilibrium, these two current densities are equal and opposite and no net hole current flows.

When an external voltage V is applied to the contact, the situation is as shown in figure 4(b) (reverse bias) and 4(c) (forward bias). The two current densities J_n^- and J_p^+ are governed by the number of carriers present in the semiconductor possessing enough energy to get over the surface potential barrier, which, when an external voltage V is applied, is of height $(V_{bi} - V)$, where $V_{bi} = \phi_M - \phi_{sc}$ is the difference between the metal and semiconductor work functions. These two current density components are given by (18)

$$J_n^- = J_{no} e^{-e(V_{bi}-V)/kT} \quad \text{and} \quad (4.4)$$

$$J_p^+ = J_{po} e^{-e(V_{bi}-V)/kT} \quad (4.5)$$

Where J_{no} and J_{po} are gross current densities due to electrons and holes respectively. The other two current density components J_p^- and J_n^+ , are dependent only upon the number of thermally generated holes available in the interior of the semiconductor, and number of electrons from the metal which can surmount the barrier respectively and these are given by (18)

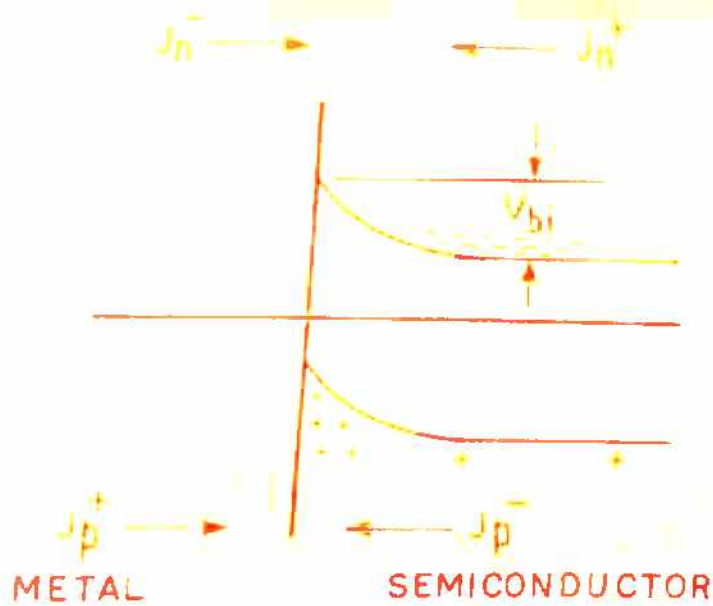
$$J_p^- = J_{po} e^{-e V_{bi}/kT} \quad \text{and} \quad (4.5a)$$

$$J_n^+ = J_{no} e^{-e V_{bi}/kT} \quad (4.6b)$$

The total current density of electrons and holes are then

$$J_n = J_n^- - J_n^+ = J_{no} e^{-e V_{bi}/kT} [e^{eV/kT} - 1] \quad \text{and} \quad (4.7)$$

$$J_p = J_p^+ - J_p^- = J_{po} e^{-e V_{bi}/kT} [e^{eV/kT} - 1] \quad (4.8)$$



(a)

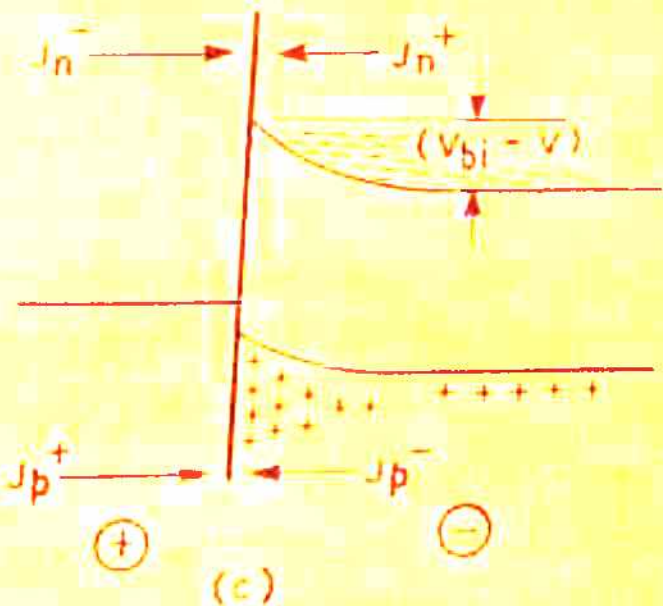
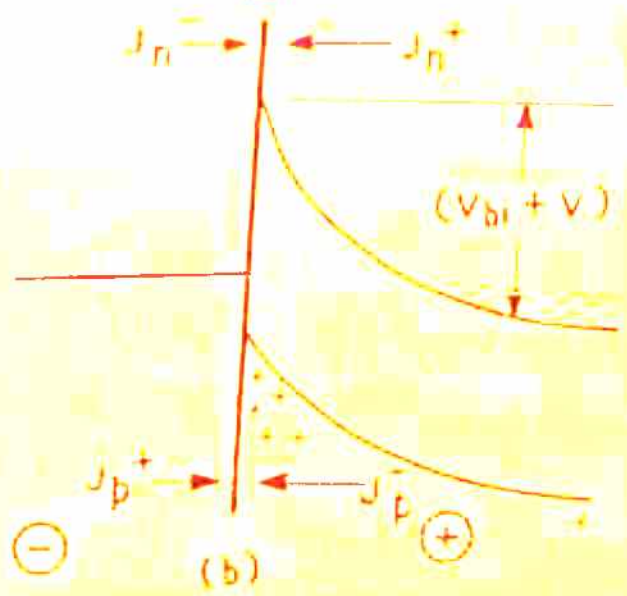


FIG. 4.4 OPERATION OF A METAL - SEMICONDUCTOR CONTACT RECTIFIER
 (a) IN THE EQUILLIBRIUM STATE .
 (b) UNDER REVERSE BIASE ($V < 0$).
 (c) UNDER FORWARD BIASE. ($V > 0$).

while the total current density is simply

$$J = (J_n + J_p) = J_o [e^{eV/kT} - 1] \quad (4.9)$$

where J_o is the saturation current density

$$J_o = (J_{po} + J_{no}) e^{-e V_{bi}/kT} \quad (4.10)$$

The metal-semiconductor rectifier thus has the same current-voltage dependence as expressed by equation (4.9) as the p-n junction, except that the saturation current is different.

According to expression (4.9) for current voltage characteristics, the characteristics of a metal-semiconductor rectifier should depend upon the difference in the work function of the metal and the semiconductor, but the experimental results of Meyerhof⁽¹⁹⁾ showed that in the case of silicon-metal contact, the rectification properties of the contact were independent of this work function difference. This situation was resolved by Bardeen⁽²⁰⁾. According to him there exist electronic states associated with the surface lying in the forbidden region between the conduction and valence bands of the semiconductor. The fundamental justification for the existence of these surface states goes back to the work of Tamm⁽²¹⁾, who showed that if a periodic square well potential such as that associated with the Kronig - Penny crystal was terminated on one side by a surface potential barrier, there would be discrete allowed energy levels within the forbidden energy regions corresponding to wave functions which

are localized near the surface. A detailed study of these surface levels was also undertaken by Shockley⁽²²⁾. According to Shockley's calculations, there should be one surface state for each surface atom. In addition to this, localized surface levels, discrete or continuously distributed, may be expected to arise from impurity atoms, oxide layer and structural imperfections at the surface. The presence of a considerable density of surface states results in the formation of depletion layer within the semiconductor even in the absence of an external metallic contact. To understand this, the case of an n type semiconductor having a substantial number of acceptor type surface states (which are negatively charged when occupied and neutral when empty) is considered, whose density and distribution in energy within the forbidden region are shown in Figure (4.5a). The electrons flow from semiconductor to the surface states. This flow of electrons will continue till thermal equilibrium is reached. In thermal equilibrium the Fermi level of the surface states coincides with that of the bulk semiconductor. The surface states will be filled upto the Fermi level creating a layer of negative charge at the surface which repels electrons within the conduction band of the semiconductor from the surface and which therefore leaves a positive space charge region arising from uncompensated donor ions adjacent to the surface. In this manner a depletion region and a built-in potential are set up as a result of equilibrium between the bulk semiconductor and surface states in the absence of a metal.

When the metal is brought into intimate contact with the semiconductor, there will be a flow of electrons from the surface states to the metal, until the Fermi levels of the metal and the surface states coincide. Thus an equilibrium is established between the metal and the surface state Fermi levels. In thermal equilibrium all the three Fermi levels coincide and this results in the formation of the barrier ϕ_B of the metal semiconductor system as illustrated in Figure (4.5).

Under thermal equilibrium the net flow of current across the metal semiconductor contact is zero. The detailed energy band diagram for metal-n type semiconductor system is shown in Figure (4.6).

4.4 EXPRESSIONS FOR DEPLETION LAYER WIDTH W, BUILT-IN POTENTIAL V_{bi} , ELECTRIC FIELD \mathcal{E} , AND BARRIER HEIGHT ϕ_{Bn} :

Before going into the details of the working of a Schottky barrier solar cell we introduce a number of terms and expressions which will be in common use throughout hereafter. The expressions, for depletion layer width W, built-in potential V_{bi} , and barrier height ϕ_{Bn} are obtained by solving the Poisson's equation. The Poisson's equation is given by

$$\frac{d^2V}{dx^2} = - \frac{\rho}{\epsilon_s} \quad (4.11)$$

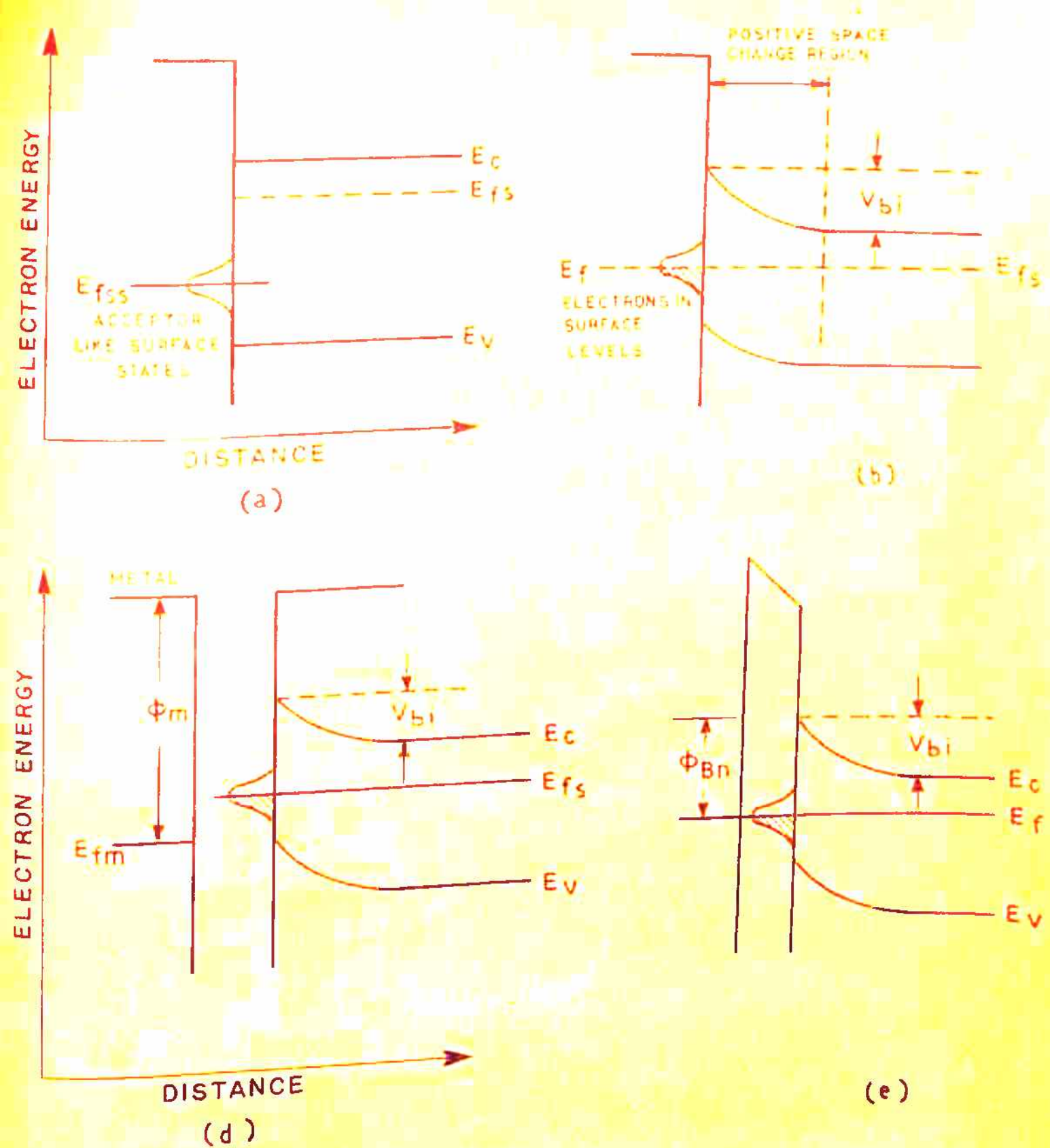


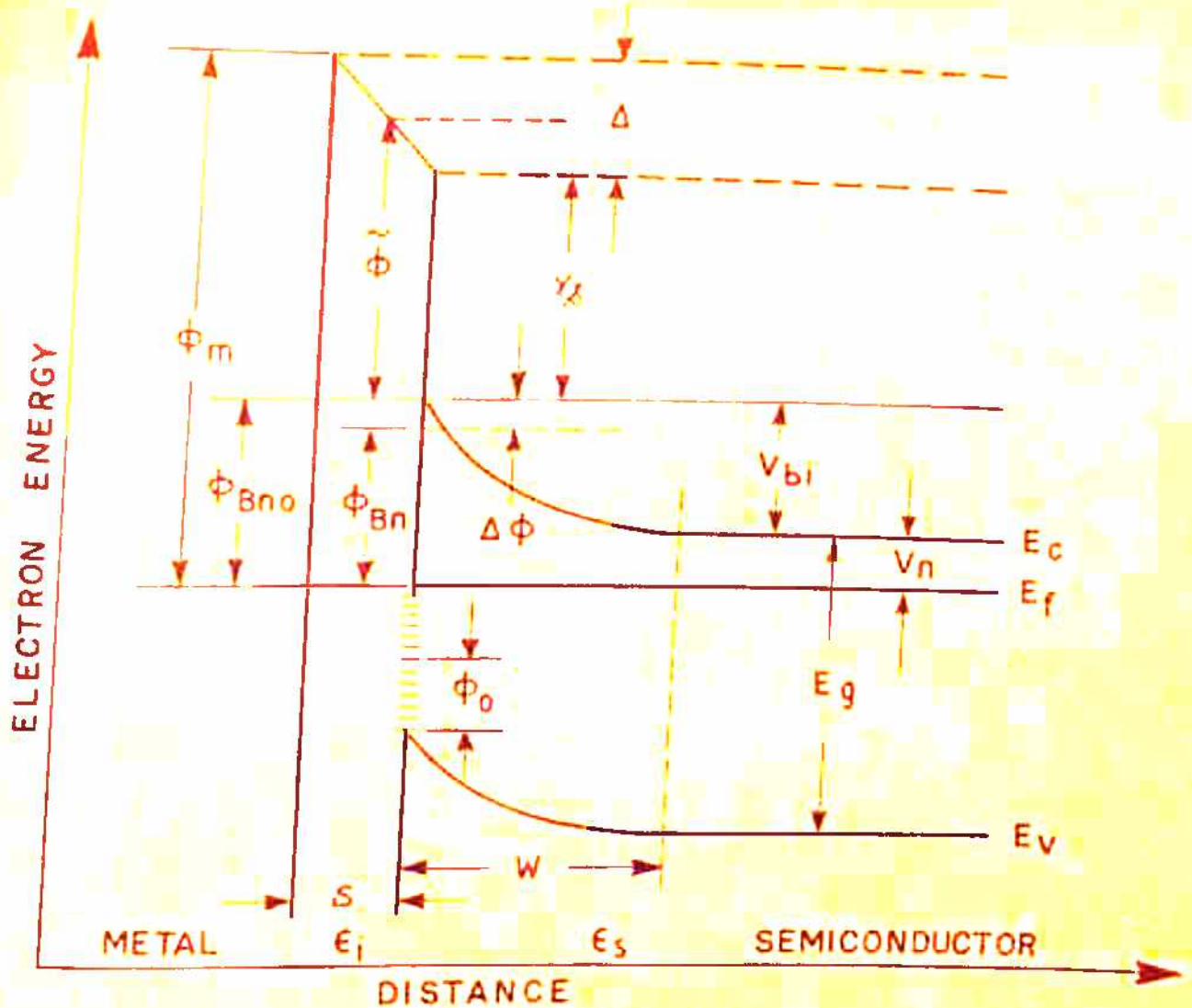
FIG. 4.5 ESTABLISHMENT OF THE THERMAL EQUILLIBRIUM BETWEEN METAL AND SEMICONDUCTOR WITH SURFACE STATES.

(a) n-TYPE SEMICONDUCTOR WITH ACCEPTOR TYPE OF SURFACE STATES.

(b) FORMATION OF A SPACE CHARGE REGION AT A FREE SEMICONDUCTOR SURFACE.

(c) METAL AND SEMICONDUCTOR WITHOUT EQUILLIBRIUM.

(d) FINAL STATE OF THE SYSTEM.



- E_{fm} = FERMI LEVEL OF METAL
- ϕ_m = METAL WORK FUNCTION
- ϕ_{Bn} = BARRIER HEIGHT OF METAL VACUUM SYSTEM
- $\Delta\phi$ = IMAGE FORCE BARRIER LOWERING
- E_c = CONDUCTION BAND
- E_v = VALENCE BAND
- V_{bi} = BUILT-IN-POTENTIAL
- $\tilde{\phi}$ = AVERAGE BARRIER HEIGHT IN INSULATOR GAP
- Δ = POTENTIAL ACROSS INTERFACIAL LAYER
- W = DEPLETION REGION WIDTH
- χ_s = ELECTRON AFFINITY OF SEMICONDUCTOR
- ϵ_s = PERMITTIVITY OF SEMICONDUCTOR
- ϵ_i = PERMITTIVITY OF INTERFACIAL LAYER
- δ = THICKNESS OF INTERFACIAL LAYER

FIG. 4.6 ENERGY BAND DIAGRAM OF A METAL-n TYPE SEMICONDUCTOR IN THERMAL EQUILIBRIUM.

where ρ is the charge density. Under abrupt approximation, that is, the doping density is constant upto the boundary between metal-semiconductor contact, the charge density $\rho = eN_D$ for $x < w$ and $\rho = 0$ for $x \geq 0$, where N_D is the donor density. The solution of the Poisson's equation (4.11) gives the following expressions for electric field \mathcal{E} , depletion region width W and the built-in potential V_{bi} ⁽¹⁷⁾,

$$\mathcal{E}(x) = \frac{e N_D}{\epsilon_s} (x - W) \quad (4.12a)$$

$$W = \left[\frac{2 \epsilon_s}{e N_D} (V_{bi} - V_n) \right]^{1/2} \quad (4.12b)$$

and

$$V_{bi} = \frac{e N_D}{2 \epsilon_s} W^2 \quad (4.12c)$$

To get the expression for the barrier height of a metal-n semiconductor with the space charge having acceptor surface states of density D_{si} states/cm²/eV, we consider D_{si} as constant over the range from ϕ_0 to the Fermi level, where ϕ_0 is the energy measured from the valence band edge at the semiconductor surface and specifies the level below which all surface states must be filled for charge neutrality at the semiconductor surface ⁽²³⁾. The surface state charge density Q_{ss} on the semiconductor is given by ⁽¹⁷⁾

$$Q_{ss} = -e D_{si} (E_g - e \phi_0 - e \phi_{Bn} - e \Delta \phi) \quad (4.13)$$

Where E_g is the energy gap of the semiconductor and $\Delta \phi$ is the schottky barrier lowering (image force lowering). The space charge, which forms in the depletion layer of the semiconductor at thermal equilibrium, is given by (17)

$$Q_{sc} = \left[2e \epsilon_s N_D (\phi_{Bn} - V_n + \Delta \phi - \frac{kT}{e}) \right]^{1/2} \quad (4.14)$$

where ϕ_{Bn} is the barrier height of the metal-semiconductor system and V_n is the difference between the semiconductor Fermi level and conduction band edge in the bulk of the semiconductor. The total equivalent surface charge density on the semiconductor surface is given by

$$Q = Q_{ss} + Q_{sc} \quad (4.15)$$

In the absence of any space charge effects in the interfacial layer, an exactly equal and opposite charge Q_m develops on the metal surface and is given by

$$Q_m = -Q = - (Q_{ss} + Q_{sc}) \quad (4.16)$$

The potential Δ across the interfacial layer can be obtained by the application of Gauss' law to the surface charge on the metal and the semiconductor and is given by (17)

$$\Delta = E \cdot \delta = - \frac{\delta Q_m}{\epsilon_i} \quad (4.17)$$

Where ϵ_i is the permittivity of the interfacial layer and δ is the thickness of the interfacial layer. At thermal equilibrium, the value of Δ can be obtained from the energy band diagram of the metal semiconductor system as shown in Figure (4.6) and given by

$$\Delta = \phi_m - (\phi_{Bn} + \chi_s + \Delta\phi) \quad (4.18)$$

where χ_s is the electron affinity of the semiconductor. If Δ is eliminated from equation (4.17) and (4.18), and substituting the value of Q_m , ϕ_{Bn} is given by (17)

$$\phi_{Bn} = [c_2(\phi_m - \chi_s) + (c_1 - c_2)(E_g/e - \phi_0) - \Delta\phi] + \left\{ \frac{c_1 \cdot c_2^2}{2} - c_2^{3/2} \right. \\ \left. \times \left[c_1(\phi_m - \chi_s) + (1 - c_2) \times (E_g/e - \phi_0) \frac{c_1}{c_2} - \frac{c_1}{c_2} (V_n + \frac{kT}{e}) \right. \right. \\ \left. \left. + \frac{c_2 \cdot c_1^2}{4} \right]^{1/2} \right\} \quad (4.19)$$

$$\text{where } c_1 = \frac{2 e \epsilon_s N_D}{\epsilon_i} \delta^2 \quad \text{and } c_2 = \frac{\epsilon_i}{\epsilon_i + e^2 \delta D_{si}}$$

The limiting value of the barrier height of the metal semiconductor system is determined by the surface states. This can be analyzed in the following manner as given by Sze (17)

(1) when $D_{si} \rightarrow \infty$, $c_2 \rightarrow 0$ then

$$\phi_{Bn} = (E_g/e - \phi_0) - \Delta\phi \quad (4.20)$$

In this case the Fermi level at the interface is pinned by the surface states at the value ϕ_0 above the valence band. The barrier height is independent of the metal work function and is determined entirely by doping and surface properties of the semiconductor.

(2) When $D_{si} \rightarrow 0$, $C_2 \rightarrow 1$, then

$$\phi_{Bn} = (\phi_m - \chi_s) - \Delta\phi \quad (4.21)$$

In this case the barrier height is determined by the difference of metal and semiconductor work functions and the amount of doping.

4.5 CHARGE TRANSPORT IN SCHOTTKY BARRIERS :

For the schottky barrier the current-voltage characteristics can be explained on the basis of three different types of approximations. The three approximations are the thermionic emission approximation, the diffusion approximation and a combination of these two known as thermionic emission diffusion approximation.

In the case of thermionic emission the assumptions involved are the following:

- (i) the barrier height $e\phi_{Bn}$ is much larger than kT ,
- (ii) electron collisions within the depletion region are neglected, and

(iii) effect of image force is also neglected.

The net current density from metal to semiconductor under this approximation is given by (17,24)

$$J_{TH} = A^* T^2 \exp(-\phi_0/kT) \left[\exp(eV/kT) - 1 \right] \quad (4.22)$$

Where A^* is the effective Richardson's constant for thermionic emission and it depends upon the effective mass of electron m_e^* . This is given by

$$A^* = \frac{4\pi e m_e^* k}{h^3} \quad (4.23)$$

Where k is Boltzmann's constant and h is the Planck's constant.

The diffusion approximation is based on the following assumptions:

- (i) the barrier height is much larger than kT ,
- (ii) the effect of electron collisions within the depletion region is included,
- (iii) the carrier concentrations at $x = 0$ and $x = W$ are unaffected by the current flow, and
- (iv) the impurity concentration of the semiconductor is non-degenerate

According to this approach the current-voltage characteristics of the schottky barrier diode is given by (17,25)

$$J_{\text{diff}} = e N_c \mathcal{E} \mu_n \exp\left(-\frac{e \phi_{Bn}}{kT}\right) \left[\exp\left(\frac{eV}{kT}\right) - 1 \right] \quad (4.24)$$

where N_c is the density of states in the conduction band, μ_n is the mobility of the electrons and \mathcal{E} is the electric field in the depletion region.

For the space charge region comparable in thickness to the diffusion length of the electrons, a combined approach yields⁽²⁶⁾

$$J_{T-D} = \frac{e N_c V_R}{1 + V_R/V_D} \exp\left(-\frac{e \phi_{Bn}}{kT}\right) \left[\exp\left(\frac{eV}{kT}\right) - 1 \right] \quad (4.25)$$

where $V_R = A^* T^2 / e N_c$ and V_D is an effective diffusion velocity. If $V_D \gg V_R$ then the expression (4.25) reduces to (4.22). In this case the thermionic emission approximation becomes dominant. If the image force effects are neglected and mobility μ_n is independent of the electric field \mathcal{E} , then $V_D = \mu_n \mathcal{E}$. If $V_D \ll V_R$ then the expression (4.25) reduces to (4.24) and the diffusion approximation becomes dominant.

4.6 SCHOTTKY BARRIER SOLAR CELLS :

Schottky barrier solar cells are rectifying metal semiconductor contacts with a very thin insulating layer

between the metal and the semiconductor . This insulating layer can be readily penetrated by tunnelling by the charge carriers. Like the p-n junction solar cell, the built-in field of the schottky barrier separates the photogenerated charge carriers. In these cells light is incident on a very thin optically transparent metal film. This light is then transmitted through the insulating layer onto the adjacent semiconductor. The motion of charge carriers modifies the built in potential in the device and power can be delivered to an external load in the same manner as in p-n junction solar cells. We consider Au-n Si system as a schottky barrier solar cell. The metal (Gold) work function in this system is greater than that of the semiconductor (Silicon).

On illuminating the schottky barrier solar cell, a voltage V appears across the cell. This voltage V acts as a forward bias on the device as in p-n junction solar cells. A part V_i of V appears across the insulating layer of thickness δ and the rest V_s appears across the semiconductor depletion region of width W . We have

$$V = V_i + V_s \quad (4.26)$$

The energy band diagram of a schottky barrier solar cell under illumination is shown in figure (4.7) . The total current through the device is given by⁽³⁾

$$I = A \left[J_{MS}^e + J_W^h + J_{DL}^h - J_{sm}^e \right] \quad (4.27)$$

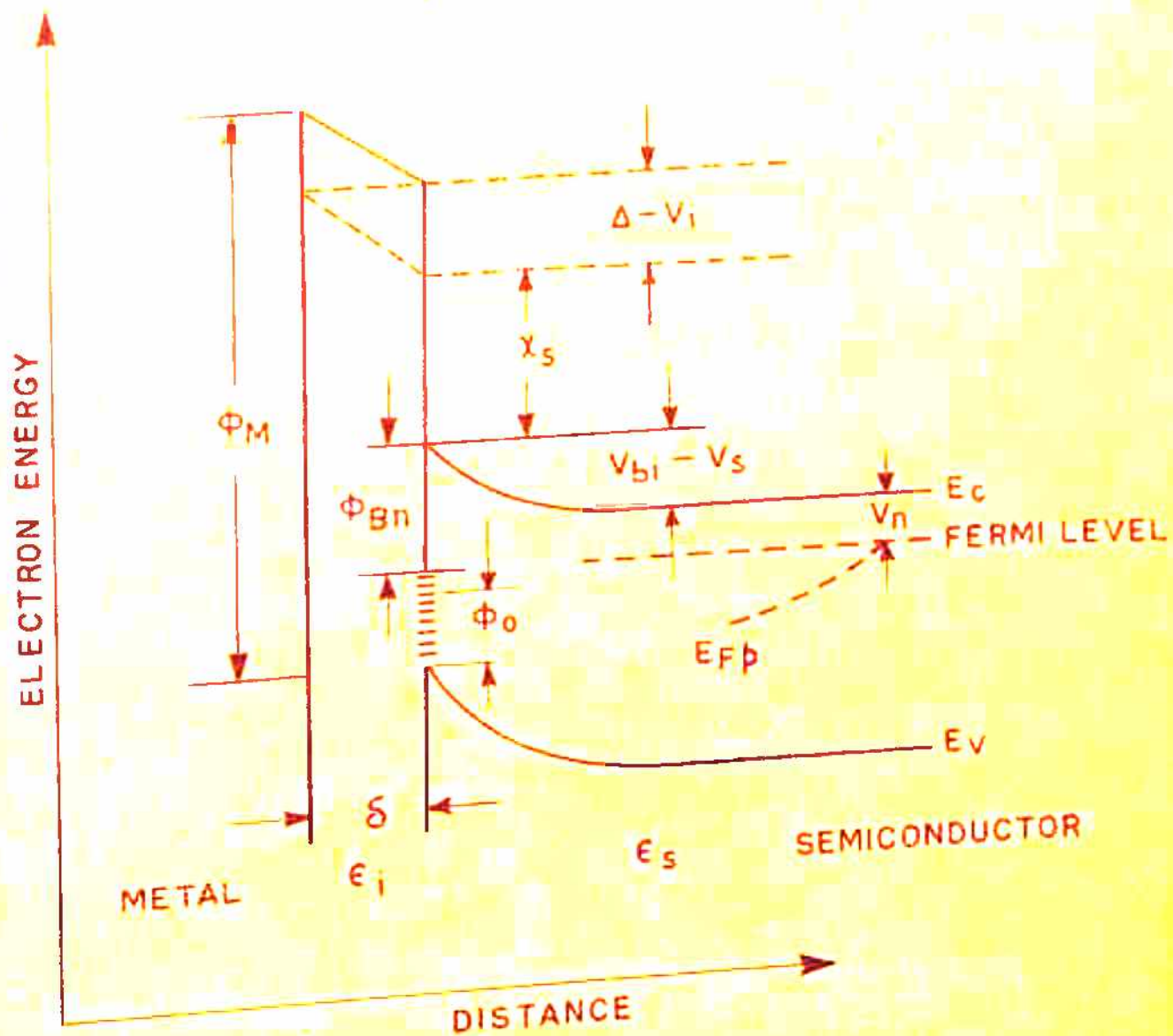


FIG. 4.7 SCHOTTKY BARRIER SOLAR CELL WITH ILLUMINATION.

Where A is the area of the device, J_{ms}^e is the current density from semiconductor to metal caused by the electrons flowing from metal to the semiconductor, J_{sm}^e is the current density from metal to semiconductor caused by electrons flowing from the semiconductor conduction band to metal, J_w^h is the current density at $x = W$ due to holes passing towards the junction from the interior of the semiconductor and J_{DL}^h is the current density on account of the photo-generated holes in the depletion region flowing towards the metal.

The current density J_{DL}^h due to carriers generated inside the depletion layer can be obtained from the generation rate $g(x)$ due to incident photons as follows⁽²⁷⁾:

$$g(x) = \alpha \phi_{flux} e^{-\alpha x} \quad (4.28a)$$

$$J_{DL}^h = e \int_0^W g(x) dx \quad (4.28b)$$

$$J_{DL}^h = e \phi_{flux} (1 - e^{-\alpha W}) \quad (4.28c)$$

Where ϕ_{flux} is the incident photon flux and α is the absorption coefficient of the semiconductor. In the case of n type silicon, the hole current density J_w^h at $x = W$ can be obtained from the solution of the continuity equation for the minority carriers⁽³⁾

$$D_p \frac{d^2 p}{dx^2} - \frac{p - p_{no}}{\tau_p} + g(x) = 0 \quad (4.29)$$

and the boundary conditions are

$$(i) \quad p \rightarrow p_{no} \text{ as } x \rightarrow \infty \quad (4.30a)$$

$$(ii) \quad p \rightarrow p_{no} e^{eV/kT} \text{ for } x = W \quad (4.30b)$$

The solution of the above equation (4.29) is

$$p(x) = p_{no} + Ae^{-x/L_p} + B e^{x/L_p} + \frac{\alpha \phi_{flux} L_p^2}{D_p (1 - \alpha^2 L_p^2)},$$

where A and B are constants.

Using the boundary condition (i) as $x \rightarrow \infty$, $p \rightarrow p_{no}$ and $B=0$ because e^{x/L_p} diverges as $x \rightarrow \infty$, the solution for excess carrier holes $p(x)$ becomes

$$p(x) = p_{no} + Ae^{-x/L_p} + \frac{\alpha \phi_{flux} L_p^2}{D_p (1 - \alpha^2 L_p^2)} e^{-\alpha x}$$

With the help of boundary condition (ii), the solution becomes

$$p(x) = p_{no} + p_{no} (e^{eV/kT} - 1) e^{W/L_p} e^{-x/L_p} - \frac{\alpha \phi_{flux} L_p^2}{D_p (1 - \alpha^2 L_p^2)} e^{-\alpha x} + \frac{\alpha \phi_{flux} L_p^2}{D_p (1 - \alpha^2 L_p^2)} e^{-\alpha x} \quad (4.31)$$

The hole current density J_w^h at $x = W$ is given by

$$J_w^h = e D_p \left. \frac{dp}{dx} \right|_{x=W} \quad (4.32)$$

where D_p is the diffusion coefficient for holes. Thus,

$$J_w^h = \frac{e \alpha L_p \phi_{flux} e^{-\alpha W}}{1 + \alpha L_p} - \frac{e p_{no} D_p}{L_p} \left[\exp(eV/kT) - 1 \right] \quad (4.33)$$

where L_p is the diffusion length for holes.

When the schottky barrier lowering effects are neglected and the transmission probability of electrons across the interfacial layer is assumed to be unity, the current density components for majority carrier electrons under thermionic emission approximation are given by

$$J_{sm}^e = A^* T^2 \exp(-e\phi_{Bn}/kT) \exp(eV_s/kT) \quad (4.34)$$

and

$$J_{ms}^e = A^* T^2 \exp(-e\phi_{Bn}/kT) \exp(-eV_i/kT) \quad (4.35)$$

Therefore, the total current flowing through the device becomes

$$I = e \phi_{flux} A \left[1 - \frac{e^{-\alpha W}}{1 + \alpha L_p} \right] - A^* T^2 A \exp[-e(\phi_{Bn} + V_i)] \times \left[\exp(eV/kT) - 1 \right] - \frac{e p_{no} D_p}{L_p} \left[\exp(eV/kT) - 1 \right] \quad (4.36)$$

In the above expression (4.36) the first term represents the photogenerated current (28) I_{ph} and second and third terms represent the dark current components due to majority and

minority carriers respectively. The current-voltage characteristics of the schottky barrier solar cell can be written as

$$I = I_{ph} - I_{oT} \left[\exp(eV/kT) - 1 \right] - I_{oD} \left[\exp(eV/kT) - 1 \right] \quad (4.37)$$

where

$$I_{ph} = e \phi_{inc} A \left[1 - \frac{e^{-\alpha W}}{1 + \alpha L_p} \right] \quad (4.38a)$$

$$I_{oT} = A^* T^2 \exp \left[- e (\phi_{Bn} + V_i) / kT \right] \quad (4.38b)$$

and

$$I_{oD} = \frac{e p_{no} D_p}{L_p} \quad (4.38c)$$

The schottky barrier solar cells can have efficiencies approaching that of the p-n junction solar cells. Fonash (3) has stressed the importance of the interfacial layer on the performance of such cells. Fonash (3) has shown that V depends on the density D_{si} of surface states. He has considered two cases. In case I the communication between the interface states and metal is extremely difficult and V is given by (3)

$$V \approx (1 + e \delta D_{si} / \epsilon_i) V_s + C \left[V_{bi}^{1/2} - (V_{bi} - V_s)^{1/2} \right] \quad (4.39)$$

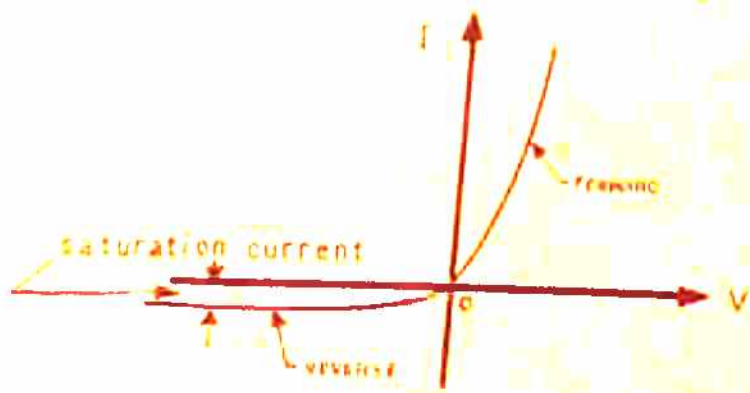
Where $C = (2e N_D \epsilon_s)^{1/2} (\delta / \epsilon_i)$. V increases with D_{si} in this case. In case II the communication between the interface states and metal is extremely efficient and V is given by (3)

$$V \simeq V_s + \frac{C}{1 + e\delta D_{si}/\epsilon_i} \left[V_{bi}^{1/2} - (V_{bi} - V_s)^{1/2} \right] \quad (4.40)$$

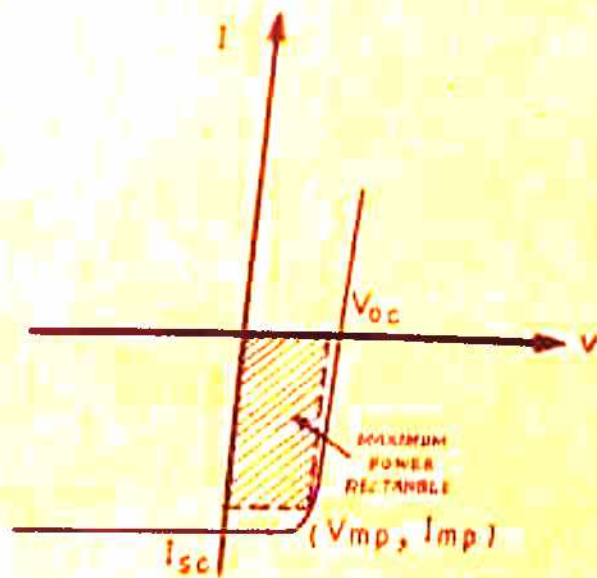
In case II V decreases with increase in D_{si} . Equations (4.39) and (4.40) show that two more parameters affect V and these are the donor density N_D and interfacial layer thickness δ . Variation of V with δ is different from that of V with D_{si} since δ also appears in C . Also Fonash⁽³⁾ has taken the tunneling probability of transmission of electrons across the interfacial layer as unity. The effect of donor density and of interfacial layer thickness δ on the performance of the schottky barrier solar cell will be presented in Chapters V and VI.

The solar cell parameters such as the short circuit current I_{sc} when $V = 0$, open circuit voltage V_{oc} when $I = 0$, the fill factor FF ($= V_{mp} \cdot I_{mp} / V_{oc} \cdot I_{sc}$) and efficiency of the solar cell η ($= FF \frac{V_{oc} \cdot I_{sc}}{P_{in}}$) can be obtained from equation (4.37) taking $\frac{\partial P}{\partial I} = \frac{\partial P}{\partial V} = 0$ for maximum power point.

The current-voltage characteristics of the schottky barrier solar cell under dark and with illumination is shown in Figure (4.8).



(a)



(b)

FIG. 4.8 CURRENT - VOLTAGE CHARACTERISTIC
 (a) FOR A SCHOTTKY BARRIER DIODE.
 (b) FOR A SCHOTTKY BARRIER SOLAR CELL.

4.7 AIM OF THE PRESENT WORK IN CONNECTION WITH SCHOTTKY BARRIER SOLAR CELL:

An alternative approach to the development of low cost solar cells for terrestrial use is through the use of metal-semiconductor schottky barriers to replace the conventional p-n junction solar cells. Schottky barrier solar cells are adaptable to low cost large area fabrication techniques and are suitable for polycrystalline devices. In addition, the collecting junction being at the surface of the device, there is increased short wavelength response and improvement in collection efficiency on account of reduced recombination. The main draw-back of schottky barrier solar cell is that the reverse saturation current I_0 in such a cell is large and the open circuit voltage V_{oc} is very small. For an ideal Au-n silicon schottky diode, for which the diode quality factor is taken as unity and ϕ_{Bn} , the barrier height at the metal semiconductor contact is 0.80 eV, the open circuit voltage V_{oc} is only 0.30 volts under AMO conditions. In recent investigations (7) it is reported that the presence of a thin oxide layer between the metal and the semiconductor can considerably increase the open circuit voltage and thereby result in a large conversion efficiency. In order to make a general comparison of the results already obtained on schottky barrier solar cells, the results obtained by different authors are presented in table (4.1).

Summary of the results already obtained for silicon semiconductors by the present method.

Type	Resistivity ohm cm	Grain thickness (\AA°)	Metall contact	T_{oc} ($^\circ\text{C}$)	I_{oc} (mA/cm^2)	η (%)
p 100	2	5-10	$50 \text{\AA}^\circ \text{Cr}^+, 50 \text{\AA}^\circ \text{Cu}^-$ $10 \text{\AA}^\circ \text{Cr}$	520	27	5.3 (8)
p	3.5-15	20-40	$30-100 \text{\AA}^\circ \text{Al}$	470	25.5	5.0 (9)
n	4.9	$10-23 \text{\AA}^\circ$ optimum 19\AA°	$100 \text{\AA}^\circ \text{Au}$	410	25.5	- (10)
n	1-10	10-40	$100 \text{\AA}^\circ \text{Au}$	550	22.0	5.75 (7)
p	-	-	$50 \text{\AA}^\circ \text{Titanium}$	500	22.0	6.0 (8)
p	1.0	-	$100 \text{\AA}^\circ \text{Au}$	400	40.0	10.5 (9)
p	1.0	-	$100 \text{\AA}^\circ \text{Al}$	550	33.0	11.7 (10)
p	1-10	-	$50 \text{\AA}^\circ \text{Sb}$	523	17.7	6.6 (11)
p	8-12	-	$100-250 \text{\AA}^\circ$	500	24.6	5.5 (12)
p (single cryst)	-	20\AA°	$31 \text{\AA}^\circ \text{Cr}$	660	26.4	12.2 (13)
p (polycryst)	-	20\AA°	$37 \text{\AA}^\circ \text{Cr}$	500	24.2	8.2 (11)
p amicryst.	5.0	$10-15 \text{\AA}^\circ$	Ni-Ni_2	558	33.3	12.76 (14)
p (single cryst)	10.0	$10-15 \text{\AA}^\circ$	Al-M_2	627	33.3	15.1 (14)

From table (4.1) it is clear that the presence of a thin interfacial insulating layer considerably improves the efficiency and the open circuit voltage of schottky barrier solar cells. The current voltage characteristics of the schottky barrier solar cell is affected by the insulating layer. It appears that the formation of a thin interfacial insulating layer and its role on the performance of the schottky barrier solar cells are the most important problems before the scientists for designing schottky barrier solar cells having maximum conversion efficiency. However, the exact role of this layer is still not clearly understood. The various parameters such as the thickness of the interfacial layer, density of surface states and doping density play an important role in determining the voltage V developed in the schottky barrier solar cell as given by Expressions (4.39) and (4.40). These very factors determine the conversion efficiency of such cells. Chapter Five deals with the introduction of transmission coefficient for electrons across the interfacial layer, its application to the experimentally grown oxide layer and the effect of the doping density on the performance of schottky barrier solar cells. Results based on a number of calculations showing the variation of the various factors with doping density are reported. A study of the schottky barrier solar cell system taking into account the transmission of holes and electrons across the interfacial layer and its effect on the conversion efficiency of such cells is the subject matter of Chapter VI.

REFERENCES:

1. W.A. Anderson and A.E. Delahoy, Proc. IEEE Vol. 60, pp. 1457 (1972).
2. R.J. Stirn and Y.C.M. Yeh, Appl. Phys. Lett. Vol. 27, pp. 95 (1975).
3. S.J. Fonash, J. Appl. Phys. Vol. 46, pp. 1286 (1975).
4. W.A. Anderson and R.A. Milano, Proc. IEEE Vol. 63, pp. 206 (1975).
5. E.J. Charlson and J.C. Lien, J. Appl. Phys. Vol. 46, pp. 3982 (1975).
6. D.R. Lillington and W.G. Townsend, Appl. Phys. Lett. Vol. 28, pp. 97 (1976).
7. J.P. Ponpon and P. Siffert, J. Appl. Phys. Vol. 47, pp. 3248 (1976).
8. E. Fabre, Appl. Phys. Lett. Vol. 29, pp. 607 (1976).
9. A.H.M. Kipperman and M.H. Omar, Appl. Phys. ^{Lett.} Vol. 28, pp. 621 (1976).
10. E. Fabre, J. Michel and V. Bandet, Twelfth IEEE Photo-voltaic specialists conference, New York, pp. 904 (1976).
11. D.R. Lillington and W.G. Townsend, Appl. Phys. Lett. Vol. 31, pp. 471 (1977).
12. Yasuliro Maeda, Appl. Phys. Lett. Vol. 33 pp. 301 (1978).
13. W.A. Anderson et al, Appl. Phys. Lett. Vol. 33 pp. 588 (1978).

14. R.B. Godfrey and M.A. Green, Appl. Phys. Lett. Vol. 33, pp. 637 (1978).
15. S. Kar, J. Appl. Phys. Vol. 49, pp. 5278 (1978).
16. D.L. Pulfrey and R.F. Mcquat, Appl. Phys. Lett. Vol. 26, pp. 167 (1974).
17. S.M. Sze, Physics of Semiconductor Devices, John Wiley and Sons Inc., New York, Chapter 8, pp. 366 (1969).
18. John P. Mckelvey, Solid State and Semiconductor Physics, Harper and Row Publishers, New York, Evnston and London, Chapter 16, pp. 478 (1966).
19. W.E. Meyerhof, Phys. Rev. Vol. 71, pp. 727 (1947).
20. J. Bardeen, Phys. Rev. Vol. 71, pp. 171 (1947).
21. I. Tamm, Physik Z, Sowjetunion Vol. 1, pp. 733(1932).
22. W. Shockley, Phys. Rev. Vol. 56, pp. 317 (1939).
23. A.M. Cowley and S.M. Sze, J. Appl. Phys. Vol. 36, pp. 3212 (1965).
24. H.A. Bethe, MIT Radiation Laboratory, Report 43, pp. 12 (1942).
25. W. Schottky , Natarwis Vol. 26, pp. 843 (1938).
26. C.R. Crowell and S.M. Sze, Solid State Electronics, Vol. 9, pp. 1035 (1966).
27. W.W. Gartner, Phys. Rev. Vol. 116, pp. 84 (1959).
28. W.A. Anderson et al, J. Appl. Phys. Vol. 45, pp. 3913 (1974).

CHAPTER-V.ELECTRON TRANSMISSION AND DONOR DENSITY EFFECT IN
SCHOTTKY BARRIER SOLAR CELLS.

5.1	Introduction.	142
5.2	Theory	144
5.3	Electron tunneling probability and effect of interfacial layer thickness.	146
5.4	Application of the results to the chemically grown and evaporated oxide layers.	150
5.5	Effect of donor density on the performance of schottky barrier solar cell.	153
5.6	Results and discussion.	157

CHAPTER V.ELECTRON TRANSMISSION AND DONOR DENSITY EFFECT IN SCHOTTKY
BARRIER SOLAR CELLS5.1 INTRODUCTION

Recent experimental investigations⁽¹⁻¹³⁾ have shown that the efficiency of Schottky barrier solar cells can be increased considerably by introducing a thin insulating layer between the metal and the semiconductor. The insulating layer helps in reducing the dark current component of the schottky barrier solar cell. The exact role of this layer is still not clearly understood. According to Fonash⁽¹⁴⁾, the density D_{si} of surface states plays an important role in the functioning of the schottky barrier solar cells. The expression for the voltage V developed by Fonash⁽¹⁴⁾ for a schottky barrier solar cell contains this factor D_{si} . Fonash⁽¹⁴⁾ considered two cases affecting the voltage developed by the cell. For case I, in which the communication between the interface states and metal is extremely difficult, the voltage V is given by⁽¹⁴⁾

$$V \approx (1 + e \delta D_{si} / \epsilon_i) V_s + C [V_{bi}^{1/2} - (V_{bi} - V_s)^{1/2}] \quad (5.1)$$

Where $C = (2eN_D \epsilon_s)^{1/2} \delta / \epsilon_i$ and the various other symbols appearing in equation (5.1) have been explained in Chapter IV. It is clear from equation (5.1) that V increases with increase

in D_{si} . The communication between the interface states and metal is difficult when the Fermi level of the interface states coincides with that of the bulk semiconductor. For case II in which the communication between the interface states and metal is extremely efficient, the voltage V is given by (14)

$$V = V_s + \frac{C}{1 + e \delta D_{si} / \epsilon_i} \left[V_{bi}^{1/2} - (V_{bi} - V_s)^{1/2} \right] \quad (5.2)$$

equation(5.2) shows that V decreases with increase in D_{si} . The communication between the interface states and metal is most efficient when the Fermi level associated with the interface states and metal coincide. From equations (5.1) and (5.2) it is seen that two more parameters, not considered by Fonash⁽¹⁴⁾, affect the voltage V developed in the solar cell. These are the interfacial layer thickness δ and the donor density N_D . Variation of V with δ is somewhat different from that of V with D_{si} since δ also appears in the constant C . Also the variation of V with N_D seems to be different from that of V with D_{si} since N_D appears only in the constant C . Fonash⁽¹⁴⁾ considered the interfacial layer to be perfectly transparent to electrons and hence took the transmission coefficient unity for electrons across the interfacial layer. These equations are modified by taking into account the transmission coefficient for electrons and thereby studying the effect of the interfacial layer thickness on the

Schottky barrier solar cell performance. Likewise the effect of the doping density on the performance of the schottky barrier solar cell is also considered.

5.2 THEORY :

We consider a schottky barrier solar cell consisting of a metal and an n type semiconductor, the metal being of higher work function than the semiconductor. Illuminating the schottky barrier solar cell results in a voltage V across the cell, a part V_i of which appears across the interfacial layer of thickness δ , while the rest $V_s (= V - V_i)$ appears across the depletion region of width W of the semiconductor. The energy band diagram of metal -n semiconductor system with and without illumination is shown in Figure (5.2). The total current I , flowing in the external circuit from metal to semiconductor under illumination, is given by

$$I = I_{ph} - I_{Dark} \quad (5.3)$$

Where I_{ph} is the photogenerated current and is given by⁽¹⁵⁾

$$I_{ph} = e \phi_{flux} \left[1 - \frac{e^{-\alpha w}}{1 + \alpha L_p} \right] \quad (5.4)$$

In expression (5.4) ϕ_{flux} represents the incident photon flux, α is the absorption coefficient of the semiconductor, w is

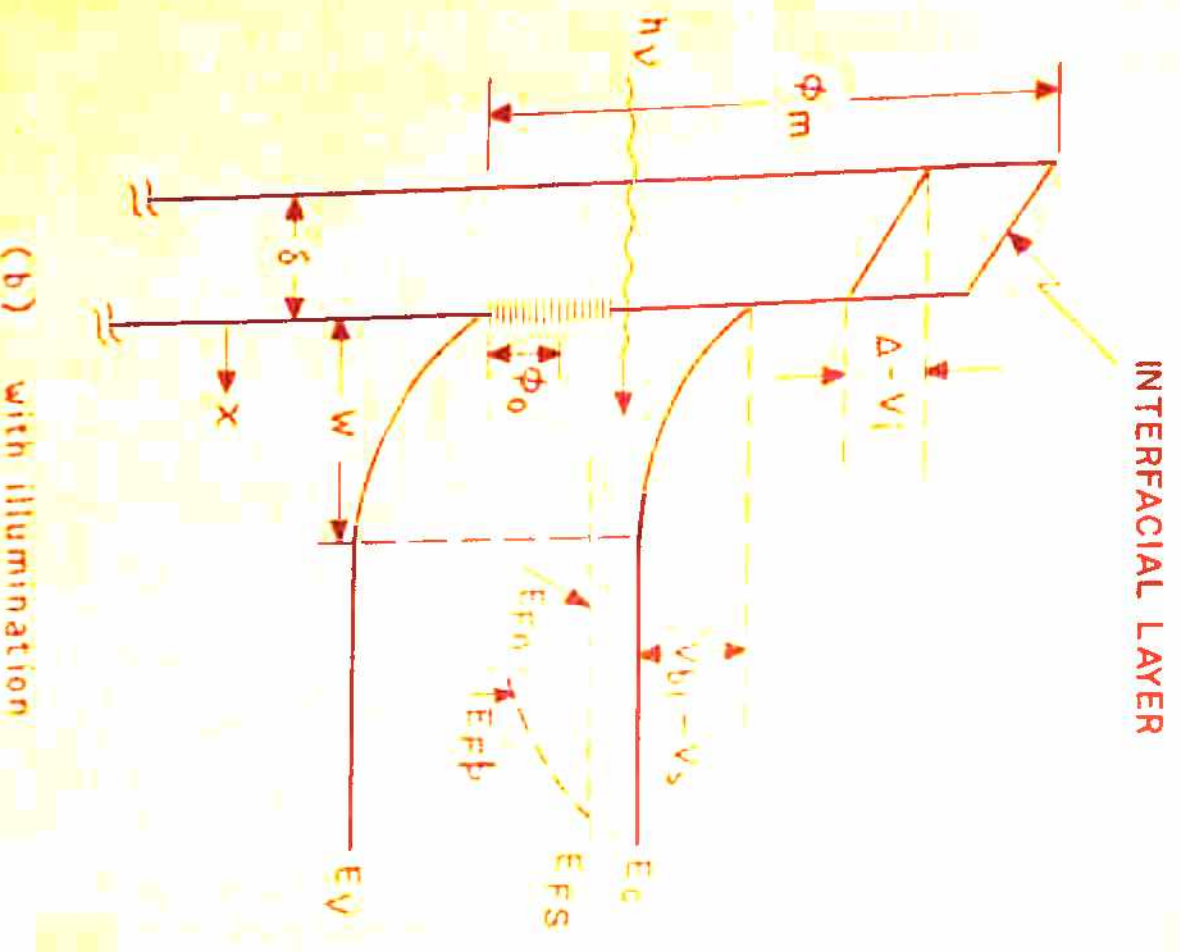
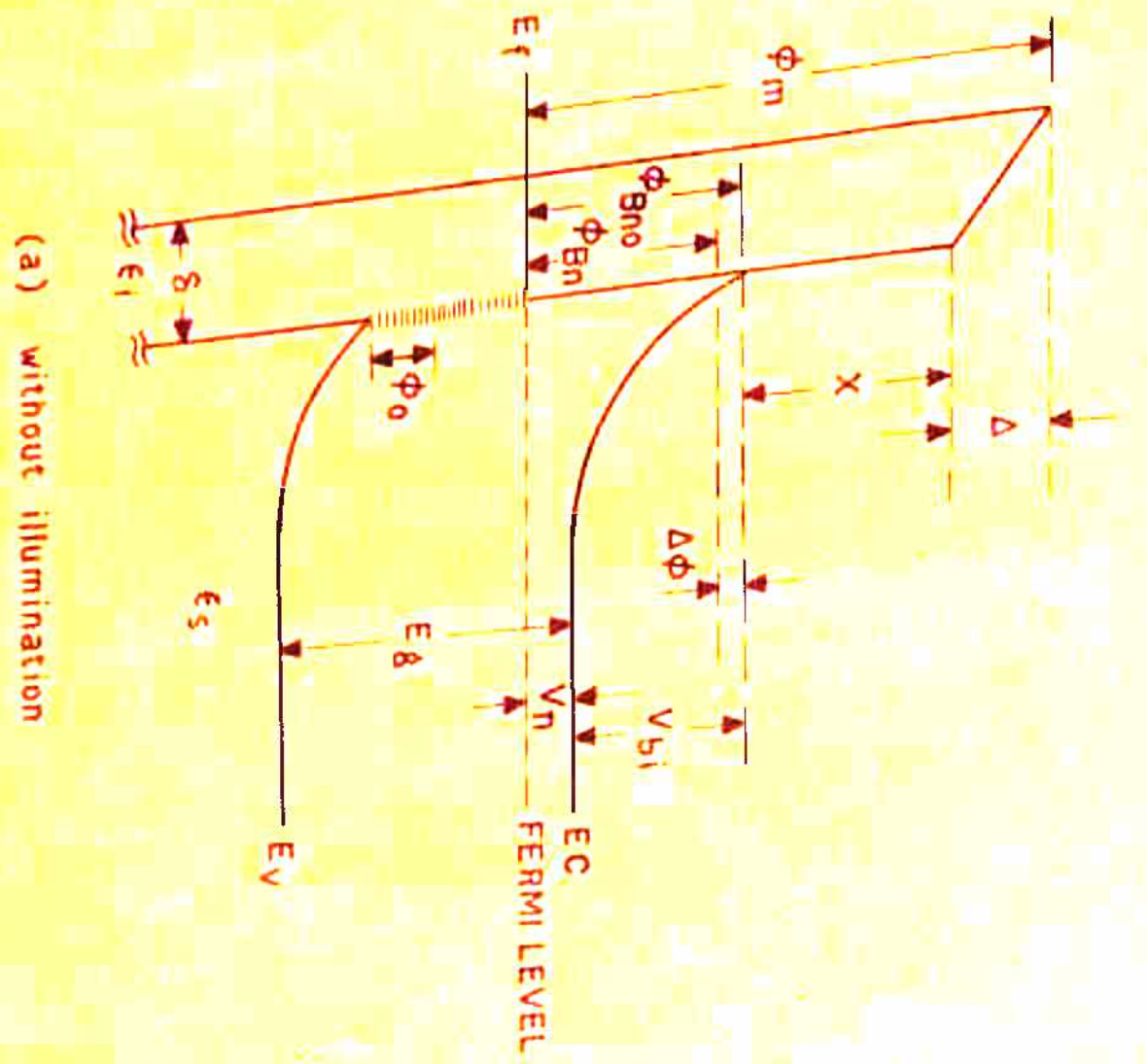


FIG. 5.1 ENERGY BAND DIAGRAM OF A M.S. SYSTEM.

the width of the semiconductor depletion region and L_p is the diffusion length for minority carrier holes.

In equation (5.3), the second term is the dark current arising because of the fact that illumination makes the device forward biased which, in turn, gives rise to the diode current or the dark current in a direction opposite to the photogenerated current I_{ph} . The dark current I_{Dark} mainly consists of two components, namely (1) the dark current I_n due to majority carrier electrons, and (2) the dark current I_h due to the minority carrier holes. The dark current component I_n due to majority carrier electrons is given by (14)

$$I_n = A^* T^2 \exp(-e \phi_{Bn}/kT) \left[\exp(eV_s/kT) - \exp(-eV_i/kT) \right] \quad (5.5)$$

In expression (5.5) A^* is the effective Richardson's constant, ϕ_{Bn} is the barrier height of the metal-semiconductor contact system, k is Boltzmann's constant and T is the operating temperature of the cell.

The dark current component due to minority carrier holes I_h is given by (14)

$$I_h = \frac{ep_{no} D_p}{L_p} \left[\exp(eV/kT) - 1 \right] \quad (5.6)$$

Where p_{no} is the equilibrium hole concentration and D_p is the diffusion coefficient for holes.

5.3 ELECTRON TUNNELING PROBABILITY AND EFFECT OF INTERFACIAL LAYER THICKNESS

In his analysis Fonash⁽¹⁴⁾ took the tunneling probability of electrons across the interfacial layer equal to unity. Srivastawa et al⁽¹⁵⁾ performed calculations to study the effect of interfacial layer thickness δ on the efficiency of schottky barrier solar cell for both the cases, namely, the case of difficult communication and that of easy communication. These authors found that the efficiency η first increases with the interfacial layer thickness δ and then gets saturated for higher values of δ for the case of difficult communication (Figure 5.2a). On the other hand the efficiency decreases with the increase in the interfacial layer thickness δ for efficient communication as shown in Figure (5.2b). A continuous increase in the efficiency η of the cell with δ in the initial stages leading finally to its (efficiency) saturation beyond a certain δ as shown in Figure (5.2a) seems quite unlikely. In the present work, expression (5.5) was modified by introducing the transmission factor T_{rn} to account for the electron tunneling across the interfacial layer and study its consequences on efficiency η .

The ratio of the current due to diffusion of minority carrier holes I_h to the current due to thermionic emission of majority carrier electrons I_n , known as injection ratio, is

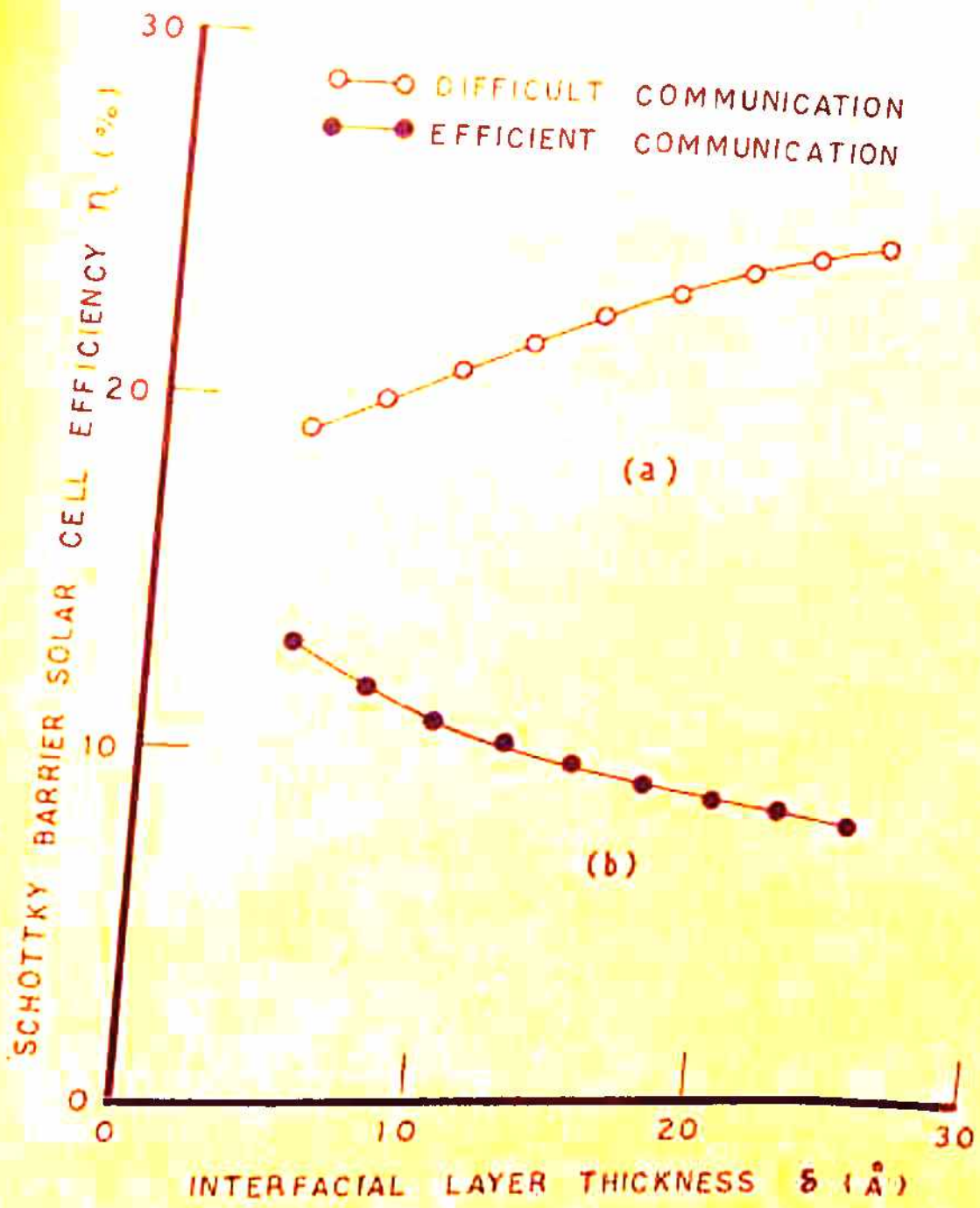


FIG. 5.2 VARIATION OF EFFICIENCY η WITH INTERFACIAL LAYER THICKNESS δ FOR DIFFICULT AND EFFICIENT COMMUNICATION BETWEEN INTERFACE STATES AND METAL.

usually of the order of $10^{-5} - 10^{-4}$ for silicon schottky diodes⁽¹⁷⁾. The expression for the dark current used by most of the authors is the one given by the thermionic emission approximation of the majority carriers^(6,15).

Introducing the transmission coefficient T_{rn} of electrons across the interfacial layer and the ideality factor n in the expression for the dark current, the dark current is given by

$$I_{\text{Dark}} = I_0 \cdot T_{rn} \cdot \left[\exp \left(\frac{eV}{nkT} \right) - 1 \right] \quad (5.7)$$

where I_0 is the reverse saturation current and given by

$$I_0 = A \cdot T^2 \exp \left(- e \phi_{Bn}^* / kT \right)$$

Where ϕ_{Bn}^* is the effective barrier height defined by $(\phi_{Bn} + V_i)$. The tunneling probability of electrons across the interfacial layer T_{rn} is given by⁽¹⁸⁾

$$T_{rn} = \exp \left\{ - \frac{8\pi}{3h} \frac{(2m^*)^{1/2} \delta}{\Delta - V_i} \left[(\tilde{\phi} + \Delta - V_i)^{3/2} - \tilde{\phi}^{3/2} \right] \right\} \quad (5.9)$$

Where Δ is the potential drop across the interfacial layer when the cell is not illuminated, $\tilde{\phi}$ is the average barrier height for electrons in the insulator gap, h is Planck's constant, m^* is the effective mass of electron and V_i is the

voltage developed across the interfacial layer on illumination. For low values of D_{si} the potential V_i developed across the interfacial layer is calculated using the boundary condition⁽¹⁸⁾

$$\epsilon_s E_s^o = \epsilon_i E_i^o = \epsilon_i \frac{\Delta - V_i}{\delta} \quad (5.10)$$

Where ϵ_s and ϵ_i are the permittivities of semiconductor and interfacial layer respectively and E_s^o and E_i^o are the electric fields associated with semiconductor and interfacial layer respectively. The ideality factor n is given by⁽¹⁸⁾

$$n = 1 + \epsilon_s \delta / \epsilon_i W \quad (5.11)$$

It is thus quite clear that the current I_{Dark} as given by equation (5.7) depends upon the transmission coefficient T_{rn} of electrons and the diode quality factor n . Taking into account the transmission coefficient T_{rn} across the interfacial layer and the ideality factor n , Srivastava et al⁽¹⁵⁾ studied the effect of δ on the conversion efficiency η of the schottky barrier solar cell. It was found that there exists an optimum thickness δ for which the conversion efficiency η is maximum as shown in Figure (5.3). The various parameters used during the computation are given in table (5.1)*. The detailed analysis to see the effect of interfacial layer thickness δ on solar cell parameters is discussed in Chapter VI.

*Work presented at National Solar Energy Convention in Jadavpur (1976) by Srivastava, Swami and Ghule.

TABLE-5.1

Parameters used in efficiency calculations of Schottky barrier
solar cell.*

e	$= 1.602 \times 10^{-19}$ Coul.	D_p	$= 10 \text{ cm}^2/\text{sec.}$
k	$= 1.380 \times 10^{-23}$ joule/ $^\circ\text{K}$	τ_p	$= 10^{-5}$ sec.
h	$= 6.625 \times 10^{-34}$ joule-sec.	α	$= 10^3 \text{ cm}^{-1}$
ϵ_0	$= 8.854 \times 10^{-14}$ farad/cm	ϕ_B	$= 0.20 \text{ eV}$
ϵ_s	$= 11.8 \epsilon_0$		
ϵ_i	$= 4.0 \epsilon_0$		
ϕ_K	$= 4.70 \text{ eV}$		
E_g	$= 1.12 \text{ eV}$		
A^*	$= 120 \text{ Amp cm}^{-2} \text{ } ^\circ\text{K}^{-2}$		
N_c	$= 2.8 \times 10^{19} \text{ cm}^{-3}$		
N_v	$= 1.02 \times 10^{19} \text{ cm}^{-3}$		
n_i	$= 1.6 \times 10^{10} \text{ cm}^{-3}$		
m	$= 9.108 \times 10^{-31} \text{ Kg.}$		
χ_p	$= 4.05 \text{ eV}$		
N_D	$= 10^{17} \text{ cm}^{-3}$		
p_{no}	$= 2560 \text{ cm}^{-3}$		
P_{input}	$= 135 \text{ m w/cm}^2$		

*The datas are taken from references 18 and 24.

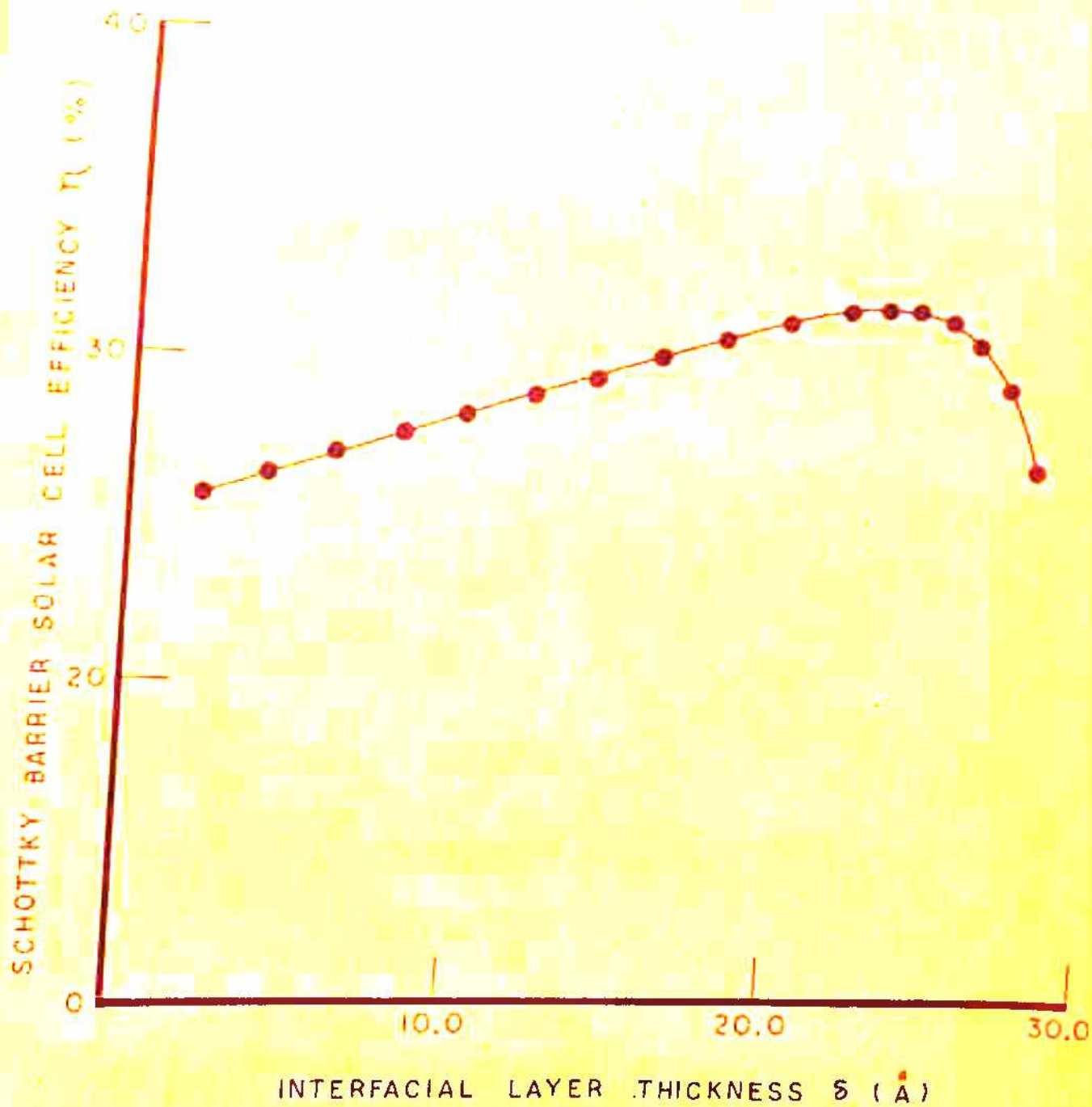


FIG. 5.3 EFFICIENCY η FOR SCHOTTKY BARRIER SOLAR CELL AS A FUNCTION OF INTERFACIAL LAYER THICKNESS δ WITH TRANSMISSION COEFFICIENT T_{rn} .

5.4 APPLICATION OF THE RESULTS TO CHEMICALLY GROWN AND EVAPORATED OXIDE LAYERS:

Schottky barrier solar cells possess many advantages over the conventional p-n junction solar cells. One great disadvantage with a schottky barrier solar cell is that the saturation current I_0 in such cells being large, the open circuit voltage V_{oc} is very small. For an ideal Au-n Si schottky diode, for which the diode quality factor n is taken as unity and ϕ_{Bn} , the barrier height at the metal semiconductor contact is 0.80 eV, the open circuit voltage V_{oc} is only 0.3 volts under AMO conditions whereas it is 0.6 volts for p-n junction solar cells. In a recent communication Ponpon and Siffert⁽⁵⁾ have shown that Au- nSi schottky barrier solar cells can be fabricated with increased V_{oc} . The interfacial layer between the metal and the semiconductor helps to attain a large values of V_{oc} . The values of V_{oc} observed experimentally by these authors range from 0.325 to 0.420 volts for the various schottky diode samples having chemically grown oxide layers. whereas the V_{oc} values range from 0.42 to 0.55 volts for evaporated oxide layer samples. The figure 0.55 volts comes closer to the 0.6 volts attainable with the conventional p-n junction solar cells. The above authors have also calculated theoretically the open circuit voltage using the observed values of

short circuit (photogenerated) current I_{sc} , effective barrier height ϕ_{Bn}^* and the diode quality factor n . It is found that the calculated V_{oc} values seem to agree with the observed values for chemical oxide layer samples. The observed and calculated values, however, do not agree for the evaporated oxide layer.

The simple theory of Fonash⁽¹⁴⁾ takes the tunneling probability of transmission for electrons, as also the ideality factor, as unity. According to Fonash⁽¹⁴⁾ the expression for the current I flowing through the device on illumination is given by

$$I = I_{ph} - I_o \left[\exp(eV/kT) - 1 \right] - I_{oD} \left[\exp(eV/kT) - 1 \right] \quad (5.12)$$

In equation (5.12) I_{o1} and I_{oD} are the reverse saturation current components due to thermionic emission of majority carrier electrons and the diffusion of minority carrier holes respectively. In the present work the dark current component due to thermionic emission of electrons has been modified by taking into account the tunneling probability of transmission of electrons across the interfacial layer. In general the current voltage characteristics can be written in the form as given below

$$I = I_{ph} - I_o' \left[\exp(eV/nkT) - 1 \right] \quad (5.13)$$

Where I'_0 is the modified reverse saturation current such that $I'_0 = I_{01}$ when the transmission of electrons across the interfacial layer is quite large and $I'_0 = I_{0D}$ when the transmission of electrons across the interfacial layer is extremely poor. The transmission coefficient of electrons T_{rn} , depends on the interfacial layer thickness δ , as given by equation (5.9). Thus the dark current also depends on δ . Beyond certain δ , the current component due to thermionic emission becomes so small that the dark current is mainly due to the diffusion of the minority carrier holes. The open circuit voltage V_{oc} is given by

$$V_{oc} = \frac{nkT}{e} \ln \left(\frac{I_{ph}}{I'_0} + 1 \right) \quad (5.14)$$

It is found from table 5.2 that the observed values for chemically grown oxide layer samples agree when $I'_0 = I_{01}$ in equation (5.14), whereas the agreement for evaporated oxide layer samples is better when $I'_0 = I_{0D}$ in equation (5.14). **

This suggests that the tunneling of the majority carrier electrons is quite appreciable in the case of chemically grown oxide layer samples, whereas the diffusion of minority carriers plays the dominant role in determining the open circuit voltage in the case of evaporated oxide layer

**Work presented at the National Solar Energy Convention
Bhavnagar (1978) by Swami, Srivastava and Ghule.

sample. In evaporated oxide layer samples the majority carrier current due to electrons, seems to be greatly attenuated by the transmission factor across the interfacial layer. This seems to be the reason why evaporated oxide layer results agree with those given by equation (5.14) with $I'_0 = I_{00}$.

Table (5. 2) shows that the experimental and theoretic values of V_{oc} agree when transmission is unity for chemically grown oxide layer, whereas table (5.3) shows a better agreement between experimental and theoretically V_{oc} values when transmission factor is not unity.

5.5 EFFECT OF DONOR DENSITY ON THE PERFORMANCE OF SCHOTTKY BARRIER SOLAR CELL:

It was pointed out earlier that the donor density N_D , also appears in the expressions (5.1-5.2) for the voltage developed in the schottky barrier solar cell. Thus apart from the interfacial layer thickness δ and the density of interfacial states D_{si} , another parameter which affects the performance of schottky barrier solar cell is the donor density N_D . Some attempts were made by Shewchun, Singh and Green⁽¹⁹⁾ to show the effect of substrate doping on the conversion efficiency of schottky barrier solar cells. These authors pointed out that the degradation in diffusion length is an important parameter which causes a decrease in schottky barrier solar

TABLE-5.2

Experimental and theoretically calculated values of V_{oc} for semiconductors

From oxide layer samples

OBSERVED VALUES			CALCULATED VALUES		
Effective barrier height ϕ_{bn}^* (eV)	Diode quality factor n	Open circuit voltage V_{oc} (mV)	V_{oc} (mV) $I_0 = I_{01}$	V_{oc} (mV) $I_0 = I_{00}$	
0.79	1.34	325	350	579	
0.80	1.11	300	301	480	
0.80	1.13	310	307	489	
0.81	1.04	312	297	451	
0.815	1.22	356	343	529	
0.825	1.15	398	361	499	
0.83	1.22	398	368	529	
0.84	1.19	405	371	517	
0.85	1.39	420	447	603	

TABLE-3.3

Experimental and theoretically calculated values for evaporated on the
layer samples

EXPERIMENTALLY OBSERVED VALUES			CALCULATED VALUES	
Effective barrier height ϕ_{Bn}^* (eV)	Diode quality factor n	Open circuit Voltage V_{oc} (mV)	V_{oc} (mV) $I_0 = I_{01}$	V_{oc} (mV) $I_0 = I_{02}$
0.83	1.59	490	460	703
0.88	1.34	550	456	593
0.88	1.25	517	423	553
0.89	1.19	536	415	527
0.92	1.21	505	456	536

cell efficiency. Experimental results to show the effect of resistivity on V_{oc} for an Al-p type silicon schottky barrier solar cell, are presented by Godfrey and Green⁽²⁰⁾. They pointed out that there is an optimum resistivity for which the open circuit voltage has the maximum value. These authors also presented theoretical calculations to show the effect of substrate resistivity on open circuit voltage V_{oc} . Their calculations show a linear variation of open circuit voltage with substrate resistivity. However, their calculated variation of open circuit voltage V_{oc} does not exhibit the behavior of experimentally observed variation of V_{oc} with substrate resistivity. This article deals with the effect of doping density on the short circuit current, open circuit voltage and efficiency of schottky barrier solar cells. Results based on a number of calculations incorporating the various factors with doping density are reported in the following articles. Results of calculations are obtained for an Au-n Si schottky barrier solar cell.^{***}

Taking into account the series resistance R_s , the current voltage characteristics is given by

$$I = I_{ph} - I_0 \left[\exp\left(\frac{e(V + IR_s)}{nkT}\right) - 1 \right] \quad (5.15)$$

Where I_0 is the reverse saturation current. The internal series resistance R_s of the schottky barrier solar cell is given by⁽²¹⁾

^{***} This paper has been accepted for publication in Indian Journal of Physics.

$$R_s = \frac{\rho_s t_s}{A} \quad (5.16)$$

where t_s is the thickness of the semiconductor, A is the area of the solar cell and ρ_s is the resistivity of the semiconductor. The resistivity of the n-type semiconductor with donor density N_D is given by

$$\rho_s = \frac{1}{e \mu_n N_D} \quad (5.17)$$

where μ_n is the mobility for majority carrier electrons.

From equation (5.15), the short circuit current $I_{sc}(V = 0)$, open circuit voltage $V_{oc}(I=0)$ and the efficiency $\eta (= P_{mp}/P_{in})$ can be obtained from the I-V characteristics.

5.6 RESULTS AND DISCUSSION:

The graphs are obtained for an Au-n Si system. The parameters used in calculations are given in table 5.1. The value for P_{in} for AMO sunlight is 135 mW/cm^2 .

5.6.1 EFFECT OF DONOR DENSITY ON SHORT CIRCUIT CURRENT :

The variation of short circuit current with donor density is shown in Figure (5.4) and it appears that it remains almost constant upto a donor density $10^{15}/\text{cm}^3$, but thereafter it decreases with donor density N_D . The short circuit current, given by

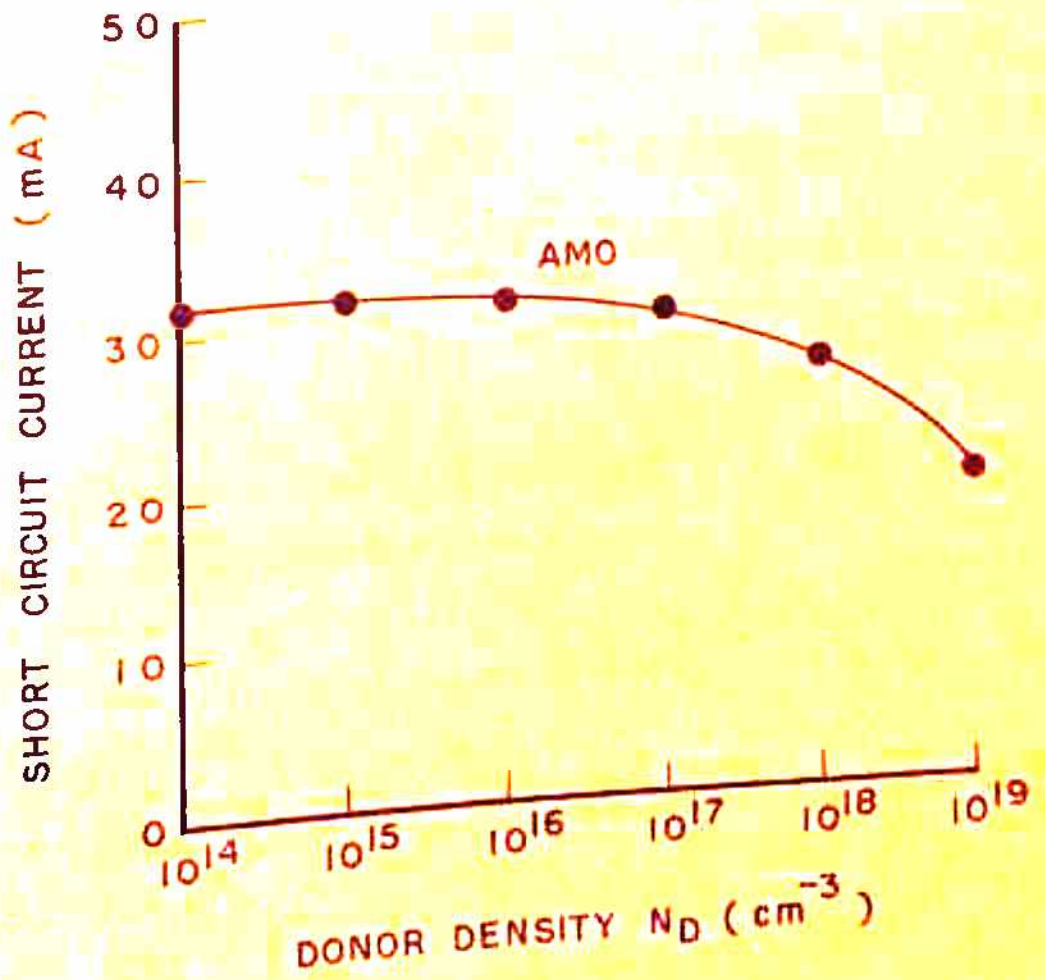


FIG. 5.4 EFFECT OF DONOR DENSITY ON SHORT CIRCUIT CURRENT OF SCHOTTKY BARRIER SOLAR CELL.

$$I_{sc} = e \phi_{flux} \left[1 - \frac{e^{-\alpha W}}{1 + \alpha L_p} \right], \quad (5.18)$$

depends upon the incident photon flux ϕ_{flux} , the absorption coefficient α , depletion region width W and the diffusion length L_p . The donor density alters the minority carrier life time, mobility, diffusion length and depletion region width W . The diffusion length, as given by $L_p = (\mu_p \tau_p)^{1/2}$, is governed by the minority carrier life time τ_p and the diffusion coefficient D_p for holes. The increased donor density provides increased majority carriers. The minority carrier holes, on the other hand, can be calculated from the relation $p_{no} = n_i^2 / n_{no}$, where n_{no} is the concentration of electrons in the n type semiconductor and is given by $n_{no} = \frac{1}{2} \left[(N_D - N_A) + \left\{ (N_D - N_A)^2 - 4 n_i^2 \right\}^{1/2} \right]$. At room temperature, for n type semiconductor, $N_D \gg N_A$ and $(N_D - N_A) \gg n_i$, the electron density n_{no} in n type semiconductor is given by N_D . Thus, the concentration of the minority carriers holes in n type semiconductor can be written in the form

$$p_{no} = n_i^2 / N_D \quad (5.19)$$

Equation (5.19) shows that an increase in the majority carrier density results in a decrease in the minority carrier density. Therefore, the minority carrier holes, which are surrounded by the majority carrier electrons, have more chances to recombine with the majority carriers available from increased donor density

The increase in the probability of recombination causes the minority carrier life time to decrease. The empirical relation for the dependence of minority carrier life time is given by (22)

$$\tau_p = \frac{3.9 \times 10^{-4}}{1 + N_D/N_{D0}} \quad (5.20)$$

where $N_{D0} = 7.1 \times 10^{15}/\text{cm}^3$.

It appears from the above expression (5.20) that increase of N_D decreases the minority carrier life time τ_p . The diffusion length also depends upon the diffusion coefficient D_p . The diffusion coefficient is determined by the operating temperature T and the mobility for holes μ_p and is given by $D_p = \frac{kT}{e} / \mu_p$. The mobility of holes decreases with increase in donor density (23). Thus for a constant value of operating temperature, the diffusion coefficient also decreases as a result of a decrease in mobility. Thus, a decrease in minority carrier life time τ_p , as also a decrease in the diffusion coefficient D_p , causes the diffusion length L_p to decrease. The diffusion length L_p plays an important role in determining the short circuit current I_{sc} and its dependence on diffusion length L_p is shown in equation (5.18). It appears from equation (5.18) that the decrease in diffusion length L_p decreases the short circuit current I_{sc} . Another factor which also appears to be

responsible for the decrease of the short circuit current is the depletion region width W . The depletion region width under short circuit conditions is given by

$$W = \left[\frac{2 \epsilon_s}{e N_D} V_{bi} \right]^{1/2} \quad (5.21)$$

where V_{bi} is the built-in potential. V_{bi} is given by

$$V_{bi} = \phi_{Bn} - V_n = \phi_{Bn} - \frac{kT}{e} \ln \left(\frac{N_c}{N_D} \right) \quad (5.22)$$

where N_c is the density of states in the conduction band and V_n is the difference between the semiconductor Fermi level and conduction band edge in the bulk of the semiconductor. The increase in V_{bi} has much less effect in increasing W than a decrease in W brought about by the factor N_D in equation (5.21). Thus, the net effect is that the depletion region width W decreases with increase in donor density. It is clear from equation (5.18) that a decrease in depletion region width W , apart from the decrease in diffusion length L_p , also decreases the short circuit current I_{sc} . Thus both the factors, namely decrease of L_p and that of W with N_D , result in a decrease of the short circuit current. This seems to explain the variation of I_{sc} with N_D (Figure 5.4).

5.6.2 EFFECT OF DONOR DENSITY ON OPEN CIRCUIT VOLTAGE V_{oc} :

The effect of donor density on the open circuit voltage V_{oc} is shown in figure (5.5). It appears from the graph that the open circuit voltage first increases with donor density N_D , attains a maximum value and thereafter decreases with N_D . The primary reason for increase in the open circuit voltage seems to be due to increase in diode quality factor n . The diode quality factor n increases with donor density N_D through decrease in the depletion region width W as given by (15)

$$n = 1 + \epsilon_s \delta / \epsilon_i W \quad (5.23)$$

The ratio of the current due to diffusion of the minority carrier holes to the current due to thermionic emission of majority carriers, known as injection ratio, is usually of the order of $10^{-5} - 10^{-4}$ for silicon schottky diodes (16). Thus, under such conditions, the dependence of open circuit voltage V_{oc} on diode quality factor n is given by

$$V_{oc} = \frac{nkT}{e} \ln \left[\frac{I_{ph}}{I_0} + 1 \right] \quad (5.24)$$

In schottky barrier solar cells $I_{ph}/I_0 \gg 1$, thus neglecting 1 and substituting $A^* T^2 T_{rn} \exp(-e \phi_{Bn}^*/kT)$ for I_0 , the expression (5.24) for V_{oc} can be written in the form

$$V_{oc} = n \left[\phi_{Bn}^* + \frac{kT}{e} \ln(I_{ph}) - \frac{kT}{e} \ln(A^* T_{rn} T^2) \right] \quad (5.25)$$

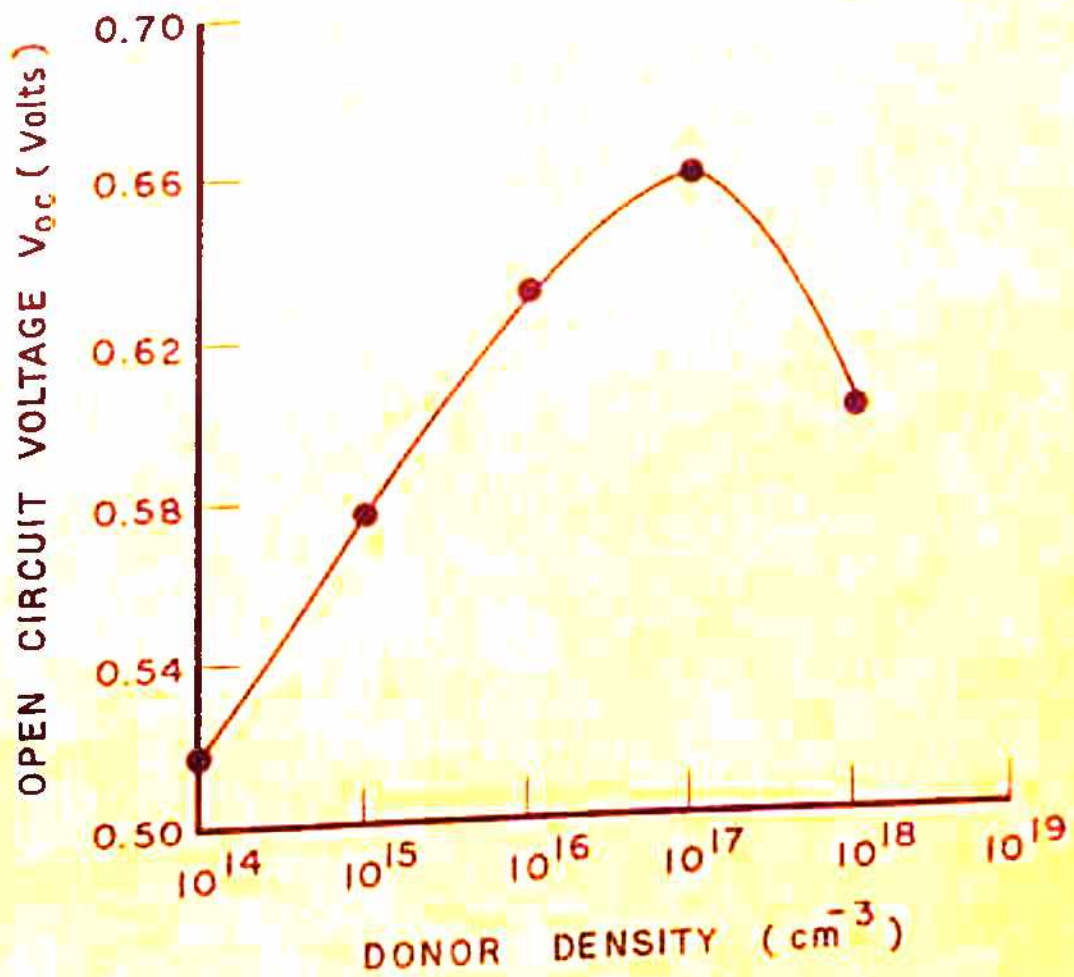


FIG.5.5 EFFECT OF DONOR DENSITY ON OPEN CIRCUIT VOLTAGE OF SCHOTTKY BARRIER SOLAR CELL .

where ϕ_{Bn}^* is the effective barrier height ($\phi_{Bn} + V_i$) of the metal semiconductor system and the remaining symbols have been explained earlier. It appears from equation (5.25) that the open circuit voltage increases with diode quality factor n in its initial stages. The increase in diode quality factor n with donor density is the consequence of the increased recombination in the space charge region. Equation (5.25) also represents the dependence of open circuit voltage V_{oc} on photogenerated current I_{ph} and ^{the} effective barrier height ϕ_{Bn}^* . V_{oc} depends upon I_{ph} as in equation (5.25). However, the dependence of I_{ph} (or I_{sc}) on N_D , as explained earlier shows that I_{ph} decreases for higher values of N_D . Therefore after $N_D = 10^{17}/\text{cm}^3$, the decrease in V_{oc} seems to be due to decrease in I_{ph} .

The effective barrier height ϕ_{Bn}^* also affects the open circuit voltage. For low values of surface states the voltage V_i developed across the interfacial layer is given by (18)

$$V_i = \Delta - (\epsilon_s / \epsilon_i) \cdot E_s^0 \delta \quad (5.26)$$

Thus, the effective barrier height becomes

$$\phi_{Bn}^* = \phi_{Bn} + \Delta - \frac{\epsilon_s}{\epsilon_i} E_s^0 \delta \quad (5.27)$$

The electric field E_s^0 associated with semiconductor is given by

$$E_s^0 = \frac{e N_D}{\epsilon_s} w \quad (5.28)$$

It appears from equation (5.28) that at higher values of donor density the electric field E_s^0 becomes quite large and decreases the effective barrier height ϕ_{Bn}^* as given by equation (5.27). The decrease in ϕ_{Bn}^* decreases the open circuit voltage V_{oc} as shown by equation (5.25). After $10^{17}/\text{cm}^3$, the decrease in photogenerated current I_{ph} and decrease in effective barrier height ϕ_{Bn}^* (25) with donor density seems to be stronger than an increase in the diode quality factor n and the net effect is a decrease in the open circuit voltage V_{oc} with N_D . At higher values of N_D the schottky barrier lowering also reduces the open circuit voltage but in the present calculations the effect of schottky barrier lowering has not been considered. The experimental results for the variation of the open circuit voltage with donor density are not available in the literature for metal -n silicon type schottky barrier solar cells. The results showing the variation of V_{oc} with substrate resistivity, presented by Godfrey and Green⁽²⁰⁾, exhibit a similar trend as the calculated dependence of V_{oc} on the donor density for n-type silicon.

5.6.3 EFFECT OF DONOR DENSITY ON EFFICIENCY:

The variation of efficiency with donor density is shown in Figure (5.6). The efficiency of the schottky barrier solar cell is determined by the maximum power point. The maximum power point depends upon the maximum area rectangle that can be inscribed in the current voltage characteristics of the schottky barrier solar cell. Figure (5.6) shows that the

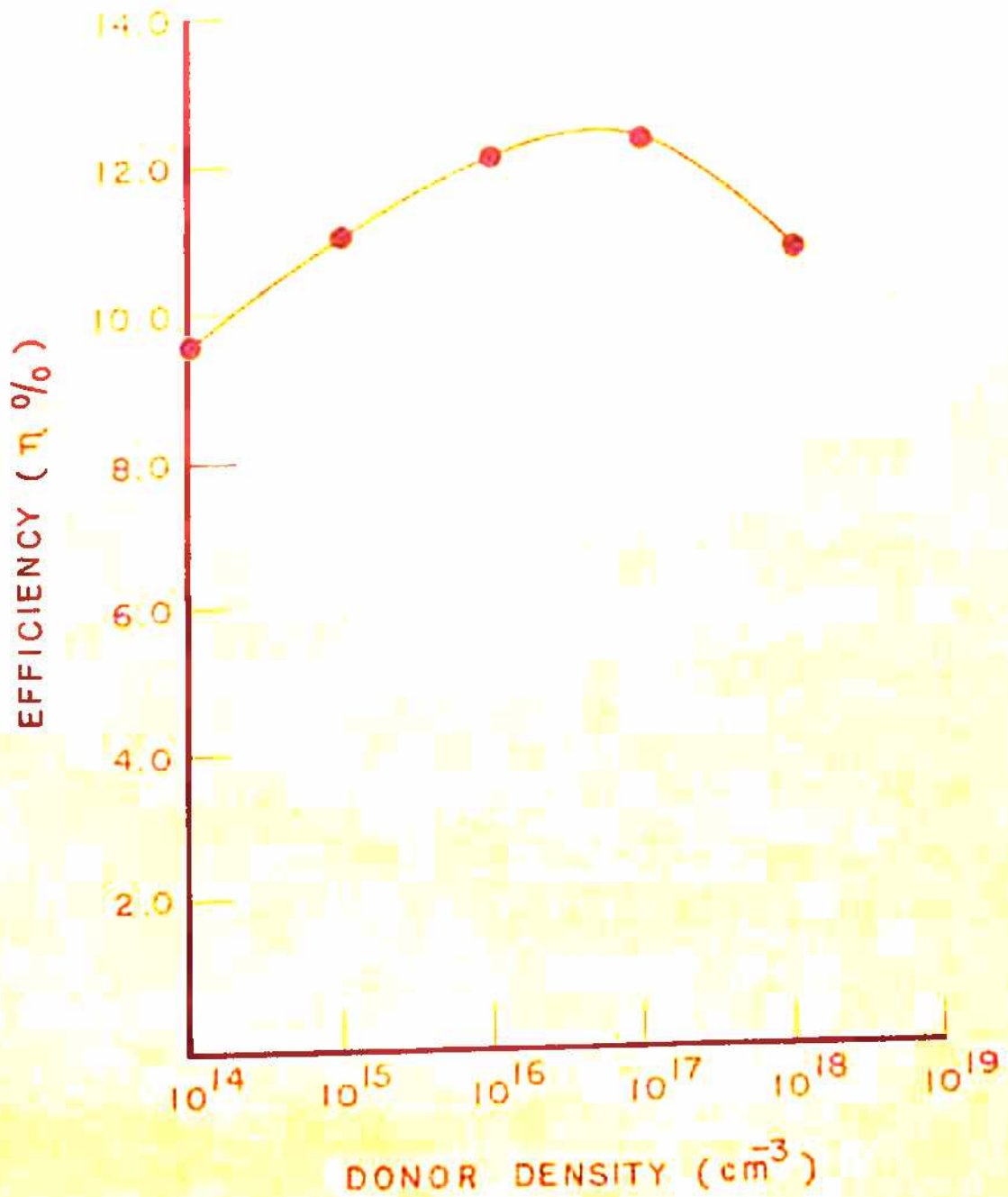


FIG.5.6 EFFECT OF DONOR DENSITY ON EFFICIENCY OF SCHOTTKY BARRIER SOLAR CELL.

conversion efficiency η first increases with the donor density but after acquiring its maximum value it starts decreasing with further increase in donor density. The increase in efficiency in the initial stages seems to be due to increase in V_{OC} . Another factor which appears to increase the efficiency of schottky barrier solar cell is a decrease in the series resistance R_s . The internal series resistance, as given by equation (5.16), is the consequence of resistivity of the semiconductor, thickness of the solar cell and area of the cell. The resistivity of the semiconductor as given by equation (5.17), appears to decrease with donor density which in turn lowers the series resistance R_s . The decrease in the series resistance R_s improves the maximum rectangle area ^sincribed in the current voltage characteristics of the solar cell and hence helps in improving the efficiency of the solar cell. After attaining its maximum value, the fall in efficiency η of the schottky barrier solar cell with further increase in donor density seems to be caused by a decrease in the short circuit current accompanied by an increase in the reverse saturation current I_0 . The net effect is a decrease in the power generating current. The open circuit voltage V_{OC} also decreases at high N_D values as discussed earlier. Thus, the decrease in the power generating current and the open circuit voltage degrades the maximum power point which in turn lowers the efficiency of the cell. This seems to explain the variation of efficiency η with donor density N_D .

References

1. G.S. Stirn and I.C.M. Yeh, Appl. Phys. Lett. Vol. 27, pp. 95 (1975).
2. W.A. Anderson and R.A. Milano, Proc. IEEE Vol. 63, pp. 206 (1975).
3. E.J. Charlson and J.C. Lien, J. Appl. Phys. Vol. 46, pp. 3982 (1975).
4. D.R. Lillington and W.G. Townsend, Appl. Phys. Lett. Vol. 28, pp 97 (1976).
5. J.P. Ponpon and P. Siffert, J. Appl. Phys. Vol. 47, pp. 3248
6. E. Fabre, Appl. Phys. Lett. Vol. 29, pp. 607(1976).
7. A.H.M. Kipperman and M.H. Omar, Appl. Phys. Lett. Vol. 28, pp 621 (1976).
8. E. Fabre, J. Michel and V. Bandet, Twelfth IEEE Photo-voltaic Specialists Conference, New York, pp 904(1976).
9. D.R. Lillington and W.G. Townsend, Appl. Phys. Lett. Vol. 31, pp 471 (1977).
10. Yasuhiro Maedo Appl. Phys. Lett. Vol. 33 pp. 501(1978).
11. W.A. Anderson et al, Appl. Phys. Lett. Vol. 33, pp 588(1978)
12. R.B. Godfrey and M.A. Green, Appl. Phys. Lett. Vol. 33, pp 637 (1978).

13. S.Kař, J. Appl. Phys. Vol. 49, pp. 5278 (1978).
14. S.J. Fonash, J. Appl. Phys. Vol. 46. pp 1286 (1975).
15. W.A. Anderson et al, J. Appl. Phys. Vol. 45 pp. 3913 (1974)
16. S.Srivastava, N.K.Swami and H.M.Ghule, Proc. National Solar Energy Convention, Jadavpur(Calcutta) pp107 (1976).
17. M. Pepper, Metal semiconductor contact, Published by the Institute of Physics Belgrave, Square London (1974).
18. V.I. Strikha, Radio Engineering and Electronics Physics, Vol. 9 pp. 552 (1964).
19. J. Shewchun, R. Singh and M.A. Green, J. Appl. Phys. Vol. 48 pp. 765 (1977).
20. R.B.Godfrey and M.A. Green, International Solar Energy Congress, Extended Abstract, New Delhi, Vol. 1, Abstract No. 0237, pp. 434 (1978).
21. P.K. Dubey, Appl. Phys. Lett. Vol. 29, pp.435 (1976).
22. J.G. Fossum, Solid State Electronics Vol. 19, pp. 269(1976)
23. Anant G. Sabnis, Solid State Electronics Vol. 21, pp 581 (1978).
24. S.M. Sze, Physics of Semiconductor Devices, John Willey and Sons. Inc. New York (1969).

CHAPTER-VI.EFFECT OF HOLE TRANSMISSION IN SCHOTTKY BARRIER SOLAR
CELLS.

6.1	Theory.	170
6.2	Transmission of electrons and holes.	173
6.3	Calculations for V_s and V_i	174
6.4	Results and discussion.	177

CHAPTER- VI.6.1. PHOTO TRANSMISSION IN SCHOTTKY BARRIER SOLAR CELLS

In Chapter V the expressions given by Fonash⁽¹⁾ for the voltage V developed under illumination by a metal - n type semiconductor system, in which the metal work-function is greater than that of the n-type semiconductor, were discussed and analysed. These expressions are

$$V = (1 + e \delta D_{si} / \epsilon_i) \cdot V_s + C [V_{bi}^{1/2} - (V_{bi} - V_s)^{1/2}], \quad (6.1)$$

for the case of difficult communication and

$$V = V_s + \left[\frac{C}{1 + e \delta D_{si} / \epsilon_i} \right] [V_{bi}^{1/2} - (V_{bi} - V_s)^{1/2}], \quad (6.2)$$

for the case^{of} efficient communication. The various symbols appearing in equations (6.1) and (6.2) and the conditions under which the communication is termed difficult or efficient have also been discussed in Chapter V. These equations were modified by incorporating a factor taking into account the tunneling probability T_{rn} of the electrons across the interfacial layer. The effect of donor density was also considered. However, the expression for the photogenerated

current used in Chapter V was independent of δ . Experiment results presented by Lillington and Townsend⁽²⁾ show that beyond a certain value of δ there is a decrease in the short circuit current. An interfacial layer of greater thickness δ will modify the potential drops across the interfacial layer and the depletion layer. This, in turn, is bound to effect the net hole current which governs the magnitude of the photogenerated current I_{ph} . The expressions giving the current I and the voltage V -even after taking account of electron transmission-need further modification, namely incorporation of a factor T_{rh} which accounts for the hole transmission across the interfacial layer. Such a factor alone can account for a decrease in I_{ph} for larger values of δ . A study of the schottky barrier solar cell system taking into account the factor T_{rh} forms the subject matter of this chapter.

Olsen⁽³⁾ worked on metal-p type silicon schottky barrier system and considered the transmission coefficient for tunneling of minority carrier electrons and the majority carrier holes across the interfacial layer. In this work the photogenerated current was considered to be independent of interfacial layer thickness δ which appears quite unlikely. Card⁽⁴⁾ also considered the effect of transmission of electrons and holes across the interfacial layer. The effect of interfacial layer thickness, taking into account electron and hole

transmission, on various parameters of a schottky barrier solar cell is presented in the following articles*.

6.1 THEORY :

We consider a schottky barrier solar cell consisting of a metal and an n type semiconductor, the metal being of higher work function than the semiconductor. Illuminating the schottky barrier solar cell results in a voltage V across the cell, a part V_i of which appears across the interfacial layer of thickness δ , while the rest $V_s (= V - V_i)$ appears across the depletion region of width W of the semiconductor. The energy band diagram of Au- n Si system with and without illumination is shown in Figure (6.1). The total current I , flowing in the external circuit from metal to semiconductor under illumination, is given by

$$I = I_{ph} - I_{Dark} \quad (6.3)$$

Where I_{ph} is the photogenerated current due to absorption of light in the depletion region and I_{Dark} is the dark current resulting on account of forward biasing of the solar cell.

I_{ph} is given by⁽⁵⁾

$$I_{ph} = e \phi_{flux} T_{rm} \beta \left\{ \left[\frac{\alpha L_p}{1 + \alpha L_p} \frac{v_p \left(\frac{T_{rh}}{4} + D_{si} C_{pi} \right)}{D_p/L_p + v_p \left(\frac{T_{rh}}{4} + D_{si} C_{pi} \right)} e^{-\alpha W} \right] + [1 - \exp(-\alpha w)] (I_{rh} + D_{si} C_{pi}) \right\} \quad (6.4)$$

*Paper entitled "Role of interfacial layer in schottky barrier solar cell" by N.K.Swami, S.Srivastava and H.M.Ghule published in J. of Phys. D. p. 765 (1979).

In equation (6.4) ϕ_{flux} is the incident photon flux, T_{rh} is the transparency of the metal film, β is the quantum efficiency of the internal photoeffect, α is the absorption coefficient of the semiconducting material, D_{si} is the density of interface states, C_{pi} is the capture cross section of holes, D_p is the diffusion coefficient for holes, L_p is the diffusion length of holes and v_p is the thermal velocity of holes through the interfacial layer. The expression (6.4) given by Deborozhanskii et al. (5) was used by these authors to explain the effect of photon energy $h\nu$ on photogenerated current I_{ph} . However, the form of the transmission coefficient for holes and the effect of interfacial layer thickness δ on the performance of a schottky barrier solar cell is not discussed by these authors. The expression (6.4) is more general than that used by several authors (1,6,7). If

$$(T_{\text{rh}} + D_{\text{si}} C_{\text{pi}}) \rightarrow 1 \text{ and } \frac{D_p}{L_p} \ll v_p \left(\frac{T_{\text{rh}}}{4} + D_{\text{si}} C_{\text{pi}} \right),$$

$$I_{\text{ph}} = \phi_{\text{flux}} T_{\text{rm}} \beta \left[1 - \frac{\exp(-\alpha \delta)}{1 + \alpha L_p} \right] \quad (6.5)$$

The expression (6.5) for I_{ph} is the same as that used by Anderson et al. (6) (1974), Fonash (1975) and Landsberg and Klimpke (7) (1977). Expression (6.5) is independent of δ . It is thus clear that for those values of δ for which the condition $D_p/L_p \ll v_p \left(\frac{T_{\text{rh}}}{4} + D_{\text{si}} C_{\text{pi}} \right)$ holds, I_{ph} will be independent

of δ . However, the transmission coefficient T_{ph} for holes across the interfacial layer, which appears in the general expression (6.4) for I_{ph} , also depends upon the thickness δ . It is therefore necessary to consider the effect of δ on the photogenerated (short circuit) current I_{ph} as also its effect on the efficiency of the schottky barrier solar cell.

The second term in equation (6.3) is the dark current arising because of the fact that illumination makes the device forward biased which in turn gives rise to diode current (dark current) in a direction opposite to the photogenerated current I_{ph} . The two components, contributing to the dark current I_{dark} , namely the thermionic emission of majority carrier electrons I_n and the diffusion^{of} minority carrier holes I_p , are discussed in article (5.2) of chapter V.

Besides the usual thermionic emission current I_n and the diffusion current I_p in the case of Au-nSi schottky barrier solar cell, the current component arising from generation recombination processes in the space charge region is given by⁽³⁾

$$I_{rec} = \frac{e n_i \delta}{\tau_p} \left[\exp (eV/2kT) - 1 \right] \quad (6.6)$$

where τ_p is the minority carrier life time and n_i is the intrinsic carrier density.

This transmission of electrons T_{rn} , the transmission of holes T_{rh} and the depletion region width W depend upon the interfacial layer thickness δ , which in turn determine the photogenerated current I_{ph} and the dark current I_{Dark} of a schottky barrier solar cell. It is therefore possible to study the effect of δ on I_{sc} , V_{oc} and η of a schottky barrier solar cell.

6.2 TRANSMISSION OF ELECTRONS AND HOLES:

The transmission coefficient for electrons across the interfacial layer is given by⁽⁹⁾

$$T_{rn} = \exp \left[- \frac{8 \pi (2m_e^*)^{1/2} \delta}{3h (\Delta - V_i)} \left\{ (\tilde{\phi}_e + \Delta - V_i)^{3/2} - \tilde{\phi}_e^{3/2} \right\} \right] \quad (6.7)$$

where m_e^* is the effective mass of electrons. $\tilde{\phi}_e$ is the average barrier height for electrons in the insulator gap and Δ is the potential drop across the interfacial layer under thermal equilibrium. The transmission coefficient T_{rn} across the interfacial layer, can also be written in a simpler form given by

$$T_{rn} = \exp \left[- \frac{4 \pi}{h} (2 m_e^* \tilde{\phi}_e)^{1/2} \delta \right] \quad (6.8)$$

To reduce expression (6.7) to the form of expression (6.8) we find that for $(\Delta - V_i) \ll \tilde{\phi}_e$ the quantity $(\tilde{\phi}_e + \Delta - V_i)^{3/2} - \tilde{\phi}_e^{3/2}$ can be approximated by

$$(\tilde{\phi}_e + \Delta - V_i)^{3/2} - \tilde{\phi}_e^{3/2} \approx \tilde{\phi}_e^{3/2} \left[1 + \frac{3}{2} \frac{\Delta - V_i}{\tilde{\phi}_e} \right] - \tilde{\phi}_e^{3/2} \quad (6.9)$$

Substituting equation (6.9) in equation (6.7) yields the expression (6.8) for the transmission coefficient T_{rn} .

The transmission coefficient for holes T_{rh} can also be expressed by a similar expression by replacing the effective mass of electrons by that of holes and the barrier height in the insulator gap for electrons by that of holes. Hence T_{rh} can be put in the form

$$T_{rh} = \exp \left[- \frac{4\pi}{h} (2 m_h^* \tilde{\phi}_h)^{1/2} \delta \right] \quad (6.10)$$

In expression (6.10) m_h^* is the effective mass of holes and $\tilde{\phi}_h$ is the barrier height for holes in the insulator gap.

6.3 CALCULATIONS FOR V_s AND V_i :

The parameters, voltage developed across the interfacial layer V_i and voltage developed across the space charge region V_s , influence considerably the conversion efficiency of schottky barrier solar cell. V_s and V_i can be obtained as follows:

If the image force lowering $\Delta\phi$ and thermal voltage kT/e are neglected, the space charge Q_{sco} per unit area of the semiconductor in thermal equilibrium is given by (10)

$$Q_{sco} = [2e \epsilon_s N_D (\phi_{Bn} - V_n)]^{1/2} \quad (6.11)$$

and the surface state charge density on the semiconductor Q_{sso} is given by (10)

$$Q_{sso} = -e D_{si} [E_G - \phi_0 - \phi_{Bn}] \quad (6.12)$$

The total equivalent surface charge density on the semiconductor surface is given by $(Q_{sco} + Q_{sso})$. The net charge developed on the metal surface Q_{mo} will be equal and opposite to the surface charge density

$$Q_{mo} = - (Q_{sco} + Q_{sso}) \quad (6.13)$$

Similarly on illumination, the charge developed in the depletion layer Q'_{sc} and the surface state charge density Q'_{ss} are given by

$$Q'_{sc} = [2e N_D \epsilon_s (\phi_{Bn} - V_n - V_s)]^{1/2} \quad (6.14)$$

and

$$Q'_{ss} = -e D_{si} [E_{fss} - \phi_0] \quad (6.15)$$

In the absence of any space charge effects in the interfacial layer, one gets the potential drop across the interfacial layer on illumination from the expression (10)

$$\Delta - V_i = \delta Q'_m / \epsilon_i \quad (6.16)$$

Substituting the values of Q_{mo} , Q'_m and $\Delta (= \delta Q_{mo} / \epsilon_i)$ in equation (6.16) the following expression is obtained

$$V = V_s \cdot C \left[V_{bi}^{1/2} - (V_{bi} - V_c)^{1/2} \right] + \frac{e N_D \delta}{\epsilon_i} [E_{rfs} + \phi_{sn} - E_c] \quad (6.17)$$

In the preceding expressions (6.11-6.17), $C = \frac{-e \epsilon_s N_D}{\epsilon_i^2} \delta^2$, N_D is the donor density, ϵ_s and ϵ_i are the permittivities of semiconductor and insulating layer respectively, E_{rfs} is the quasi Fermi level dictating the population of the density of interface states and it is measured from semiconductor valence band edge at interface and ϕ_0 is the energy level at the surface measured from the valence band edge at the semiconductor surface and specifies the level below which all surface states must be filled for the charge neutrality at the semiconductor surface (11).

The general expression for the current in a schottky barrier solar cell is then given by

$$I = I_{ph} - I_n - I_h - I_{rec} \quad (6.18)$$

substituting for I_{ph} (equation 6.4), I_n (equation 5.5), I_h (equation 5.6) and I_{rec} (equation 6.6), we get the current voltage characteristics represented by

$$I = e \phi_{flux} T_{rm} / \beta \left[\frac{\alpha L_p}{1 + \alpha L_p} v_p \frac{\left(\frac{1}{4} T_{rh} + D_{si} C_{pi} \right)}{D_p / L_p + v_p (T_{rh} / 4 + D_{si} C_{pi})} e^{-\alpha W} + (1 - e^{-\alpha W}) (T_{rh} + D_{si} C_{pi}) \right] - A^* T^2 T_{rn} \exp\left(\frac{-e\phi_{Bn}^*}{kT} \right) \left[\exp(eV/kT) - 1 \right] - e p_{no} \frac{D_p}{L_p} \left[\exp(eV/kT) - 1 \right] - \frac{e n_i W}{\tau_p} \left[\exp(eV/2kT) - 1 \right] \quad (6.19)$$

From equation (6.19), the open circuit voltage V_{oc} ($I=0$), the short circuit current I_{sc} ($V=0$) and the efficiency η ($= \frac{V_{mp} \cdot I_{mp}}{P_{in}}$) can be obtained for the schottky barrier solar cell. P_{in} is the input power and V_{mp} and I_{mp} represent the voltage and current for the maximum power.

6.4 RESULTS AND DISCUSSION:

Taking into account the transmission of electrons and holes across the interfacial layer, the variation of I_{sc} , V_{oc} and η with interfacial layer thickness δ are shown in Figures (6.2-6.4). The plots are obtained for an Au-n Si system taking the values of parameters as given in table (6.1).

From Figure (6.2) we find that the short circuit current is independent of δ in the initial stages, but later on starts decreasing with δ . In the initial stages the transmission of holes across the interfacial layer is quite high and its effect on short circuit current is negligible for small values of δ . For small values of δ , $v_p \left(\frac{T_{rh}}{4} + D_{si} C_{pi} \right) \gg$ in equation (6.4) and transmission of holes across the interfacial layer is very high as compared to $D_{si} C_{pi}$. Under these conditions the short circuit current given by

$$I_{sc} = e \phi_{flux} T_{rm}/3 \left[1 - \frac{e^{-\alpha W}}{1 + \alpha L_p} \right] \quad (6.20)$$

TABLE-6.1Parameters used in efficiency calculations of Schottky barrier Solar Cell.

e	$= 1.602 \times 10^{-19}$ coul.	C_{Si}	$= 2.20 \times 10^{-16}$ cm ⁻²
k	$= 1.38 \times 10^{-23}$ joule K ⁻¹	D_{Si}	$= 10^{11}$ /cm ² /eV
h	$= 6.625 \times 10^{-34}$ Joule-sec	m_{e0}	$= 9.108 \times 10^{-31}$ Kg.
ϵ_0	$= 8.854 \times 10^{-14}$ farad/cm	m_{e0}^*	$= 1.1 m_0$
ϵ_s	$= 11.80 \epsilon_0$	m_{h0}^*	$= 0.55 m_0$
ϵ_i	$= 4 \cdot \epsilon_0$	λ^*	$= 120$ cm ⁻² K ⁻²
ϕ_{Bn}	$= 1.12$ eV		
ϕ_{Bn}	$= 0.30$ eV		
$\tilde{\phi}_e$	$= 0.20$ eV		
\tilde{A}_1	$= \tilde{A}_2$		
T_{rm}	$= 1$		
β	$= 1$		
N_c	$= 2.3 \times 10^{19}$ cm ⁻³		
N_D	$= 10^{17}$ / cm ³		
D_p	$= 11$ cm ² sec ⁻¹		
τ_p	$= 10^{-6}$ sec ⁻¹		

*The datas are taken from references 9 and 10.

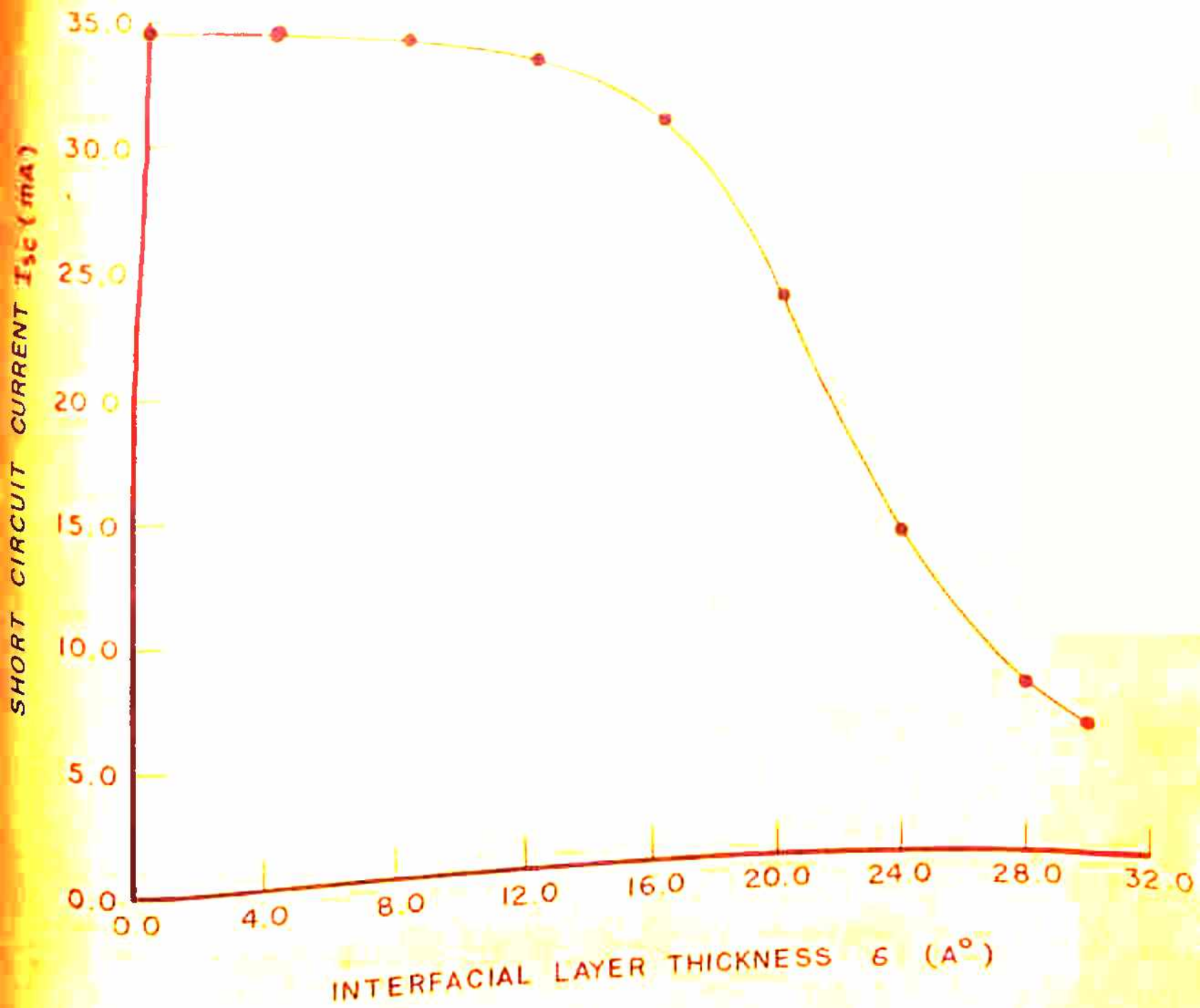


FIG 6.2 EFFECT OF INTERFACIAL LAYER THICKNESS δ ON SHORT CIRCUIT CURRENT I_{sc} .

is independent of δ . Thus I_{sc} will show no variation with δ as long as the condition $v_p \left(\frac{T_{rh}}{4} + D_{si} C_{pi} \right) \gg \frac{D_p}{L_p}$ is satisfied. However, for large values of δ the transmission coefficient T_{rh} for holes decreases according to equation (6.10) and for smaller values of T_{rh} the short circuit current I_{sc} remains no more independent of δ . Thus I_{sc} becomes sensitive to δ . When the term $v_p \left(\frac{T_{rh}}{4} + D_{si} C_{pi} \right)$ becomes smaller than D_p/L_p , the short circuit current starts decreasing with interfacial layer thickness δ . Under this condition, the expression for short circuit (photogenerated) current I_{sc} can be reduced to

$$I_{sc} = e \phi_{flux} T_{rm} / \beta \left[\frac{\alpha L_p^2}{1 + \alpha L_p} v_p / D_p \left(\frac{1}{4} T_{rh} + D_{si} C_{pi} \right) e^{-\alpha W} + (1 - e^{-\alpha W}) (T_{rh} + D_{si} C_{pi}) \right] \quad (6.21)$$

It is clear from equation (6.21) that I_{sc} decreases as the transmission coefficient T_{rh} decreases. The independence of I_{sc} for small values of δ followed by a decrease of I_{sc} with increase of δ for larger values of δ thus appears to be determined whether $v_p \left(\frac{T_{rh}}{4} + D_{si} C_{pi} \right)$ is very large or very small compared to D_p/L_p . This is in accord with the experimentally observed behaviour of Lillington and Townsend⁽²⁾.

The physical processes in the device appear to be as follows: The potential barrier in the depletion region is

actually "down hill" for holes and the slope of this potential barrier depends upon the thickness δ of the interfacial layer. At small values of δ the transmission of holes is quite high and the motion of holes 'down hill' of the potential barrier is also large. As δ increases the transmission factor T_{rh} for holes decreases as also the slope of the potential barrier which drives the holes towards the metal. The net effect of both these factors, namely T_{rh} and the slope of the barrier, is a decrease in the short circuit current I_{sc} at larger δ values. This explains why I_{sc} starts falling after certain interfacial layer thickness δ .

Figure (6.3) shows the increase in V_{oc} with δ . The open circuit voltage V_{oc} is determined by the dark current I_{dark} and the photogenerated current I_{ph} under the condition that the current I flowing through the device is zero. That is, under open circuit condition

$$I_{ph} = I_{Dark}$$

(6.22)

In expression (6.19) different components contributing to the dark current have been incorporated separately. The dark current I_{Dark} depends upon the transmission of electrons T_{rn} across the interfacial layer of thickness δ . An increase in the interfacial layer thickness δ hampers the transmission of electrons across the interfacial layer. A decrease in transmission of electrons will reduce the reverse saturation current without,

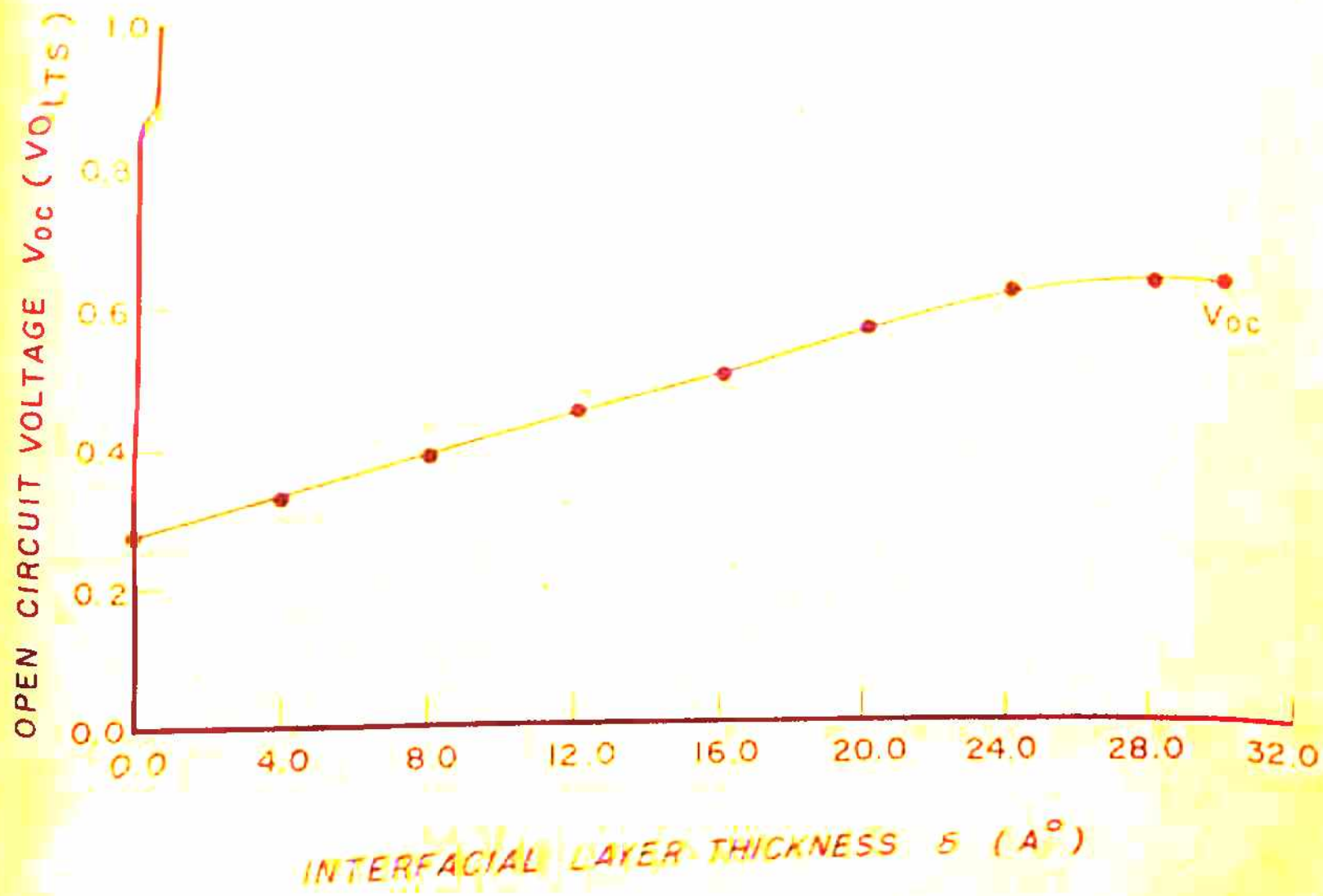


FIG.6.3 EFFECT OF INTERFACIAL THICKNESS ON OPEN CIRCUIT VOLTAGE V_{oc} .

however, affect the photogenerated current in the initial stages, resulting thereby in an increased open circuit V_{oc} . Later on, the open circuit voltage V_{oc} becomes saturated because, for smaller values of δ , the photogenerated current I_{ph} starts decreasing and it seems that the net effect of an increase in V_{oc} is to bring about a saturation for further increase in δ .

In Figure (6.4) the variation of efficiency η with δ is also shown. It increases with δ in the initial stages. The primary reason for this increase is the increase in the power generating current I flowing through the device. Increase in δ implies a smaller value of T_{rn} which means that the dark current component, which is opposing the photogenerated current I_{ph} , is very small. Thus for a range of δ values the reverse saturation current goes on decreasing as T_{rn} decreases with δ and thus power generating current increases. This results in an increase in the power obtained as also in the efficiency of the device. Beyond a certain value of δ , the efficiency, after attaining a maximum value, exhibits a decrease. This decrease, as shown in Figure 6.2, in efficiency can be ascribed to a fall in the short circuit current brought about by a decrease in the hole transmission.

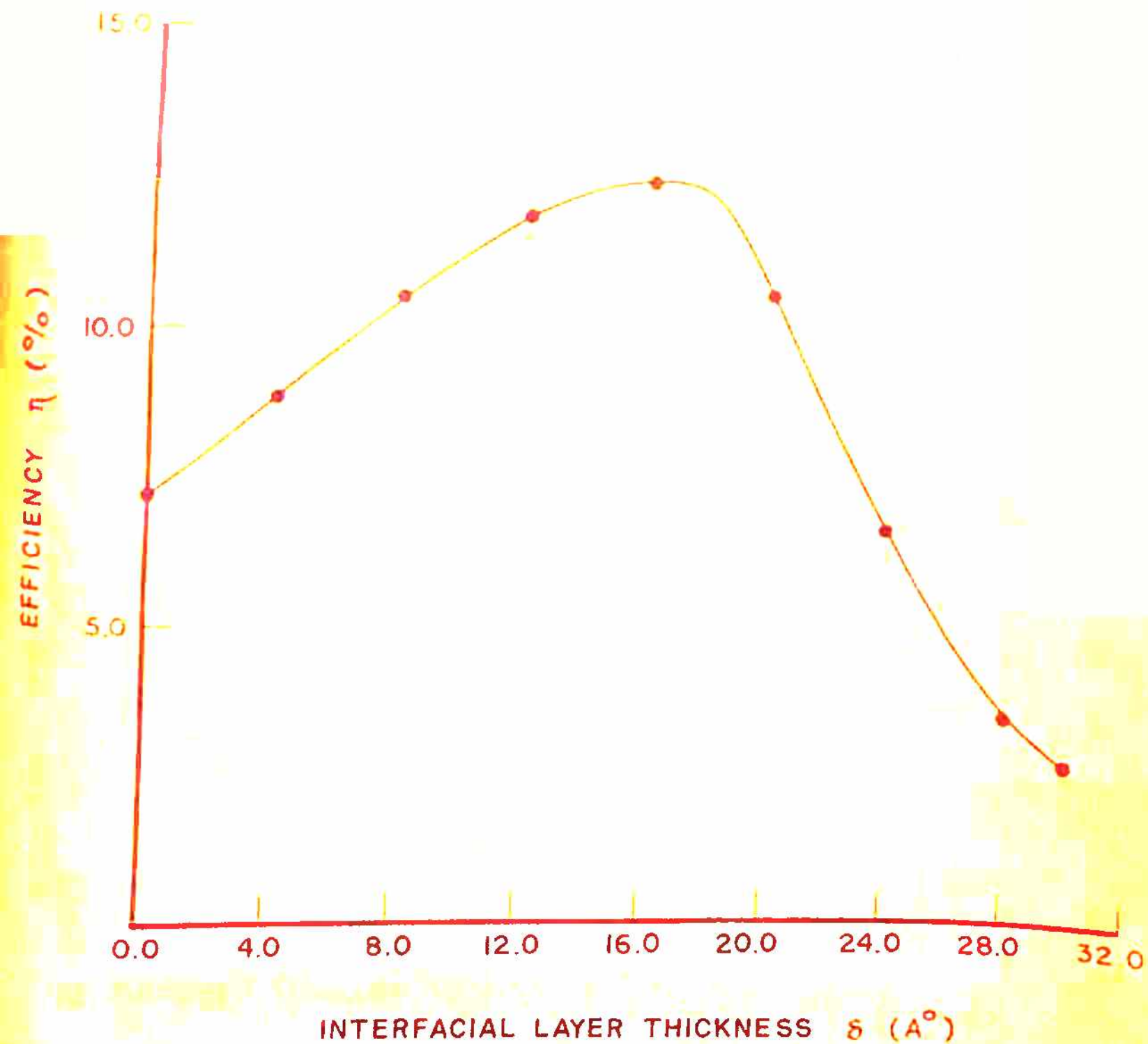


FIG. 6.4 EFFECT OF INTERFACIAL LAYER THICKNESS ON EFFICIENCY η .

REFERENCES:

1. S.J. Fonash, J. Appl. Phys. Vol. 46, pp. 1286 (1975).
2. D. R. Lillington and W.G. Townsend Appl. Phys. Lett. Vol. 28, pp. 97 (1976).
3. L.C. Olsen, Solid State Electronics Vol. 20, pp. 741 (1977)
4. H.C. Card, Solid State Electronics Vol. 20, pp 971 (1977).
5. Deborozhanskii et al, Soviet Physics Semiconductor Vol. 9, pp. 1348 (1976).
6. W.A. Anderson et al , J. Appl. Phys. Vol. 45, pp. 3913 (1974).
7. P.T. Landsberg and C. Klimpke, Proc. Royal Society, London, Vol. A354 pp. 101 (1977).
8. M. Pepper, Metal Semiconductor contact, Chapter I, Published by the Institute of Physics Belgrave Square London (1974).
9. V.I. Strikha, Radio Engineering and Electronics Physics Vol. 9, pp. 552 (1964).
10. S.M. Sze, Physics of Semiconductor Devices, John Wiley and Sons, Inc. (1969).
11. A.M. Cowley and S.M. Sze, J. Appl. Phys. Vol. 36, pp. 3212 (1965).

Solar cells have been an important part of the space program for over a decade and are also capable of making a significant impact on terrestrial energy needs. It is interesting to note that, although the principles of solar energy conversion have been known for a long time, only very recently has there been research and development on a scale large enough to permit practical application of the various types of solar cells. Because of the importance of the solar energy and the increasing amounts of research being done, it is felt to present in some detail the studies on the efficiency considerations in conventional and schottky barrier solar cells. This thesis presents results of studies carried out for p-n junction solar cells and schottky barrier solar cells.

The principles underlying the operation of a p-n junction solar cell are described in Chapter I. A number of parameters, which determine the conversion efficiency of a solar cell, are described. Of the various factors which limit the conversion efficiency, some are basic limiting factors. For such factors improvement in conversion efficiency is not possible beyond a certain limit. There are other factors which are technique oriented and improvement in these factors can increase the conversion efficiency of the solar cell. Both factors are discussed in brief in this chapter.

The current voltage characteristics of the p-n junction solar cell deviates from the ideal current-voltage characteristics if the internal series resistance is sufficiently large. The internal series resistance of the solar cell can be minimized using improved fabrication techniques. Techniques allow application of grids, called fingers to be placed at suitable distances from each other. The internal series resistance arises from various factors. These factors are discussed in Chapter II. A simple method, termed as power formulation method, is presented in Chapter II to evaluate the contribution to the series resistance by the doped layer for various types of grid structures. In this method one evaluates the quantity $(\delta I) \cdot dR$ for an element. Integrating this across all the elements of a unit or subunit gives the power term P, $P = \int (\delta I)^2 dR$, for the unit or subunit. Dividing this P by the square of the total current flowing through the unit or subunit gives resistance of the unit or the subunit. The results obtained by this method are compared with those of Bordina et al. Contribution to the internal series resistance by other factors are also determined. Various experimental techniques to determine the internal series resistance of the solar cell are discussed in brief. The experimental technique of Evdokimov is used for the determination of series resistance of the solar cell. This technique enables the determination of a number of

parameters like series resistance, shunt resistance, thermal voltage etc. from a single set of observations of the I-V plot. The experimental results are compared with the theoretical results. It was earlier thought that most of the contribution to the series resistance comes from the doped layer. This is not always true. In small area solar cells, the maximum contribution is due to contact resistance. However, in large area solar cells, doped layer may contribute quite a lot.

Since, the cost of silicon solar cells and other semiconducting material is high and is likely to remain that way, the use of almost any method to obtain more power output from a given set of solar cells is justified. One technique that has received considerable attention to get more power output from a solar cell is through the use of concentrators. The use of concentrators results in two main disadvantages. Firstly the increased power generating current I , brought about by higher concentration of incident solar radiation, flowing through the device, causes an additional voltage drop across the cell from the internal series resistance R_s and as a result the $I^2 R_s$ loss due to series resistance becomes significant. This in turn affects the maximum power point and degrades the performance of the solar cell. Secondly, the cell operating under concentrated sunlight has a tendency to operate at a temperature higher than the ambient. The

increase in temperature increases the dark current which
 oases the photogenerated current, which in turn decreases
 the efficiency of the solar cell. The concentration of inci-
 dent solar radiation and the operating temperature are impor-
 tant parameters to determine the power output from a given
 solar cell. Experimental determination of a number of solar
 cell parameters at various temperatures keeping concentration
 of incident light fixed and also at various concentrations
 without varying the temperature of the solar cell is
 presented in chapter III and the physical processes under-
 lying their dependence analysed.

The main stress at present in solar energy technology
 is on the development of cheap and efficient methods for con-
 verting incident solar radiation into electrical power. The
 only barrier in the way of conventional p-n junction silicon
 solar cell technology is the cost of these devices. Another
 device which is drawing the attention of a large number of
 scientists in recent years is the fabrication of schottky
 barrier solar cells. This is because of the fact that
 schottky barrier solar cells are adaptable to low cost large
 area fabrication techniques and are suitable for polycrys-
 talline devices. The theoretical limit of conversion effi-
 ciency of these devices can reach that of the p-n junction
 silicon solar cells. The fourth chapter describes an intro-
 duction to schottky effect, metal-semiconductor contact, the
 current voltage characteristics of schottky diodes and ^{the} theory
 of schottky barrier solar cells (SBSC's).

The main draw-back with schottky barrier solar cells is that the reverse saturation current I_0 in such a cell is large and the open circuit voltage is very small. It has been observed that the open circuit voltage and the conversion efficiency of such type of solar cells can be increased by introducing a thin insulating layer in between the metal-semiconductor contact. The current I in a schottky barrier solar cell can be expressed as

$$I = I_{ph} - I_{Dark},$$

where I_{ph} is the photogenerated current and I_{Dark} is the current arising out of forward biasing of the cell under illumination. The insulating layer helps in reducing the dark current component I_{Dark} of the schottky barrier solar cell. However, the exact role of this layer is still not clearly understood. The various parameters such as the thickness of the interfacial layer, density of interface states and donor density play an important role in determining the conversion efficiency of such cells. A factor T_{rn} taking into account the transmission of electrons across the interfacial layer is introduced in Chapter V in the expression for the dark current I_{Dark} . This factor helps in reducing the dark current and thereby improve the conversion efficiency of the schottky barrier solar cell. The performance of T_{rn} on SBSC, incorporating T_{rn} in the expression for I , is discussed in Chapter V. Results based on a number of calculations

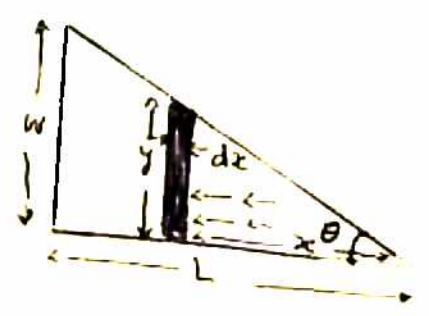
showing the variation of various factors with doping density are reported in this chapter. The schottky barrier solar cell model considered for theoretical study consists of metal -n silicon, in which the metal is of higher work function than the semiconductor.

However, the transmission factor T_{rn} for electrons across the interfacial layer is not the only factor affecting the performance of SBSC's. The photogenerated current is also affected by the thickness δ of the interfacial layer. In chapter VI an additional factor T_{rh} taking into account the minority carrier (holes) transmission across the interfacial layer has been incorporated in the expression for the current $I = I_{ph} - I_{Dark}$ and its effect is seen on the efficiency of the model considered, namely the metal - n silicon schottky barrier solar cell. The analysis shows the existence of an optimum thickness of the interfacial layer for which the efficiency of the solar cell is a maximum.

APPENDIX-2.1

(a) To obtain the resistance of the doped layer for the grid configuration shown in Figure 2.1, we divide it into two parts of length L and width W. The resistance of one part can be obtained as follows: The total current flowing in the element dx is given by

$$\delta I = \frac{1}{2} j \tan \theta dx = \frac{1}{2} j dx \tan \theta$$



$$R_{dx} = \frac{\rho_d dx}{W \cdot \delta I} = \frac{\rho_d dx}{W \cdot \frac{1}{2} j dx \tan \theta}$$

$$R_{dx} = \frac{2 \rho_d}{W j \tan \theta} = \frac{1}{4} \frac{\rho_d}{d_j} j^2 x^3 \tan \theta dx$$

$$R_{dx} = \int dx = \frac{1}{4} \frac{\rho_d}{d_j} j^2 \tan \theta \int_0^L x^3 dx$$

$$R_{dx} = \frac{1}{4} \frac{\rho_d}{d_j} \frac{L}{3} j^2$$

$$R_{dx} = \frac{1}{4} \frac{\rho_d}{d_j} \frac{L}{W}$$

Similarly the resistance of the second part is

$$R_{dx} = \frac{1}{4} \frac{\rho_d}{d_j} \frac{W}{L}$$

These two are in parallel, thus

$$R_d = \frac{1}{4} \frac{\rho_d}{d_j} \frac{WL}{(W^2 + L^2)}$$

- (b) The resistance of the grid configuration shown in Figure 2.6(d) can be obtained by dividing it into 2 subunits of length $L/2$ and width W of the type shown in Figure (2.7c). These are in parallel thus,

$$R_d = \frac{1}{2} \frac{\rho_d}{d_j} \frac{WL}{(4W^2 + L^2)}$$

- (c) The grid configuration shown in Figure (2.6 e) comprises of four subunits, each of length $L/2$ width $W/2$ of the type shown in Figure (2.7c). These are in parallel, thus

$$R_d = \frac{1}{16} \frac{\rho_d}{d_j} \frac{WL}{(W^2 + L^2)}$$

- (d) The resistance of the doped layer for the grid configuration shown in Figure (2.6f) can be evaluated as follows: The current flowing in the element of width dr is given by

$$\delta I = j \pi r^2 \text{ and } dR = \frac{\rho_d}{d_j} \frac{dr}{2 \pi r}$$

$$P = (\delta I)^2 dR = \frac{\rho_d}{d_j} \frac{\pi}{2} j^2 r^3 dr$$

$$P = \int dP = \frac{\rho_d}{d_j} \frac{\pi}{2} j^2 \int_0^a r^3 dr$$

$$P = \frac{\rho_d}{d_j} \frac{1}{8 \pi} I^2$$

$$R_j = \frac{1}{8 \pi} \frac{\rho_d}{d_j}$$

LIST OF PUBLICATIONS.

1. Dependence of Schottky barrier solar cell efficiency on the thickness of the interfacial layer, (Mrs.) S. Srivastava, N.K. Swami and H.M. Ghule, Proc. of National Solar Energy Convention, Jadavpur (Calcutta), pp 157, (1976).
2. Temperature effect on p-n junction solar cell parameters, (Mrs.) S. Srivastava, H.M. Ghule, Proc. of Symposium on Electron Devices, CS&RI (Pilani) pp 1.14 (1978).
3. Role of interfacial layer in Schottky barrier solar cells, N.K. Swami, (Mrs.) S. Srivastava and H.M. Ghule, Proc. of Symposium on Electron Devices, CS&RI (Pilani) pp 1.23 (1978).
4. Effect of ultraviolet sunlight on the various parameters of the p-n junction solar cell, N.K. Swami and H.M. Ghule, Proc. of National Solar Energy Convention, Bhavnagar, pp 43 (1978).
5. Role of oxide layer in Schottky barrier solar cells, N.K. Swami, (Mrs.) S. Srivastava and H.M. Ghule, Proc. of National Solar Energy Convention, Bhavnagar, pp 433 (1978).
6. A study of Schottky barrier solar cell system, (Mrs.) S. Srivastava, N.K. Swami and H.M. Ghule, Proc. of National Solar Energy Convention, Bhavnagar, pp 468 (1978).
7. Role of interfacial layer in Schottky barrier solar cells, N.K. Swami, (Mrs.) S. Srivastava and H.M. Ghule, J. of Phys. D., Vol. 12, pp 765 (1979).
8. Effect of doping density on the efficiency of a Schottky barrier solar cells, N.K. Swami and H.M. Ghule, Indian J. of Physics (Accepted).
9. Temperature effect in Schottky barrier solar cells, (Mrs.) S. Srivastava, P. Nopany, N.K. Swami and G.P. Srivastava, Accepted for presentation in National Solar Energy Convention to be held in Bombay in Dec. (1979).